
THE UNIVERSITY OF QUEENSLAND

AUSTRALIA

# Low Optical Gap Materials for Organic Solar Cells - Research and Application

Ajeesh Chandrasekharan

*A thesis submitted for the degree of Doctor of Philosophy at*

*The University of Queensland in 2015*

School of Chemistry and Molecular Biosciences

# Abstract

In spite of the cost of silicon solar cells decreasing in recent years, there is considerable interest in solar cells with lightweight and flexible forms. Organic semiconductor-based photovoltaic cells (OPVs) have the potential to offer low cost, lightweight and flexible devices. At this stage there is still much to be improved for OPVs as the efficiencies are still lower than their inorganic counterparts. Polymeric materials have been more widely studied than their non-polymeric counterparts. In recent years OPVs polymeric donor materials have emerged with efficiencies reaching 10% with quite a range of materials now providing efficiencies of around 7%. However, the problem with semiconducting polymers is that control of the regioregularity, poly(dispersity), and molecular weight from batch-to-batch is not a simple process. Solution-processable non-polymeric semiconductors are attractive for opto-electronic applications as they are simpler to synthesise, purify, characterise, and the optical properties can be more easily fine-tuned. In this context, diketopyrrolopyrrole (DPP) based small molecules have shown promising results with devices efficiencies reaching around 5-6%. Key properties of the DPP unit are strong π-π interactions, and suitable and tunable energy levels. These properties have been the main drivers in their use in OPVs.

This thesis consist of the synthesis, characterisation, and bulk hetrojunction (BHJ) devices properties of novel DPP(ThAr)$_2$ non-polymeric materials. Accordingly, a first series of compounds was synthesized with different electron affinity groups such as fluorenone (Fl) [**EhDPP(ThFl)$_2$** and **OddDPP(ThFl)$_2$**] and benzothiadiazole (Bt) [**OddDPP(ThBt)$_2$**] attached to the distal ends of a bisthienyl-diketopyrrolopyrrole unit DPP(Th)$_2$ unit. The 'DPP(ThAr)$_2$' derivatives were synthesised under standard Suzuki-Miyaura cross-coupling or by direct arylation reaction conditions and the rate of the direct arylation reaction was found to be faster than for the Suzuki-Miyaura cross-coupling reactions. The solubility of the compounds was poor when the 2-ethylhexyl (Eh) moiety was used as the solubilising group for **DPP(ThFl)$_2$**. 2-Octyldodecyl (Odd) solubilising groups gave better solubility in chlorinated solvents, which are typically used in OPV fabrication. The three non-polymeric DPP materials exhibited bipolar charge transport in organic field effect transistors (OFETs), with hole and electron mobility in the order of $10^{-2}$–$10^{-3}$ cm$^2$ V$^{-1}$ s$^{-1}$, and in a diode architecture **OddDPP(ThFl)$_2$** and **OddDPP(ThBt)$_2$** exhibited mobilities of the order of $10^{-4}$ cm$^2$ V$^{-1}$ s$^{-1}$ for pristine films. In BHJ devices using [6,6]-phenyl-C70-butyric acid methyl ester (PC70BM) as the acceptor, different solvent mixtures were used for device fabrication to achieve the maximum efficiency. The EQE spectra of the blend film suggested that charge generation due to absorption at

wavelengths longer than 750 nm occurred through the Channel I pathway, and at wavelengths shorter than 750 nm, both Channel I and II pathways were in play. **OddDPP(ThFl)$_2$** was found to be the best material when acting as an electron donor in BHJ device and achieved maximum PCE of 4.1%.

To further study the charge transporting properties of **OddDPP(ThFl)$_2$** based materials, its dithiane derivative (SS) [**OddDPP(ThFl(SS)$_2$)$_2$**)] was prepared. **OddDPP(ThFl(SS)$_2$)$_2$** exhibited different thermal and optical properties, which had a direct impact on the OPV device performance and the devices performed poorly. Next, a series of **OddDPP(ThBt)$_2$** derivatives were prepared with different electron withdrawing groups, dicyanovinylene (DCV) [**OddDPP(ThBt-DCV)$_2$**] and *n*-butyl-2-cyanoacetate (B2A) [**OddDPP(ThBt-B2A)$_2$**] as end groups. The end groups had a drastic effect on both the thermal and optoelectronic properties. The materials exhibited a similar electron affinity to that of [6,6]-phenyl-C60-butyric acid methyl ester (PC60BM) and hence were used as an electron acceptor with poly(3-*n*-hexylthiophene) as the electron donor. **OddDPP(ThBt-DCV)$_2$** lacked sufficient solubility to be solution processed, but **OddDPP(ThBt-B2A)$_2$** could be. The EQE spectra of the OPVs suggested that the Channel II mechanism was responsible for charge generation for wavelengths above 650 nm and both Channels (I and II) wavelengths shorter than 650 nm. However, the best device efficiency was only 0.1%.

A final series of materials consisted of 9,9'-bifluorenylidene (BF) and its derivatives as end groups. BF-based materials have been previously reported to give rise to electron accepting materials. In this series the basic structure was kept same, with the difference being simple addition of methoxy groups (OMe) or fluorine (F) atoms to **OddDPP(ThBF)$_2$** to form **OddDPP(ThBF(OMe)$_2$)$_2$**) and (**OddDPP(ThBF(F)$_2$)$_2$**), respectively. However, only the parent **OddDPP(ThBF)$_2$** and the methoxy derivative, **OddDPP(ThBF(OMe)$_2$)$_2$** could be purified and characterised. The materials exhibited different thermal phase transition behaviours, but had similar optoelectronic properties. Devices fabricated with BF derivatives and the acceptor (PC70BM) from chloroform and chloroform with 10% dichlorobenzene exhibited similar device performance. However, the device performance was poor. Interestingly, the film fabricated from chloroform with 0.5% 1,8-diiodooctane (DIO) exhibited the best device performance and the **OddDPP(ThBF)$_2$**:PC70BM OPV had an efficiency of 2.6%.

**Declaration by author**

This thesis is composed of my original work, and contains no material previously published or written by another person except where due reference has been made in the text. I have clearly stated the contribution by others to jointly-authored works that I have included in my thesis.

I have clearly stated the contribution of others to my thesis as a whole, including statistical assistance, survey design, data analysis, significant technical procedures, professional editorial advice, and any other original research work used or reported in my thesis. The content of my thesis is the result of work I have carried out since the commencement of my research higher degree candidature and does not include a substantial part of work that has been submitted to qualify for the award of any other degree or diploma in any university or other tertiary institution. I have clearly stated which parts of my thesis, if any, have been submitted to qualify for another award.

I acknowledge that an electronic copy of my thesis must be lodged with the University Library and, subject to the policy and procedures of The University of Queensland, the thesis be made available for research and study in accordance with the Copyright Act 1968 unless a period of embargo has been approved by the Dean of the Graduate School.

I acknowledge that copyright of all material contained in my thesis resides with the copyright holder(s) of that material. Where appropriate I have obtained copyright permission from the copyright holder to reproduce material in this thesis.

**Publications during candidature**

"No publications".

**Publications included in this thesis**

No publications included.

**Contributions by others to the thesis**

Prof. P.L. Burn - Conception and design of project, analysis and interpretation of research data, critical revision of thesis.

Dr Shih-Chun Lo - Analysis and interpretation of research data.

Dr Paul shaw was responsible for optical gap and electron affinity measurement and calculation from solid state for **EhDPP(ThFl)$_2$**, **OddDPP(ThFl)$_2$**, and **OddDPP(ThBt)$_2$**.

Dr Hui Jin and Dr Mike Hambsch was responsible for the bulk heterojunction device manufacture and measurements of **OddDPP(ThFl)$_2$**, and **OddDPP(ThBt)$_2$**. Dr Mike Hambsch was also responsible for transporting properties measurements in diode configuration for the same compounds.

Dr Hui Jin was responsible for the bulk heterojunction device manufacture and measurements of **OddDPP(ThFl(SS)$_2$)$_2$**.

Dr Mike Hambsch was responsible for the bulk heterojunction device manufacture and also for the transporting properties measurements in diode configuration of **OddDPP(ThBt-B2A)$_2$**.

Dr Hui Jin was responsible for the bulk heterojunction device manufacture and measurements of **OddDPP(ThBF)$_2$**, and **OddDPP(ThBF(OMe)$_2$)$_2$**.

Ms Fatemeh Maasoumi fabricated all of the organic field effect transistor (OFET) devices and measured the performance of the materials within the devices.

Dr. Dani Stoltzfus was responsible for all of the Photo Electron Spectroscopy in Air (PESA) measurements.

**Statement of parts of the thesis submitted to qualify for the award of another degree**

"None".

**Acknowledgements**

I would like to thank my advisor, Professor Paul Burn, for giving me the opportunity to come and study in Australia and for allowing me to carry out this project under his supervision. I am grateful for the support he provided throughout my candidature, and acknowledge the dedicated and optimistic attitude he takes towards his research and students. I also thank him for enabling me to attend and present at the 2015 MRS Conference in San Francisco. I also express thanks to Dr. Shih-Chun Lo, my co-advisor, for all the helpful suggestions and practical advice he gave me, and to Rob Kembery for all his administrative and organizational support.

Firstly, thank you to Dr. Hui Jin and Mike Hambsch for fabricating and testing the performance of the materials within OPV devices. Ms Fatemeh Maasoumi for OFET device fabrication and measurments. I also thank Dr. Dani Stoltfuz for carrying out PESA measurements and discussions on synthesis. Dr. Paul Shaw for optical gap measurements. Dr Ross Jansen-Van Vuuren for helping with MALDI measurments and inviting me for the hikings trips. I also thank them all for the many discussions we have had and for their encouragement and advice throughout the time as a member of COPE.

I thank Yuvan, Fan, Rob, Larry, Xin, Steve, Sarah, Renji and Ravi for encouragement, helpful discussions and, most importantly, friendship and a good sense of humor.

I thank Dr. Tri Le for assisting with NMR experiments and Mr. Graham McFarlane with mass spectrometry.

I acknowledge the University of Queensland for providing me with financial support *via* a University of Queensland Research Scholarship (UQRS) and University of Queensland International Research Award (UQIRA).

Lastly, I thank my family for their support and love over the course of my studies. I thank my parents, for encouraging me to take on the PhD, and for providing a shoulder to lean on and an ear to listen through the challenges. Special thanks to my brother and sister for encouragement.

**Keywords**

Narrow optical gap, Electron donor, electron acceptor, bulk heterojunction solar cell, synthesis, Diketopyrrolopyrrole, hole mobility, electron mobility

**Australian and New Zealand Standard Research Classifications (ANZSRC)**

ANZSRC code: 030503, Organic Chemical Synthesis, 60%

ANZSRC code: 030301, Chemical Characterisation of Materials, 40%

**Fields of Research (FoR) Classification**

FoR code: 0305, Organic Chemistry, 60%

FoR code: 0303, Macromolecular and Materials Chemistry, 40%

# Table of contents

# List of Figures, Schemes and Tables

## List of Figures

## List of Schemes

## List of Tables

## List of Abbreviations

| | |
|---|---|
| OPV | Organic Photovolatics |
| $E_b$ | Excition binding energy |
| IP | Ionisation Potential |
| EA | Electron Affinity |
| HOMO | Highest Occupied Molecular Obiatal |
| LUMO | Lowest Unoccupied Molecular Orbital |
| $T_g$ | Glass transition temperature |
| DIO | 1,8-Diiodooctane |
| Da | Daltons |
| MEH- PPV | Poly[2-methoxy-5-(2'-ethylhexyloxy)-*p*-phenylenevinylene] |
| P3HT | Poly(3-*n*-hexylthiophene) |
| PCPDTBT | Poly[2,6-(4,4-bis-(2-ethylhexyl)-4*H*-cyclopenta[2,1-b;3,4-b']-dithiophene)-*alt*-4,7-(2,1,3-benzothiadiazole)] |
| PCE | Power Conversion Efficinecy |
| DPP | Diketopyrrolopyrrole |
| BDT | Benzo[2,1-b:3,4-b']dithiophene |
| PC60BM | [6,6]-Phenyl-C60-butyric acid methyl ester |
| PC70BM | [6,6]-Phenyl-C70-butyric acid methyl ester (same as PCBM) |
| Ar | Argon (reaction scheme) |
| Fl | Fluorenone |
| Bt | Benzothiadiazole |
| DCV | Dicyanovinylene |
| B2A | *n*-Butyl-2-cyano acetatae |
| 1,3-ind | 1,3-Indanedione |
| BF | 9,9'- Bifluorenylidene |
| OMe | Methoxy |
| F | Fluorine |
| OFET | Organic Filed Effect Transistor |
| NBS | *N*-Bromosuccinimide |
| PdCl2(dppf) | [1,1'-Bis- (diphenylphosphino)ferrocene]dichloropalladium(II)] |
| $T_d$ | Decomposiiton temperature |
| $T_c$ | Crystallisation temperature |
| DSC | Differentail Scanning Calorimetry |

| | |
|---|---|
| TGA | Thermal Gravimetic Analysis |
| CV | Cyclic Voltamettry |
| PESA | Photoelectron Spectroscopy in Air |
| MIS-CELIV | Metal Insulator Semiconductor-Charge Extraction by Linearly Increasing Voltage |
| $\mu_h$ | Hole mobilities |
| $\mu_e$ | Electron mobilities |
| SCLC | Space Charge Limited Current |
| DCB | 1,2-Dichlorobenzene |
| EQE | External Quanum Efficiency |
| UV-vis | Ultraviolet-visibl |
| Voc | Open Circuit Voltage |
| $\eta$ | External Efficiency |
| OLED | Organic Light Emitting Diode |
| nm | Nanometres |
| IR | Infrared |
| b.pt | Boiling point |
| $\lambda$max | Wavelength of maximum absorption |
| MALDI-ToF | Matrix-Assisted Laser Desorption/Ionisation – Time of Flight |
| mg | Milligram |
| g | Grams |
| KHz | KiloHertz |
| mmol | Millimoles |
| M | Molar concentration, mol $L^{-1}$ |
| mM | Millimolar concentration, mmol $L^{-1}$ |
| ESI-MS | Electrospray Ionisation-Mass Spectrometry |
| Fc/Fc+ | Ferrocene/Ferrocenium couple |
| ICT | Intramolecular charge transfer |
| $^1H$ | NMR Proton Nuclear Magnetic Resonance |
| $\mu$ | Micro ($10^{-6}$) |
| D/A | Donor-Acceptor |
| S/D | Source/Electrode |
| $^{13}C$ | NMR Carbon Nuclear Magnetic Resonance |
| Min | Minutes |
| *J* | Coupling constant |
| PEDOT | Poly[3,4-(ethylenedioxy)-thiophene] |

| | |
|---|---|
| PSS | Poly(styrenesulfonate) |
| TGA(5%) | Thermal decomposition (corresponding to 5% weight loss) |

# 1. Introduction

## 1.1 Background

With increasing industrialisation and world population, energy demands are a global concern. The International Energy Agency (IEA) has projected that, energy consumption will rise to somewhere around 17 to 18 billion tonne oil equivalents by 2035. Energy is available from many sources such as coal, nuclear power, wind, solar, geothermal, hydropower and, oil fuels. However, the major portion of the energy used for generating electricity is still derived from fossil fuels.

Fossil fuels are a non-renewable source of energy upon which the human race has depended to raise the standard of living. However, the sources of such fuels are dwindling due to the rapidly increasing rate at which they are being utilized[1]. Fossil fuel power plants burn fuels such as coal, oil or gas to generate steam that drives large turbines that produce electricity. Energy Outlook, predicts that the global carbon dioxide ($CO_2$) emissions will go up 25% from fossil fuel burning by 2035 compared to what they were in 2013[2]. The major consequence of burning any fossil fuel is that, the process generates greenhouse gases, mostly carbon dioxide, but also sulphur dioxide, both of which can contribute to global warming. Considering these issues it is important to generate electricity from an alternative source, which is renewable and environment friendly.

Sun light is a permanent source of carbon free energy. Every hour the Earth receives solar energy more than enough to satisfy global energy needs for an entire year. It has been estimated that the total annual solar radiation falling on the earth is more than 7 500 times the world's total annual primary energy consumption of 450 Energy Joules (EJ)[3]. Hence, over the last few decades while different renewable energy sources have being actively explored. It is recognised that solar energy will be a key contributor to the renewable energy mix. However, the overall share of global power generation using solar cell technology is still small, less than 0.8%, which in the past was mainly due to the high cost of conventional solar cells.

## 1.2 Photovoltaics

Photovoltaic (PV) cells are capable of converting light energy directly into electricity. This process is called photovoltaic effect. The photoelectric effect was first noted by, Edmund Bequerel, in 1839, who found that certain materials would produce an electric current when exposed to light.

### 1.2.1 Silicon solar cells

The photovoltaic effect of crystalline silicon solar cells was discovered at Bell laboratories in 1941[4]. By 1954, a crystalline silicon solar with a Power Conversion Efficiency (PCE) of 6% was developed at the same facility[5]. The vast majority (90%) of solar cells manufactured today are based on 'crystalline' silicon using thin silicon wafers of 300 microns. The silicon wafers used for solar cells are Czochralski (CZ) single crystalline, produced by directional solidification, or cast to give, multicrystalline (mc) material. On a commercial scale silicon solar cell have PCE of around 15–18% with the exception of certain high-efficiency modules capable of efficiencies greater than 20%[6]. The highest reported silicon based solar cell, however, is capable of converting sunlight into electricity with efficiencies as high as 40%[7]. Silicon solar cells have been very successful commercially, especially with the decrease in manufacturing costs in recent years[8]. However, the disadvantages of silicon solar cells are low light absorption coefficient, which requires wafers to be thick, and the cost and waste of sawing the silicon wafers is still high. Hence, in an effort to produce solar cells even more cheaply there has been much work on the development of thin film cells based on inorganic (e.g. CdTe) and organic semiconductor-based, and more recently on perovskite-based photovoltaic cells, which have the potential to offer even lower cost devices due to their relative ease of manufacturing[9-11].

One of the advantages of organic and perovskite semiconductor based thin-film solar cells is that they can be manufactured from solution or vacuum deposition techniques. Using these techniques, the materials can be printed on a roll-to-roll flexible substrate using conventional processing techniques. Materials deposited using solution processing techniques e.g., printing; often have the advantage because of their low temperature requirements, as well as the potential for cost reduction and minimal impact on environment[12].

### 1.2.2 Perovskite solar cells

Lead halide perovskite-based solar cells have gained substantial attention in the last four years, owing to their rapid increase in reported power conversion efficiency[11]. In 2014 alone, there has been a number reports of perovskite cells with PCEs above 20%[13, 14]. The best perovskites, $CH_3NH_3PbI_{3-X}Cl_X$, contain lead with varying proportions of chloride and iodide (x from 0 to 3). This material can be solution processed or vacuum evaporated to make thin film devices, which makes it an eligible candidate for commercialisation and large scale production of solar cells with

high power conversion efficiency. However, the best performing perovskite solar cells all have lead, which is a real area of concern. The toxicity of handling lead during device fabrication, deployment and disposal, is a major concern and has to be addressed, if they are to make it to the market. This is similar to the CdTe cells in which first solar cell have to dispose of used molecules. Also, perovskite solar cells are reported to undergo degradation (sometimes quite rapid) on exposure to moisture and ultraviolet radiation[15]. To overcome these issues, the research community has been working on perovskite materials that are lead free and there have been a few reports in this regard recently[16, 17]. However, the device efficiencies of such devices are always much smaller (6%). At this stage there is still much to be done before perovskite can be considered commercialisable. While it is important to watch the development of perovskite cells the steady improvement in terms of the efficiency and stability of organic photovoltaic cells means that they must also be considered as been a technology of importance in the future energy mix.

## 1.3 Organic Photovoltaic (OPV) Cells

Over the last 25 years organic semiconductors have been used in field effect transistors[18], light emitting diodes[19] and organic photovoltaic (OPV) devices[20]. Although commercially used solar cells are primarily based on silicon solar cells, there has been tremendous amount of effort that has been put into to develop organic semiconductors based solar cells, both by industries and research labs. With industry and research laboratory effort the performance of OPV devices have been steadily improving with the best devices having efficiencies of 12%[21].

### 1.3.1 Brief history and device architectures

Research on organic semiconductor based photovoltaic cells began sometime in the 1950. However, the power conversion efficiencies of those cells were reported to be generally poor and in the range of $10^{-3}$ to $10^{-2}$ [22, 23]. Later in 1986, Tang introduced the bilayer heterojunction concept[24] (see Figure 1.1.a). In a typical bilayer structure, the p-type and n-type organic semiconductor are stacked upon each other, and sandwiched between the electrodes. The reported solar cells consisted of a p-type semiconductor a phthalocyanine derivative (CuPc) as the hole transporting material, see Figure 1.2a and an n-type semiconductor a perylene tetracarboxylic (PT) derivative as electron transporting material, see Figure 1.2b. This first bilayer device was reported to have achieved a power conversion efficiency of 1%[24]. This result was the benchmark for OPV cells for many years, until the turn of millennium.

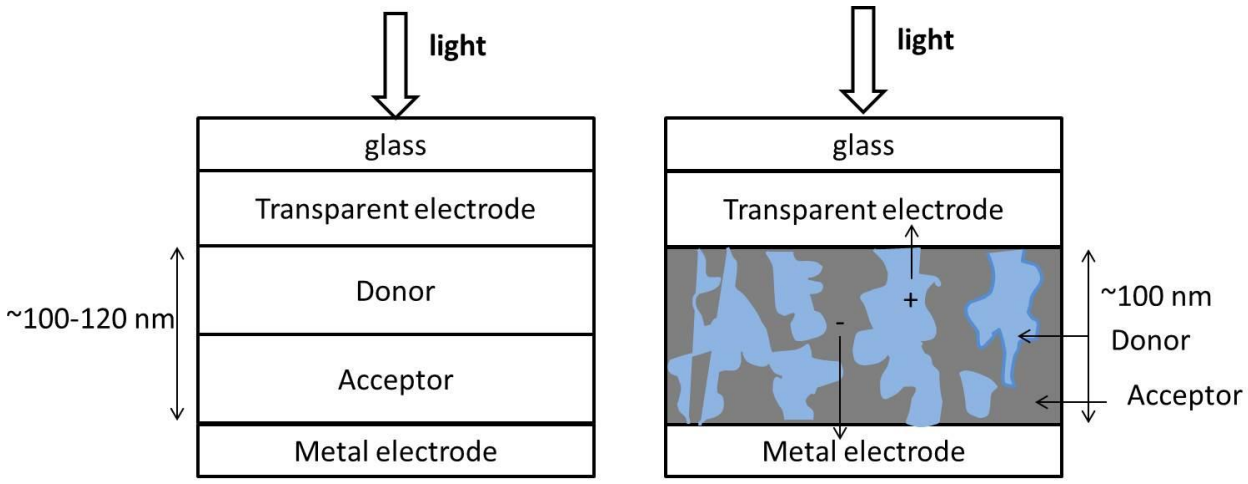


**Figure 1.1.** a) Bilayer device structure b) Bulk hetrojunction (BHJ) device structure.

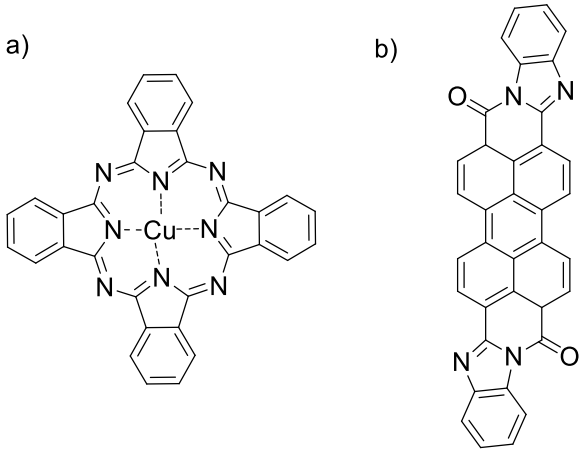


**Figure 1.2.** Chemical structures of a) CuPc, and b) PT

One of the major breakthroughs in OPV technology was achieved with the introduction of C60 (see Figure 1.3a) and its derivatives such as [6,6]-phenyl-C61-butyric acid methyl ester, PC61BM, see Figure 1.3b, as an n-type semiconductor. Furthermore, the bilayer hetrojunction has its own limitations as charge separation occurs only at an interface, resulting in low efficiency. This issue was addressed with the introduction of bulk hetrojunction concept (see Figure 1.1b). This concept was first demonstrated by Hiramoto *et al.* through the co-evaporation of a p-type, phthalocyanine (PC) derivative and an n-type perylene derivative[25]. In 1995, Heeger *et al*. and Yoshino *et al.* individually demonstrated the photoinduced electron transfer from a p-type conjugated polymer

material to a fullerene derivative blended, together[26, 27]. It was reported that the devices exhibited better photocurrent generation when compared with bilayer cells. After these discoveries polymer–fullerene blends dominated the field of high-efficiency OPVs. However, recently non-polymeric material has gained attention and efficiencies on par with many polymer-based solar cells have been reported. Summary of different types of semiconductors will be discussed in section 1.4.

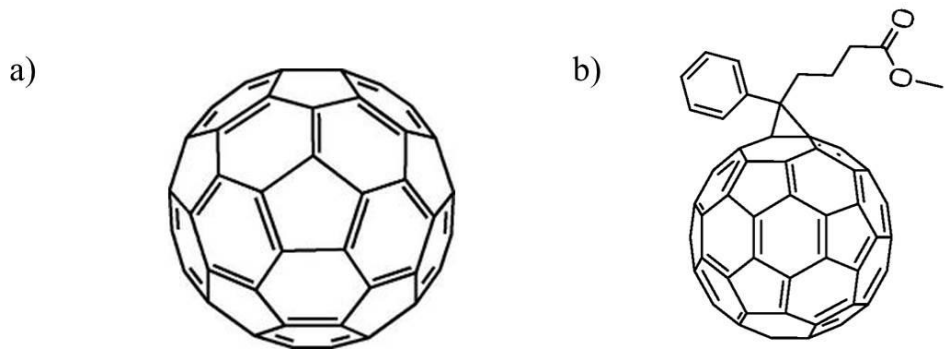


**Figure 1.3.** Chemical structures of a) C60 and, b) PC61BM.

With bulk hetrojunction layers it is important that the two components are mixed in such a way that the photogenerated exciton can reach the Donor/Acceptor (D/A) interface before recombination - the exciton diffusion length in most of the organic semiconducting materials is ~<10 nm.[28] On the other hand, the BHJ active layer needs to have a bicontinuous pathway for transport of the generated charges to the electrodes and hence fine control over the film structure is required.[29] Based on the molar extinction coefficient and charge transport properties of many active materials, and the optical effects within the device, the active layer thickness of many devices are around 100-200 nm. This thickness enables maximum utilization of the incident light.

### 1.3.2 Charge generation and extraction

In many of the inorganic semiconductors light absorption generates a free hole and electron. However, in organic solar cells, when the photoactive layer is irradiated with sunlight it generates an exciton in which the hole and electron are bound by columbic forces. The exciton then diffuses through the layer to a donor/acceptor interface, where the exciton is split into free holes (positive charge carriers) and electrons (negative charge carriers), provided the energy offset between the donor and acceptor is sufficient to overcome the Columbic binding forces of the exciton ($E_b$) (see Figure 1.4a). The binding energy of excitons in organic semiconductors is estimated to be around

~0.1-0.5 eV[30]. The holes and electrons then move to the corresponding electrodes by flowing through either the donor or acceptor phase, respectively.

In a typical organic solar cell, both donor and acceptor are capable of absorbing sunlight and, the charge generation process can occur by either the 'Channel I' or 'Channel II' mechanism, respectively (see Figure 1.4b, and c). Over many years it was thought that charge generation occurs primarily through Channel I mechanism i.e, the donor absorbs the light, which generates excition in donor phase and at the donor/acceptor interface electron is transferred to the material with higher electron affinity (the acceptor). Hence, there has been significant effort in developing narrow optical gap donor materials that have a strong molar absorptivity co-efficient in the visible region to increase the efficiency of charge generation. Conversely, for Channel II it is assumed that the absorption of light primarily occurs in the acceptor phase which creating an exciton, which migrates to the interface of donor where hole transfer occurs from the acceptor to the material with lower ionisation potential (donor). Often the Ionisation Potential (IP) and Electron Affinity (EA) are used interchangeably with the energy of the Highest Occupied Molecular Orbital (HOMO) and Lowest Unoccupied Molecular Orbital (LUMO), respectively. Given the possibility of Channel II generation recently there has been an effort to design acceptor materials with large excition coefficients in the visible region to enhance the light absorption in the active layer. Koster *et al.*, proposed that, by optimising both Channels (I and II) in a complementary fashion the power conversion efficiency beyond the Shockley-Queisser limit could be achieved in organic solar cells. One way of doing this is by designing donor and acceptor materials that have complementary absorptions which would increase the charge generation efficiency. Along with the relevant energy levels the donor and acceptor materials in a blend have to have the requisites ordering in a film for free charge carrier generation and the subsequent extraction of the charges to their respective electrodes. The optimised film structure is required to avoid complex recombination processes that can occur at the donor/acceptor interface, e.g., if separated charges recombine (geminate recombination) [31].

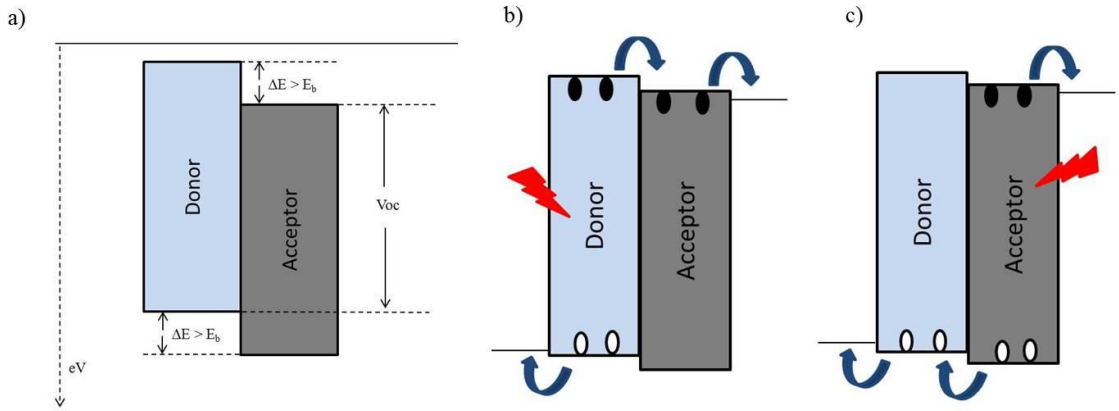


**Figure 1.4.** A simple energy level diagram of a donor and acceptor solar cell device (a) depicting energy difference required for charge transfer from donor to the acceptor ($\Delta E > E_b$), where $E_b$ is excition binding energy and the origin of the Voc (b) excitation of the donor and Channel I mechanism – electron transfer (c) excitation of the acceptor and Channel II mechanism – hole transfer. Solid circles represent the path of electron, with clear circles representing the movement of free holes.

Optimising the film structure has been achieved using various techniques such as thermal annealing[32, 33], solvent annealing[34], solvent mixtures/or the use of additives solvent[35-39] or a combination of all these. Thermal and solvent annealing is techniques that are normally used to achieve the optimised film blend structure after the films have been fabricated. For example, in the case of thermal annealing the blend film is general heated above the glass transition temperature ($T_g$) or in some case above melting point of the donor or acceptor material to bring about an ordered film structure on cooling. In contrast, solvent mixtures/and solvent additive combination involve fabricating the blend film from a 'master solvent' with small amounts of a high boiling point solvent such as xylenes, chlorobenzene, or additives such as 1,8-diiodooctane (DIO). The use of different solvents or additives works on the principle that the donor and acceptor have different solubilities and precipitate out at different times in the presence of the bad solvent. In addition the higher boiling point of the additives allows the film to dry slowly, which can result in a better film structure for maximum charge extraction. In the literature, a mixture of small amount of high boiling point solvent with the master solvent has been referred as a solvent mixture[39] although in some cases it is called as a solvent with additive[36].

Efficiency of a solar cell is described with respect to a number of parameters including Fill Factor (FF), open circuit voltage (Voc) and short circuit current ($J_{sc}$), as defined by the following equations:

$$\eta(PCE) = FF\ J_{sc}\ Voc/\ P_{IN} \quad (1)$$

$$FF = I_{mpp}\ V_{mpp}/J_{sc}\ Voc \quad (2)$$

The FF is given by equation (2) and is an indication of the diode quality. $I_{mpp}$ and $V_{mpp}$ are the current and voltage at the maximum output power, respectively. $J_{sc}$ is the short circuit current and Voc is the open circuit voltage. In an organic solar cell, Voc is governed to first order by the difference in energy of the EA of the acceptor and the IP of the donor material[40] (see Figure1.4a). $P_{IN}$ is the total power into the cell and the external power conversion efficiency η, is defined as the ratio of the maximum power delivered by the device to the incident light that falls on the cell, Pin. Therefore PCE is essentially a measurement of the power produced by a solar cell in relation to the incoming power. In summary, the key requirements for organic photoactive materials are: good absorption of photons within the solar spectrum, adequate phase separation and appropriate energy levels (IP/EA) of the materials to enable exciton separation and charge transport, and ideally solution processable for ease of manufacture, particularly for large area modules.

## 1.4 Materials

There are primarily two types of organic semiconductors: polymeric and the other is non-polymeric. In the literature, usually non-polymeric materials are mostly referred as small molecules although it is technically incorrect as their molecular weight is generally too high. In this thesis, small molecules are discussed under the topic non-polymeric materials, as the work is primarily based on non-polymeric materials having molecular weights of around 1 500 Daltons (Da).

### 1.4.1 Polymer donor materials for OPV

Polymeric based materials are well studied in comparison to non-polymeric materials in OPV. The main drive in polymeric materials development has been on narrow optical gap (so called low band

gap polymers), which are usually mixed with fullerene acceptors to form bulk heterojunction devices.

One of the earliest polymers to be used in an OPV device was poly[2-methoxy-5-(2'-ethylhexyloxy)-*p*-phenylenevinylene] (MEH-PPV) (see Figure 1.5a), which when blended with C60 gave a higher energy conversion efficiency compared to earlier reported polymers.[41] However, polymer based OPVs really only gained momentum after poly(3-*n*-hexylthiophene) (P3HT) (see Figure 1.5b), which had a smaller optical gap and broader spectrum coverage, gave efficiencies of around 4-5%, making it a standard material for studying polymer solar cells. However, the Voc of the device with P3HT:PCBM blends was low, around 0.6 eV[38]. It was seen in the previous section that, Voc is one of the important parameters for achieving high efficiency solar cells. Hence, to fine tune the IP the donor polymers units with relatively low IP were incorporated into the polymer backbone to improve the Voc. For example, Cao *et al*., and Leclerc *et al*., demonstrated that by combining 9,9- di-*n*-octylfluorene (PFO-DBT) and *N*-9′-heptadecanyl-2,7-carbazole units (PCDTBT) with the 4,7-dithien-2-yl-2,1,3-benzothiadiazole unit, devices with high Voc (~0.9 eV) could be obtained[42, 43] (see Figure 1.5c and d, respectively). Another important parameter governing the PCE of organic solar cells is $J_{sc}$. $J_{sc}$ value is primarily determined by the charge generation efficiency of the active layer in OPVs, which is directly related to the number of photon absorbed. By engineering materials with a narrower optical gap, materials with better solar spectral coverage can be obtained. The most common approach of obtaining materials with narrower optical gap is by having alternating Donor-Acceptor moieties along the polymer backbone. In this regards, Bazan *et al*., combined 4,4-bis-(2-ethylhexyl)-4*H*-cyclopenta[2,1-b;3,4-b]dithiophene unit with a 2,1,3-benzothiadiazole unit, which are considered to be units with relatively high IP and EA, respectively to give a material with a near infrared absorption. This material poly[2,6-(4,4-bis-(2-ethylhexyl)-4*H*-cyclopenta[2,1-b;3,4-b']-dithiophene)-*alt*-4,7-(2,1,3-benzothiadiazole)] (PCPDTBT) exhibited a narrow optical gap of 1.4 eV, and with PC71BM as acceptor gave OPV devices that exhibited a PCE of 5.5%[44] (see Figure 1.5e). However, a reduction in the optical gap of donor material leads to, a straight forward consequence of reduction in the Voc value. Hence, materials have to be carefully designed, to incorporate units with suitable energy levels, to obtain devices with high efficiency. As stated earlier another important parameter is FF, which is dependent on the charge collection at the electrodes. One of the factors that can determines the charge collection efficiency at the electrode is the transporting properties of the donor and acceptor material. Price *et al*., reported two polymers, one having a fluorine atom (PBnDT-FTAZ, see Figure 1.5f) attached to the 2-alkyl-benzo[d][1,2,3]triazole unit with the second without the fluorine atom (PBnDT-HTAZ, see Figure 1.5g). The two polymers exhibited similar absorption properties, however, they had different hole

mobilities. PBnDT-FTAZ ($\mu_h$ = 6.7 x $10^{-5}$) exhibited a hole mobility one order of magnitude more than PBnDT-HTAZ ($\mu_h$ = 3.3 x $10^{-6}$) leading the former polymer exhibiting a better PCE of 6.8% with FF = 0.73. PBnDT-HTAZ, had a PCE and FF of 4.3% and FF = 0.55, respectively[45]. In recent years, there have been reports of polymer donor materials with fullerene acceptors giving OPV devices with efficiencies reaching 10%, and quite a range of donor materials now have efficiencies of around 7%[45, 46]. However, disadvantages of conjugated semiconducting polymers are issues relating to the control of the regioregularity, polydispersity, and molecular weight and hence batch-to-batch reliability is not a simple process. Hence, there has been a developing interest in the research community and in industry to develop non-polymeric materials.

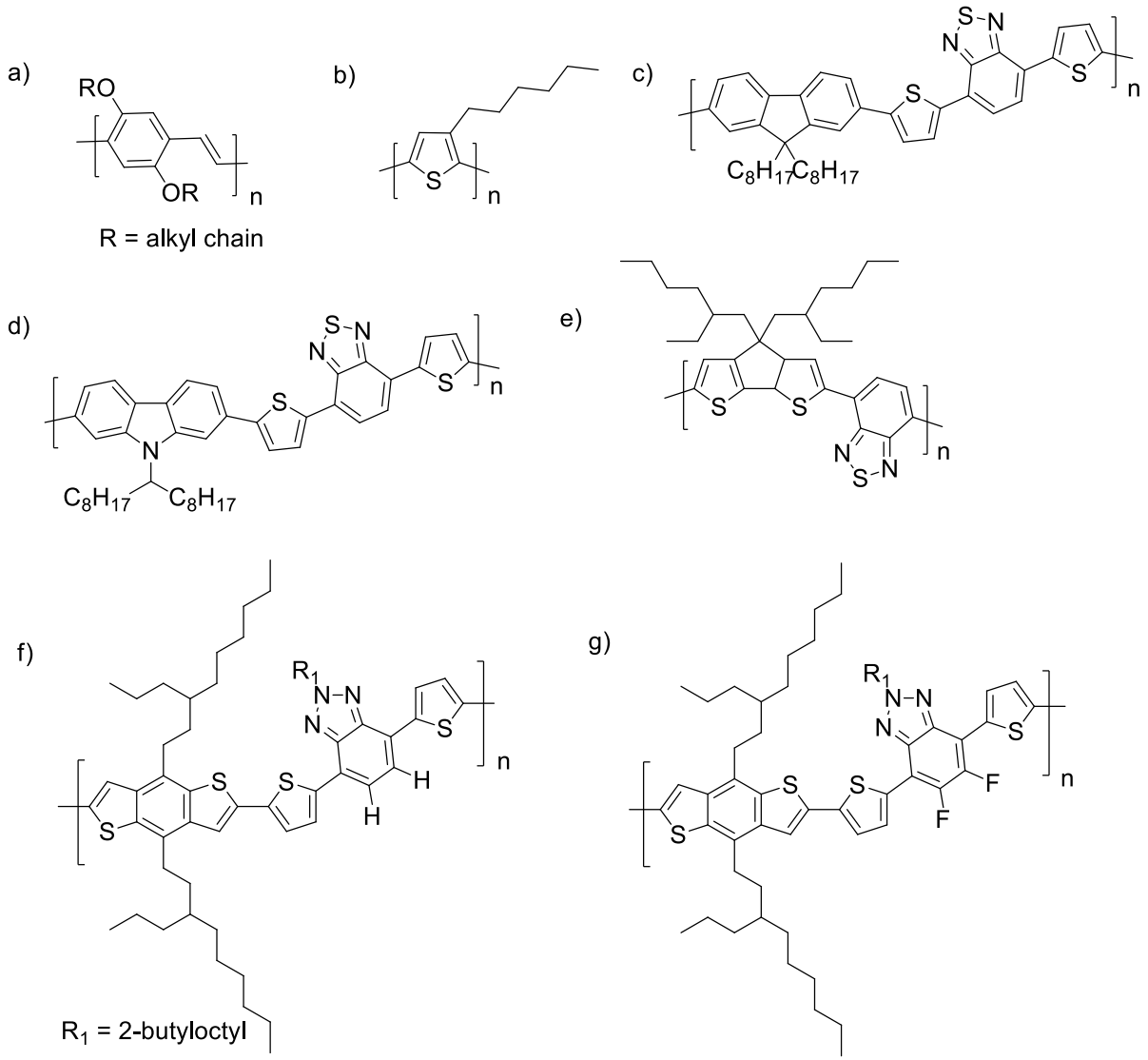


**Figure 1.5.** Chemical structures of polymer donor materials developed to fine tune the IP/EA, optical properties, and charge transport properties.

### 1.4.2 Non-polymer donor materials for OPV

Non-polymeric chromophores possess certain advantages over polymeric materials such as the ease of synthesis and purification, and they can often have better charge carrier mobility (better for charge extraction) with values as high as 15 $cm^2 V^{-1} s^{-1}$ reported[47]. The optical properties of small molecules can also be fine-tuned more precisely, compared to polymers, where even a small structural change can alter either the optical or physical properties to a great extent. Non-polymeric materials can also have large molar absorption co-efficients, be soluble in common organic solvents, and can in some cases be both solution and vacuum processed.

The increasing number of reports on OPV devices containing non-polymeric materials was started, when BHJ type devices with polymers gained attention. The early reports mainly focused on using phthalocyanine (see Figure 1.6a) or hexabenzocoronene (see Figure 1.6b) as donor material and a perylene derivative (see Figure 1.6c) as the acceptor material. However, the devices had poor efficiency compared to the polymers at that time. The poor device performances discouraged the research community at the time to use non-polymeric materials in OPV devices. It was not until 2006, that the situation changed with reports from Lloyd *et al*., Sun *et al*., Kopidakis *et al*., and Roncali *et al*., of high efficiency non-polymeric OPV devices[48-51]. However, the efficiency was still not on par with the polymer devices. The reports used materials that were primarily based on oligothiophenes. For, example Kopidakis *et al*., reported a series of star shaped oligothiophenes with 1,3,5 or 1,2,4,5 substituted phenyl cores with the intent of forming two- and three-dimensional conjugated networks with PC61BM as an acceptor. The best device efficiency (PCE 1.7%) was for a material with a 1,2,4,5 substituted phenyl core with each arm consisting of six thiophene rings[51] (see Figure 1.6d). At, the same time, several other research groups were working on soluble rubrenes and pentacenes. However, the highest device efficiency with the acenes was reported only in 2009. Winzenberg *et al*., reported that a 1:1 mixture of an acetyl triethylsilyl substituted dibenzo[b,def]chrysene material (see Figure 1.6e) with PCBM exhibited PCE of 2.3% with Voc = 0.83 eV, FF = 0.41, $J_{sc}$ = 6.55 mA $cm^2$ [52]. Nguyen *et al*., in 2008, reported the first soluble bisthienyl-diketopyrrolopyrrole (DPP) based material with oligothiophene incorporated at the ends[53]. The material was reported to have a *t*-carbamate group (see Figure 1.6f) at the nitrogen positon of the DPP unit, which was thermally less stable. However, when the carbamate group was replaced with a 2-ethylhexyl solubilising groups (see Figure 1.6g), the material exhibited better stability and with PCBM as acceptor gave a PCE of 3.0%[54].

Recent research on non-polymeric materials have shown that, they are capable to achieve efficiency, on par and even ahead of some polymeric materials-based devices[55]. In last two years there have been quite a few reports of non-polymeric donor materials based OPV devices that have shown efficiencies greater than 6%[56, 57]. For example, Kan *et al*., in 2014 reported a non-polymeric material 'named' DR3TSBDT with a dialkylthiol-substituted benzo[1,2-*b*:4,5-*b*]dithiophene (BDT) as the central unit, with *tri*-octlythiophenes as linkers and rhodanine end groups (see Figure 1.6h). With PC71BM as an acceptor the donor material exhibited an average PCE of 9.6% based on 50 devices. They have also have reported that when the dialkyloxy solubilising groups (see Figure 1.6i) were replaced with dialkylthiol groups the material exhibited more ordered molecule packing, which resulted in a higher PCE. As the charge transport in non-polymeric materials are largely dependent on interchromophore π-π interactions unlike polymers that can also have intrachain transport. The recent progress in some non-polymeric materials are focused on incorporating groups that can induce better molecular packing[58, 59].

a)

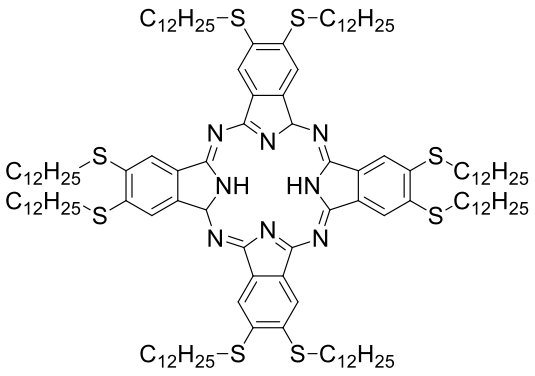

b)

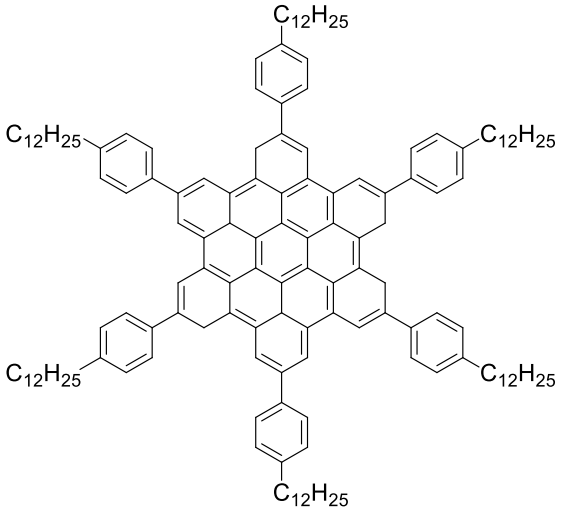

c)

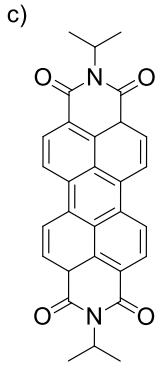

d)

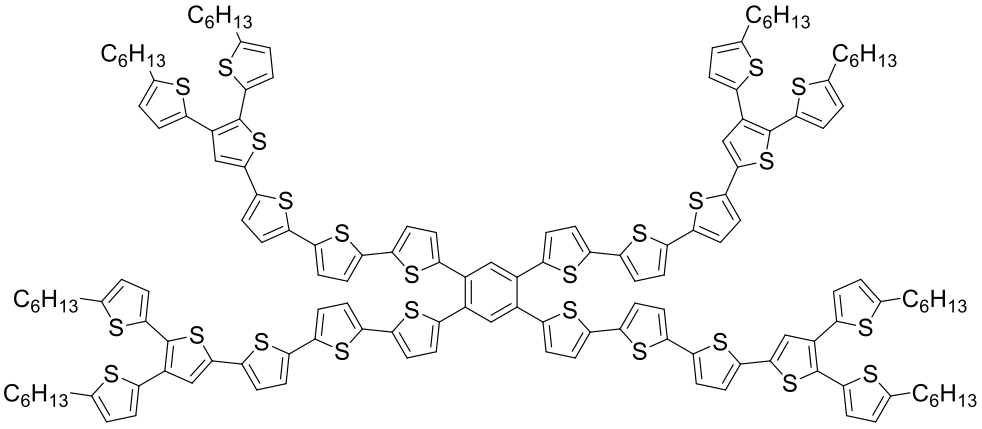

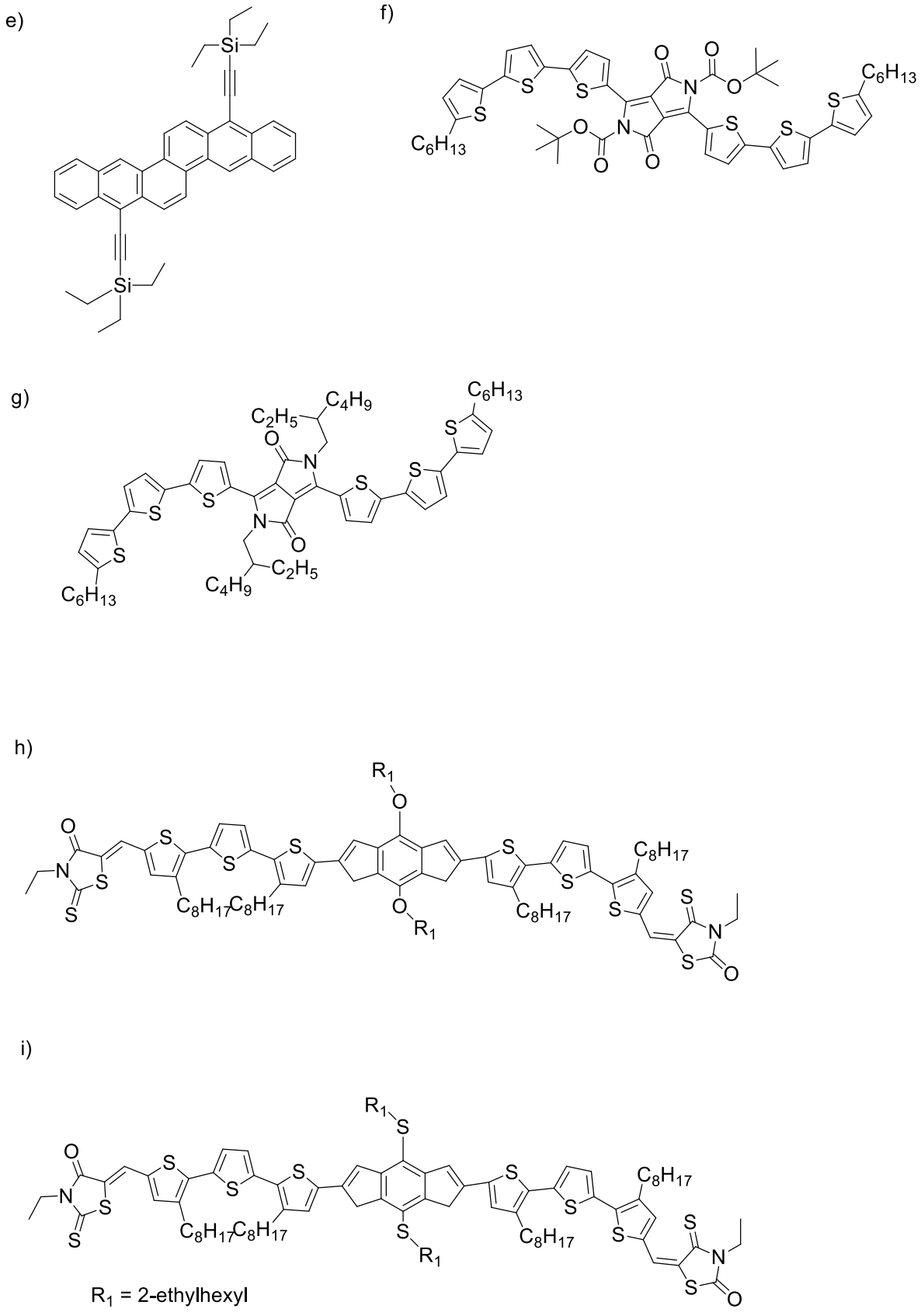


**Figure 1.6.** Structures of non-polymeric donor materials with variations used to fine tune the optoelectronic properties and induce ordered molecular packing in solid state.

General trends in non-polymeric donor materials in OPV devices show that, they usually have a high Voc mostly in the range of 0.7-0.9 eV, compared to their polymeric counterparts, while the FFs and $J_{sc}$s tend to be lower. The non-polymeric materials also exhibit high molar absorptivity and in some cases better charge transporting properties than the polymeric materials. However, polymers are known to form interpenetrating percolated pathways with the PCBM acceptors creating the necessary bicontinuous network for charge transport, resulting in the better FF. Non-polymeric materials have relatively shorter conjugated backbone length limiting the ability to form interpenetrating networks when blended with PCBM derivatives and other acceptors. The fact that charge transport in a non-polymeric material is primarily due to π-π interactions between the adjacent molecules in the solid state, and negligible intrachain contribution, can result in a decrease in the FF. Hence to overcome these issues, the recent focus on non-polymeric materials has been to design materials having alternating Donor-Acceptor chromophores (the so called push-pull structure) and also by incorporating groups or units at the end that can induce planarisation of the molecule or strong π-π interactions in solid state. In this context, it has been demonstrated that the molecular packing and optical properties of the bisthienyl-diketopyrrolopyrrole [DPP$(Th)_2$] based material can be tuned by different alkyl substituents (solubilising groups) at the nitrogen positions and by having different aromatic groups attached to the 5-positions of the thiophenes. As a consequence substituted DPP derivatives have now attracted considerable research effort in optoelectronic applications[60] such as chemsensors[61], two–photon absorption[62], organic light emitting diodes[63], organic thin film transistors[64], and in the context of this work in organic solar cells[65].

## 1.5 Diketopyrrolopyrrole (DPP)

The first synthesis of the Diketopyrrolopyrrole (DPP) chromophore unit was reported by Furam, *et al*., with the structure having a phenyl group attached to each of the lactam rings (see Figure 1.7)[66]. Iqbal *et al*., further developed the synthetic pathway, and found that by treating one mole of a disuccinate with two moles of an aromatic nitrile in the presence of a strong base at elevated temperature it was possible to get better yields[67].

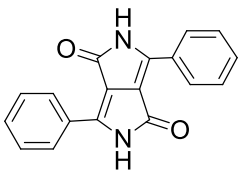


**Figure 1.7.** A 1,4-diketo-3,6-diphenylpyrrolo[3,4-c]pyrrole

The unsubtituted DPP derivative showed a bathochromic shift in the absorption spectrum in the solid state compared to solution. This was caused by hydrogen bonding, π–π and van der Waals interactions, which can be simply understood from the x-ray crystal structures[68]. Owing to their strong light absorption, photochemical stability and the feasibility for large scale synthesis, DPP derivatives have rapidly became an important class of high-performance pigments used in inks, paints, and plastics[69]. However, due to their insolubility in most common organic solvents, their early application was largely limited to the pigment industry. More recently it has been found that facile addition of alkyl groups onto the nitrogens of the lactams can lead to soluble DPP derivatives.

Key properties of the DPP core unit are strong π-π interactions a relatively high electron affinity, and tenability of the optoelectronic properties, and these have been the main drivers in their use in solar cell applications. Narrow optical gap materials are one of the important parameters for better performance in organic solar cells. Increasing the chain length of the substituents at the 3 and 6-positions of the DPP core can lead to a narrowing of the optical gap, a broadening of the absorption, and a tendency to self-assemble into ordered film structures upon thermal annealing[70]. More recently, there have been reports of using additives in processing solvents, to improve blend film structure, for films based on DPP donor materials and PCBM acceptors[35, 36]. Although DPP-based polymer material do not form part of this thesis work, a brief discussion on the DPP based polymer material will be included in the introduction as the early work on the DPP chromophore was mainly focused on narrow optical gap donor polymer materials.

### 1.5.1 DPP based polymer materials for OPVs

DPP derivatives have been used as either the donor or acceptor material in OPV devices. However, the major focus of the research has been to focus on using the DPP unit within the donor polymer material[65]. In particular by using various coupling reactions (generally palladium catalysed) a broad range of different lower IP building blocks have been co-polymerized with 3,6-dithiophen-2-yl-2,5-dihydropyrrolo[3,4-c]pyrrole-1,4-dione (DPP-bithiophene) to fine tune the optical gap, and ionisation energies and electron affinities[71]. In 2009, Yang *et al*., reported a series of narrow optical gap polymers with different IP units copolymerized with the DPP-bithiophene unit (see Figure 1.8). The materials exhibited narrow optical gap in the range of ~1.3-1.6 eV. Polymers with benzo[2,1-b:3,4-b']dithiophene (BDT) (see Figure 1.8d), exhibited the best device efficiencies, and the better performance was attributed to the broad solid state absorption from 350-850 nm. Recently, a series of polymers was reported where the structures were based on DPP and BDT units, but with

alkylthienyl and alkylphenyl moieties were attached to the BDT. The devices with alkylthienyl groups incorporated onto the BDT achieved over 8% in a tandem solar cell and 6.6% in single junction solar cells, which is one of the highest efficiencies reported with a DPP based polymer[72]. Thomson *et al*., synthesized novel semi- random polymers containing poly(3-*n*-hexylthiophene) (P3HT) and differing amounts of DPP unit (5-15%), and these had broad absorption and high short circuit current density, leading to OPV devices with Power Conversion Efficiencies (PCE) on average greater than devices containing only regioregular P3HT[73]. DPP based materials have shown to have high hole mobilities in diode (closer to OPV device operational conditions) and OFET configuration[74]. In this regard, Ong et al., reported a polymer based on DPP-bithiophene unit copolymerised with a dithienylthieno[3,2-b]thiophene (DTT) unit. The material exhibited a very high hole mobility of up to 10.5 $cm^2$ $V^{-1}$ $s^{-1}$, which is one of the highest reported for any polymer material[75]. Thus DPP core unit can impact good properties in to polymeric materials such that they can match the solar energy distribution and allow for the necessary IP/EA arrangement for charge carrier generation as well as good charge transport is optimised.

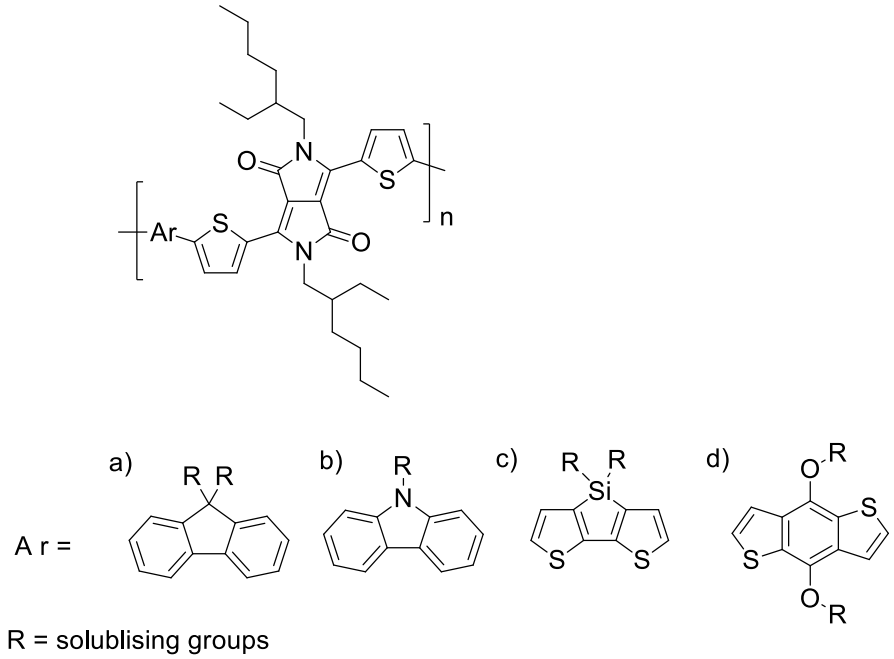


**Figure 1.8.** Structures of DPP-based copolymers with different building blocks to tune the optical gap, and ionisation energies and electron affinities.

### 1.5.2 DPP based non-polymeric materials for OPVs

Earlier work on DPP-based materials were focused on using oligothiophenes attached to the DPP(Th)$_2$ unit. The devices made using those materials exhibited a moderate PCE of 3.0% with $J_{sc}$ = 9.2 mA cm$^2$ and Voc = 0.75 eV [36]. More recently Chandrasekharam *et al*. reported two compounds based on the DPP(Th)$_2$ unit having relatively high IP (difluoro-phenyl) and low IP (di-n-butyloxy phenyl) units attached at the end (see Figure 1.9a and b). The material having difluorophenyl exhibited a higher Voc (0.80 eV) in OPV devices compared to the material with di-*n*-butyloxy phenyl units (Voc 0.74 eV)[76]. Although the difference in Voc are only marginal, these results suggest that both in case of polymer and non-polymeric materials, the same design strategy can be used to obtain compounds with higher Vocs. In addition, Fréchet *et al*. reported that incorporation of units that are planar onto the ends of the DPP(Th)$_2$ unit can facilitate favorable end-to-end π–π interactions, leading to enhanced charge transport between adjacent molecules. They reported a series of compounds having different end units such as triphenylamine, BDT, or pyrene units with the groups chosen based on their ability to form planar structures in films (see Figure 1.9c, d and e). It was found that the material having the pyrene end units, exhibited a better FF (nearly approaching 0.6), a better PCE. X-ray studies of the crystals of those materials showed that the one with pyrene unit exhibited a more planar structure in solid state[58]. DPP-based non-polymeric materials have gained wider attention from the research community after the non-polymeric DPP based molecule DPP(TBFu)$_2$ (Figure 1.9f) showed an OPV efficiency of 4%[32]. More recently, efficiencies above 5% were reported for BDT-2DPP moieties which had 5-alkylthiophene-2-ylsubstituted BDT unit and bisthienyl-diketopyrrolopyrrole units at the end[77] (Figure 1.9g).

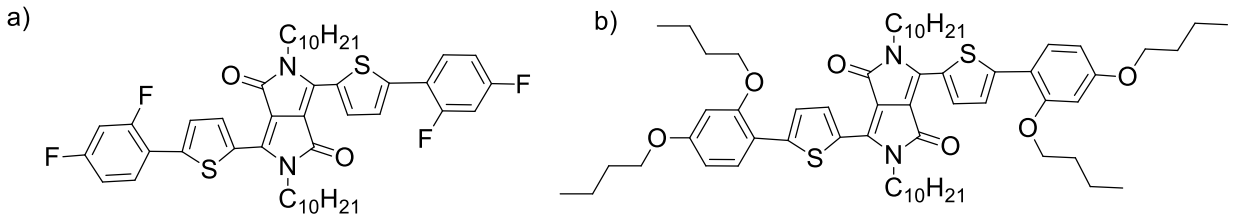

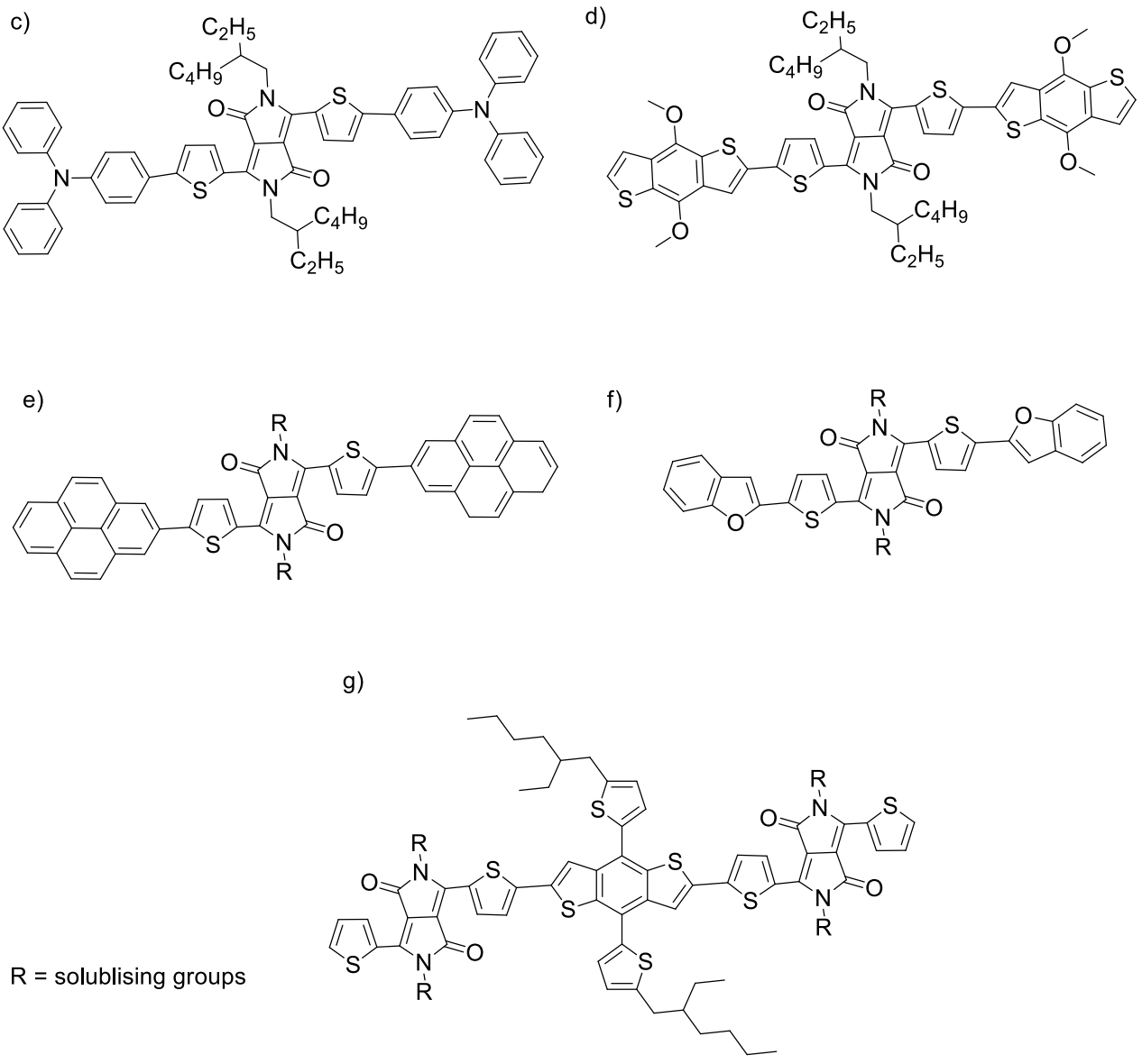


**Figure 1.9.** Structure of DPP based non-polymeric materials having different IP/EA, optical gaps, and charge transport properties.

Surprisingly, although small molecule based organic semiconductors are not generally known to have good film forming properties compared to their polymer counterparts, these structures that couple the rigid planar units onto the DPP core have tended to have good film forming properties, which is required for high PCEs[32]. This thesis consist of Chapters were fullerene derivative, [6,6]-phenyl-C70-butyric acid methyl ester (PC70BM) has been used as acceptor and in another Chapter, non-fullerene acceptor has been explored. Hence, a brief summary on both fullerene and non-fullerene acceptors has been provided in the next section.

# 1.6 Fullerenes acceptor and non-fullerene acceptors

### 1.6.1 Fullerene acceptors

For both polymers and non-polymeric materials, fullerene derivatives have been widely used as acceptor for OPV devices. Reasons for this is the spherical shape of fullerenes allows for the effective packing in solid state and charge transfer in all directions, which leads to high electron mobilities $10^{-2}$ $cm^2$ $V^{-1}$ $s^{-1}$ [78, 79]. Another important advantage of these fullerenes is the high electron affinity of ~ -3.6 eV[80], which allows energetically favorable electron transfer from the donor to the acceptor, which was previously discussed in Section 1.3.1. With the introduction of soluble fullerene derivatives of C60 such as [6,6]-phenyl-C60-butyric acid methyl ester (PC60BM), interest in the solution processable polymer-fullerene blends grew quickly. However, PC60BM has a low absorption profile in the visible region, which can limit the efficiency of charge generation in the blend films, especially in the case when the extinction co-efficient on the donor is low. This issue was, however, partially overcome by using PC70BM (see Figure 1.10) as an acceptor, which has higher optical density over a wide range of wavelengths in the visible region[80]. The other main drawbacks of these PCBMs are the limited scope of synthetic modification[81]. Hence, the optical properties of the PCBMs cannot be fine-tuned precisely to have complementary absorption to the donor materials. Although the polymer-fullerene devices exhibit the best PCEs before they can be commercialized on a large scale the costs need to be reduced and in case of the polymers batch-to-batch need to be reduced.

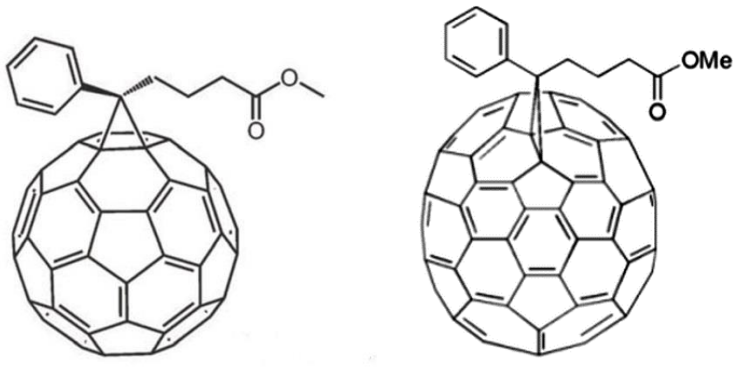


**Figure 1.10.** Chemical structure of PC60BM (left) and PC70BM (right).

Hence, with the aim of overcoming these drawbacks, the research community have been developing non-polymeric donor and acceptor materials (the latter are generally referred to as non-fullerene acceptors), which have high molar absorptivity in the visible region and can be solution processed. It should be noted that, there are small number of acceptor polymers are also referred as non-fullerene acceptors. However, the focus in the next section is on solution processed non-polymeric acceptor materials in OPV devices.

### 1.6.2 Non-fullerene non-polymeric acceptor materials

A comparison of the PCE and brief discussion of each class of acceptors will be given with the examples using polymer as donor materials. The progress in non-fullerene based acceptors has been primarily based small molecule compounds, as the EA and optical properties can be fine-tuned to suit more widely used donor polymer materials, such as P3HT. There are only few reports of other polymer materials used as donor for investigating non-fullerene acceptors. This is because P3HT can be solution processed from wide range of solvents and the film forming properties are well understood and hence useful comparison can be made.

Perylene-diimide (PDI) derivatives were among the first acceptor materials studied in BHJ organic solar cells[24]. However, due to the original low PCE that was reported, PDI based acceptor materials were not much explored till more recently. PDI derivatives have been reported to form long range ordered aggregates in a film, limiting their ability to form the favorable film structure for charge generation and extraction[82]. However, more recently it was shown that, by using dimers or star-shaped PDI derivatives, the aggregation can be reduced, resulting in better device efficiencies in the range of 3–4%[83]. The best device result reported so far for a PDI derivative [($SF\text{-}PDI_2$), see Figure 1.11a] was from Zhao et al., who reported PCE of 6.3% with a Voc of 0.98 eV. In that report, a difluorobenzothiadiazole based polymer was used as the electron donor[84]. Moreover, the PDI derivatives were reported to have a high electron mobility measured in the FET configuration. For example, *N*,*N*-ditridecyl-3,4,9,10-perylenetetracarboxylic diimide [(PTCDI-C13) see Figure 1.11b] thin-film transistors had an electron mobility of 2.1 $cm^2 V^{-1} s^{-1}$ [85].

In 2010 Wudl *et al*., reported a non-fullerene acceptor based on the 9,9'-bifluorenylidene (99'BF) unit[86]. The 99'BF unit is forced to be coplanar in the ground state due to the double bond (see Figure 1.11c). However, addition of electron leads to strain relief[87] and a gain in aromaticity to a 14-π-electron system[88]. In OPV devices, 99'BF and its derivatives were used as electron acceptors

with P3HT as the electron donor. The best devices exhibited a PCE of around 2% with a high Voc of 1.10 eV, which is essentially double that of standard P3HT:PC60BM, blend[86]. One of the important parameters for achieving high PCE is to have high Voc. Normally it is important to ensure that the energy offset between donor and acceptor is sufficient for charge transfer(~0.4 eV)[30]. However, Gong *et al*., have demonstrated ultrafast charge transfer from P3HT to the 99'BF derivative D99'BF (see Figure 1.11d), even though the EA energy offset between the donor and the acceptor was only 0.12 eV. This value is considerably less than the minimum energy offset requirement for charge generation led to a high Voc 1.2 eV[89].

More recently, there have been quite a few reports based on using EA units such as benzothiadiazole[90], vinazene derivatives[91], perylene diimide[83], diketopyrrolopyrrole[92], 1,3-indanedione[93] and rhodanine units[94] with or without electron withdrawing groups such as dicyanovinylene[80] or alkyl cyanoacetate[95] groups to obtain acceptor material with suitable EA to facilitate charge generation with P3HT. The basic design strategy in most of these materials is to incorporate high EA units/groups at the end or ends of the molecule that can also contain units with different IP to obtain material with narrower optical gap. In this regard, Holiday *et al*., reported a compound having a fluorene unit in conjugation with a benzothiadiazole-rhodanine unit at the end[96] (FBR, see Figure 1.11e). The material exhibited an EA of -3.6 eV, and under the same conditions they also measured the EA of PC60BM (-3.8 eV). The P3HT:FBR device exhibited a PCE of 4.1%. In order to understand the charge generation process they carried out transient and steady state optical spectroscopy measurements for the P3HT:FBR blend film, and reported that there was ultrafast charge generation and efficient photocurrent generation from both P3HT and FBR, indicating both Channel I and II charge generation. However, PCEs based on non-fullerene acceptors, still lag behind the fullerene derivatives. Hence, there is a need to engineer better non-polymeric non-fullerene materials to absorb over a wide range of solar spectrum. Further, by investigating the charge generation process and film forming properties of the new acceptor materials, is expected to generate better performing non-polymeric donor and acceptor materials. In this regard, DPP based non-polymeric materials have not been exploited widely as an alternate acceptor materials.

Sonar et al., reported a series of DPP-based acceptor materials having trifluoromethylphenyl or trifluorophenyl units at the end[92]. The materials exhibited EAs in the range of ~-3.5 eV to -3.7 eV. The materials were reported to have high molar absorptivities over the range of 700 to 300 nm, which was proposed to be due to charge transfer transition between the low IP phenylene-thienylene unit and the EA diketopyrrolopyrrole core. The best device result was achieved for the material

having trifluoromethylphenyl has end groups (see Figure 1.11f). The device exhibited a PCE of 1% using P3HT as the donor material under simulated AM1.5 solar irradiation of 100 mW $cm^2$. These results have encouraged the research community to further explore DPP-based molecule has electron acceptors with P3HT as donor. Janssen *et al*., in 2010, reported a series of DPP-derivatives incorporating low reduction potential groups, such as 3-*n*-octylthiophene and the corresponding aldehyde (see Figure 1.11g and h, respectively). As a result of the low FF and $J_{sc}$, the device exhibited a poor PCE, with the best device efficiency of 0.31%[97]. In 2014, there were two reports of DPP based acceptor materials. In those reports different aromatic units such as fluorene or benzothiadiazole was used as the central unit and the $DPP(Th)_2$ unit was incorporated at both ends (see Figure 1.11i and j). In both reports, the best devices exhibited a Voc above 1.0 eV, and efficiency of around 1%[98, 99]. More recently, Kim *et al*. reported three $DPP(Th)_2$ based acceptor materials. The end groups consisted of phenyl ring having electron-withdrawing cyanide groups attached at different position (*p*ara, *m*eta, and *ortho*) of the phenyl ring (see Figure 1.11k, l and m). The materials were reported to be investigated as Channel II acceptor materials and it was suggested that the EQE of 13% of P3HT:*p*-DPP-PhCN blend film above 650 nm was due to charge generation through Channel II mechanism[100]. Hence, these results suggest that, by incorporating EA groups onto $DPP(Th)_2$ unit, the electron affinity of the resultant material should be higher facilitating charge separation at the donor/acceptor interface in BHJ based OPV devices.[92]

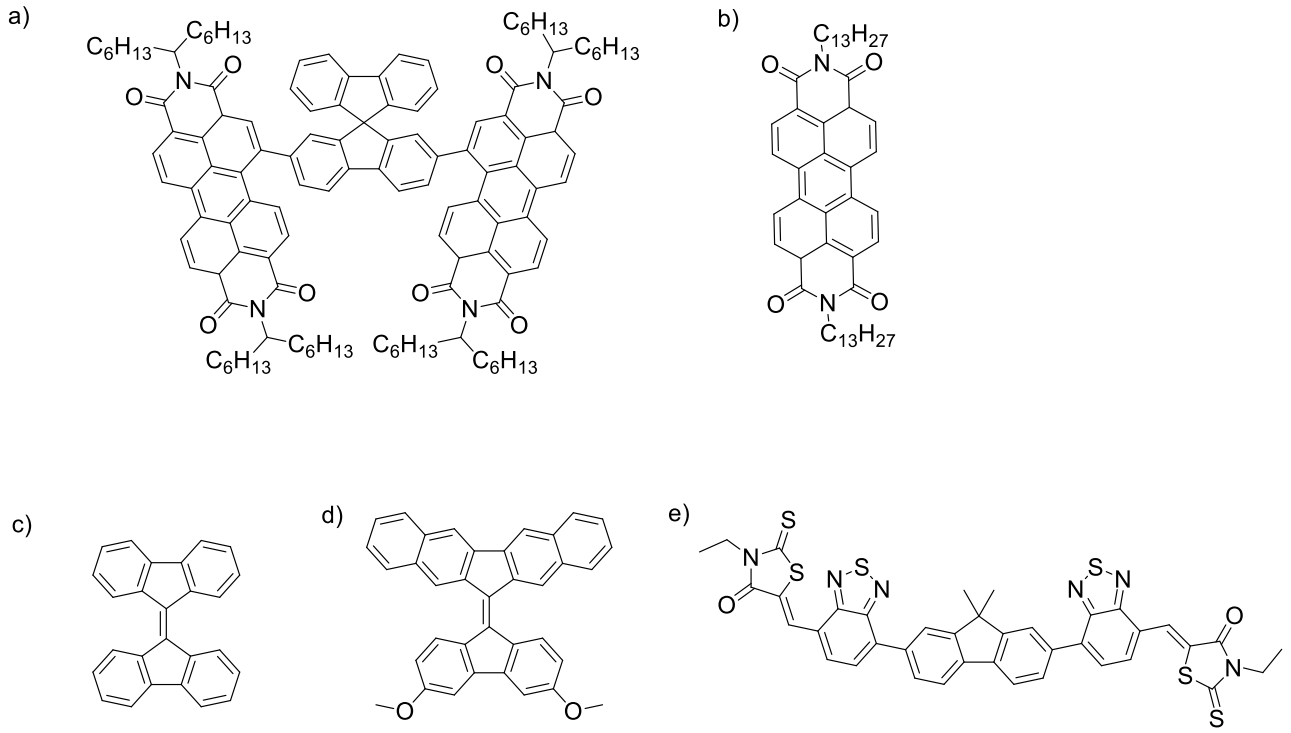

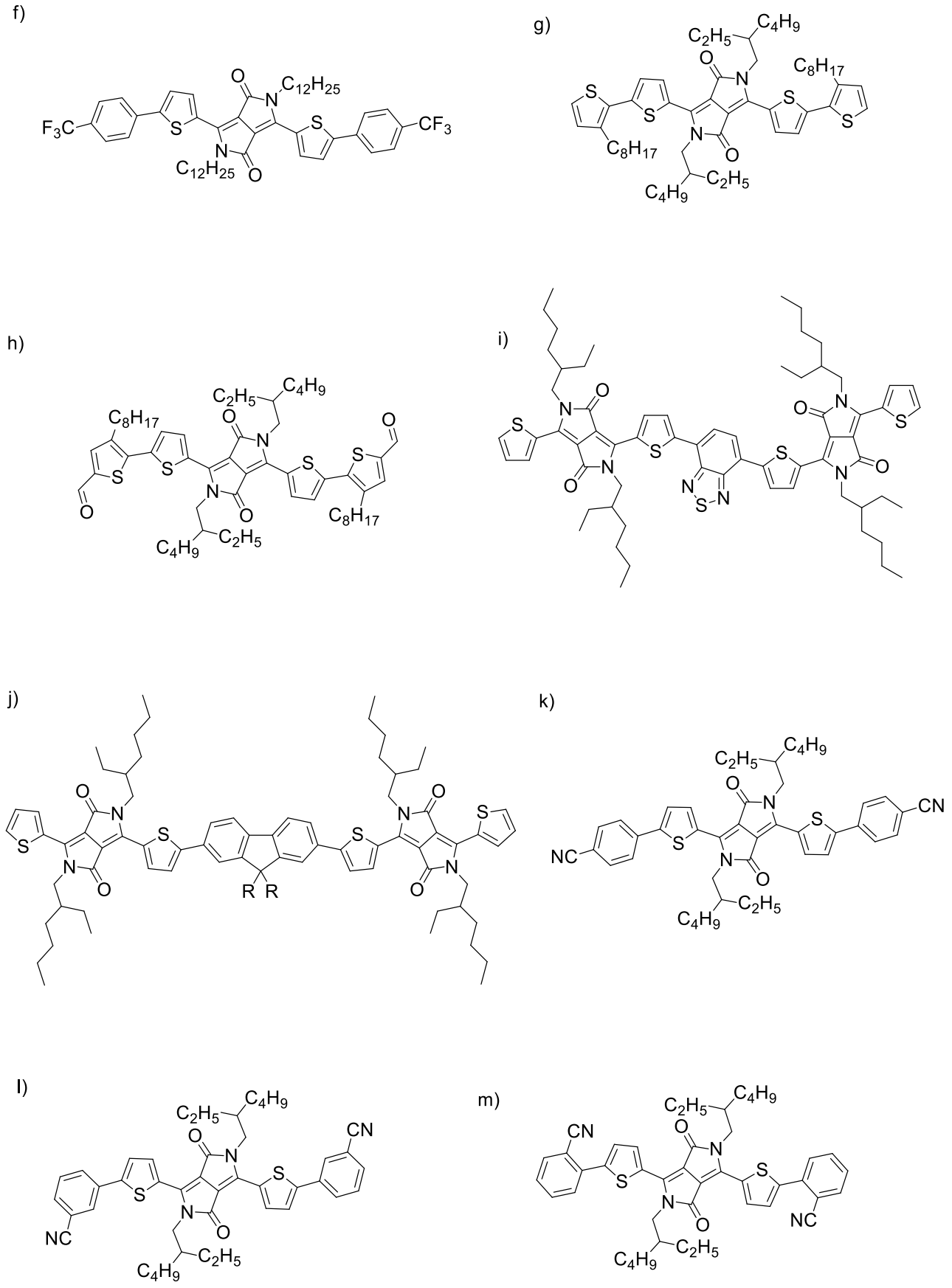


**Figure 1.11.** Chemical structures of non-fullerene acceptors.

## 1.7 Aims

Given the advantageous properties of the diketopyrrolopyrrole (DPP) unit the key aims of the thesis were to: use bisthienyl-diketopyrrolopyrrole DPP(Th)$_2$ as the basic building block for new non-polymeric materials for OPV. Incorporate electron affinity groups at the distal end of DPP(Th)$_2$ unit and investigate the effect on the electron affinity and ionisation potential, absorptivity, charge transport and physical properties. Measure the performance of the new materials on an OPV device to gain insight into the structure property relationship.

# Chapter 2 – Synthesis of non-polymeric bisthienyl-DPP based materials with fluorenone or benzothiadiazole end groups

## 2.1 Introduction

This chapter details the synthetic procedures and purification techniques used in preparing a series of targets based on the bisthienyl-diketopyrrolopyrrole unit [DPP(Th)$_2$], see Figure 2.1. (below). Diketopyrrolopyrrole (DPP) has a thiophene ring attached at 3 and 6 positions of the DPP core unit. The DPP core-bisthiophene has a narrow optical gap and broad absorption in the visible region. It was decided to attach the electron affinity fluorenone (Fl) or benzothiadiazole (Bt) moieties onto the 5-positions of thiophenes. It was anticipated that this would lead to materials with narrower optical gap with an absorption onset wavelengths longer than above 700 nm where PC70BM at the best, has a low optical density. The materials were then investigated as Channel I materials. Fluorenone has been previously used as an electron affinity unit in conjunction with thiophene in non-polymeric materials, with the compound showing good charge-carrier mobilities in OFETs[101]. In OPVs, materials compressed of fluorenone coupled with an oligothiophene gave a PCE of 1.2%[102]. The rationale for using benzothiadiazole at the distal ends of the DPP(Th)$_2$ unit is that it has been widely used as an electron acceptor in both non-polymeric compounds and π-conjugated polymers[103].

Based on this, the first target was prepared with 2-ethylhexyl (solubilizing groups) attached at the nitrogen position of the DPP(Th)$_2$, with fluorenones connected to the 5-positions of both thiophenes using Suzuki-Miyaura cross-coupling conditions (**EhDPP(ThFl)$_2$** (**2.1**) see Figure 2.1). However, the **EhDPP(ThFl)$_2$** lacked sufficient solubility in organic solvents commonly used to prepare devices, and hence a second target (**OddDPP(ThFl)$_2$** (**2.2**) see Figure 2.1) that contained the longer alkyl solubilizing group, 2-octyldodecyl, was prepared to ensure sufficient solubilities. The final target (**OddDPP(ThBt)$_2$** (**2.3**) see Figure 2.1) contained two 2-octyldodecyl solubilizing groups and benzothiadiazoles as the end groups and was prepared *via* direct arylation with a Pd-catalysis.

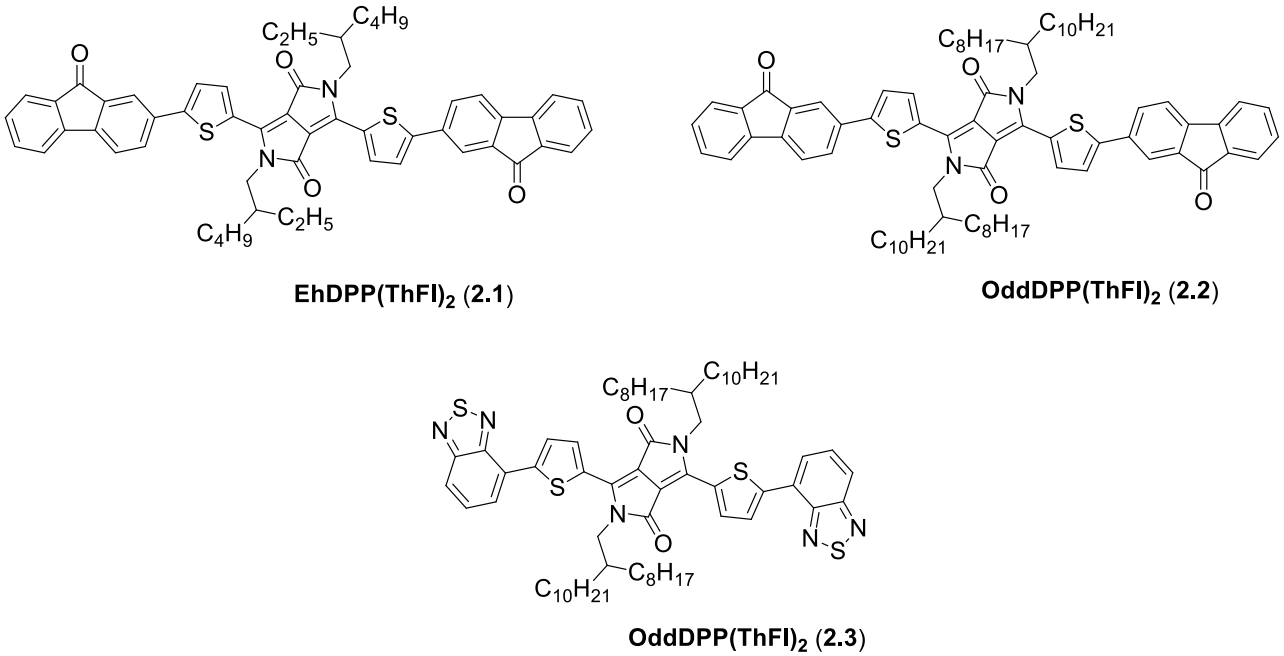


**Figure 2.1.** Chemical structure of **EhDPP(ThFl)$_2$ (2.1), OddDPP(ThFl)$_2$ (2.2)** and **OddDPP(ThBt)$_2$ (2.3).**

## 2.2 Synthesis of EhDPP(ThFl)$_2$

### 2.2.1 Synthesis of DPP(Th)$_2$ with 2-ethylhexyl solubilising groups

Among the different synthetic routes to the DPP moiety[104-108], the most commonly employed method uses aromatic nitriles with a succinic ester in the presence of a strong base[104, 109] and this was selected for the synthesis of the series, of the compounds described in this thesis. The first step in the synthesis of DPP core with two thiophenes attached was therefore the formation of the 2-cyanothiophene **2.6**, and two routes were investigated (Scheme 2.1).

The first route used the Rosenmund-von Braun reaction, wherein 2-bromothiophene **2.4** was treated with an excess of copper(I) cyanide in *N*-methyl-2-pyrrolidone at 135 °C to give **2.6** in 52% yield. In the second route, 2-thiophenecarboxyaldehyde **2.5** was converted to the corresponding aldoxime using hydroxylamine hydrochloride and triethylamine followed by rapid dehydration of the aldoxime intermediate using oxalyl chloride[110] to give **2.6** in a 66% yield. The advantage of the latter route is that it avoids the use of copper(I) cyanide, which is highly toxic to the environment and extra consideration must be given to its disposal.

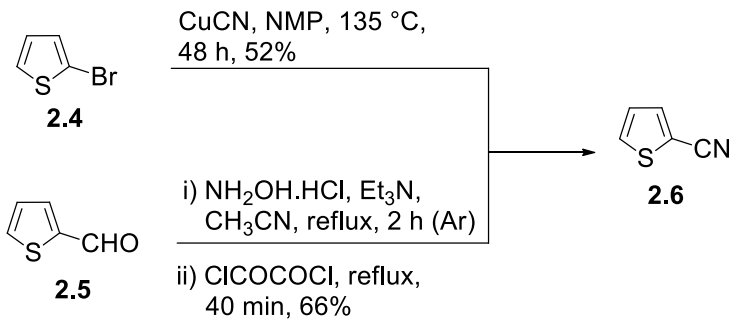


**Scheme 2.1.** Synthetic scheme to **2.6**.

Di-*iso*–propylsuccinate was prepared from readily available succinic acid **2.7**. **2.7** was converted to the corresponding di-*iso*-propylester **2.8** by in situ formation of the acid chloride[110] to give **2.8** in a 93% yield (Scheme 2.2).

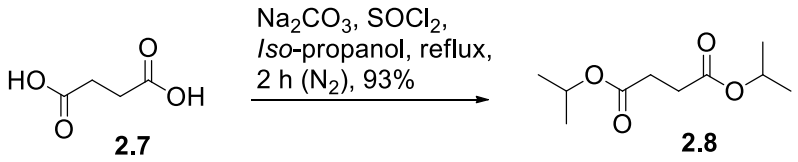


**Scheme 2.2.** Synthetic scheme to **2.8**.

The next step in the synthesis was the preparation of the DPP core with two thiophenes attached (**DPP(Th)$_2$**). A review of the literature revealed two different bases but same process were commonly employed to prepare **DPP(Th)$_2$**: where **2.6** and **2.8** were added sequentially at ≈50 °C and 100 °C, respectively, to a solution of base (potassium *tert*-butoxide in *tert*-amyl alcohol[71] or sodium *tert*-amyloxide[111]). Potassium *tert*-butoxide was first investigated as the base as it requires less precaution while handling compared to sodium metal. However, the absence of any bright colours in the final reaction mixture indicated that no product was formed (the product is highly coloured).

Therefore, sodium *tert*-amyloxide was used (the second route). The sodium *tert*-amyloxide was freshly prepared by adding sodium in *tert*-amyl alcohol and heating at reflux (b.pt of *t*-amyl alcohol = 102 $^{o}$C) for 17 h. **2.6** and **2.8** were added to this solution sequentially at ≈60 °C and 100 °C, respectively. During the addition of **2.8**, the reaction mixture turned dark purple and after a few hours of reacting at 100 $^{o}$C the solution became black. After cooling to room temperature, the reaction mixture was filtered, but no product was obtained. Adding a catalytic amount of iron(II)

chloride led to the desired **DPP(Th)$_2$** (**2.9**), but the yield was low (15%), compared to previously reported yields in literature which were above 60%[7] under similar reaction conditions. To achieve a better yield, the number of sodium equivalents (w.r.t succinic ester), and the addition rate of **2.8** was varied. As the sodium equivalents (w.r.t succinic ester) increased from 2.1 to 5, yields of ≈15-81 % of **DPP(Th)$_2$** were obtained. The highest yield (81%) was obtained with 5 equivalents (w.r.t succinic ester) of sodium metal and the slow addition of **2.8** over a 5 h period (Scheme 2.3). Thereafter, for the subsequent syntheses of **DPP(Th)$_2$**, sodium *tert*-amyloxide was prepared using catalytic amount of iron(II) chloride for sodium dissolution and 5 equivalents of sodium was used.

The basic bisthienyl-diketopyrrolopyrrole (**DPP(Th)$_2$**) was insoluble in organic solvents such as dichloromethane, tetrahydrofuran, toluene. However, it was sufficiently soluble in *N*,*N*-dimethylformamide, and this was the solvent of choice for the *N*-alkylations. Potassium carbonate was chosen as the base and 2-ethylhexyl alkyl chains were used as these have been widely used in organic semiconductors[57] and in non-polymeric DPP(Th)$_2$ based materials as solubilizing groups[32] (especially useful for solution processing; i.e., as it provides good solubility in solvents used for preparing OPV devices). The reaction to prepare **EhDPP(Th)$_2$** (Scheme 2.3) was carried out by treating **DPP(Th)$_2$** with 2-ethylhexyl bromide and using potassium carbonate as base in *N*,*N*-dimethylformamide at 80 °C for 13 h, and the desired product was obtained in a 44% yield. In order to investigate the effect of reaction temperature on yield, the reaction was also carried out at 140 °C under similar reaction conditions for 17 h. However, under these conditions a low yield of 14% was obtained. This is likely due to O-alkylation, which has been reported to occur[112]. Aprotic polar solvents generally favour substitution at the hard centre (O-alkylation), and that by choosing a protic solvent it can be minimized. However, due to insolubility of **DPP(Th)$_2$** in polar protic solvents the reaction could not be used to improve the *N*-alkylation.

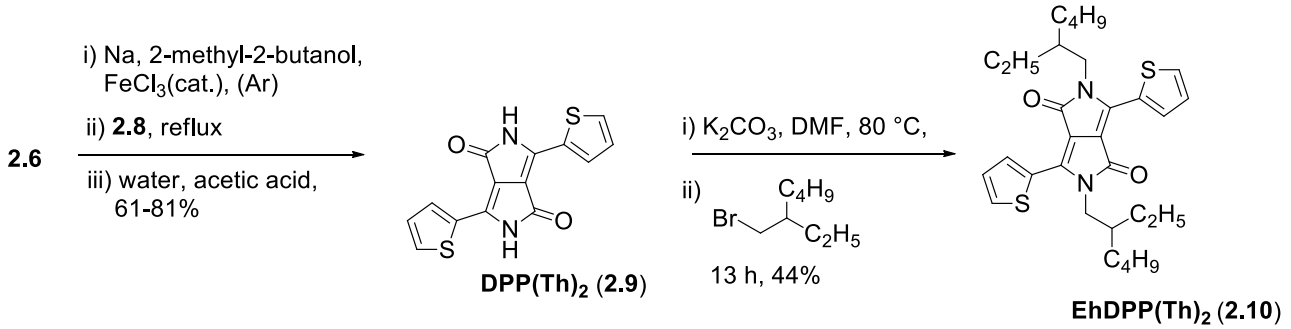


**Scheme 2.3.** Synthetic scheme to **DPP(Th)$_2$** (**2.9**) and **EhDPP(Th)$_2$** (**2.10**).

### 2.2.2 Synthesis and purification of EhDPP(ThFl)$_2$

The final step before the fluorenones could be attached to the **DPP(Th)$_2$** core unit was the regioselective bromination of the thiophene units. This was achieved using *N*-bromosuccinimide (NBS) in chloroform in the dark, and gave selective bromination of **EhDPP(Th)$_2$** at 5-position of both the thiophene units in an overall yield of 79% (Scheme 2.4).

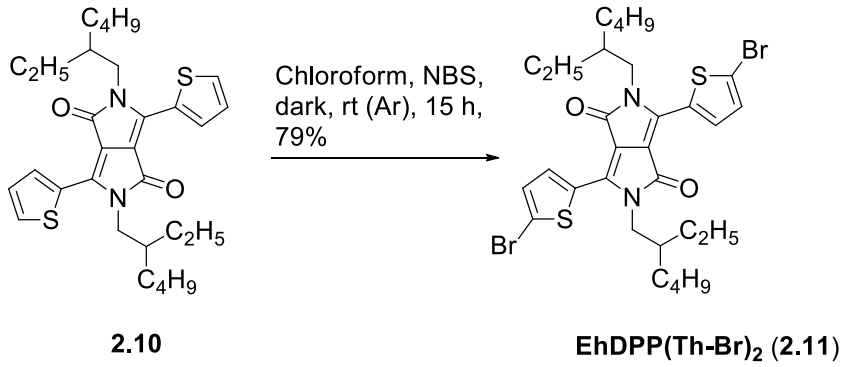


**2.10** **EhDPP(Th-Br)$_2$ (2.11)**

**Scheme 2.4.** Synthetic scheme to **EhDPP(Th-Br)$_2$** (**2.11**).

With the DPP-bithiophene unit in hand the next step in the synthesis was the formation of the fluorenone boronate ester ready for coupling. The conversion of 2-bromofluorene **2.12** to fluorenone **2.13** is an oxidation reaction, and so potassium permanganate was first tried as the oxidizing agent with potassium hydroxide as the base. However, the yield was only moderate (48%). Increasing the number of equivalents of potassium permanganate did not increase the yield further and after a number of experiments using different base concentrations and oxidizing agents, it was found that simply adding 10 M concentrated solution of sodium hydroxide in air was all that was needed to form the fluorenone in a **2.13** in 92% yield (Scheme 2.5).

Conversion of **2.13** to the boronic ester **2.14** was first attempted using [1,1'-bis-(diphenylphosphino)ferrocene]dichloropalladium(II) $PdCl_2$(dppf) as the catalyst and bis(pinacolato)diboron in *N*,*N*-dimethylformamide. The removal of trace *N*,*N*-dimethylformamide was problematic using Buchi vacuum, but the addition of diethyl ether enabled precipitation of the desired crude product. The solid residue could be collected, which was then purified using column chromatography to give **2.14** in a 45% yield (Scheme 2.5). The low yield was in part due to the boronic ester getting adsorbed onto the silica and it could not be totally eluted even with ethyl acetate. However, it was subsequently found that if the reaction was carried out in 1,4-dioxane,

which could be completely removed at the end of the reaction, the product could be purified simply by recrystallisation from ethanol to give a 60% yield (Scheme 2.5).

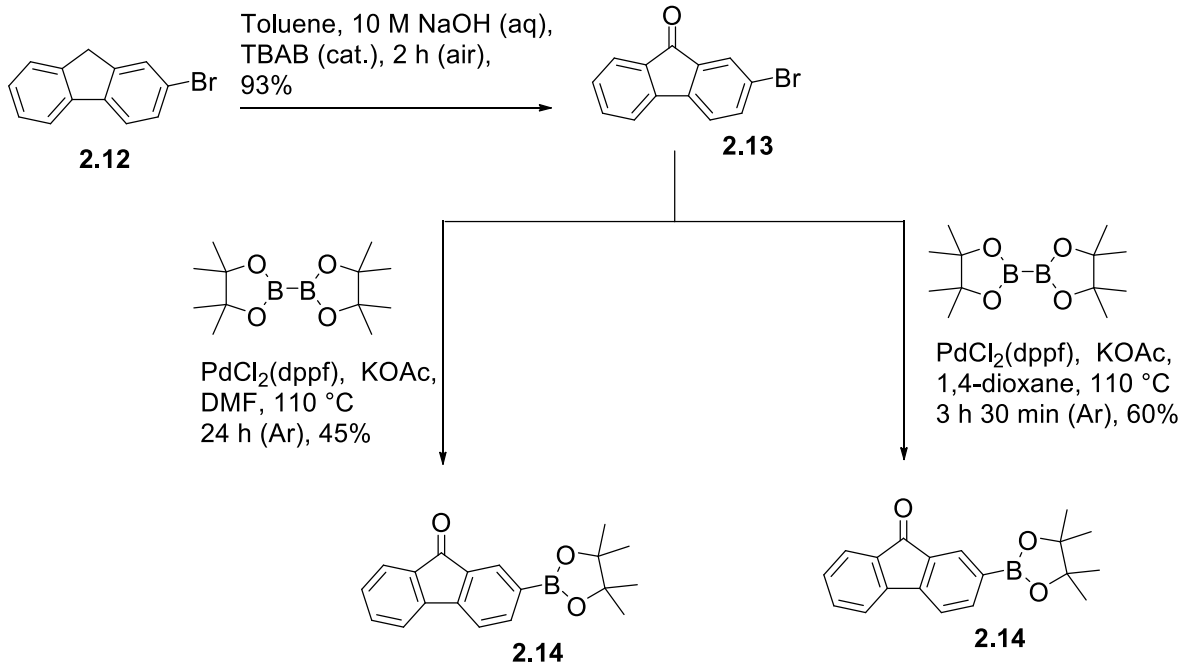


**Scheme 2.5.** Synthetic scheme to **2.14**.

The target molecule **EhDPP(ThFl)$_2$** was finally synthesized by using a standard Suzuki coupling reaction (Scheme 2.6). **EhDPP(Th)$_2$** was reacted with **2.14** in tetrahydrofuran and aqueous potassium carbonate (base). The mixture was deoxygenated by sparging with argon, before the tetrakis(triphenylphosphino)palladium(0) catalyst was added to the mixture which was sparged again before being heated to reflux. However, it was found that the product had poor solubility in most organic solvents, with the exception of chlorinated solvents (dichloromethane and chloroform), in which it was partially soluble. Purification of the desired product was first attempted using column chromatography over silica with dichloromethane and light petroleum (4:1) as eluent, with the column flushed with chloroform to completely elute the product and all the possible side-products. However, no pure product was obtained. Purification by recrystallization was attempted with a range of different solvents and solvent mixtures (dichloromethane/toluene, chloroform/light petroleum, and *N*,*N*-dimethylformamide). However, again the product could not be completely purified. Sublimation (230 °C, 1.6 mbar) did not remove the impurities either. An interesting (and potentially useful) observation that occurred during collecting the $^1$H NMR was that neat deuterated toluene dissolved the impurity and not the product. However, recrystallization from neat toluene was unsuccessful (see Fig. 2.2a, arrows showing unknown impurity peaks). The

desired product was eventually obtained pure via Soxhlet extraction (Figure 2.2b) in a 10% yield. The reaction was then repeated on a larger scale and purification carried out by chromatography followed by Soxhlet extraction with toluene to afford **EhDPP(ThFl)$_2$** in a 37% yield. It is important to note that the purity of the materials is crucial for optimal device performance for all class of organic semiconductors[47].

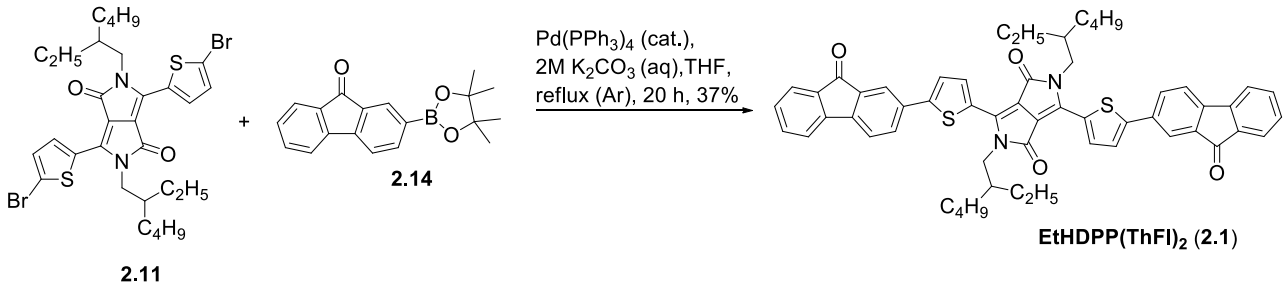


**Scheme 2.6.** Synthetic scheme to **EhDPP(ThFl)$_2$** (**2.1**).

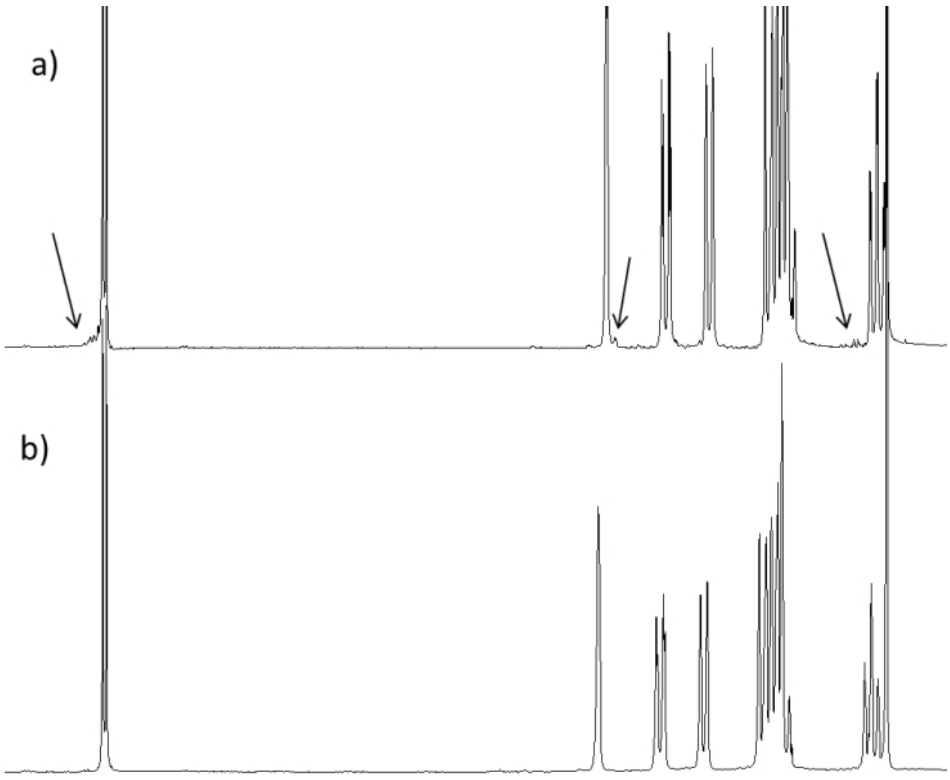


**Figure 2.2** a) $^1$H NMR of filtrate from toluene recrystallization of **EhDPP(ThFl)$_2$** b) $^1$H NMR after soxhlet extraction of **EhDPP(ThFl)$_2$**.

## 2.3 Synthesis of OddDPP(ThFl)$_2$ and OddDPP(ThBt)$_2$

### 2.3.1 Synthesis of DPP(Th)$_2$ with 2-octyldodecyl solubilising group

As **EhDPP(ThFl)$_2$** has poor solubility in organic solvents it was expected that, when solution processed the quality of the film formed would be poor for OPV devices. So to overcome the solubility issue, the longer branched alkyl chain 2-octyldodecyl was chosen. However, 2-octyldodecylbromide **2.16** was not commercially available and hence 2-octyldodecan-1-ol **2.15** was converted to the bromide **2.16** using a literature procedure[113]. **2.15** was converted to **2.16** using NBS and triphenyl phosphine in dichloromethane in an 84% yield (Scheme 2.7).

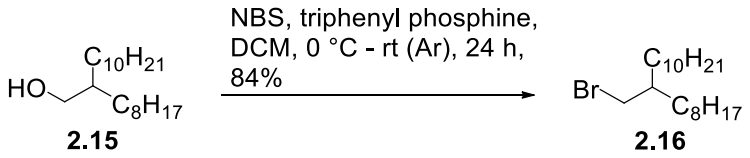


**2.15** **2.16**

**Scheme 2.7.** Synthetic scheme to **2.16**.

The *N*-alkylation of **DPP(Th)$_2$** with 2-octyldodecylbromide **2.16** was first carried out under similar reaction conditions used for preparation of **EhDPP(Th)$_2$** (see Table 2.1 reactions 1). However, low yields (18-20%) led to an investigation into optimizing the reaction conditions. Two different synthetic procedures were found for the preparation of **OddDPP(Th)$_2$**, one using potassium carbonate as base in DMF at 130 °C[114] and another using cesium carbonate as base and 2-octyldodecyl iodide as alkylating agent at 140 °C[58]. However, from the preparation of **EhDPP(Th)$_2$** it was observed that a higher reaction temperature (140 °C) led to lower *N*-alkylated product (see section 2.2.1). A test reaction was carried out using cesium carbonate as base in *N*,*N*-dimethylformamide at 80 °C with **2.16**, but, the yield was ~ 5% less than the reaction carried out using potassium carbonate as base (see Table 2.1 reactions 2).

A literature review showed that *N*-alkylation of heterocyclic compounds like pyrrole and indole are usually obtained in high yield when treated with an appropriate base and phase transfer catalyst followed by the reaction of the resulting salt with an alkylating agent.[115] 18-Crown-6 was chosen as the phase transfer catalyst as crown-complexed potassium ion is loosely associated with a 'soft' centre (nitrogen) compared to a 'hard' centre (oxygen), which will facilitate alkylation at

nitrogen position. The *N*-alkylation was then carried out using potassium carbonate as base and 18-Crown-6 in DMF at 80 °C and the yield improved to 30-34%. With sufficient material in hand **OddDPP(Th)$_2$** was then converted to the bromo derivative, **OddDPP(Th-Br)$_2$** regioselectively using *N*-bromosuccinimide (NBS) in chloroform under dark to give in a 82% yield (Scheme 2.8).

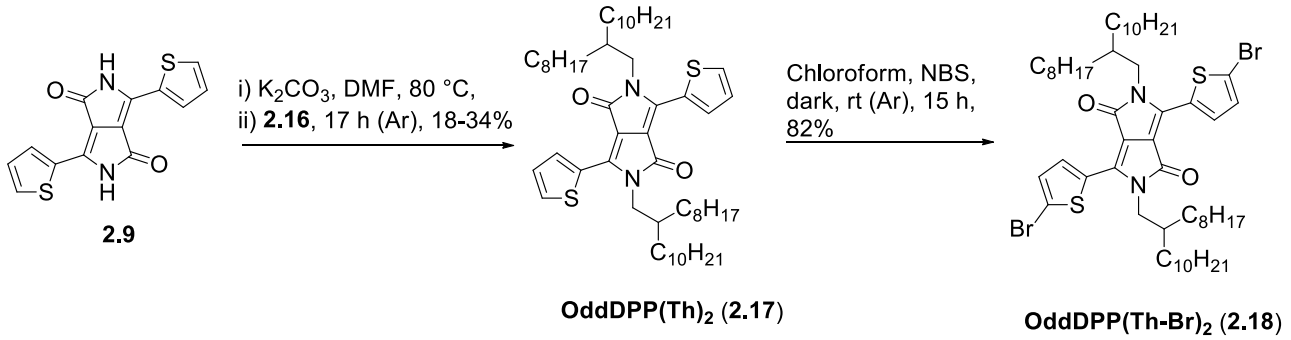


**Scheme 2.8.** Synthetic scheme to **OddDPP(Th)$_2$** (**2.17**), and **OddDP(Th-Br)$_2$** (**2.18**).

| Reactions | Alkylating agent | Base | Solvent | Phase Transfer Catalyst | Temp. | Time | yield |
|---|---|---|---|---|---|---|---|
| 1 | 2.10 | $K_2CO_3$ | DMF[a] | - | 80 °C | 13-17 h | 18-20% |
| 2 | 2.10 | $Cs_2CO_3$ | DMF[a] | - | 80 °C | 17 h | 15% |
| 3 | 2.10 | $K_2CO_3$ | DMF[a] | 18-crown-6 | 80 °C | 17 h | 30-34% |

[a] *N*,*N*-dimethylformamide

**Table 2.1.** Investigation of *N*-alkylation reaction conditions with 2-octyldodecylbromide.

### 2.3.2 Synthesis and purification of OddDPP(ThFl)$_2$ and OddDPP(ThBt)$_2$

**OddDPP(ThFl)$_2$** was synthesised by reacting **OddDPP(Th-Br)$_2$** with **2.14** under standard Suzuki-Miyuara cross coupling conditions (Scheme 2.9). The residue obtained after reaction showed better solubility in dichloromethane and chloroform in comparison to **EhDPP(ThFl)$_2$** and was purified by column chromatography followed by recrystallisation from toluene to give **OddDPP(ThFl)$_2$** in a 54% yield.

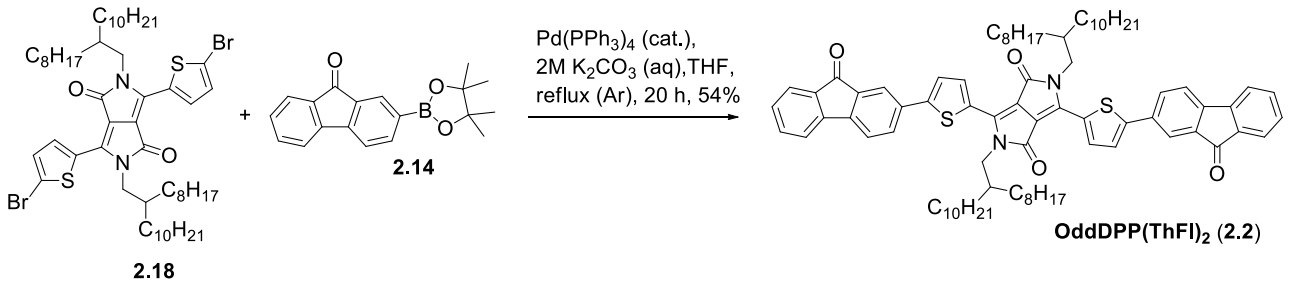


**Scheme 2.9.** Synthetic scheme to **OddDPP(ThFl)$_2$** (**2.2**).

The final target of this series involved attaching 2,1,3-benzothiadiazole **2.19** to form **OddDPP(Th)$_2$**. As the previous targets were successfully prepared under Suzuki-Miyuara cross coupling conditions, a similar synthetic route was first considered which required the synthesis of boronic ester of the benzothiadiazole moiety **2.20** (Scheme 2.10).

In order to get to the precursor **2.20**, **2.21** was first converted to the mono-brominated derivative with bromine and hydrobromic acid (37%) and purified by recrystallisation from methanol to give **2.20** in a 62% yield. It was observed that slow addition (5h) of bromine was crucial in obtaining **2.20** in a moderate yield. The synthesis of boronic ester derivative of **2.20** was then investigated under standard Miyuara cross coupling conditions using bis(pinacolato)diboron and potassium acetate as base in 1,4-dioxane with [1,1'-bis(diphenylphosphino)ferrocene]dichloropalladium(II) as the catalyst. The reaction mixture was heated at 110 °C (oil bath temperature) and after 22 h, no starting material was found (monitored by TLC). The purification of the crude (pink colour oil) was carried out by adding diethyl ether which initiated precipitation and the solid obtained was recrystallized from ethanol. However, the solid obtained was not pure and from the $^1$H NMR it was observed that unreacted boronate ester (impurity) was still present. Purification using column chromatography was not attempted as it was observed before that boronate esters tend to adsorb on to silica and the product would not be eluted completely (see section 2.2.2). With only 27 mg in hand a test reaction was carried out with **EhDPP(Th-Br)$_2$** under standard Suzuki reaction conditions (Scheme 2.10). However, the reaction failed to provide any of the target molecule (**2.22**). The $^1$H NMR experiment of the fraction collected from the column showed no peaks related to the target product. It should be noted that for this test reaction **DPP(Th)$_2$** with 2-ethylhexyl solubilising groups was used. However, the subsequent reactions were carried out with **DPP(Th)$_2$** unit having 2-octyldodecyl as the solubilising groups.

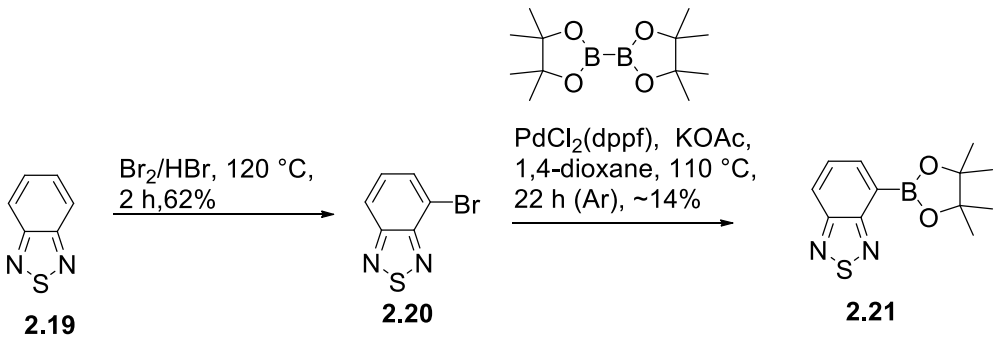


**Scheme 2.10.** Synthetic scheme to **2.20** and **2.21**.

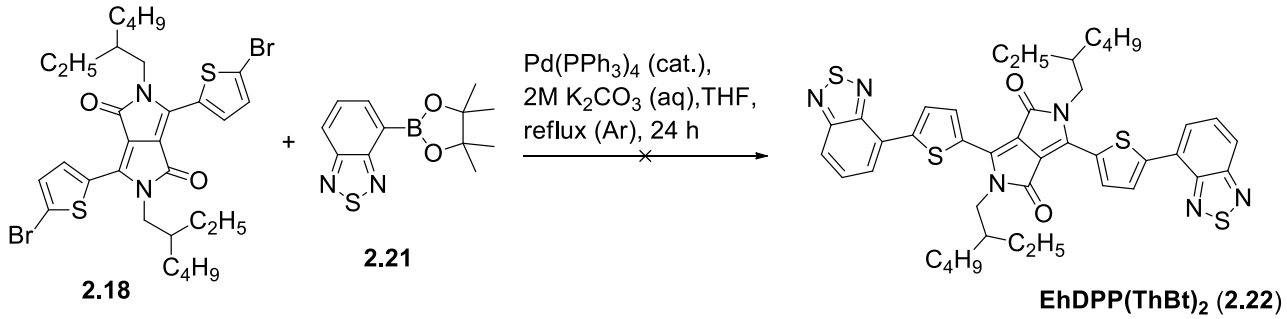


**Scheme 2.11.** Synthetic scheme to synthesis **EhDPP(ThBt)$_2$** (**2.22**).

A survey of the literatures showed that the most commonly employed methods for attachment of aromatic rings onto **DPP(Th)$_2$** was through palladium catalysed Suzuki-Miyaura[35], Stille[116] or Negishi[76] cross-coupling reactions, which require synthesis of the respective aryl boronic acids, tin or zinc precursors from their aryl halides. However, more recently metal catalysed direct arylation has been reported as a promising approach for synthesis of DPP(Th)$_2$ derivatives.

### 2.3.3 Direct arylation reaction by C-H activation of thiophene

In general direct arylation reaction involves activation of a carbon-hydrogen bond followed by subsequent formation of carbon-carbon bond (C-H functionalization). A typical C-H activated arylation conditions of simple arenes unit utilises palladium acetate as catalyst and pivalic acid as co-catalyst with an inorganic base (potassium carbonate, potassium acetate and cesium carbonate) in polar aprotic solvents such as *N*,*N*-dimethylacetamide (DMA), *N*,*N*-dimethylformaldehyde (DMF) and *N*,*N*-dimethylsulphoxide (DMSO)[117]. Marc Lafrance *et al.* reported that pivalate anion formed during the reaction is a key component in C-H bond cleaving and acts as a catalytic proton shuttle from arenes to the base. More recently Shi-Yong Liu *et al*. showed that for DPP(Th)$_2$ direct

arylation reactions, addition of pivalic acid increases the reaction rate by six times and can lead to high yields[118]. The advantages of using direct arylation reactions in comparison with cross coupling reactions are (i) fewer synthetic steps, as it is not necessary to prepare organometallic intermediates, (ii) faster rate of reaction, and (iii) comparable to better overall yield[117, 118].

With the **2.20** in hand and the first attempt to get to the target molecule under standard Suzuki conditions failed, a test reaction was first carried out with **OddDPP(Th)$_2$** and **2.20** using palladium acetate as catalyst, pivalic acid as co-catalyst, and potassium carbonate as base, in *N*,*N*-dimethylacetamide at 110 °C (oil bath temperature). It is important to note that the potassium carbonate was heated at 150 °C for 17 h under vacuum (~0.2 mbar), prior to use. After 30 min of stirring the reaction mixture at 110 °C, the colour changed from purple to blue and after 5 h, no starting material was observed (monitored by TLC). The reaction mixture was cooled to room temperature to give a dark blue residue. The residue was purified using column chromatography over silica using dichloromethane/light pet spirit (3:2) as eluent to afford **OddDPP(ThBt)$_2$** in a 31% yield. Later, a larger scale reaction (1.1 g) was carried out to give **OddDPP(ThBt)$_2$** in a 49% yield (Scheme 2.12). In the later reaction the stoichiometry of reactants remained the same, a significantly more concentrated solution was used, potentially explaining the improved yield.

The **OddDPP(ThBt)$_2$** was soluble in chlorinated solvents like chloroform, dichloromethane and in non-chlorinated solvents such as tetrahydrofuran. During this work on **OddDPP(ThBt)$_2$** Sonar et al., reported a similar molecule but with different alky chain 2-butyloctyl.[35] The reported molecule was prepared using standard Suzuki conditions which took 72 h for completion and gave a 87% yield. In comparison, it was obvious that under palladium catalysed direct arylation reaction conditions, the rate of reaction was fast. To investigate whether an increase in number of equivalents of **2.20** used (w.r.t **OddDPP(Th)$_2$**) could give a better yield, a reaction (152 mg scale) was carried out with 3.5 equivalents of **2.20**, however, there was only 2% increase in yield (33%) in comparison with the test reaction (31%).

Encouraged by the results and to investigate the feasibility of the reaction conditions with different aryl halides, a direct arylation reaction was carried out with **OddDPP(Th)$_2$** and 2.5 equivalents of fluorenone **2.13** (w.r.t to **OddDPP(Th)$_2$**). Unlike the Suzuki cross coupling reaction, the reaction went to completion in 4 h, and it was possible to isolate **OddDPP(ThFl)$_2$** in a 49% yield (Scheme 2.12). However, it has to be noted that the Suzuki reaction was carried out on a large scale compared to the direct arylation reaction and so the comparison must be taken with caution.

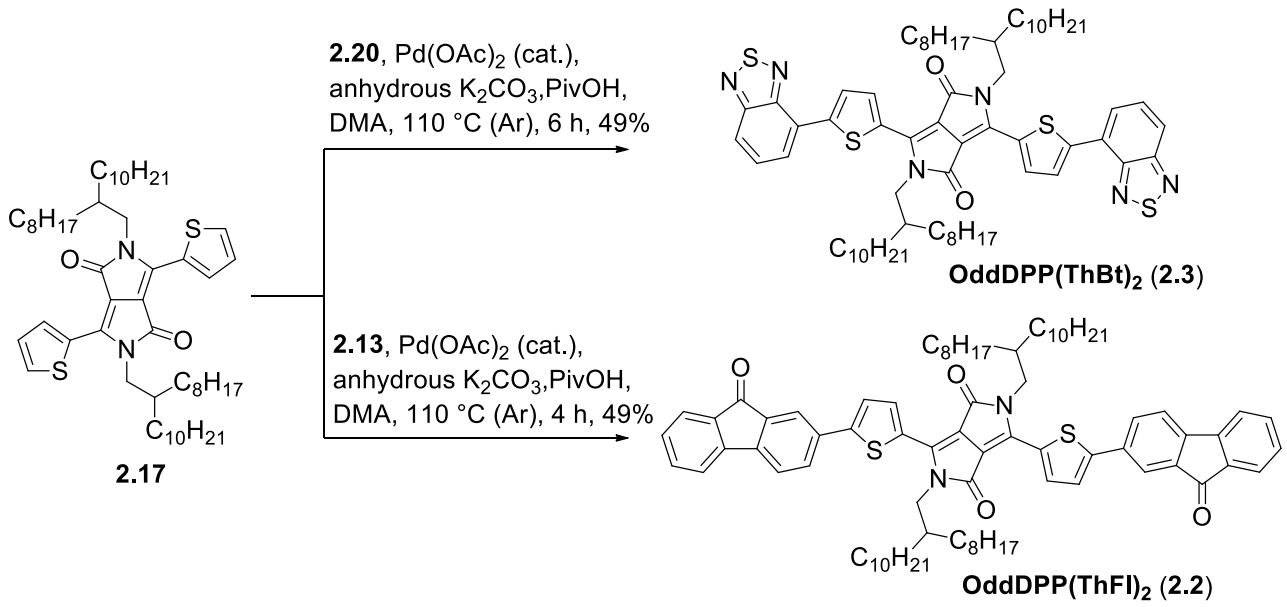


**Scheme 2.12.** Synthetic scheme to **OddDPP(ThBt)$_2$** (**2.3**) and **OddDPP(ThBt)$_2$** (**2.2**).

## 2.4 Conclusion

In this chapter, it has been shown that a better yield can be obtained for **DPP(Th)$_2$** preparation when 5 equivalents of sodium are used and catalytic amount of iron (II) chloride is used for sodium dissolution. By using the phase transfer catalyst 18-crown-6 for *N*-alkylation of the DPP(Th)$_2$ unit a better yield can be obtained. DPP(ThAr)$_2$ can be either prepared under Suzuki-Miyaura cross-coupling reaction conditions or by direct arylation of an aryl halide with DPP(Th)$_2$ in a moderate yield. The direct arylation reaction is a more convenient way to prepare DPP(ThAr)$_2$ as it does not require preparation of organometallic intermediates, which are toxic and labour intensive and add an extra step. The rate of the direct arylation reaction was found to be faster than for the Suzuki-Miyaura cross-coupling reactions. The solubility was poor when the 2-ethylhexyl moiety was used as the solubilising group for **DPP(ThFl)$_2$**. 2-Octyldodecyl solubilising groups gave better solubility in chlorinated solvents which are typically used in device fabrication.

The structure-property relationships and OPV device performance and OFETs device performance of these compounds are discussed in Chapter 3.

# Chapter 3 – Physical, charge transporting and photovoltaic properties of EhDPP(ThFl)$_2$, OddDPP(ThFl)$_2$ and OddDPP(ThBt)$_2$

# 3.1 Introduction

In this chapter the thermal, electrochemical and optoelectronic properties of the non-polymeric DPP(ThAr)$_2$s (Figure 3.1), which were introduced in the previous chapter are compared. The **EhDPP(ThFl)$_2$** that has 2-ethylhexyl solubilizing groups lacked sufficient solubility in most of the organic solvents for solution processing. Whereas, **OddDPP(ThFl)$_2$** and **OddDPP(ThBt)$_2$**, which have the longer 2-octyldodecyl solubilizing groups showed better solubility, hence, can be solution processed. The primary aim in this chapter is to investigate materials that are solution processable as Channel I (hole transporting) materials with PC70BM in bulk hetrojunction (BHJ) solar cells. However, for comparison the thermal, electrochemical, optoelectronic properties of **EhDPP(ThFl)$_2$** material was also investigated. A secondary aim was to investigate these materials as the active channel layer in OFETs. Hence, for OFETs, **EhDPP(ThFl)$_2$** was thermal evaporated, while **OddDPP(ThFl)$_2$** and **OddDPP(ThBt)$_2$** were solution processed from chloroform.

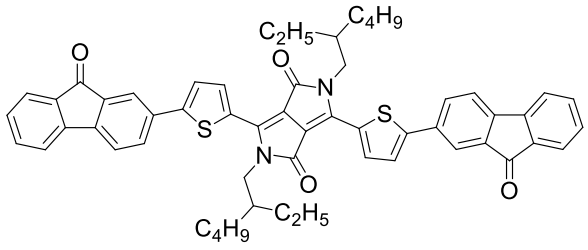

**EhDPP(ThFl)$_2$ (2.1)**

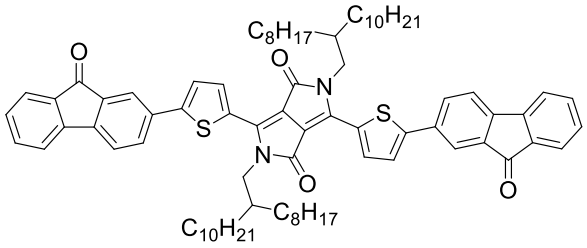

**OddDPP(ThFl)$_2$ (2.2)**

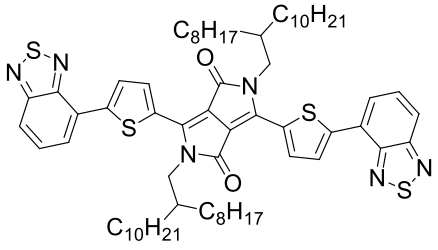

**OddDPP(ThBt)$_2$ (2.3)**

**Figure 3.1.** Chemical structures of **EhDPP(ThFl)$_2$ (2.1), OddDPP(ThFl)$_2$ (2.2)** and **OddDPP(ThBt)$_2$ (2.3)**

## 3.2 Physical properties

### 3.2.1 Thermal properties

Given the insolubility of the **EhDPP(ThFl)$_2$**, it could only be thermal evaporated to form a film capable of being used in a device. Hence, it was necessary to investigate the thermal stability to ensure it did not decompose during processing. It was also important to investigate the thermal stability of **OddDPP(ThFl)$_2$** and **OddDPP(ThBt)$_2$** to make sure they are stable enough to be used in OPV cells. In all three cases it was also important to understand whether they underwent any phase transition. The thermal stability to decomposition temperature ($T_d$ ) of the new DPP materials was investigated using Thermal Gravimetric Analysis (TGA). The DPP derivatives, irrespective of their different alkyl groups and end groups were thermally stable to high temperature. The materials exhibited a 5% weight loss occurred at 405, 399 and 404 °C, under nitrogen for **EhDPP(ThFl)$_2$**, **OddDPP(ThFl)$_2$** and **OddDPP(ThBt)$_2$** (see Figure 3.2), respectively. These results show that the three new DPPs exhibit good thermal stability, well above the operational conditions encountered in OFETs and OPV, indeed in the case of **EhDPP(ThFl)$_2$** during thermal evaporation.

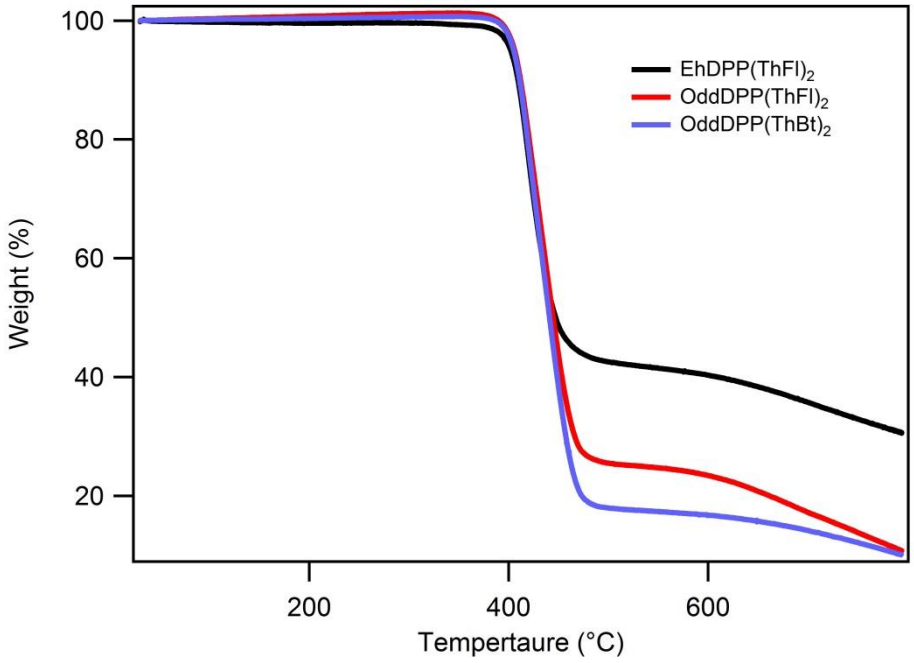


**Figure 3.2.** TGA traces for **EhDPP(ThFl)$_2$**, **OddDPP(ThFl)$_2$** and **OddDPP(ThBt)$_2$** heating at 10 $^{o}$C min$^{-1}$ under $N_2$.

Next, to understand whether the materials had any thermal transitions such as a glass transition temperature ($T_g$) or crystallisation temperature ($T_c$). Differential Scanning Calorimetry (DSC) was used. The melting point for **EhDPP(ThFl)$_2$**, was first measured and was observed to be 282-284 °C. The melting point was above the temperature range we could measure using the PerkinElmer Diamond DSC (280 °C) at Centre for Organic Photonics and Electronics (COPE). However, the STA 6000 simultaneous thermal analyzer records both TGA (Weight loss *versus* temperature) and DSC (heat flow *versus* temperature) and has a temperature range from 15°C to 1000 °C. The **EhDPP(ThFl)$_2$** sample was heated and cooled from 30 °C to 320 °C at a scan rate of 10 °C min$^{-1}$ (see Figure 3.3). The first heating scan exhibited a $T_g$ at 233 °C and a broad endothermic transition around 280 °C corresponding to the melting point. A closer look at the melting point peak revealed that there are two melts occurring simultaneously. A small difference in the melts could be seen, with the distinct first melt observed at 286 °C. The slow cooling rate allowed the transition from the melt to crystals, with two different crystallisation temperatures (225 °C and 249 °C) observed. The two distinct crystallisation process exhibited in the DSC scans suggest that the molecule can exist in two different polymorphs in the solid state with similar melting points. The second heating and cooling scans was identical to the first scans. During thermal evaporated it is not clear as to whether **EhDPP(ThFl)$_2$** would form an amorphous film. However, if it did then it would require heating above the melt to instigate a crystallisation process, which is not practical.

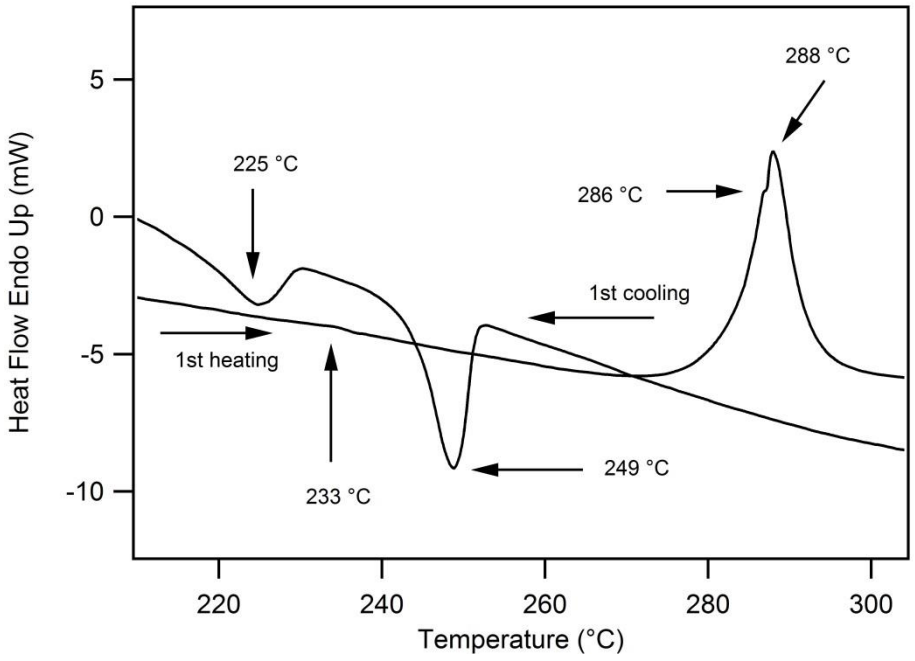


**Figure 3.3.** DSC traces for **EhDPP(ThFl)$_2$** at 10 $^{o}$C min$^{-1}$.

The melting point for **OddDPP(ThFl)$_2$**, was observed at 238-240 °C and hence the thermal transition studies were investigated using the PerkinElmer Diamond DSC. A similar trend in the thermal transitions were exhibited for the **OddDPP(ThFl)$_2$** sample at a scan rate of 10 °C min$^{-1}$ (see Figure 3.4). During the first heating no $T_g$ was observed although there were two melting point. However, the different melting points (241 °C and 263 °C) of the crystals (recrystallized from toluene) was quite obvious for **OddDPP(ThFl)$_2$** sample, unlike the **EhDPP(ThFl)$_2$**. On cooling crystallisation was observed at 229 °C with a small feature at 114 °C. During the second heating cycle the first thermal transition corresponding to melting was observed at 118 °C with the second at 241 °C. The melt at 118 °C corresponds to the $T_c$ at 114 °C (1$^{st}$ cooling scan). It is clear that **OddDPP(ThFl)$_2$** has propensity to crystallise, and this needs to be kept in mind when preparing devices. It is important to control the crystallinity in the active layers and in the case of OPV devices to bring about ideal phase separation for maximum charge extraction. The third heating and cooling scan was identical to the second scan.

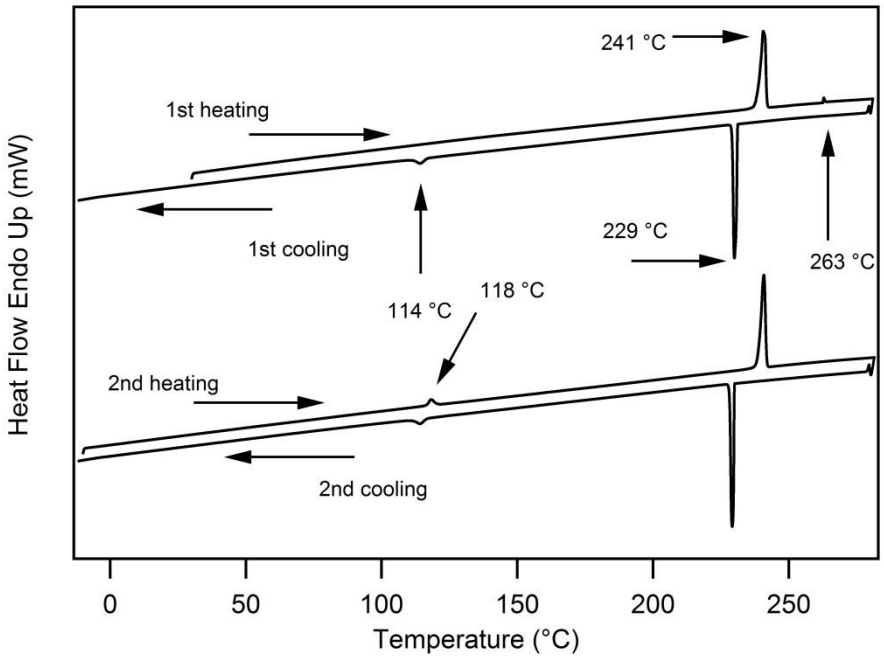


**Figure 3.4.** DSC traces for **OddDPP(ThFl)$_2$** at 10 $^{o}$C min$^{-1}$.

The **OddDPP(ThBt)$_2$** sample exhibited a weak thermal transition around 70 $^{o}$C at a scan rate of 10 $^{o}$C min$^{-1}$ (see Figure 3.5a). However, it was not obvious whether it corresponded to a $T_g$ as the scan rate was low. $T_g$s are often more easily observed at faster heating rates. Hence, the sample was heated at a scan rate of 200 $^{o}$C min$^{-1}$ and a clear $T_g$ was observed at 91 °C (see Figure 3.5b). At a scan rate of 10 $^{o}$C min$^{-1}$, the melting transition was observed at 139 °C and an exothermic transition

corresponding to crystallisation process was observed at 124 °C, during cooling cycle (see Figure 3.5a). The second heating and cooling exhibited identical transactions at a scan rate of 10 $^{o}$C min$^{-1}$. Interestingly, this material exhibited only one crystalline process, unlike the other two materials which exhibited polymorphs.

The thermal transitions observed for each of the DPP derivatives in this series are at an accessible temperature (around 100 to 250 °C) allowing annealing techniques to be employed to optimize the film structure.

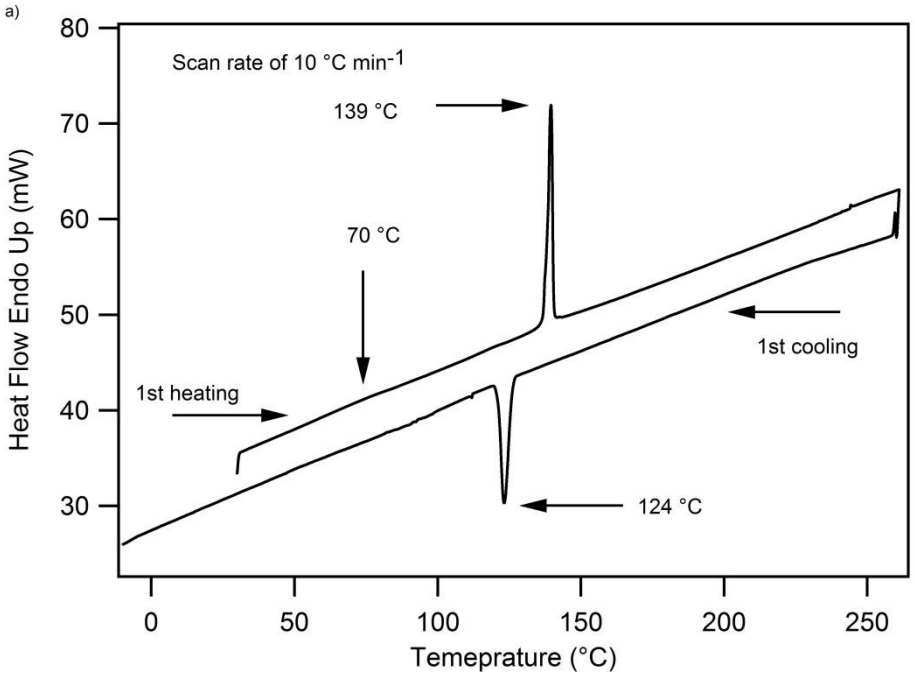

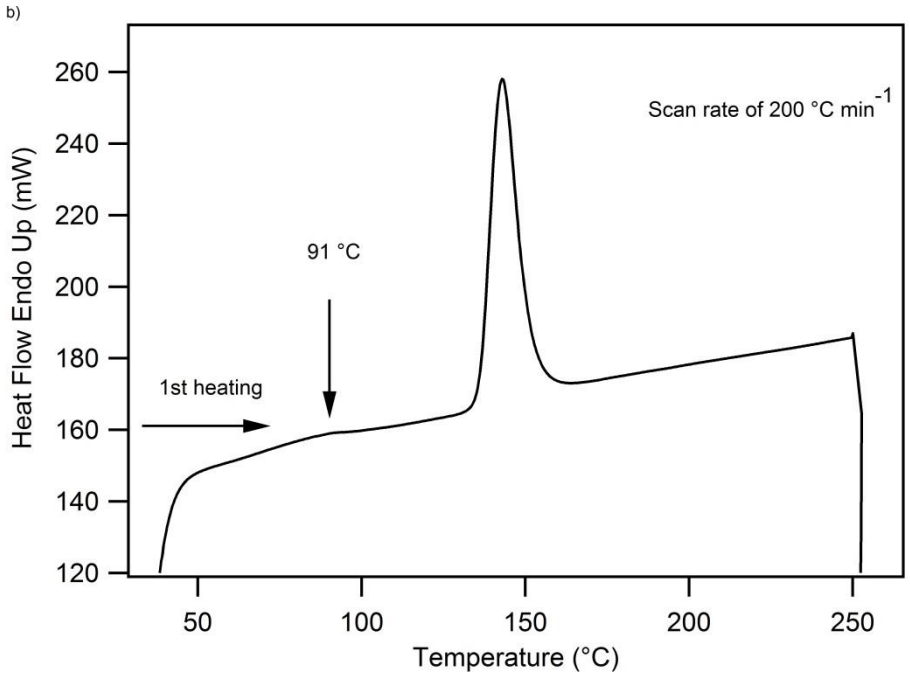


**Figure 3.5.** DSC traces for **OddDPP(ThBt)$_2$** at a) 10 $^{o}$C min$^{-1}$and b) 200 $^{o}$C min$^{-1}$.

| Material | $T_d$ (°C) | $T_g$ (°C) | $T_m$ (°C) | $T_c$ (°C) |
|---|---|---|---|---|
| **EhDPP(ThFl)$_2$** | 405 | 233 | 286, 288 | 225, 249 |
| **OddDPP(ThFl)$_2$** | 399 | - | 241, 263 (1$^{st}$ heating)<br>118, 241(2$^{nd}$ heating) | 229, 114 |
| **OddDPP(ThBt)$_2$** | 404 | 91 | 139 | 124 |

**Table 3.1.** Summary of the results from TGA and DSC measurements.

### 3.2.2 Optical properties

The optical properties of the DPPs were investigated in solution and thin film using UV-vis absorption spectroscopy (see figure 3.6). The longest wavelength absorption for **EhDPP(ThFl)$_2$** and **OddDPP(ThFl)$_2$** exhibited maxima at 581 nm and 617 nm in dichloromethane with molar absorptivity of 53 000 M$^{-1}$ cm$^{-1}$, 52 000 M$^{-1}$ cm$^{-1}$, and 49 000 M$^{-1}$ cm$^{-1}$, 48 000 M$^{-1}$ cm$^{-1}$, respectively. However, the longest wavelength absorption for **OddDPP(ThBt)$_2$**, with the

benzothiadiazole end group exhibited maxima at 597 nm and 636 nm with molar absorptivity of 49 000 $M^{-1}$ $cm^{-1}$ and 43 000 $M^{-1}$ $cm^{-1}$, respectively. In the literature it is proposed that the absorption at wavelengths longer than 600 nm being characteristic of intramolecular charge transfer (ICT) transitions of **DPP(Th)$_2$** with dual-band vibronic features[119]. The bands in the visible region of the spectrum (400−500 nm) arise from the aryl π-π* transitions localised on thiophenes, fluorenones, and benzothiadiazoles[35, 119, 120].

The thin film absorption was investigated next. A thin film of **EhDPP(ThFl)$_2$** was thermally evaporated on to a quartz substrate to give a 110 nm thin film. The **OddDPP(ThFl)$_2$**, and **OddDPP(ThBt)$_2$**, showed sufficient solubility in chloroform and formed a thin film (~ 90 nm) when spin-coated. All three DPP derivatives display significant red-shifts in their absorption particularly in the ICT bands. The shift of around 95 nm, could arise from the planarisation of the molecule in solid state or intermolecular interactions in the neat film. Compared to **EhDPP(ThFl)$_2$** and **OddDPP(ThFl)$_2$**, **OddDPP(ThBt)$_2$** shows much broader and more pronounced red-shifts around 105 nm in the solid-state absorption profiles, and has a maximum in the absorption bands at 731 nm (See Table 3.2). In line with the literature it is proposed that the larger red shift is due to stronger intermolecular interaction in solid state for **OddDPP(ThBt)$_2$** than **DPP(ThFl)$_2$**, indicating stronger Donor-Acceptor (D-A) interactions.

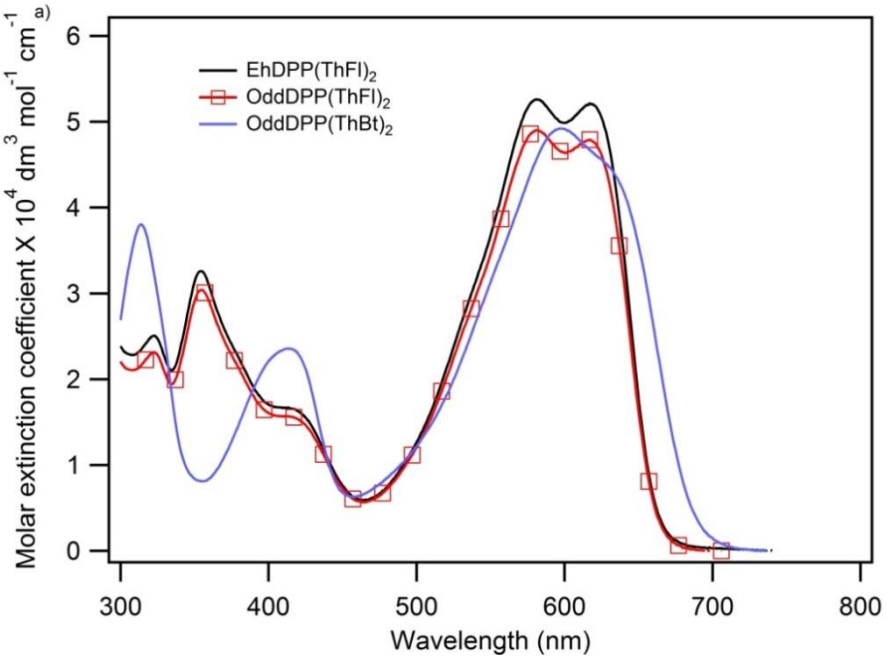

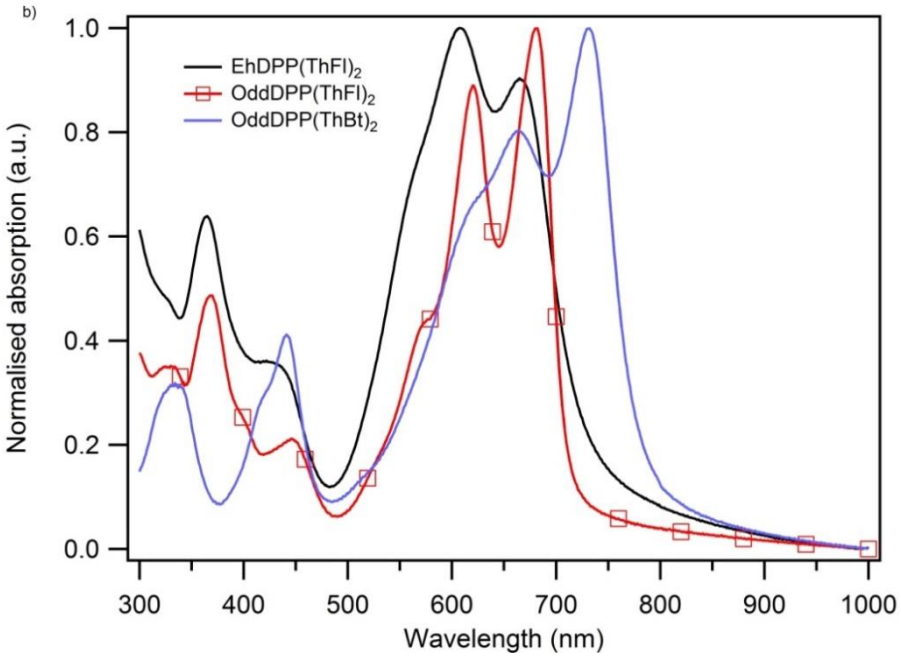


**Figure 3.6.** a) Solution (in dichloromethane) and, b) neat film UV-vis absorptions of **EhDPP(ThFl)$_2$**, **OddDPP(ThFl)$_2$**, and **OddDPP(ThBt)$_2$**.

| **Material** | **$\lambda_{max}$ (nm) solution** | **$\lambda_{max}$ (nm) film** |
|---|---|---|
| **EhDPP(ThFl)$_2$** | 617, 581, 412, 354, 323 | 666, 608, 423, 365 |
| **OddDPP(ThFl)$_2$** | 617, 581, 412, 354, 323 | 680, 621, 575, 448, 371, 333 |
| **OddDPP(ThBt)$_2$** | 636, 597, 415, 314 | 731, 664, 621, 441, 412, 335 |

**Table 3.2.** Summary of the absorption measurements from solution and film.

The normalised absorption spectrum of **OddDPP(ThFl)$_2$**, and **OddDPP(ThBt)$_2$**, which can be solution processed with PC70BM are shown in Figure 3.7. Comparing the DPP and PC70BM absorption spectra would suggest that OPV devices made with these materials should have charge generation *via* the Channel I mechanism at wavelength around 700 nm, where the DPP materials have strong absorption and PC70BM have low optical density. **OddDPP(ThBt)$_2$** has a much broader absorption spectrum than **OddDPP(ThFl)$_2$** allowing greater photon absorption at

wavelengths longer than 700 nm. At these shorter wavelength charges could be generated by Channel II, whereby PC70BM absorbs and a hole is transferred to the DPP donor material or the excited PC70BM could transfer its energy to the DPP donor material by Foster or Dexter transfer followed by Channel I generation.

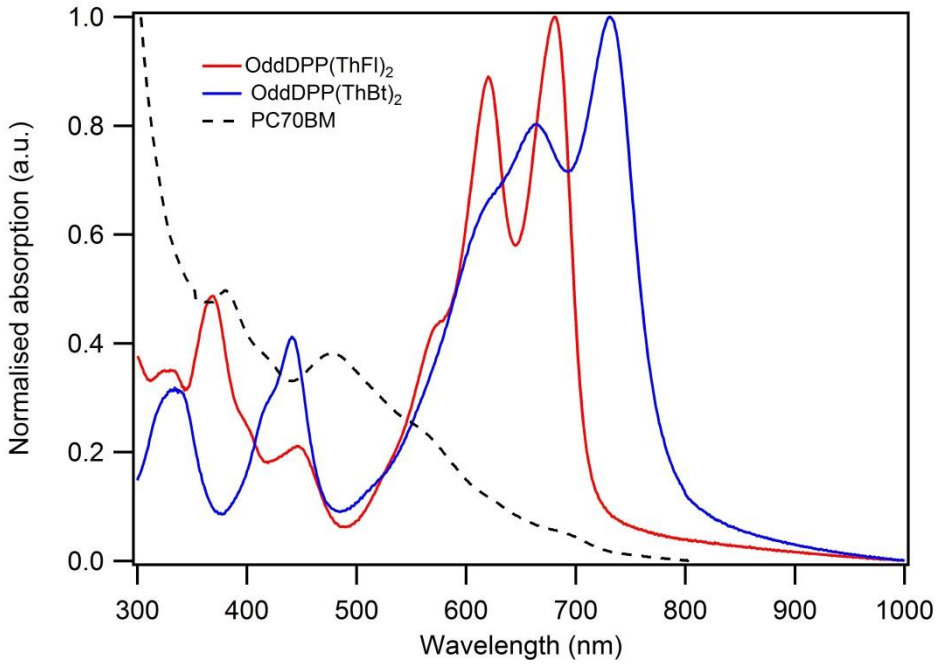


**Figure 3.7.** Normalised absorption spectrum of **OddDPP(ThFl)$_2$**, and **OddDPP(ThBt)$_2$** with PC70BM in thin films to compare the ranges of photon absorption.

### 3.2.3 Electrochemical properties

It was necessary to determine the IP and electron affinity EA of materials before being incorporated to OPV devices, to understand whether when **OddDPP(ThFl)$_2$** or **OddDPP(ThBt)$_2$**, were blended with PC70BM there would be sufficient energy offset for charge generation. **OddDPP(ThFl)$_2$** exhibited insufficient solubility in dichloromethane/electrolyte solution at room temperature for cyclic voltammetry (CV) measurements. However, **OddDPP(ThBt)$_2$** was soluble in dichloromethane and was found to have two chemically reversible waves in both oxidation and reduction at $E_{1/2}$ = 0.4 V & 0.7 V and –1.5 V & –1.8 V, respectively (see Figure 3.8), *versus* the ferrocene/ferrocenium couple. The IP (HOMO) and EA (LUMO) were then calculated by adding the $E_{1/2}$ of the first oxidation and reduction to the offset in potential to the reported IP of ferrocene (4.8 eV)[121] as shown in equation, IP = -[4.8 + 0.4] = -5.2 eV; EA = -[4.8 + (-1.5)] = -3.3 eV. This

gave an estimated IP and EA energies of –5.2 eV and –3.3 eV for **OddDPP(ThBt)$_2$**, (see Table 3.1).

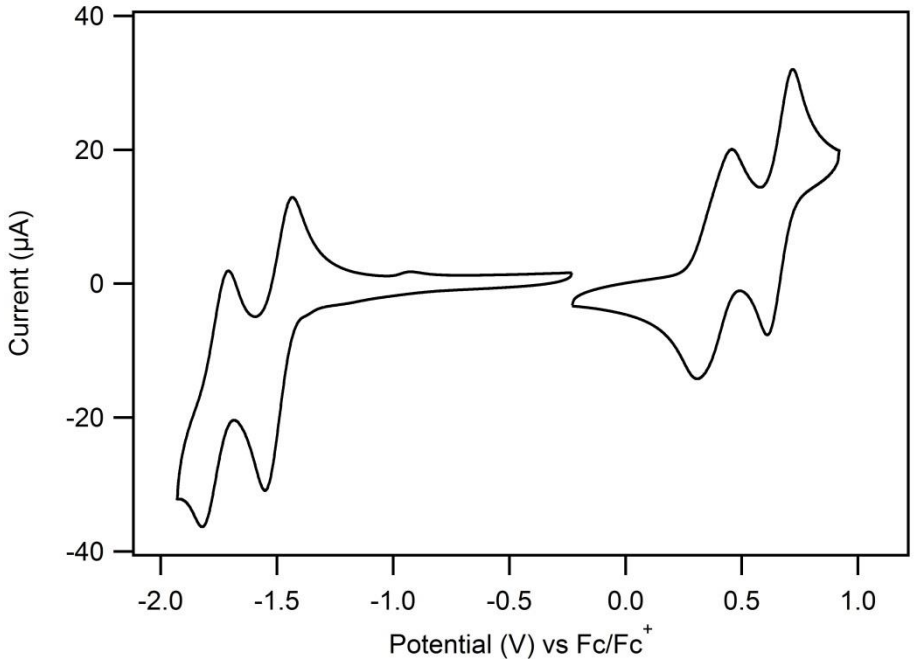


**Figure 3.8.** Cyclic voltammograms for **OddDPP(ThBt)$_2$** measured in dichloromethane solution under an argon atmosphere at a scan rate of 100 mV $s^{-1}$ with glassy carbon as the working electrode.

Since, the IP and EA of the **EhDPP(ThFl)$_2$** and **OddDPP(ThFl)$_2$** could not be estimated using CV. The IP of films of the materials were measured using photoelectron spectroscopy under air (PESA). **EhDPP(ThFl)$_2$** was thermally evaporated on to a glass substrate to give a 110 nm thick film. The **OddDPP(ThFl)$_2$** and **OddDPP(ThBt)$_2$** films were fabricated by spin-coating from chloroform solution to give ~60 nm thick films. During the PESA measurement the surface of the film is bombarded with a slowly increasing energy of ultraviolet photons and at particular energy levels photoelectrons start to emit. The energy level at which the emission starts is the work function or IP of the material. This gave an IP value and it was found the IP was −5.3 eV for all three DPP derivatives. The PESA measurements were performed by Dr. Dani Stoltzfus.

However, for the material **OddDPP(ThFl)$_2$** to be used as donor material, it is important to know the EA. There are numerous ways reported for estimating the optical gap with the best using the absorption and PL spectra[122]. Hence it was measured from the solid state by adding the optical gap to the IP, measured form PESA. Thin films were prepared for all the DPP derivatives to estimate the optical gap in the solid state. The optical gaps each of the three DPPs in solid state was

estimated from film absorption and photoluminescence (PL) spectra. First the corrected absorbance and PL spectra were obtained by dividing the absorbance by eV and PL by eV[123]. The spectra were then normalized and plotted against eV. And, finally the optical gap was taken at the crossover of the absorption and PL spectra[122]. The EA were then calculated by adding optical gap to the ionization potentials from solid-state measurements. The measurements and calculations were undertaken by Dr Paul Shaw. Within experimental errors these EA values (see Table 3.3) are identical. It should be noted that these energy values should not be taken as absolute due to the difference in the experimental methods used in their determination. For example, for **OddDPP(ThBt)$_2$** CV gave a EA energy of -3.3 eV while PESA/optical gap gave the energy as -3.7 eV. Nevertheless, they are useful guides to determine whether or not the charge separation might or might not occur with particular acceptor.

| **Materials** | **CV** | | **PESA/Optical Gap** | | |
|---|---|---|---|---|---|
| | **IP (eV)**[a] | **EA (eV)**[b] | **IP (eV)**[c] | **EA (eV)**[d] | **$E_g$ (eV)**[e] |
| **EhDPP(ThFl)$_2$** | -[f] | -[f] | –5.3 | –3.6 | 1.7 |
| **OddDPP(ThFl)$_2$** | -[f] | -[f] | –5.3 | –3.5 | 1.8 |
| **OddDPP(ThBt)$_2$** | -5.2 | -3.3 | –5.3 | –3.7 | 1.6 |

[a] determined from the $E_{1/2}$ of the first oxidation; [b] determined from the $E_{1/2}$ of the first reduction; [c] determined from PESA; [d] estimated from IP and the optical gap; [e] derived from the crossover of absorption and emission in solid state; [f] not determined.

**Table 3.3.** Summary of the results from CV measurements, PESA and optical gap measurements.

Although the actual mechanism of charge generation is still not completely understood in OPV devices, it is believed that the energy offset between the EAs (in case of Channel I) must be sufficient to generate free charges. This energy offset must be greater than the binding energy of the excitons, which is estimated to be around ~0.1-0.5 eV[30]. The DPP donors all have an EA of -3.5 eV whereas PC70BM has been reported to have an EA of -4.2 eV[78]. Therefore, each of the derivatives could be used as Channel I materials with PC70BM (see Figure 3.9). In addition given the difference in IP between the DPP derivatives and PC70BM Channel II generation could also occur.

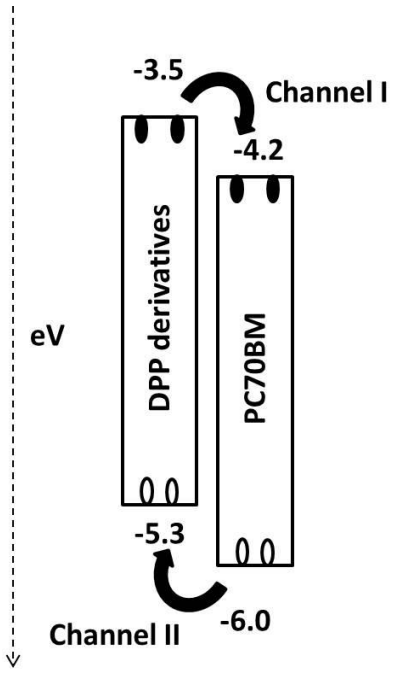


**Figure 3.9.** Diagrams showing the routes for charge generation between **OddDPP(ThFl)$_2$** and PC70BM. Solid circles represent the electrons and holes represented by hollow ovals.

## 3.3 Transporting properties

In an organic solar cell, photoexcitation creates an excition and at the donor-acceptor interface free charges are generated which then are collected at the respective electrodes. Therefore the charge mobility of material is one of the important parameters that determine the efficiency of charges collected as it influences charge extraction and recombination dynamics[124]. In this context, for the DPP derivatives to function as donor material, it must be able to transport holes to the respective electrode. Hence, it was important to investigate the hole transporting properties of these materials. Mobilities in the solid state were investigated by two methods; first in OFETs mode (undertaken by Ms Fatemeh Maasoumi) and second by MIS-CELIV technique (undertaken by Mr Martin Stolterfoht). The later technique is a diode configuration and hence more representative of an OPV device.

### 3.3.1 Mobility in an OFET configuration

An important aspect of an organic semiconductor is its charge carrier mobility. Based on the dominant charge transport carriers the semiconductors are classified as p-type (hole transporter), n-type (electron transporter) and bipolar (hole and electron transporter). The performance of

semiconductor in devices as p or n type strongly depending on IP and EA of the materials and work function of electrodes in device architecture. The DPP derivatives have IPs of around -5.3 eV and EAs of around -3.6 eV, and by choosing an appropriate electrode as Source/Drain (S/D) contact electrode, the charges can be injected and collected at the electrodes. The gold was chosen as the S/D contact electrode and has a work function of gold is ~-4.5 to 5.1 eV[125, 126], which made it a suitable electrode for hole/electron injection.

For organic semiconductors to feature a high charge mobility they typically must be able to form highly ordered films and/or crystalline film[127]. Hence, it is important to control the degree of crystallinity and uniformity of the organic semiconductor film to improve the device performance. The degree of crystallinity can be controlled by using techniques such as thermal and solvent annealing. The DSC studies of the DPP derivatives indicated that they had a rich thermal landscape. Hence, the OFETs device films were optimized using thermal annealing, to achieve maximum charge carrier mobility.

The FET devices were fabricated in a bottom gate with top contact configuration, using $SiO_2$ as the gate dielectric as illustrated in Figure 3.10. For better performance devices different surface passivation layers were used such as: poly(methylmethacrylate) (PMMA), or divinyltetramethyldisiloxane-bis(benzocyclobutane) (BCB), or octadecyltrichlorosilane (OTS). **EhDPP(ThFl)$_2$** films were deposited under vacuum (3 x $10^{-6}$ mbar) at 0.2 Å $S^{-1}$ with a substrate temperature of 26 $^{o}$C to give films of about 40 nm thickness. The **OddDPP(ThFl)$_2$** films were spin-cast from 8 mg/ml in chloroform solution at 2500 rpm for 30 sec to give films of 50 nm thickness. **OddDPP(ThBt)$_2$** films were spin-cast from 8 mg/ml chloroform solution at 2500 rpm for 30 sec to give of about 40 nm thickness. All thickness were measured by Dektak 150 profilometer.The OFETs were completed by deposition of gold under vacuum (2 x $10^{-6}$ mbar) to form the top S/D contacts (40 nm) through shadow masks prepared by deep reactive ion etching with a channel length of 80 μm and channel width of 16 mm.

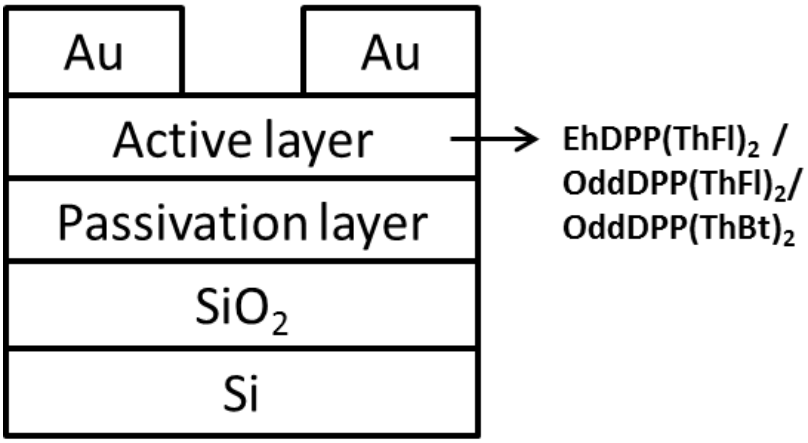


**Figure 3.10.** Schematic diagram of the OFET architecture.

The carrier mobilities of **EhDPP(ThFl)$_2$** films before annealing were poor, were the source-drain and gate currents were at the same order. However, after annealing at 225 °C (around the $T_c$ see Figure 3.3) for 30 sec, the source-drain current improved by three orders of magnitude, which led to devices exhibiting with maximum hole and electron mobilities of $\mu_h = 1.4 \times 10^{-3}$ cm$^2$ V$^{-1}$ s$^{-1}$ and $\mu_e = 3.6 \times 10^{-3}$ cm$^2$ V$^{-1}$ s$^{-1}$, respectively. These mobilities were achieved with PMMA as passivation layer. However, the device had a poor ON/OFF ratio of less than 10, and the threshold voltages ($V_{TH}$) of -15 and +23 V, respectively, were relatively high (See Table 3.4). The output curves shows bipolar characteristics with distinct linear and saturation regimes for both p-channel mode (Vg < 0) and n-channel mode (Vg > 0) (see Figure 3.11).

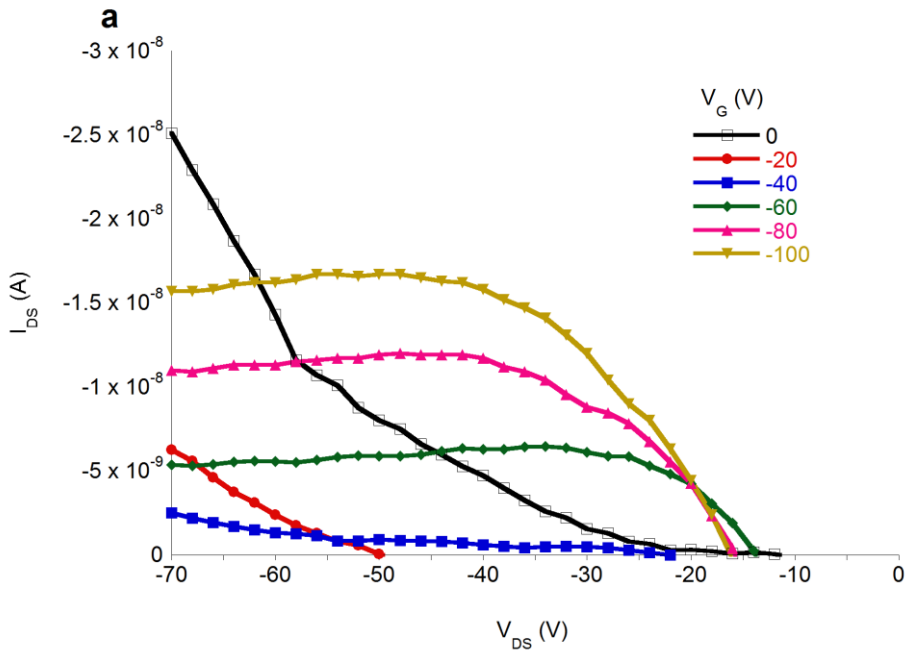

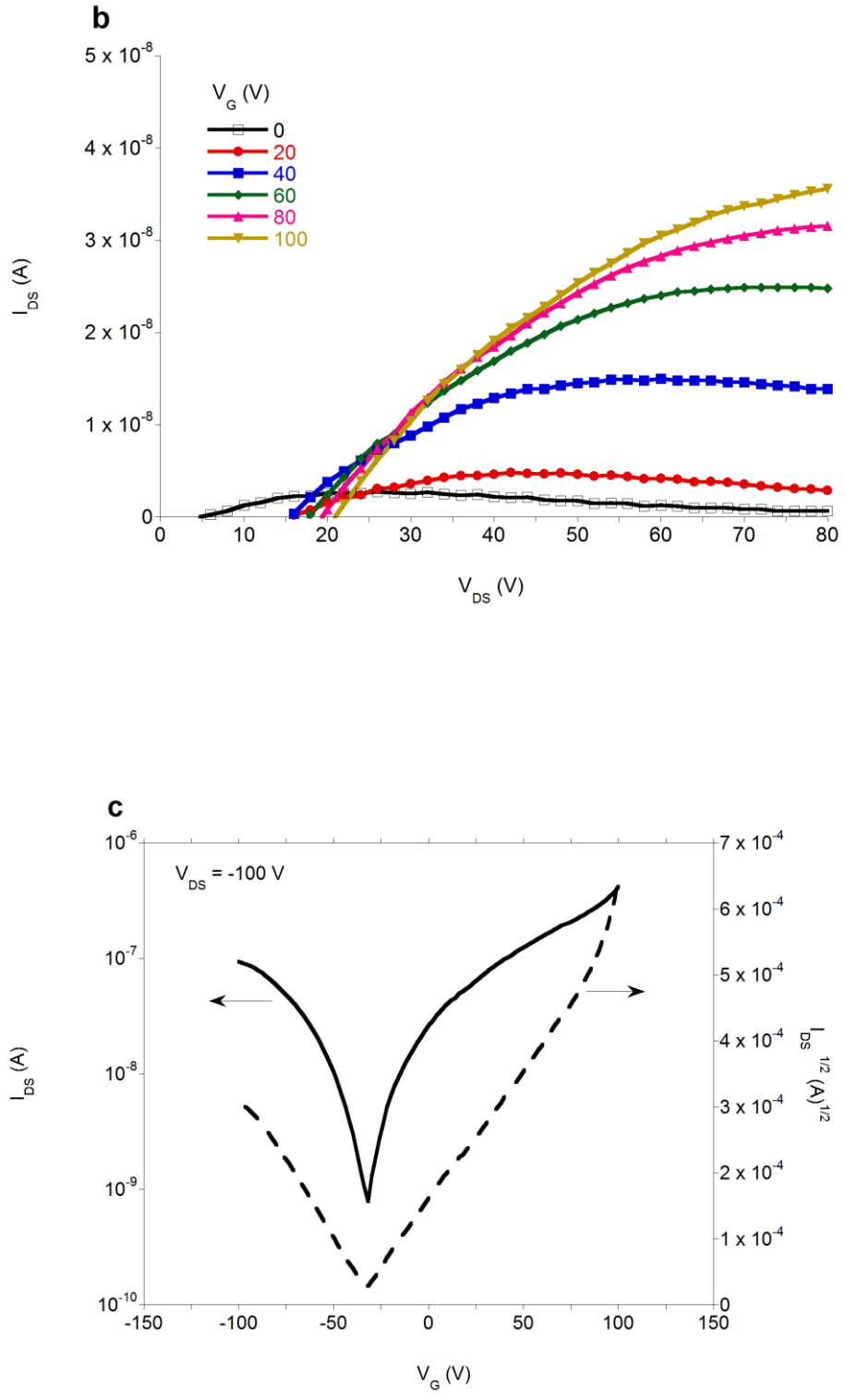


**Figure 3.11.** a and b) Output characteristics of **EhDPP(ThFl)$_2$** in p-type and n-type mode respectively, and c) Transfer characteristic for the OFET operating in p-type mode in the saturation regime (VDS = - 100 V).

Figures 3.12 and 3.13 illustrate a typical examples of OFETs comprised of **OddDPP(ThFl)$_2$** and **OddDPP(ThBt)$_2$** active layers, respectively, and their performance and shows clear p-type and n-type modes. The maximum hole mobility of the two solution processed DPP derivatives were exhibited by **OddDPP(ThBt)$_2$**, which had a maximum hole mobility of $\mu_h$ = 9.8 x $10^{-2}$ $cm^2$ $V^{-1}$ $s^{-1}$ with OTS as the passivation layer. The ON/OFF ratio was 2 x $10^5$ and the threshold voltage = −32 V. The maximum electron mobility of $\mu_e$ = 1.3 x $10^{-2}$ $cm^2$ $V^{-1}$ $s^{-1}$, ON/OFF ratio of 1.1 x $10^5$, and $V_{TH}$ of + 21 V was found for **OddDPP(ThFl)$_2$** with BCB as passivation layer (See Table 3.4). The highest mobilities for **OddDPP(ThFl)$_2$** was achieved after annealing the films at 200 °C, and above this temperature, the mobilities decreased. For **OddDPP(ThBt)$_2$**, the best device mobility was achieved when the film was annealed at 150 °C for 30 sec which is above its $T_g$ (125 °C).

In general, the as cast films prepared from evaporation or spin coating exhibited lower mobility compared to films, after annealing. A possible explanation for this is that the material form amorphous as disordered films on processing, which when on heating becomes more ordered. Hence, the mobilities of all the DPP derivatives increased by at least an order of magnitude, after annealing. All the three DPP derivatives showed bipolar mobility with reasonably balanced hole and electron mobilities. The FET mobilities of the **OddDPP(ThFl)$_2$** containing OFETs is amongest highest reported for bipolar non-polymeric DPP based materials[128, 129].

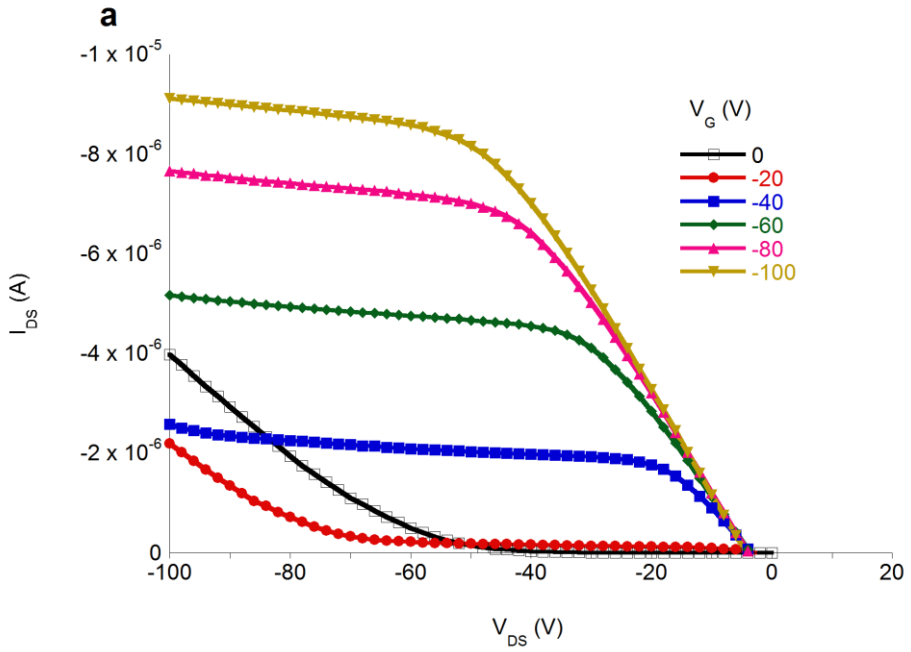

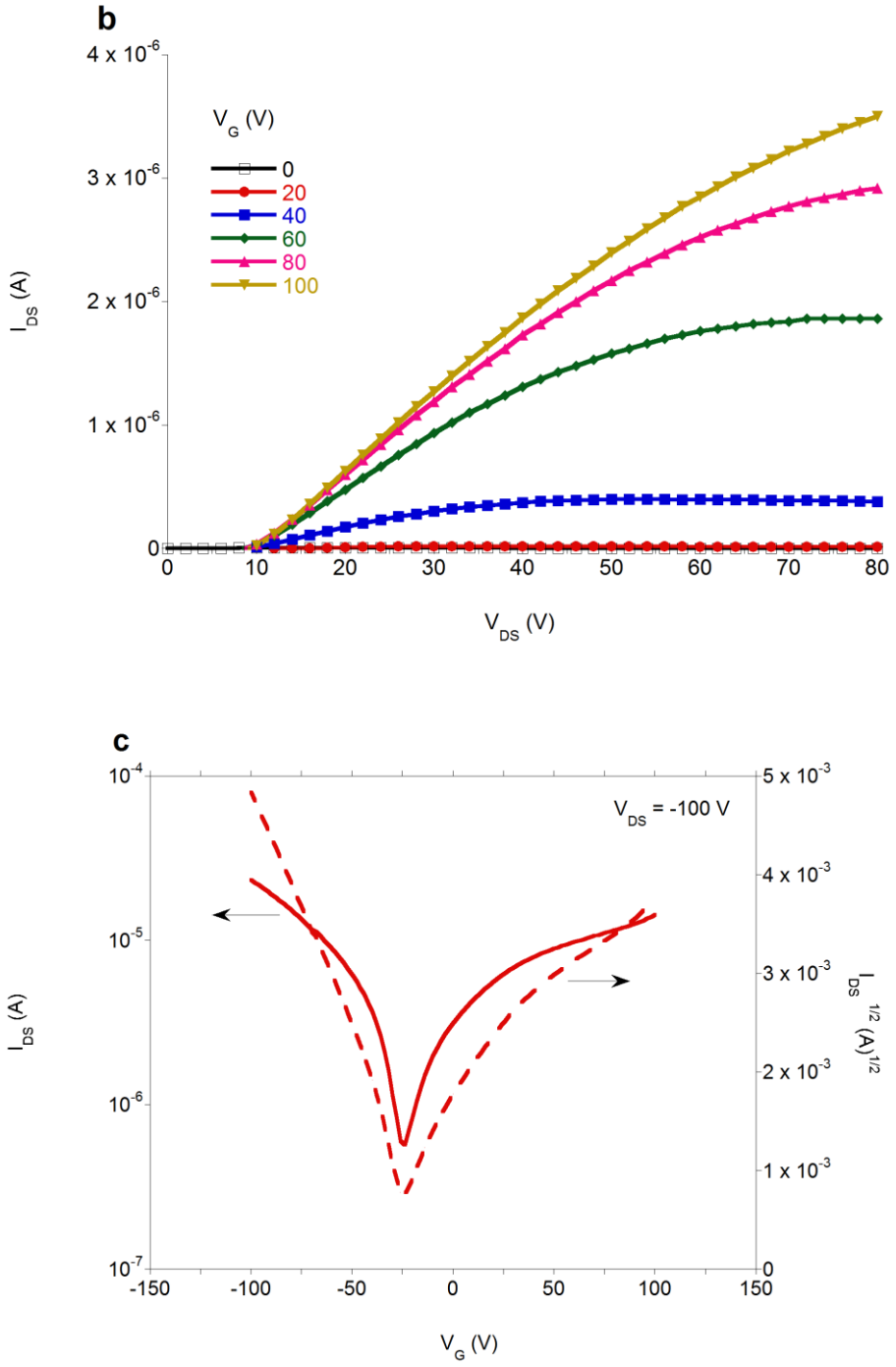


**Figure 3.12.** a and b) Output characteristics of **OddDPP(ThFl)$_2$** for p and n modes respectively, and c) transfer characteristics for the OFET operating in p-type mode in the saturation regime (VDS = - 100 V).

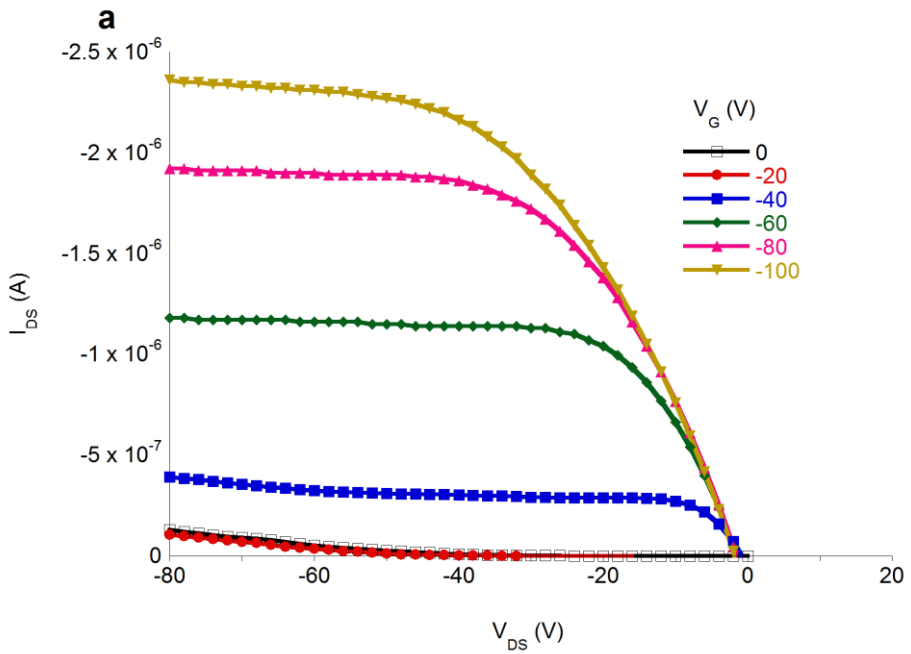
a
-2.5 x 10-6
-2 x 10-6
-1.5 x 10-6
-1 x 10-6
-5 x 10-7
0
IDS (A)
VG (V)
0
-20
-40
-60
-80
-100
-80
-60
-40
-20
0
20
VDS (V)

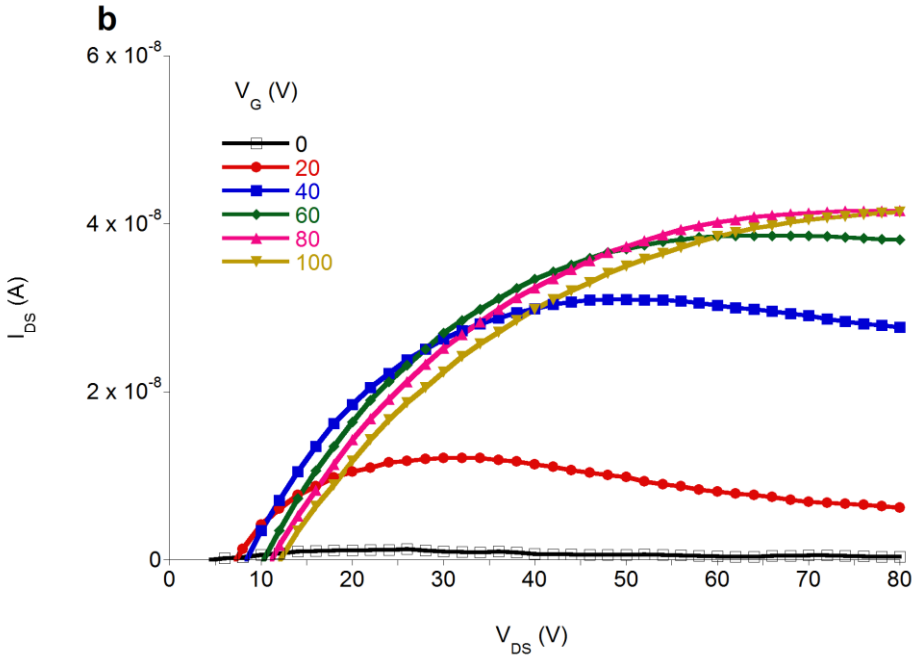
b
6 x 10-8
4 x 10-8
2 x 10-8
0
IDS (A)
VG (V)
0
20
40
60
80
100
0
10
20
30
40
50
60
70
80
VDS (V)

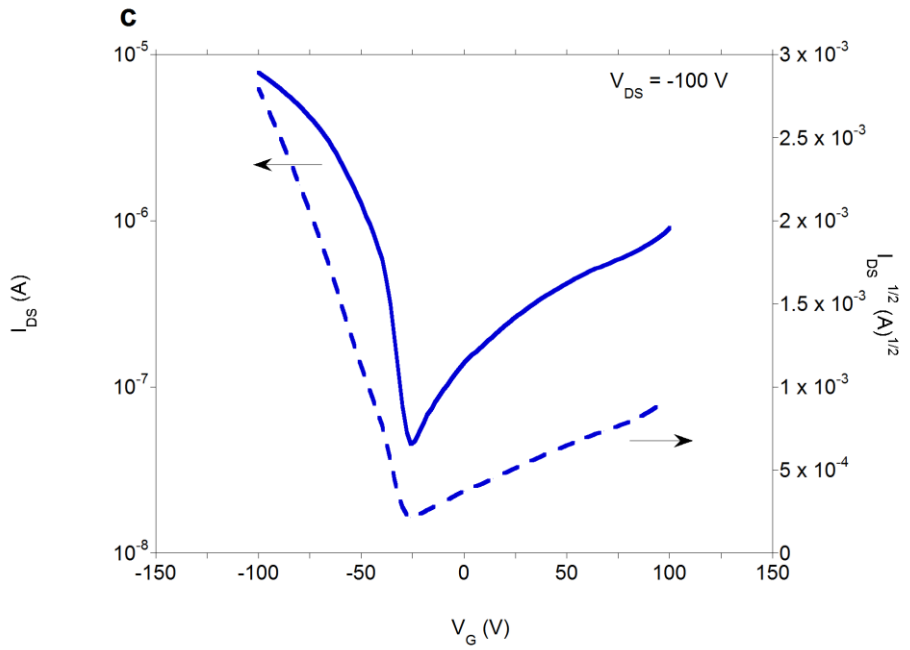


**Figure 3.13.** a and b) Output characteristics of **OddDPP(ThBt)$_2$** for p and n modes respectively, and c) transfer characteristics for the OFET operating in p-type mode in the saturation regime (VDS = - 100 V).

| **Materials** | **Dielectric** | **Max $\mu_h$ ($cm^2 V^{-1} s^{-1}$)** | **Max $\mu_e$ ($cm^2 V^{-1} s^{-1}$)** | **On/off ratio** | **$V_{TH}$ (V)** |
|---|---|---|---|---|---|
| **EhDPP(ThFl)$_2$** | OTS | 3.1 x $10^{-4}$ | –[a] | 3.1 x $10^3$ | −31 / –[a] |
| | BCB | 4.5 x $10^{-5}$ | 5.2 x $10^{-6}$ | 1.2 x $10^2$ / 8 x $10^2$ | −15/ –[a] |
| | PMMA | 1.4 x $10^{-3}$ | 3.6 x $10^{-3}$ | Less than 10 | -15/ +23 |
| **OddDPP(ThFl)$_2$** | OTS | 9.8 x $10^{-2}$ | - | 2 x $10^5$ | -32 |
| | BCB | 7.6 x $10^{-3}$ | 1.3 x $10^{-2}$ | 1.3 x $10^2$/ 1.1 x $10^5$ | +10/ +21 |

| | | | | | |
|---|---|---|---|---|---|
| | PMMA | $7.2 \times 10^{-5}$ | $1.2 \times 10^{-4}$ | Less than 10 | –[a] / –[a] |
| **OddDPP(ThBt)$_2$** | OTS | $9.8 \times 10^{-2}$ | –[a] | $2 \times 10^5$ | −32 / –[a] |
| | BCB | $4.3 \times 10^{-3}$ | $1.0 \times 10^{-3}$ | $3.2 \times 10^2$ / $3.4 \times 10^3$ | -19/ -10 |
| | PMMA | $1.5 \times 10^{-3}$ | $3.6 \times 10^{-5}$ | $4 \times 10^2$ / 10 | -/ +12 |

[a] not measurable.

**Table 3.4.** Summary of charge carrier mobility of **EhDPP(ThFl)$_2$**, **OddDPP(ThFl)$_2$** and **OddDPP(ThBt)$_2$** under different field-effect transistor conditions. All reported values are averages over >6 devices and the standard deviations are reported accordingly.

### 3.3.2 Mobility study *via* MIS-CELIV technique

Although, FETs mobilities have been used in literature[130] to report the transport properties of the materials used in OPV devices, the charge carrier mobility from OFETs measurements only provides information about the charge transport horizontally along the active channel close to the dielectric layer. Hence, further mobility measurements were carried out using the Metal insulator semiconductor-charge extraction by linearly increasing voltage (MIS-CELIV)[78] technique to provide insights into the charge transport in vertical direction. This technique allows for both electron and hole mobility measurements separately in devices that are close in architecture to operational organic solar cell devices.

In the MIS-CELIV structure, a dielectric (insulator) is deposited on the top or bottom of the organic semiconductor film, which is sandwiched between two metal electrodes. $MgF_2$ was used as dielectric layer as it has wide optical gap (−20 eV)[131]. The idea behind using such a large optical gap material is to block both electrons and holes. Holes or electrons can then be injected when a forward bias voltage is applied and trapped by the insulator. The Holes can be injected from ITO when, the insulator is adjacent to the samarium/aluminium electrode (see Figure 3.14a). And the electrons can be injected through samarium/aluminium, when the insulator is adjacent to ITO (see

Figure 3.14b). Subsequently, by linearly increasing the reverse via voltage, charges are extracted and the transport properties determined.

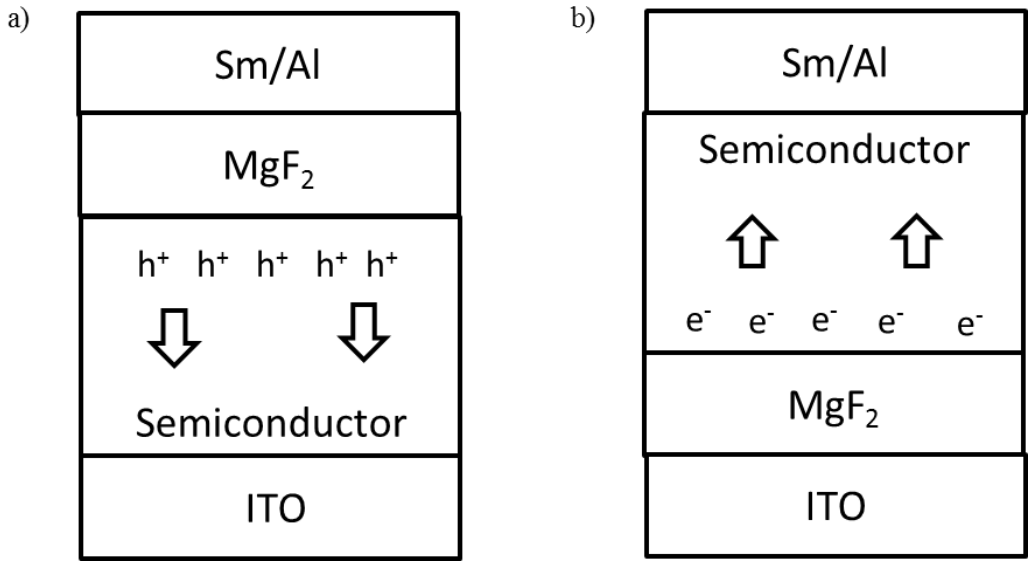


**Figure 3.14.** Schematic of the MIS diode in the case of a) hole only and, b) electron only.

As the main aim of the project was to develop new solution processable materials for OPV devices only **OddDPP(ThFl)$_2$** and **OddDPP(ThBt)$_2$** were further investigated. Indium tin oxide (ITO) coated glass substrates were patterned by photolithography and cleaned by sonicating in sequence with Alconox (detergent), de-ionized water, acetone and 2-propanol for 10 min each. The cleaned substrates were coated with a 20 nm layer of PEDOT:PSS by spin coating at 5000 rpm for 60 s. **OddDPP(ThFl)$_2$** and **OddDPP(ThBt)$_2$** were solution processed from chloroform solution to give about ~150 nm thick films. Finally, 1 nm of samarium and 100 nm of aluminium were deposited to complete the device by thermal evaporation under a $10^{-6}$ mbar vacuum. A 100 nm layer of magnesium fluoride was evaporated under a $10^{-6}$ mbar vacuum either on the PEDOT:PSS layer or underneath the aluminium cathode for electron only and hole only devices, respectively.

In the MIS-CELIV experiment a voltage offset is applied in forward bias prior to charge extraction, which causes an accumulation of injected charges at the semiconductor-insulator interface, as illustrated in Figure 3.14. Subsequently, a triangular voltage pulse is applied in reverse bias to extract this charge (CELIV). The current transients start from the displacement current value $j_0$, which is defined by the total capacitance of the device. The time at which the current transient reaches the doubled value of $j_0$ corresponds to the transit time ($t_{tr} = 4\pi * t_{2j0}$). From the transit time, the mobility can be calculated from the equation given below:

$$\mu = \frac{2d_s^2}{At_{tr}^2}\left(1 + \frac{\varepsilon_s d_i}{\varepsilon_i d_s}\right)$$

Where $\varepsilon_0$ is absolute dielectric permittivity of vacuum, $\varepsilon_s$ ( $\varepsilon_i$ ) is the dielectric constant of the semiconductor (insulator) and $d_s$ is the thickness of the semiconductor layer and $d_i$ is the thickness of the insulator. The hole and electron mobilities calculated for **OddDPP(ThFl)$_2$** from this technique were $\mu_h = 9 \times 10^{-5}$ cm$^2$ V$^{-1}$ s$^{-1}$ and $\mu_e = 1 \times 10^{-5}$ cm$^2$ V$^{-1}$ s$^{-1}$, respectively (See Table 3.5). For **OddDPP(ThBt)$_2$**, $\mu_h = 6 \times 10^{-5}$ cm$^2$ V$^{-1}$ s$^{-1}$ and $\mu_e = 5 \times 10^{-5}$ cm$^2$ V$^{-1}$ s$^{-1}$. The similarity in the charge carrier mobilities of **OddDPP(ThFl)$_2$** and **OddDPP(ThBt)$_2$** measured *via* MIS-CELIV technique, indicates that they are bipolar. The hole mobilities (~$10^{-5}$ cm$^2$ V$^{-1}$ s$^{-1}$) measured for these materials are comparable to those previously reported for solution processable donor materials based on DPP such as DPP(TBFu)$_2$ (4 X $10^{-5}$ cm$^2$ V$^{-1}$ s$^{-1}$)[32], *tri* –DPP (~1 x $10^{-5}$ cm$^2$ V$^{-1}$ s$^{-1}$)[132], which were used as donor material with PC70BM as acceptor. Comparison of the mobilities has to be taken with caution as the measurement techniques used in the literature is by Space Charge Limited Current (SCLC) technique. This suggests that the DPP derivatives (**OddDPP(ThFl)$_2$** or **OddDPP(ThBt)$_2$**) when blended with PC70BM, can act as a hole charge transporter.

| **Materials** | **$\mu_h$ (cm$^2$ V$^{-1}$ s$^{-1}$)** | **$\mu_e$ (cm$^2$ V$^{-1}$ s$^{-1}$)** |
|---|---|---|
| **OddDPP(ThFl)$_2$** | 9 x $10^{-5}$ | 1 x $10^{-5}$ |
| **OddDPP(ThBt)$_2$** | 6 x $10^{-5}$ | 5 x $10^{-5}$ |

**Table 3.5.** Summary of mobility measurements using MIS-CELIV technique.

The mobilities of **OddDPP(ThFl)$_2$ and OddDPP(ThBt)$_2$** measured under FETs mode exhibited two orders of magnitude higher than that measured using MIS-CELIV technique. However, it has to be considered that, MIS-CELIV technique device architecture allows for mobility measurements close to operational organic solar cells device.

## 3.4 OddDPP(ThFl)$_2$ and OddDPP(ThBt)$_2$ in heterojunction devices

In the previous sections it has been shown that both **OddDPP(ThFl)$_2$** and **OddDPP(ThBt)$_2$** have suitable IPs (see Figure 3.9) and sufficient hole mobility to perform as an electron donor with PC70BM as an acceptor in an OPV device. It was also shown that these materials have higher optical density around 700 nm compared to the PC70BM (see Figure 3.7). The detailed OPV device characteristics were studied by Dr. Hui Jin and Dr. Mike Hambsch and a summary of the key properties will be discussed here.

### 3.4.1. Device manufacture and results

One of the key issues with the BHJ architecture is to ensure the ideal phases of the donor and acceptor in the blend are generated for excition dissociation and efficient charge extraction. To achieve the ideal separation in blend films different processing techniques can be employed such as thermal annealing,[32, 133] solvent vapour annealing,[34] and use of solvent mixtures/solvent additive[37]. Recently, the use of small amount of additives in the solvent has been reported to bring about ideal phase separation in films consisting of non-polymeric donor materials and PCBM acceptors[36, 134]. Additives are organic solvents with a higher boiling point, which are added to the master solvent in small quantity before spin coating onto the substrate. This allows the films to dry slowly, to achieve the ideal film structure. The most commonly employed additives in a BHJ solar cells are 1,8-diiodooctane (DIO), 1-chloronaphthalene (CN)[132]. However, during characterization of these materials, a report on material similar to **OddDPP(ThBt)$_2$**, but with a different solubilising group,[35] described that by using small quantity (1%) of DIO as additive in chloroform the PCE increased from 0.26% to 0.89%. Considering this, DIO was first, chosen as the solvent additive while fabricating blend films. The optimization of the devices was achieved in two stages; first, the effect of additive concentration followed by determination of the optimal donor:acceptor blend ratio. The devices had the following structure ITO (100 nm)/PEDOT:PSS (≈25 nm)/**OddDPP(ThFl)$_2$**:PC70BM/Ca (15 nm)/Al (100 nm). The active layer thickness for **OddDPP(ThFl)$_2$**:PC70BM devices were 90-120 nm, whereas for **OddDPP(ThBt)$_2$**:PC70BM was around ~90-110 nm.

The blend films were fabricated using chloroform as the ‘master solvent’, followed by gradual increment in the volume of additive (DIO) (0.5% V/V, 1% V/V, 1.5% V/V, 2% V/V, 2.5% V/V, 3%V/V). The first set of experiments were carried out with 1:1 ratio of

**OddDPP(ThFl)$_2$**:PC70BM. The film cast from chloroform exhibited current density of 3.2 ± 0.1 mA cm$^{-2}$ (see Figure 3.15). However, the film fabricated from chloroform with 0.5% DIO exhibited an increase in current density by three fold achieving maximum PCE of 3.2%, $J_{sc}$ = 9.1 ± 0.1 mA cm$^{-2}$, $V_{OC}$ = 0.90 ± 0.01 V and FF = 0.49 ± 0.01%.

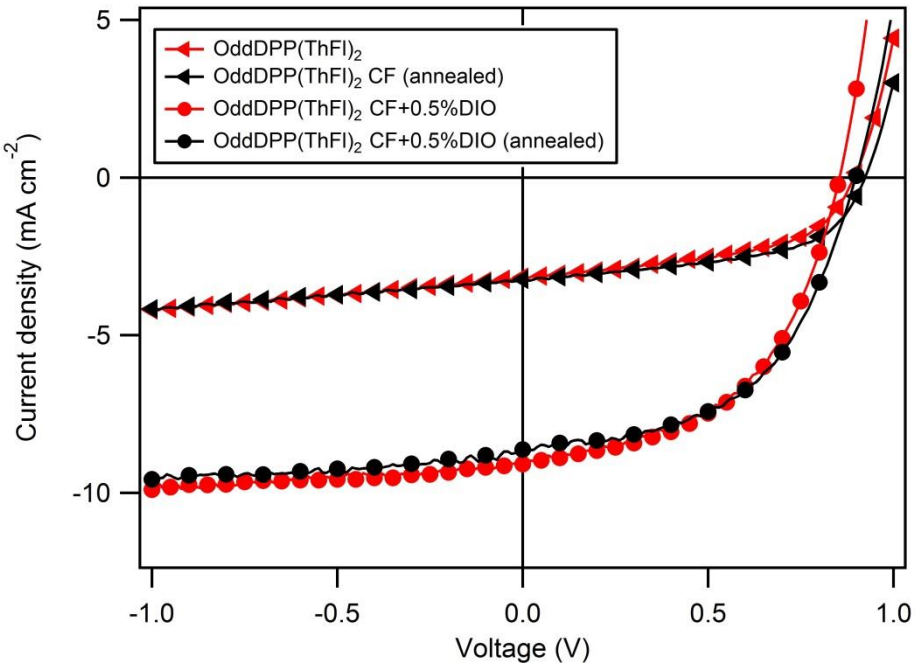


**Figure 3.15.** *J-V* curve of **OddDPP(ThFl)$_2$** devices showing current density as a function of voltage for different materials and DIO loading.

Next, the best ratio of **OddDPP(ThFl)$_2$**:PC70BM was determined by fabricating device from chloroform with 0.5% DIO as the additive. A device with ratio of 3:2 (**OddDPP(ThFl)$_2$**:PC70BM) exhibited maximum charge generation with an EQE of 56% at 687 nm. The EQE spectrum of blends (see Figure 3.16), shows a similar shape to the absorption spectrum as seen in Figure 3.9. This suggest that at wavelength longer than 600 nm charge generation is primarily through the Channel I mechanism, with electron transfer from **OddDPP(ThFl)$_2$** to PC70BM. Charge generation *via* absorption can also play an important role although it is not possible to determine whether it is by Channel I or II. At shorter wavelength absorption by **OddDPP(ThFl)$_2$** and PC70BM both contribute to charge generation. For the, **OddDPP(ThFl)$_2$** devices the maximum PCE was 4.0%, with $J_{sc}$ = 9.1 ± 0.1 mA cm$^{-2}$, $V_{OC}$ = 0.85 ± 0.01 V and FF = 0.52 ± 0.01%. Thermal annealing at 90 ºC showed a slight drop in current density, however, exhibited an increase in Voc (0.91) leading to PCE of 4.1% (see Table 3.6). It was observed that annealing above 90 ºC, resulted in poorer device performance, which is likely to occur from an unfavourable change in the film structure.

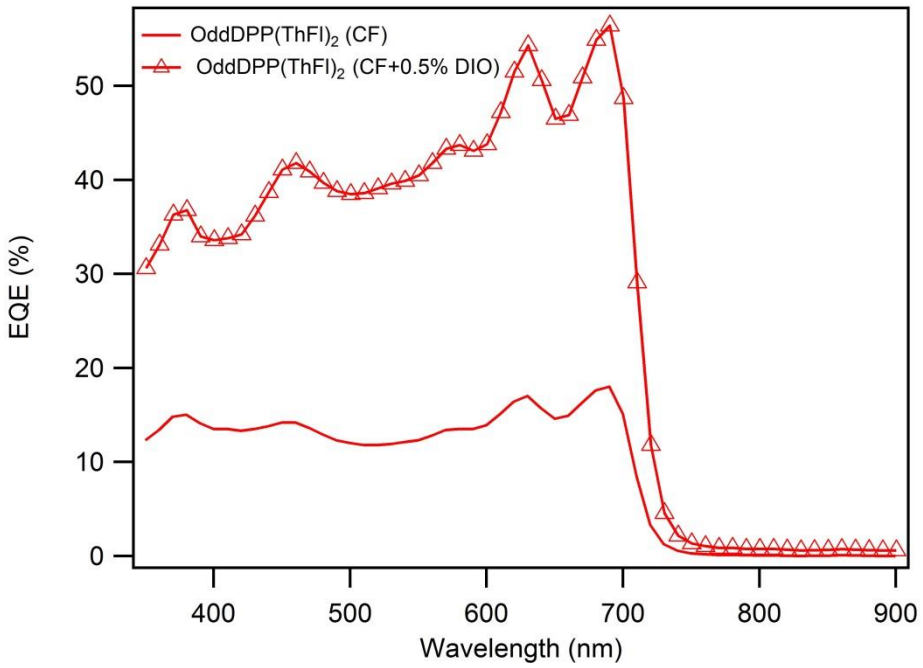


**Figure 3.16.** Plot of EQE against wavelength for **OddDPP(ThFl)$_2$**:PC70BM devices.

Given, the best device efficiency for **OddDPP(ThFl)$_2$** was achieved when the film was fabricated from chloroform with 0.5% additive it was decided to investigate the device performance of different ratios of **OddDPP(ThBt)$_2$**:PC70BM films cast from chloroform and chloroform with 0.5% DIO. The best ratio was found to be 3:1 for **OddDPP(ThBt)$_2$**:PC70BM. In contrast to the **OddDPP(ThFl)$_2$** case the film cast from chloroform exhibited a current density almost five times higher than that cast from chloroform with 0.5% DIO (see Figure 3.17). The best device exhibited maximum PCE 2.1%, $J_{sc}$ = 5.6 ± 0.1 mA cm$^{-2}$, $V_{OC}$ = 0.92 ± 0.01 V and FF = 0.46 ± 0.01.

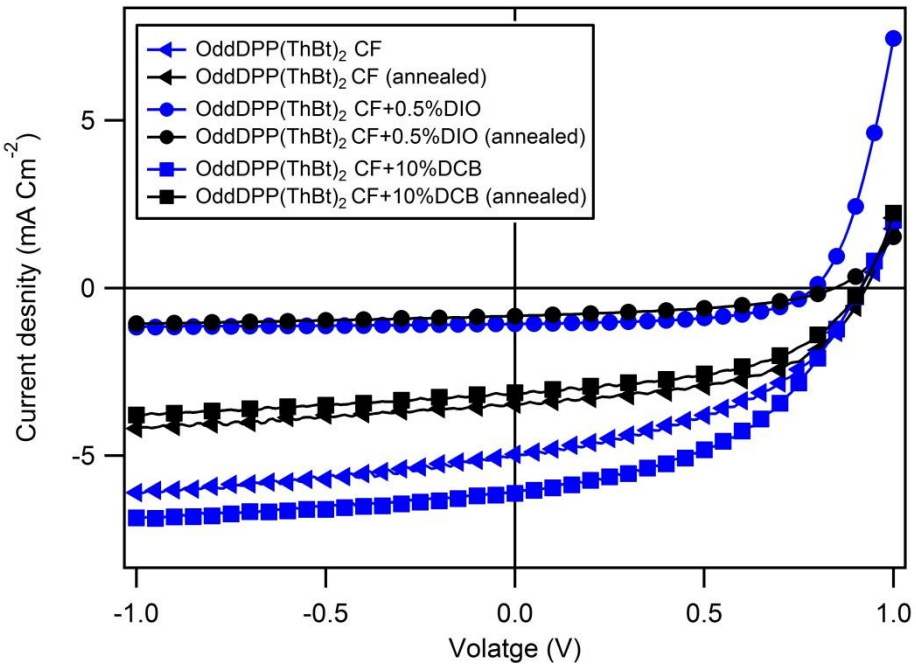


**Figure 3.17.** *J-V* curve of **OddDPP(ThBt)$_2$** devices showing current density as a function of voltage.

However, one of the most commonly employed solvent mixtures for donor polymer and fullerene acceptors are 1,2-dichlorobenzene (DCB) and chlorobenzene (CB). This is because the, higher boiling point allows for slow drying of the films, resulting in ideal film structure in donor polymer and fullerene blends. Considering PC70BM has good solubility in DCB[37], and the addition of DCB to chloroform would allow slow drying of the films to bring about a different film structure. It, was therefore decided to employ chloroform with DCB for fabricating films of **OddDPP(ThBt)$_2$**:PC70BM blend. The films were fabricated from chloroform with 5% and 10% DCB. The films fabricated from the latter showed an increase in current density to 6.1 ± 0.1 mA cm$^{-2}$ leading to maximum PCE of 2.6%, $V_{OC}$ = 0.91 ± 0.01 V and FF = 0.47 ± 0.01. Compared to the films fabricated from chloroform solution the one with 10% DCB would take longer time for the film to dry, allowing more time for the components to order in the solid state. A comparison of EQE spectrum of films fabricated from chloroform, chloroform with 0.5% DIO, and chloroform with 10 % DCB are shown in Figure 3.18. In In both these films bands above 700 nm, corresponds to the absorption of DPP derivative, suggesting charge generation primarily through Channel I mechanism. However, the films fabricated from chloroform with 0.5% DIO, exhibited a maximum EQE of 7% at 440 nm, suggesting less ordered film structure, resulting in poor charge generation.

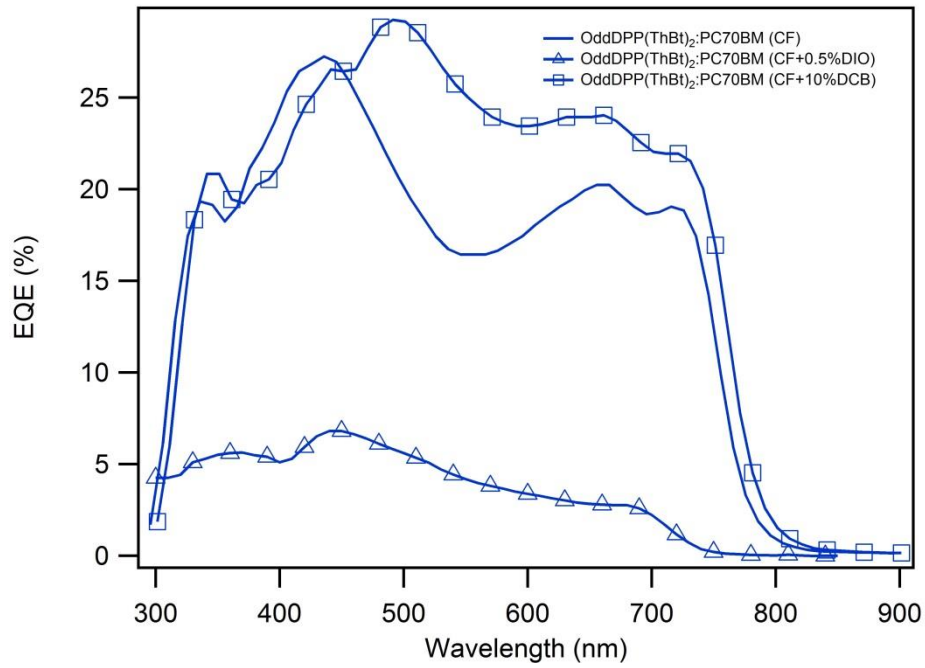


**Figure 3.18.** Plot of EQE against wavelength for **OddDPP(ThBt)$_2$**:PC70BM devices.

In case of **OddDPP(ThBt)$_2$** films thermal annealing at 90 ºC resulted in reduction of the current density (see Table 3.3). This is in direct contrast to the thermal properties of this material, which showed a $T_g$ around 91 ºC, in the DSC measurements (see Figure 3.5). In general, it is expected that when the film is annealed above $T_g$ it would results in molecular ordering and subsequently would enhance the charge transport. However, that was not the case in these devices. A possible explanation for this is due the unfavourable film structure, resulting in poorer device performance.

| Device | Blend ratio (Donor:PC70BM) (by weight) | Thickness (nm) | Annealing temperature (°C) | $J_{sc}$ (mA cm$^{-2}$) ±0.1 | $V_{oc}$ (V) ±0.01 | FF ±0.01 | PCE (%) ±0.1 |
|---|---|---|---|---|---|---|---|
| **OddDPP(ThFl)$_2$** (CF) | 3:2 | 90 | - | 3.2 | 0.89 | 0.5 2 | 1.5 |
| | | | 90 | 3.2 | 0.92 | 0.55 | 1.6 |
| **OddDPP(ThFl)$_2$** (CF + 0.5% DIO) | 3:2 | 90 | - | 9.1 | 0.85 | 0.52 | 4.0 |
| | | | 90 | 8.5 | 0.91 | 0.53 | 4.1 |
| **OddDPP(ThBt)$_2$** (CF) | 3:1 | 100 | - | 5.0 | 0.92 | 0.46 | 2.1 |
| | | | 90 | 3.5 | 0.92 | 0.53 | 1.7 |
| **OddDPP(ThBt)$_2$** (CF + 0.5% DIO) | 3:1 | 110 | - | 1.1 | 0.79 | 0.56 | 0.5 |
| | | | 90 | 0.8 | 0.84 | 0.45 | 0.3 |
| **OddDPP(ThBt)$_2$** (CF + 10% DCB) | 3:1 | 110 | - | 6.1 | 0.91 | 0.47 | 2.6 |
| | | | 90 | 3.1 | 0.91 | 0.51 | 1.5 |

**Table 3.6.** BHJ solar cell parameters of the best devices of **OddDPP(ThFl)$_2$** and **OddDPP(ThBt)$_2$** blended with PC70BM processed from different solvents. CF = chloroform, DIO = 1,8-diiodooctane, DCB = dichlorobenzene.

## 3.5 Conclusion

The DPP materials described in Chapter 2 and 3 showed a broad absorption across the UV-visible spectrum with $\lambda_{max}$ above 600 nm. In the OFET configuration the materials showed hole mobilities in the range of $10^{-2}$-$10^{-3}$ $cm^2$ $V^{-1}$ $s^{-1}$. The mobility measurements from MIS-CELIV technique showed that the two solution processable materials had sufficient mobility to be used in OPV devices. In OPV devices the role of solvent additives and solvent mixtures was found to be important in optimizing the ideal film structure to bring about maximum excition dissociation and efficient charge extraction. The EQE spectrum of **OddDPP(ThFl)$_2$** and **OddDPP(ThBt)$_2$** suggest charge generation through channel I mechanism, above 700 nm. However for **OddDPP(ThBt)$_2$**, an EQE of 29% at 500 nm, suggest charge generation through channel II mechanism, at this wavelength. The photovoltaic device results show that both **OddDPP(ThBt)$_2$** and **OddDPP(ThFl)$_2$** are good electron donor candidate for use with PC70BM as the electron acceptor. However, **OddDPP(ThFl)$_2$** performed better as an electron donor in BHJ device and achieved maximum PCE of 4.1%.

# Chapter 4 – Synthesis, Physical and photovoltaic properties of OddDPP(ThFl)$_2$ derivative

# 4.1 Introduction

In Chapter 3, **OddDPP(ThFl)$_2$** was shown to be a good electron donor candidate with PC70BM as the acceptor in BHJ solar cells. The best device **OddDPP(ThFl)$_2$**:PC70BM films exhibited a PCE of 4.1% , with, $J_{sc}$ = 8.5 ± 0.1 mA cm$^{-2}$, $V_{OC}$ = 0.91 ± 0.01 V and FF = 0.53 ± 0.01%. However, this is short of the one of the highest reported PCE for non-polymeric based material which is 9%. In the best device the FF was reported to be 0.75[135]. Charge carrier recombination losses usually are believed to be one of contributors to a low FF[136]. While efforts to engineer materials in order to improve the light absorption have been the main focus, it is also important to have materials with higher charge carrier mobilities and reduce bimolecular recombination losses. One approach to improving the charge carrier mobility is by incorporating groups or atoms that can induce a more ordered film structure. In this context, it has been well documented that molecules having sulphur atoms can improve charge transport through sulphur-sulphur interactions, generally represented in literature as S…S[137, 138]. Yanming *et al.,*[138] fabricated OFETs devices based on a single-crystalline micrometer wire of perylo[1,12-b,c,d]thiophene (PET) (see Figure 4.1a) which demonstrated p-type (hole) mobilities of up to 0.8 cm$^2$ V$^{-1}$ s$^{-1}$. More recently, Wei Jiang *et al.,*[139] synthesized a derivative of PET, dithioperylene (see Figure 4.1b), which had two sulfur atoms to facilitate better S…S interactions. The compound exhibited hole mobilities as high as 2.13 cm$^2$ V$^{-1}$ s$^{-1}$ in OFETs. These results show that S…S interactions can induce better packing in solid state which can lead to devices with high hole mobilities in OFETs. It was shown in Chapter 3 (section 3.3.1) that the mobilities of **OddDPP(ThFl)$_2$** measured in a diode configuration were three orders of magnitude lower than when used as the active layer in an OFET. It was therefore postulated that by incorporating sulphur atoms into the basic **OddDPP(ThFl)$_2$** would lead to an increase in the hole mobility.

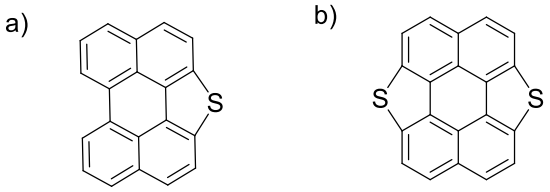


**Figure 4.1.** Chemical structures of a) PET, and b) Dithioperylene

Thus, the first synthetic target was the thione-analogue of **OddDPP(ThFl)$_2$**: the conversion of the carbonyl groups of fluorenones in **OddDPP(ThFl)$_2$** to thiones [**OddDPP(ThFlS)$_2$** (**4.1**) see Figure

4.2]. In addition, it has also been previously reported that compounds containing thiones usually exhibit a absorption bands in the visible region that are broader and considerably red-shifted compared to those of simple carbonyls[140].

In a second variation on the basic **OddDPP(ThFl)$_2$** structure it was decided to convert fluorenones carbonyl groups of **OddDPP(ThFl)$_2$** to dicyanovinylene moieties using malononitrile to give [**DPP(ThFlCN)$_2$** (**4.3**) see Figure 4.2]. It was proposed that addition of the dicyanovinylene groups would increase the EA of **OddDPP(ThFl)$_2$**, turning it from being an electron donor into an electron acceptor. It has been previously reported that, by incorporating dicyanovinylene groups into materials with high n-type (electron) mobilities are obtained in OFETs. For example, a compound comprised of dicyanovinylene groups incorporated at the distal ends of DPP(Th)$_2$ unit gave a material with good electron mobility of $\mu_e$ = 0.64 cm$^2$ V$^{-1}$ s$^{-1}$ [141]. Interestingly, in OPV devices compounds comprised of dicyanovinylene groups have been previously used as an electron acceptor as well as electron donors. For example, a molecule having dicyanovinylene group in conjunction with a dithienosilole-benzothiadiazole unit was reported gave a PCE of 1.43%[80] as an electron acceptor. In contrast, Wessendorf *et al*.,[142] reported series of compounds having oligothiophenes with dicyanovinylene at the ends and dithieno[3,2-b:2',3'-*d*] pyrrole (DTP) as the central unit. The material was used as electron donor with PC61BM as electron acceptor and the best device was reported to have PCE of 6.1%. The synthetic approaches to **4.1** and **4.2** are discussed in the following sections.

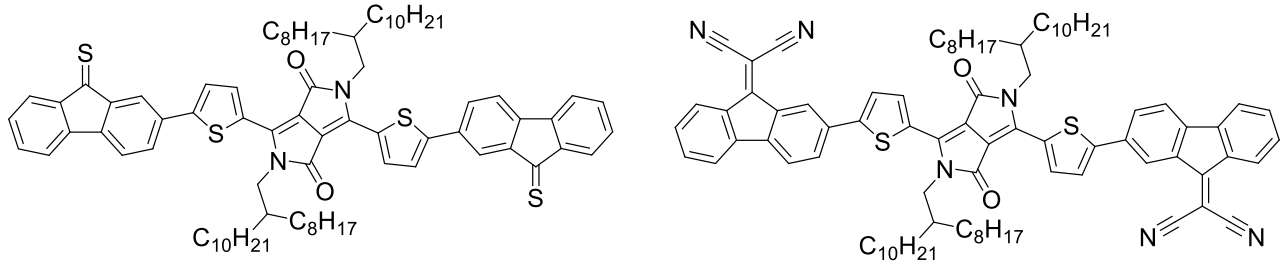


**Figure 4.2.** Chemical structure of **OddDPP(ThFlS)$_2$** (**4.1**), and **OddDPP(ThFlCN)$_2$** (**4.2**).

# 4.2 Synthesis of targets OddDPP(ThFlS)$_2$, and OddDPP(ThFlCN)$_2$

### 4.2.1 Synthesis of OddDPP(ThFlS)$_2$

A review of literature revealed that the carbonyl group of fluorenone are generally converted to the thione using one of two routes: i) reaction of fluorenone in methanol with a combination of hydrogen chloride and hydrogen sulphide[143], or ii) treatment of fluorenone with Lawesson's reagent in refluxing toluene or benzene[144]. The later method was chosen as hydrogen sulphide gas is a toxic, and an extremely flammable gas and hard to use than Lawesson's reagent. Toluene was chosen as the solvent due restriction on the use of benzene.

Conversion of **OddDPP(ThFl)$_2$** carbonyl groups to thiones was investigated with different equivalents of Lawesson's reagent [w.r.t to **OddDPP(ThFl)$_2$**]. First, **OddDPP(ThFl)$_2$** was reacted with 2 equivalents of Lawesson's reagent in toluene by heating at reflux for 3 hr (Scheme 4.1). After completion of reaction, the solvent was completely removed using in *vaccuo* and purified using column chromatography with a dichloromethane/light petroleum spirit mixture as eluent. Comparison of the Infrared spectrum of **OddDPP(ThFl)$_2$** and product showed that both the carbonyl stretching peak (1717 cm$^{-1}$) and carbonyl (amide) peak (1646 cm$^{-1}$) had gone (see Figure 4.3). In the literature[145] the thiocarbonyl stretch peak is reported to be at 1140 ± 80 cm$^{-1}$, although it is dependent on the neighbouring atoms to which the thione carbon atom is bonded[146]. Taking this into account the stretch at 1261 cm$^{-1}$ and 1119 cm$^{-1}$ were assigned to the thiocarbonyl and thioamide moieties. However, IR spectrum cannot provide a measure of the purity of the sample. However, $^1$H NMR experiment exhibited a complex spectrum (see Figure 4.4), suggesting the product was not pure. Further, purification using column chromatography failed to give any desired product in pure form.

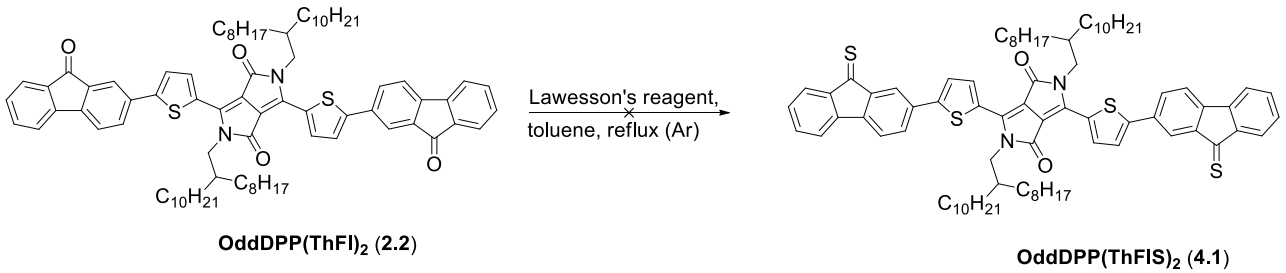


**OddDPP(ThFl)$_2$ (2.2)** **OddDPP(ThFlS)$_2$ (4.1)**

**Scheme 4.1.** Synthesis scheme to **OddDPP(ThFlS)$_2$** (**4.1**).

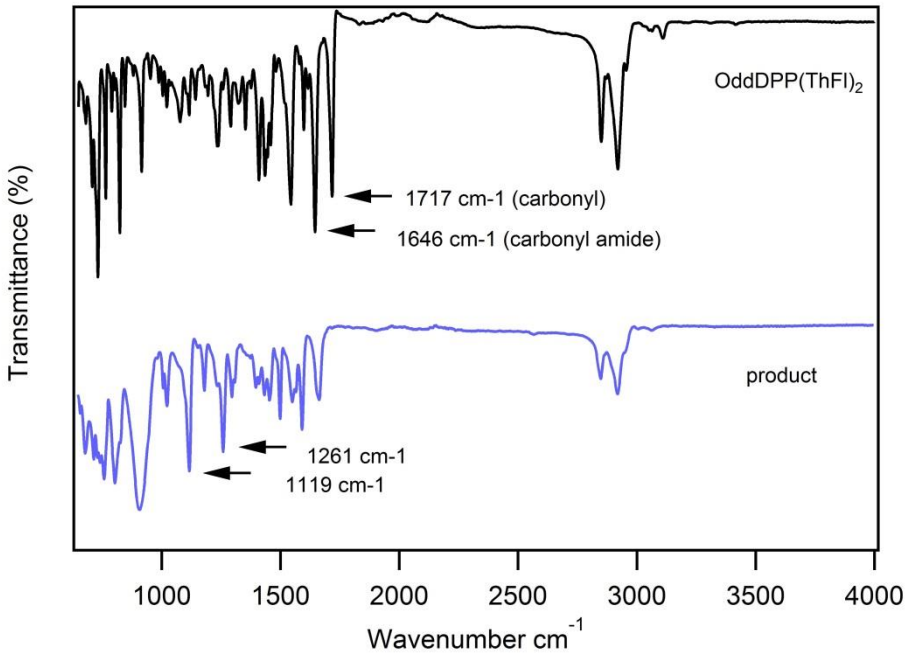


**Figure 4.3.** IR spectrum of the product for the reaction using 2 equivalents of Lawesson's reagent (blue).

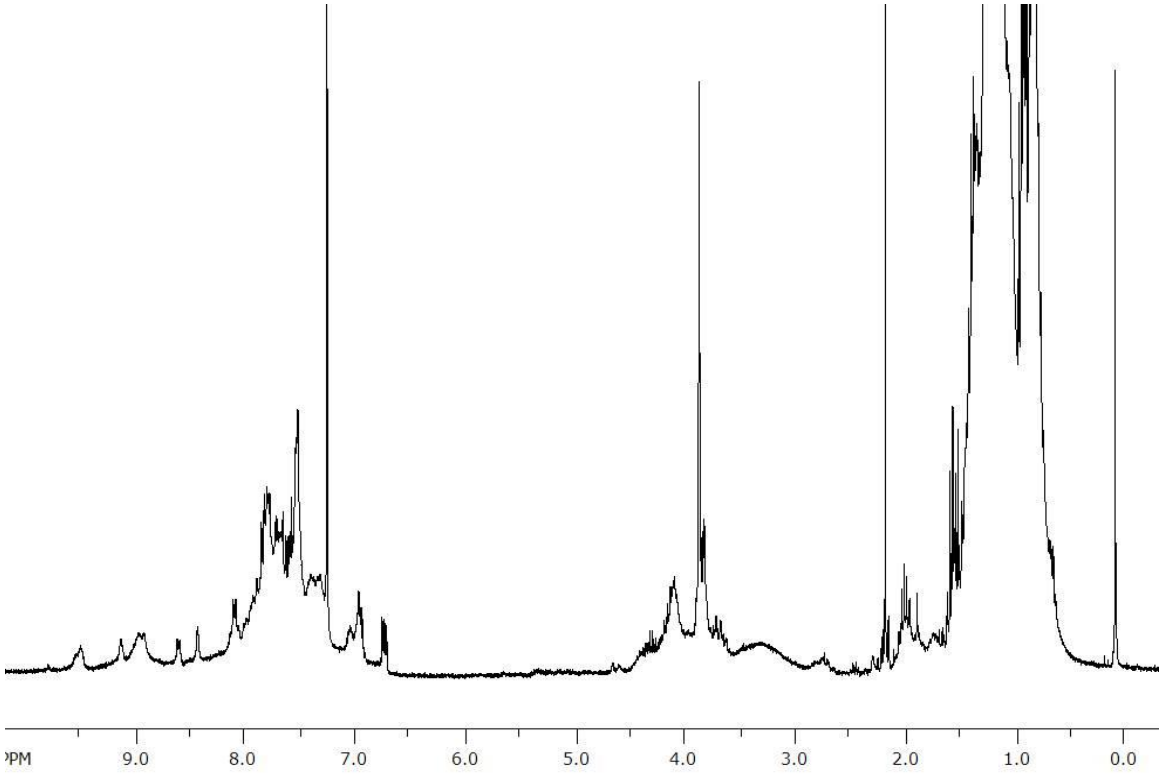


**Figure 4.4.** $^{1}$H NMR of the product for the reaction using 2 equivalents of Lawesson's reagent.

When of Lawesson's reagent is in solution it can exist in an equilibrium with a more reactive dithiophosphine ylides (**1,2**) (see Figure 4.5), which exists in two mesomeric forms (**1,2**). Both these forms can react with the carbonyl group to form the corresponding thione[147]. Hence, it is more likely that, when 2 equivalents of Lawesson's reagent were used, all the carbonyl groups of **OddDPP(ThFl)$_2$** were converted to thiones.

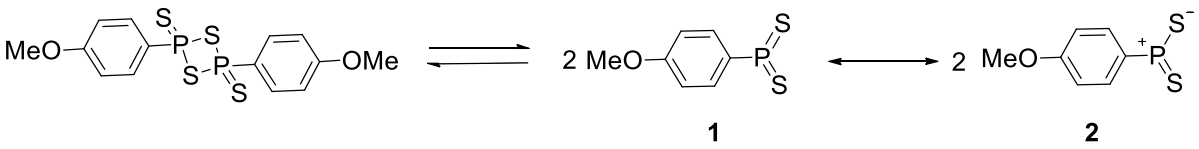


**1** **2**

**Figure 4.5.** Schematic diagram of Lawesson's reagent in solution in equilibrium with the ylides (**1,2**).

Considering that both the mesomeric forms of Lawesson's reagent can react with the carbonyl group, it is logical to consider that for conversion of two more electrophilic carbonyl groups on the fluorenone of **OddDPP(ThFl)$_2$** only 1 equivalent of the Lawesson's reagent would be sufficient. Hence, for the next reaction only 1 equivalent of Lawesson's reagent was used. Purification was carried out using flash column chromatography over silica. However, again from the $^1$H NMR experiment showed that the material was not pure. One of the reasons for not being able to purify the product using a silica column might be the instability of the thione groups to silica. In general, the silica used for column chromatography is lightly acidic and this combined with slightly wet solvents might hydrolyse the thione groups. Hence, purification by recrystallisation using a dichloromethane/light petroleum spirt mixture was attempted. However, this also proved unsuccessful.

Thiones are generally regarded as being unstable and not easy to obtain, but this relative instability also means that they react readily with large variety of reagents and, in this context, it is not surprising that they can undergo self-condensation in refluxing toluene to form bifluorenylidene [86]. The conditions used for the reactions is very much similar to one used for preparing bifluorenylidene. It is highly likely therefore that this may have resulted in the formation of many side products during the reaction, which would have made the purification of target molecule difficult.

### 4.2.2 Synthesis of OddDPP(ThFlCN)$_2$

The final derivatisation of **OddDPP(ThFl)$_2$** was the conversion of carbonyl groups to dicyanovinylene moieties, and was first investigated using Knoevenagel reaction conditions (Table 4.1). **OddDPP(ThFl)$_2$** was reacted with malononitrile, using piperidine as a base in dichloromethane heated at reflux for 12 h. An IR spectrum of the crude exhibited no peaks related to the nitrile, but, showed peaks corresponding to the carbonyl groups at 1717 cm$^{-1}$. The reaction as thus failed to give any of the desired product but the starting materials could recovered and hence the approach taken had to be reviewed. It has been reported that, fluorenone can also be converted to the dicyanovinylene derivatives by reacting with malononitrile and piperidine in ethanol[148] or by reacting malononitrile with fluorenone (without base) in *N*,*N*-dimethyl sulfoxide at 110 °C[149]. The first synthetic route is similar to the first one that was investigated. Hence, the *N*,*N*-dimethyl sulfoxide route was investigated. The **OddDPP(ThFl)$_2$** was therefore reacted with malononitrile in *N*,*N*-dimethyl sulfoxide and heated at 110 °C for 12 h. An IR spectrum again exhibited no peaks related to the nitrile. A reaction was then carried out under similar conditions using *N*,*N*-dimethyl sulfoxide at 110 °C, but, using piperidine as base. After few hours, the reaction mixture turned brownish yellow in colour, and $^1$H NMR of the crude (following work up but before purification) exhibited no presence of any aromatic protons, which suggests that the material had degraded under these conditions. There is only one report of direct conversion of an elaborated fluorenone to the equivalent containing dicyanovinylene. In this case the fluorenone was in conjugation with indeno[1,2-b]fluorene unit and was converted to dicyanovinylene groups using an excess of malononitrile along with pyridine and titanium tetra chloride in chlorobenzene. Hence, the next reaction was carried out using **OddDPP(ThFl)$_2$**, malononitrile with pyridine and titanium tetrachloride in chlorobenzene at room temperature. However, within a few minutes of addition of titanium tetrachloride, the reaction turned to a brownish yellow colour again and the analysis of the crude showed that the reaction failed to give any desired product (Table 4.1 provides a summary of the reaction conditions tried in the synthesis of **4.2**).

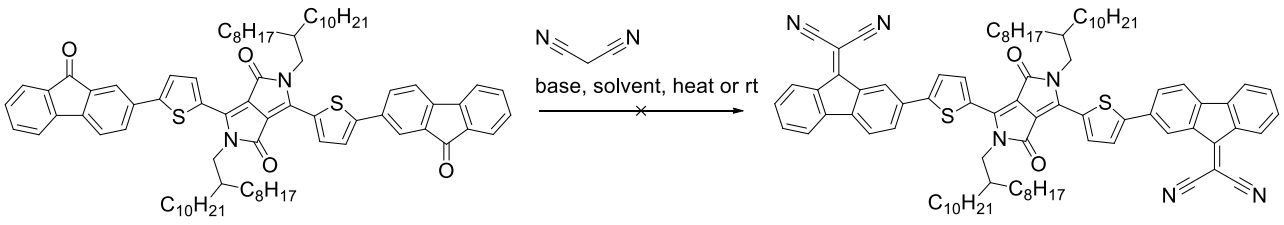


**OddDPP(ThFl)$_2$ 2.2** **OddDPP(ThFlCN)$_2$ 4.2**

**Scheme 4.2.** Synthesis scheme to **OddDPP(ThFlCN)$_2$** (**4.2**).

| Reactions | Base and reagent(s) | Solvent | Temperature | Result |
|---|---|---|---|---|
| 1 | piperidine and malononitrile | DCM[a] | reflux | starting material recovered |
| 2 | malononitrile | DMSO[b] | 110 °C | starting material recovered |
| 3 | piperidine and malononitrile | DMSO[b] | 110 °C | reaction mixture degraded |
| 4 | pyridine, malononitrile and titanium tetrachloride | Chlorobenzene | room temperature | reaction mixture degraded |

[a]dichloromethane, [b]*N*,*N*-dimethyl sulfoxide

**Table 4.1.** Summary of reactions carried out in an attempt to synthesize **4.2**.

### 4.2.3 Synthesis of OddDPP(ThFl(SS)$_2$)$_2$

Faced with difficulties in obtaining the thione derivative of **OddDPP(ThFl)$_2$** pure, it was decided to convert the carbonyl group to the corresponding dithiane. Dithiane groups can be used as protecting group for aldehyde and ketone groups. However, the effect of dithiane groups on the OPV device performance has never been investigated. It was thought that the four sulphur atoms would facilitate S…S interactions giving rise to strange interchromophore interactions.

In order to synthesize **4.3**, **OddDPP(ThFl)$_2$** was reacted with 1,3-propanedithiol and aluminium chloride in 1,2-dichloroethane (1,2-DCE) at 60 $^{o}$C (Scheme 4.3), according to the procedure reported by Ong *et al*.,[150]. The residue obtained after reaction was soluble in most common organic solvents and was purified using column chromatography to give **OddDPP(ThFl(SS)$_2$)$_2$** in a 79% yield. The ditihiane groups were stable on silica, thus enabling the product to be obtained in a good yield.

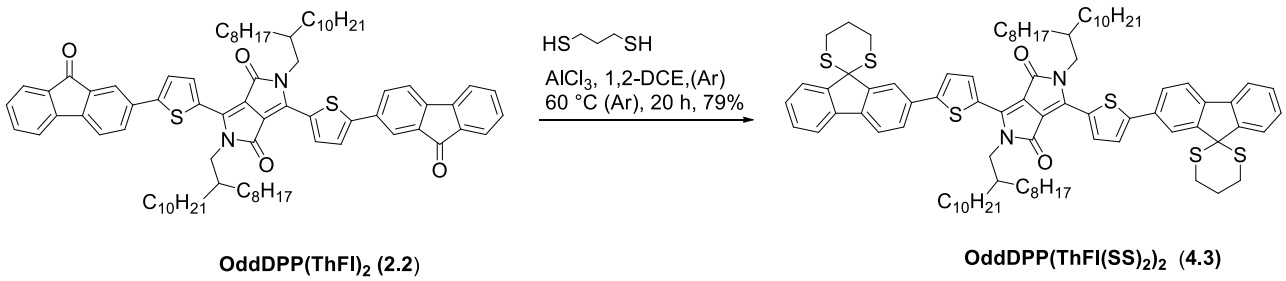


**OddDPP(ThFl)$_2$ (2.2)** **OddDPP(ThFl(SS)$_2$)$_2$ (4.3)**

**Scheme 4.3.** Synthesis scheme to **OddDPP(ThFl(SS)$_2$)$_2$** (**4.3**).

# 4.3 Physical properties of OddDPP(ThFl(SS)$_2$)$_2$

As only **OddDPP(ThFl(SS)$_2$)$_2$** (**4.3**) could be successfully synthesized and importantly, purified, the focus turned to its analysis of **4.3**.

### 4.3.1 Thermal properties

The stability to the thermal degradation of **OddDPP(ThFl(SS)$_2$)$_2$** was measured by TGA at a scan rate of 10 °C min$^{-1}$. Thermal decomposition temperature ($T_d$), with a 5% weight loss, occurred at 303°C (see Figure 4.6). Converting the fluorenone carbonyl groups of **OddDPP(ThFl)$_2$** (5% weight loss occurred at 399°C) to dithiane groups therefore lowers the $T_d$. It was found that, the first decomposition curve exhibited around 300 °C in TGA, corresponds to decomposition of the dithiane groups.

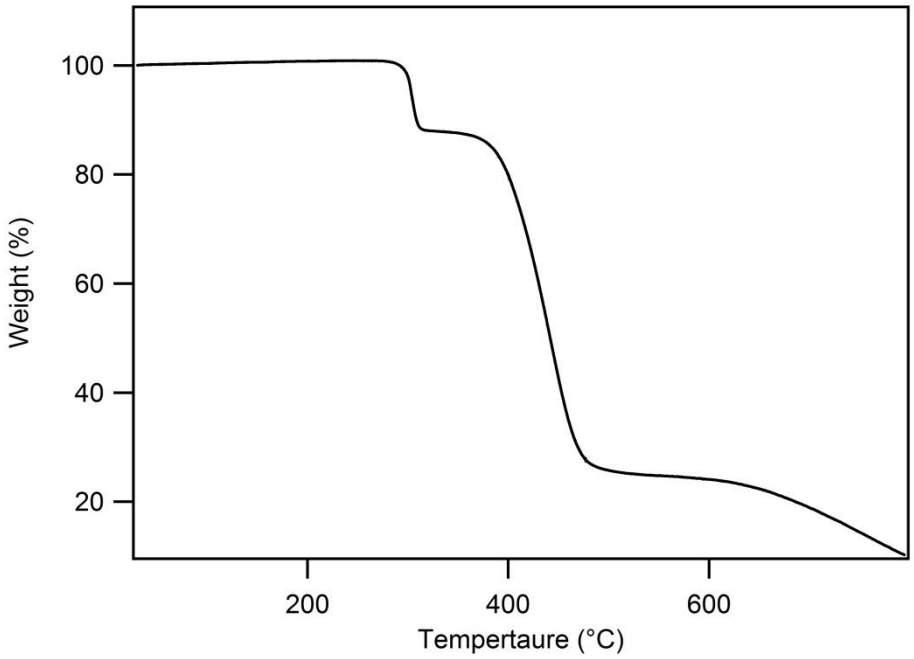


**Figure 4.6.** TGA traces for **OddDPP(ThFl(SS)$_2$)$_2$** at a heating rate of 10 $^{o}$C min$^{-1}$ under $N_2$.

DSC analysis of **OddDPP(ThFl(SS)$_2$)$_2$** sample at a scan rate of 100 $^{o}$C min$^{-1}$ showed an endothermic transition corresponding to melting point at 147 $^{o}$C, in the first heating scan. However, on cooling no crystallisation process was observed (see Figure 4.7). During second heating scan $T_g$ was observed at 52 $^{o}$C and the second cooling scan was identical to the first (at the same rate). The thermal properties of **OddDPP(ThFl(SS)$_2$)$_2$** are clearly different to the **OddDPP(ThFl)$_2$** which exhibited two crystallisation processes on cooling during the DSC measurements (see chapter 3, Figure 3.4). The fact that **OddDPP(ThFl(SS)$_2$)$_2$** forms an amorphous solid on rapid cooling from the melt suggests that the material would form an amorphous film when spin-coated as the solvent evaporation can be considered to attain rapid cooling. The inability of the film to reorganise on heating above the $T_g$ (there is no crystallisation peak) is expected to lead the material having poor charge carrier mobility.

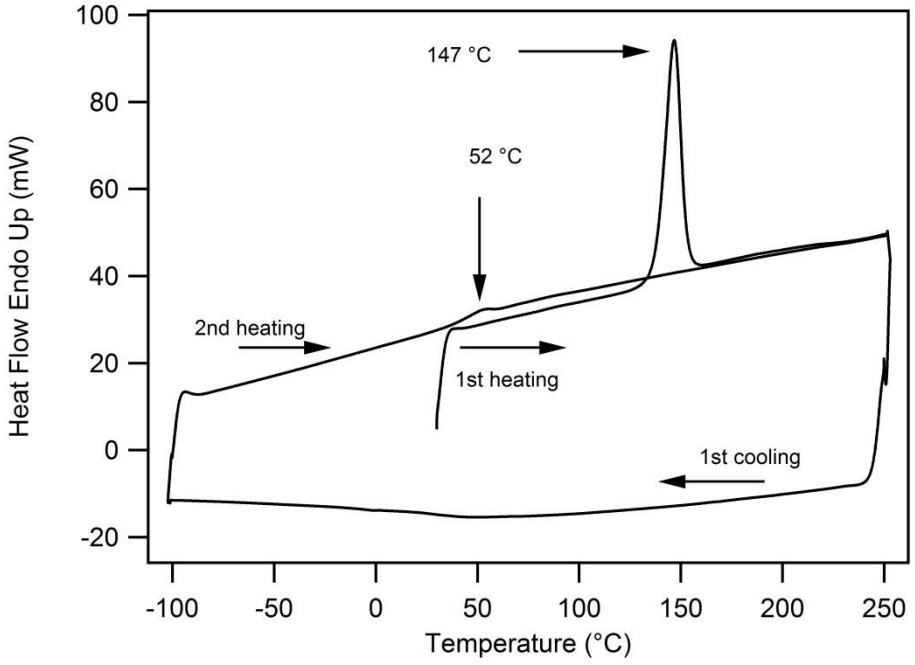


**Figure 4.7.** DSC traces for **OddDPP(ThFl(SS)$_2$)$_2$** at a scan rate of 100 $^{o}$C min$^{-1}$.

### 4.3.2 Optical and redox properties

The UV-Vis absorption spectra of **OddDPP(ThFl(SS)$_2$)$_2$** in dichloromethane and thin film are compared in Figure 4.8. In solution, **OddDPP(ThFl(SS)$_2$)$_2$** exhibited a similar absorption profile to **OddDPP(ThFl)$_2$**. **OddDPP(ThFl(SS)$_2$)$_2$** exhibited long wavelength absorption maxima at 615 nm and 578 nm with molar absorptivities of 60 000 M$^{-1}$ cm$^{-1}$ and 58 000 M$^{-1}$ cm$^{-1}$, respectively. In solid state for longest wavelengths, the **OddDPP(ThFl(SS)$_2$)$_2$** exhibited absorption maxima at 637 nm and 591 nm, which is slightly red-shifted compared with the material in solution. In general, a shift in absorption to longer wavelength and broadening of the absorption from the solution to solid states suggest, better planarisation of the molecule in solid state and/or strong intermolecular interactions. The weak red shift seen for **OddDPP(ThFl(SS)$_2$)$_2$** in moving from solution to solid state is consistent with the planarisation of the chromophore in solid state. However, in solid state, **OddDPP(ThFl)$_2$** had exhibited longer wavelength absorption maxima at 681 nm and 621 nm, in solid state, which suggest **OddDPP(ThFl)$_2$** exhibited better solid state planarisation compared with the dithiane derivative, **OddDPP(ThFl(SS)$_2$)$_2$**.

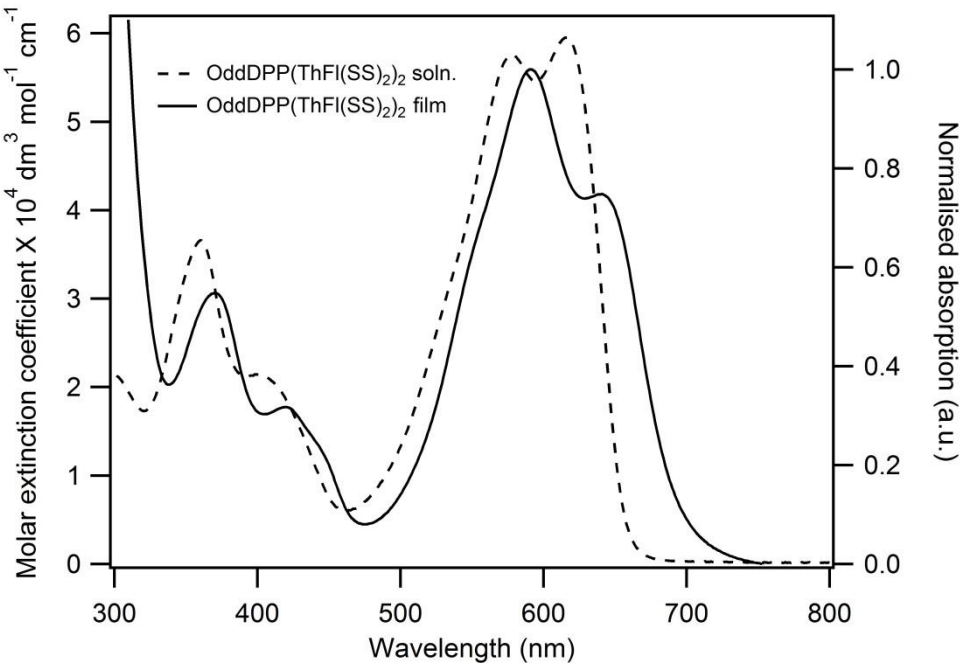


**Figure 4.8.** Solution (in dichloromethane) and neat film UV-Vis absorption of **OddDPP(ThFl(SS)$_2$)$_2$**.

| **Material** | $T_d$ **(°C)** | $T_g$ **(°C)** | $T_m$ **(°C)** | $\lambda_{max}$ **(nm) solution** | $\lambda_{max}$ **(nm) film** |
|---|---|---|---|---|---|
| **OddDPP(ThFl(SS)$_2$)$_2$** | 303 | 52 | 147 | 578, 616, 403, 361 | 591, 640, 420, 370 |

**Table 4.2**. Summary of TGA, DSC and absorption measurements of **OddDPP(ThFl(SS)$_2$)$_2$**.

In order to investigate the capability of **OddDPP(ThFl(SS)$_2$)$_2$** to facilitate charge generation, when blended with PC70BM as an acceptor, the relative positions of the IP and EA of the dithiane derivative need to determined: cyclic voltammetry. Using freshly dried and doubly distilled dichloromethane was used for both the oxidation and reduction measurements. Measurements were carried out with a 0.1M tetra-*n*butylammonium perchlorate electrolyte (TBAP) solution (see Figure 4.9). During the oxidation process, the **OddDPP(ThFl(SS)$_2$)$_2$** exhibited two chemically reversible oxidation at 0.5 V and 0.7 V. Using the same scan rate, a chemically reversible reduction was observed to occur at -1.6 V. The IP and EA were then estimated by adding the $E_{1/2}$ of the first oxidation and reduction with the offset in potential to the reported IP of ferrocene (4.8 eV)[121] to give **OddDPP(ThFl(SS)$_2$)$_2$** with an IP and EA of –5.3 eV and –3.2 eV, respectively. The IP of films of the materials were then measured using PESA, this gave an IP of -5.4 eV for

**OddDPP(ThFl(SS)$_2$)$_2$**. The IP and EA are essentially the same of **OddDPP(ThFl)$_2$**, –5.3 eV and –3.5 eV (IP measured using PESA and EA from optical gap), for IP and EA, respectively. Acknowledging that, these values are only a useful guide, the energy offset between **OddDPP(ThFl(SS)$_2$)$_2$** and PC70BM are considered sufficient for charge generation.

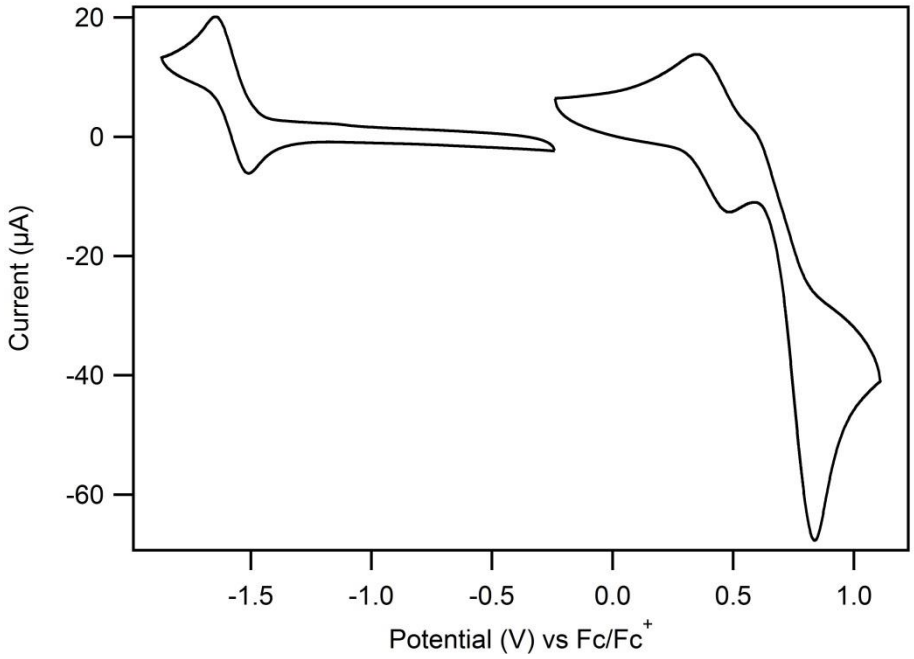


**Figure 4.9.** Cyclic voltammograms for **OddDPP(ThFl(SS)$_2$)$_2$** measured in dichloromethane solution under an argon atmosphere at a scan rate of 100 mV $s^{-1}$ with a glassy carbon working electrode.

## 4.4 Bulk Heterojunction OPV devices

Before fabricating the BHJ device, the effect of dithiane groups on the charge carrier mobilities would normally be investigated. However, neat films of sufficient quality for charge transport measurements in the diode configuration, e.g, MIS-CELIV technique, could not be formed and hence OPV devices were directly prepared and tested. The device architecture used as the following structure, ITO (100 nm)/MoOx (15nm)/ **OddDPP(ThFl(SS)$_2$)$_2$**:PC70BM/Ca (15 nm)/Al (100 nm) and the active layer thickness were around 50-70 nm. Building on the results from the study on **OddDPP(ThFl)$_2$** the devices were fabricated using different blend of **OddDPP(ThFl(SS)$_2$)$_2$**:PC70BM but always using in chloroform with 0.5% DIO as the processing solvent. The devices were fabricated and tested by Dr Hui Jin.

Different ratios (1:1, 1:2, 1:3, 1:4, and 2:3) of donor:acceptor blends were investigated. As shown in Figure 4.10, for **OddDPP(ThFl(SS)$_2$)$_2$**:PC70BM blend ratios of 1:1 and 2:3, the EQE spectra exhibited a flat-like shape, indicating the existence of both electron photoexcitation transfer (EPT) – Channel I and hole photoexcitaion transfer (HPT) – Channel II. When the acceptor (PC70BM) content was increased the peak around 380 nm and 600 nm turned to be higher and a spectral valley was shown around 440 nm, and the whole spectral shapes were to be similar with the absorption spectrum of PC70BM. The Maximum EQE spectrum was exhibited for 1:4 ratio of **OddDPP(ThFl(SS)$_2$)$_2$**:PC70BM, with an EQE value of 12% at 568 nm and more efficient HPT.

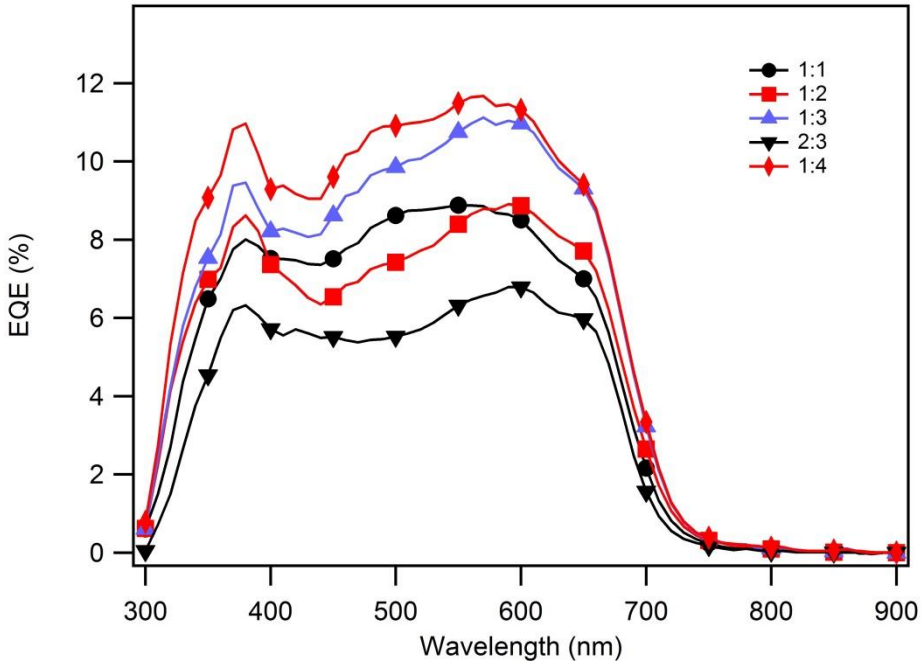


**Figure 4.10.** EQE spectra as a function of wavelength for different ratios of **OddDPP(ThFl(SS)$_2$)$_2$**:PC70BM blend devices.

The device efficiencies for the different blend ratios are summarised in Table 4.2. The devices fabricated from 1:1 and 1:2 ratios of **OddDPP(ThFl(SS)$_2$)$_2$**:PC70BM blend films exhibited similar $J_{sc}$ (see Figure 4.11). As the PC70BM content were further increased in the blend to 1:4, the device exhibited improvement in $J_{sc}$ to 1.5 ± 0.1 mA cm$^{-2}$ with a marginally lower Voc and FF (Table 4.3). This lead to device with a PCE of 0.4%, for a blend ratio of **OddDPP(ThFl(SS)$_2$)$_2$**:PC70BM. However, for a film with 2:3 blend ratio exhibited an increase in Voc to 0.90 ± 0.01 (V), but both $J_{sc}$ and FF was lower. The marginal increases in $J_{sc}$ of the film with 1:4 ratio of **OddDPP(ThFl(SS)$_2$)$_2$**:PC70BM suggest that, the blend had a favourable film structure to form

percolation pathway for both electrons and holes. The differences in the values are marginal and hence, should not be over interpreted.

| Blend ratio OddDPP(ThFl(SS)$_2$)$_2$:PC70BM | $J_{sc}$ (mA cm$^{-2}$) ±0.1 | $V_{oc}$ (V) ±0.01 | FF ±0.01 | PCE (%) ±0.01 |
|---|---|---|---|---|
| 1:1 | 1.2 | 0.80 | 0.28 | 0.30 |
| 1:2 | 1.1 | 0.82 | 0.31 | 0.30 |
| 1:3 | 1.3 | 0.80 | 0.33 | 0.40 |
| 2:3 | 0.9 | 0.90 | 0.24 | 0.20 |
| 1:4 | 1.5 | 0.78 | 0.32 | 0.40 |

**Table 4.3.** BHJ solar cell parameters for the devices with an active layers of **OddDPP(ThFl(SS)$_2$)$_2$** blended with PC70BM processed from chloroform containing 0.5% DIO.

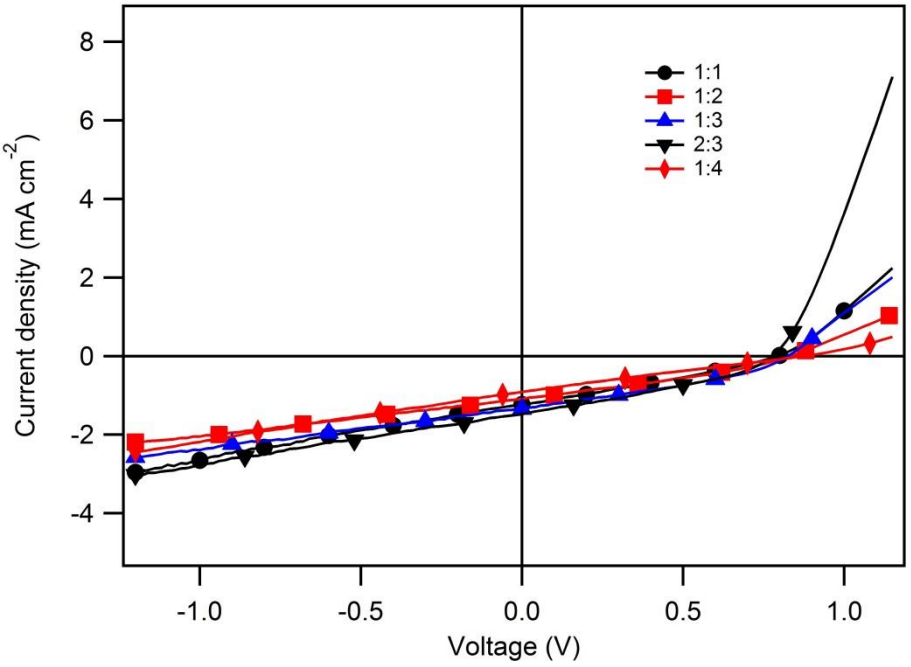


**Figure 4.11.** *J-V* curves of different ratios of **OddDPP(ThFl(SS)$_2$)$_2$**:PC70BM blend devices.

## 4.5 Conclusion

Although the conversion of carbonyl groups to thiones was not successful using Lawesson's reagent, the carbonyl group was successfully converted to the dithiane derivative (**OddDPP(ThFl(SS)$_2$)$_2$**) in high yields. Synthesis of **DPP(ThFlCN)$_2$** under Knoevenagel reaction conditions or using titanium tetrachloride as Lewis acid also failed to give the desired product. The thermal and optical properties of the dithiane derivative suggested weaker intermolecular interaction in film for **OddDPP(ThFl(SS)$_2$)$_2$** than **OddDPP(ThFl)$_2$**. The effect of the dithiane groups was to decrease the performance of OPV devices. The BHJ devices showed marginal improvement in $J_{sc}$ with increase in PC70BM content. However, the devices exhibited poor PCE, with the highest only being 0.40%.

# Chapter 5 – Synthesis, Physical, transporting and photovoltaic properties of OddDPP(ThBt)$_2$ derivatives

# 5.1 Introduction

Previously it has been thought that the photon absorption generates excitons only in the donor material and charge generation occurs only through the Channel I mechanism. However, recently it has been well established that both donor and acceptor can absorb light leading to charge generation through both Channels (I and II)[80, 151, 152]. In Chapter 3 it was found that for **OddDPP(ThBt)$_2$** for wavelengths above 700 nm charge generation was primarily through Channel I and wavelengths shorter than 700 nm both Channels were in play. Thus, PC70BM also played a significant role in light absorption and charge generation. However, PC70BM has a low excition coefficient in the visible region, which limits its ability to absorb light in thin films.

In order to improve the light absorption, one approach that has been taken by the research community is to engineering acceptor materials that have a larger excition coefficient in the visible region[83, 96]. It has also been demonstrated that by engineering an acceptor material to have complementary absorption with the donor material, the blend films can absorb over a wide range of wavelengths[80, 152]. In this context at COPE, a non-fullerene acceptor material [YF25 (see Figure 5.1)] was designed to have narrower optical gap than P3HT (2 eV) and high electron affinity[80]. The material was comprised of a dicyanovinyl-benzothiadiazole unit in conjugation with dithienosilole unit, and it exhibited a optical gap of 1.7 eV and an electron affinity of -3.7 eV. From the EQE and time-resolved microwave conductivity (TRMC) measurements it was demonstrated at wavelengths longer than 650 nm, the charge generation was solely through the Channel II mechanism.

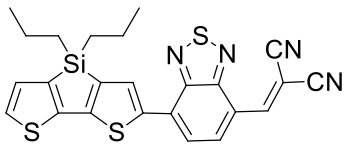


**Figure 5.1**. Chemical structure of YF25.

It was also shown in Chapter 3 that **OddDPP(ThBt)$_2$** that contained a 2,1,3-benzothiadiazole unit at had an optical gap of 1.9 eV and from cyclic voltammetry an EA of -3.3 eV. Although the energy offset between the electron affinity of **OddDPP(ThBt)$_2$** and P3HT (-3.0eV) should be sufficient for charge generation *via* Channel I, it is still considered lower. The EA of the fullerene acceptors PC60BM and PC70BM, have an EA of around -3.6 eV. By incorporating groups such as dicyanovinylene and *H*-indene-1,3(2*H*)-dione (1,3-indandione) groups, onto the **OddDPP(ThBt)$_2$** unit, it was anticipated that the resulting materials would have a narrower optical gap and larger EA,

with a view to them being used as Channel II materials with P3HT. Based on these ideas, the first target [**OddDPP(ThBt-DCV)$_2$** (**5.1**) see Figure 5.2] is comprised of dicyanovinylene groups atatched to the **OddDPP(ThBt)$_2$** unit. However, **OddDPP(ThBt-DCV)$_2$** lacked sufficient solubility in organic solvents to be solution processable for OPV device fabricated and hence, the second target had *n*-butyl-2-cyanoacetate groups [**OddDPP(ThBt-B2A)$_2$** (**5.2**) see Figure 5.2] attached to the **OddDPP(ThBt)$_2$** unit. The solubilising groups (*n*-butyl) in the ester moieties provided the solubility necessary for solution processing. Alkyl cynaoacetate groups have been previously reported in conjunction with 2,1,3-benzothiadiazole to increase the EA of the non-fullerene acceptors which gave OPV devices with a PCE of 0.21% with P3HT as the donor material[95]. The third target [**OddDPP(ThBt-1,3-ind)$_2$** (**5.3**) see Figure 5.2] was comprised of 1,3-indandione incorporated into the **OddDPP(ThBt)$_2$** unit. In OPVs, an acceptor material comprised of 1,3-indandione coupled with thiophene-fluorene unit gave a PCE of 2.4%[93].

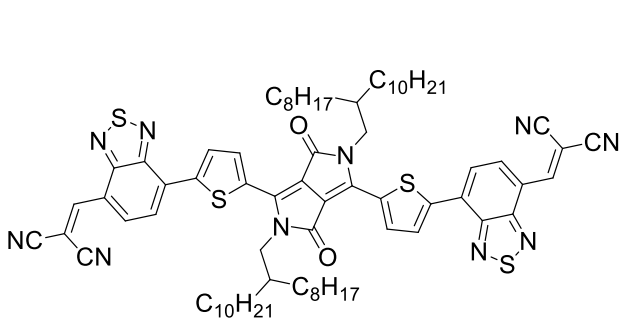


**OddDPP(ThBt-DCV)$_2$ (5.1)**

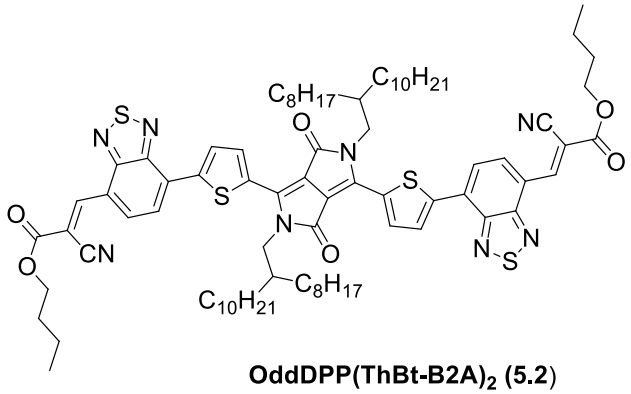


**OddDPP(ThBt-B2A)$_2$ (5.2)**

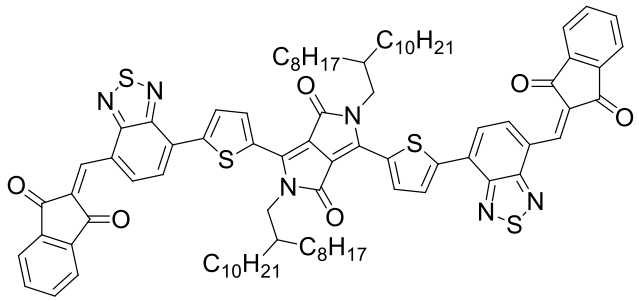


**OddDPP(ThBt-1,3-ind)$_2$ (5.3)**

**Figure 5.2.** Chemical structure of **OddDPP(ThBt-DCV)$_2$** (**5.1**), **OddDPP(ThBt-B2A)$_2$** (**5.2**), and **OddDPP(ThBt-1,3-ind)$_2$** (**5.3**).

Although **OddDPP(ThBt-DCV)$_2$** lacked sufficient solubility for solution processing, the thermal and optical properties of the material were investigated to compare the effect of incorporating dicyanovinylene groups on the **OddDPP(ThBt)$_2$** unit.

## 5.2 Synthesis of OddDPP(ThBt-CHO)$_2$ (5.11)

The key intermediate in the design strategy for the synthesis of new non-fullerene acceptor targets was the synthesis of [**OddDPP(ThBt-CHO)$_2$** (**5.11**)] (see Figure 5.3). The aldehyde moieties then enable the EA groups (dicyanovinylene, *n*-butyl-2-cyanoacetate, and 1,3-indandione) to be incorporated, under various condensation reaction conditions.

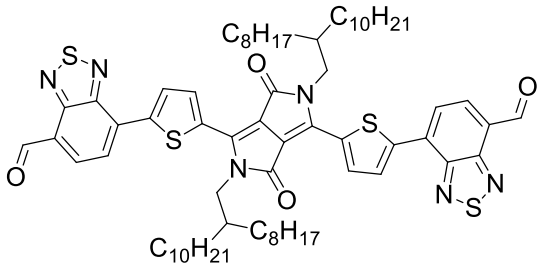


**OddDPP(ThBt-CHO)$_2$ (5.11)**

**Figure 5.3.** Chemical structure of **OddDPP(ThBt-CHO)$_2$** (**5.11**).

The initial step in the synthesis of **5.10**, which is required for the preparation of **5.11** was the reduction of commercially available 2-methyl-6-nitroaniline (**5.4**) to 3-methylbenzene-1,2-diamine (**5.5**) (Scheme 5.1). The reduction of aromatic nitro group to amine is generally carried out *via* activated metal[153, 154] such as zinc, iron, or tin, in the presence of an acid, or transition metal catalyzed hydrogenation[155] using Ni, Pd/C, and $PtO_2$. However, these methods require harsh conditions. One of the simplest methods that has been previously reported for converting nitro to amine is by reacting nitro compound with a mixture of aluminum metal and ammonium chloride in methanol and, sonicating the mixture at 35 KHz in a sonic bath maintained at 25 °C for 24 h[156]. Following the literature procedure **5.4** was reacted with aluminum foil and ammonium chloride in methanol. However, instead of sonicating the reaction mixture, the reaction was heated at reflux for 20 h to give **5.5** in a ~90%. The crude product was taken to the next step without purification.

The next, step in the synthesis was a ring closure reaction to form 4-methylbenzo[c][1,2,5]thiadiazole (**5.6**) (Scheme 5.1). A review of literatures revealed that the most commonly employed methods for preparation of **5.6** is by slow addition of thionyl chloride or thionylaniline to a solution of **5.5** in benzene followed by steam distillation of the product[157]. Thionyl chloride was readily available and dichloromethane was used instead of benzene as it is less toxic and can be readily removed at low temperature. Hence, to a solution of **5.5** and triethyl

amine in dichloromethane, thionyl chloride was added dropwise and heated at reflux for 3 h before being allowed to cool down to room temperature (Scheme 5.1). After completion of the reaction dichloromethane was first distilled out at atmospheric pressure to reduce the volume by one third. Then to that water was added and stirred. After quenching with water the product was collected by steam distillation at 140 °C (oil bath temperature) to give **5.6** in a 46% yield, for the two steps.

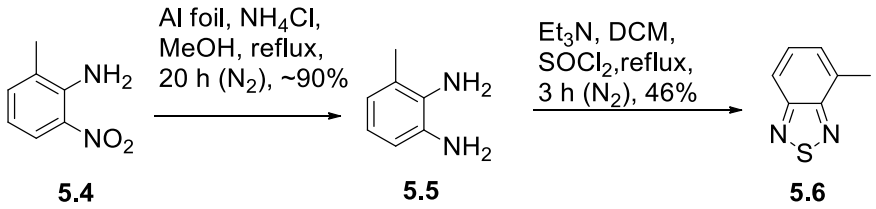


**5.4** **5.5** **5.6**

**Scheme 5.1.** Synthetic scheme to **5.5** and **5.6**.

The subsequent step required selective bromination at the 7-position of **5.6** to get **5.7**. However, bromination of **5.6** using bromine and hydrobromic acid (37%) gave a mixture of products **5.7** and **5.8** (Scheme 5.2). The reason for obtaining mixture of products was the excess use of bromine (w.r.t to **5.6**), which resulted in bromination at benzylic carbon to give **5.8**. Bromination at benzylic carbon of **5.6** has been previously reported when bromine was used in excess[158]. As the next step was to be bromination at benzylic carbon to get **5.9**, the mixture of **5.7** and **5.8** was taken to the next step without purification. In general benzylic bromination is carried out using *N*-bromosuccinimide (NBS) with a radical initiator in chlorinated solvents[159]. Hence, NBS was used as brominating agent with 1,1'-azobis(cyclohexanecarbonitrile) (ABCN) as a radical initiator in chlorobenzene to give **5.9** in a 52% yield, for the two steps (Scheme 5.2).

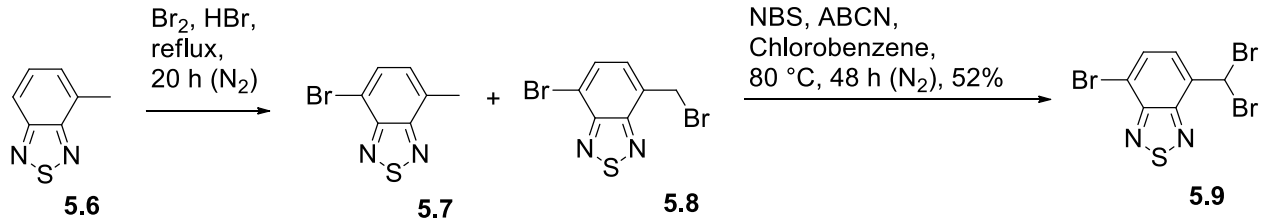


**5.6** **5.7** **5.8** **5.9**

**Scheme 5.2.** Synthetic scheme to **5.9**.

The final step to **5.10** was the hydrolysis of dibromomethyl group of **5.9** to give the aldehyde. This was achieved by treating **5.9** with sodium acetate in acetic acid at reflux to give **5.10** in a 64% yield (Scheme 5.3).

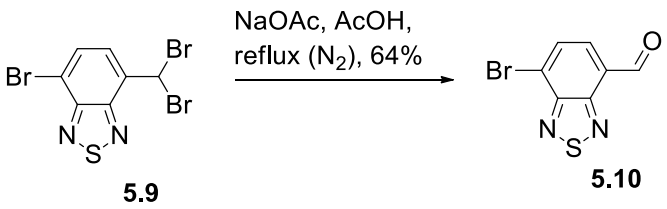


**5.9** **5.10**

**Scheme 5.3.** Synthesis scheme to **5.10**.

With, sufficient **5.10** in hand the next step was the attachment of **5.10** onto the **OddDPP(Th)$_2$** unit. It was shown in chapter 2 that under direct arylation reaction conditions the 2,1,3-benzothiadiazole unit could be connected to the **OddDPP(Th)$_2$** unit. Based on that result a test reaction was carried out with **5.10** and **OddDPP(Th)$_2$** using potassium carbonate as base and palladium acetate as catalyst in *N*,*N*-dimethylacetamide (DMA) (Scheme 5.4). However, the yield was low (30%). The drawbacks of direct arylation reactions are the possible side reactions such as homocoupling and functional group interference[117].

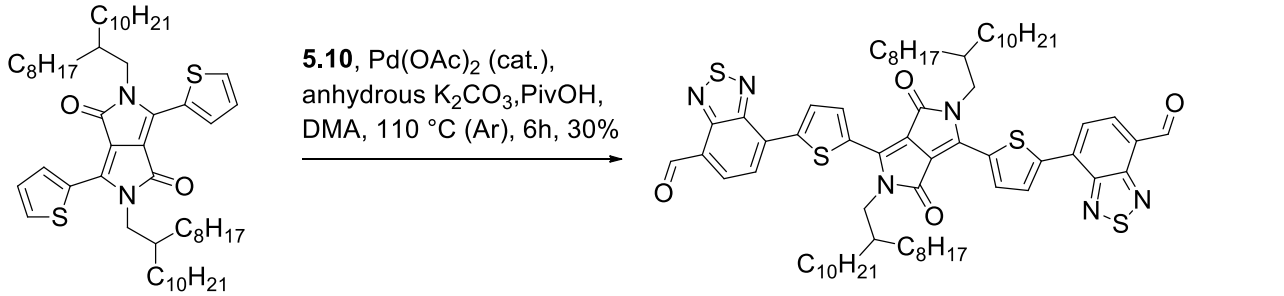


**2.17** **OddDPP(ThBt-CHO)$_2$ (5.11)**

**Scheme 5.4.** Synthesis scheme to **OddDPP(ThBt-CHO)$_2$** (**5.11**).

To investigate the effect of functional group interference on the yield; the aldehyde group on **5.10** was protected using ethane-1,2-diol. This was achieved by reacting **5.10** with an excess of the ethane-1,2-diol with p-toluenesulfonic acid as acid catalyst in toluene under Dean-Stark conditions to give **5.12** in an 86% yield (Scheme 5.5).

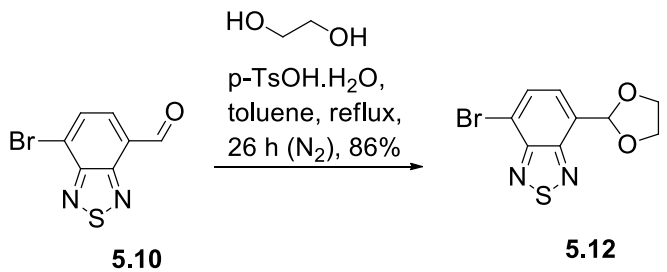


**5.10** **5.12**

**Scheme 5.5.** Synthesis scheme to **5.12**.

**5.12** was then reacted with **OddDPP(Th)$_2$** under direct arylation reaction conditions and the reaction went to completion in 6h to give a **5.13** (Scheme 5.6). It was anticipated that the cyclic acetal group might hydrolyze on the silica during purification and since, the next step was the hydrolysis of acetal groups to give **OddDPP(ThBt-CHO)$_2$** the product was taken to next step without further purification. **5.13** was treated with 2 M hydrochloric acid in tetrahydrofuran heated at reflux to give **OddDPP(ThBt-CHO)$_2$** as dark green solid in an 89% yield, for the two steps (Scheme 5.6). The high yield obtained when the aldehyde group was protected under the direct arylation reaction suggests that the low yield in the previous reaction (Scheme 5.6) is due to the aldehyde group interference.

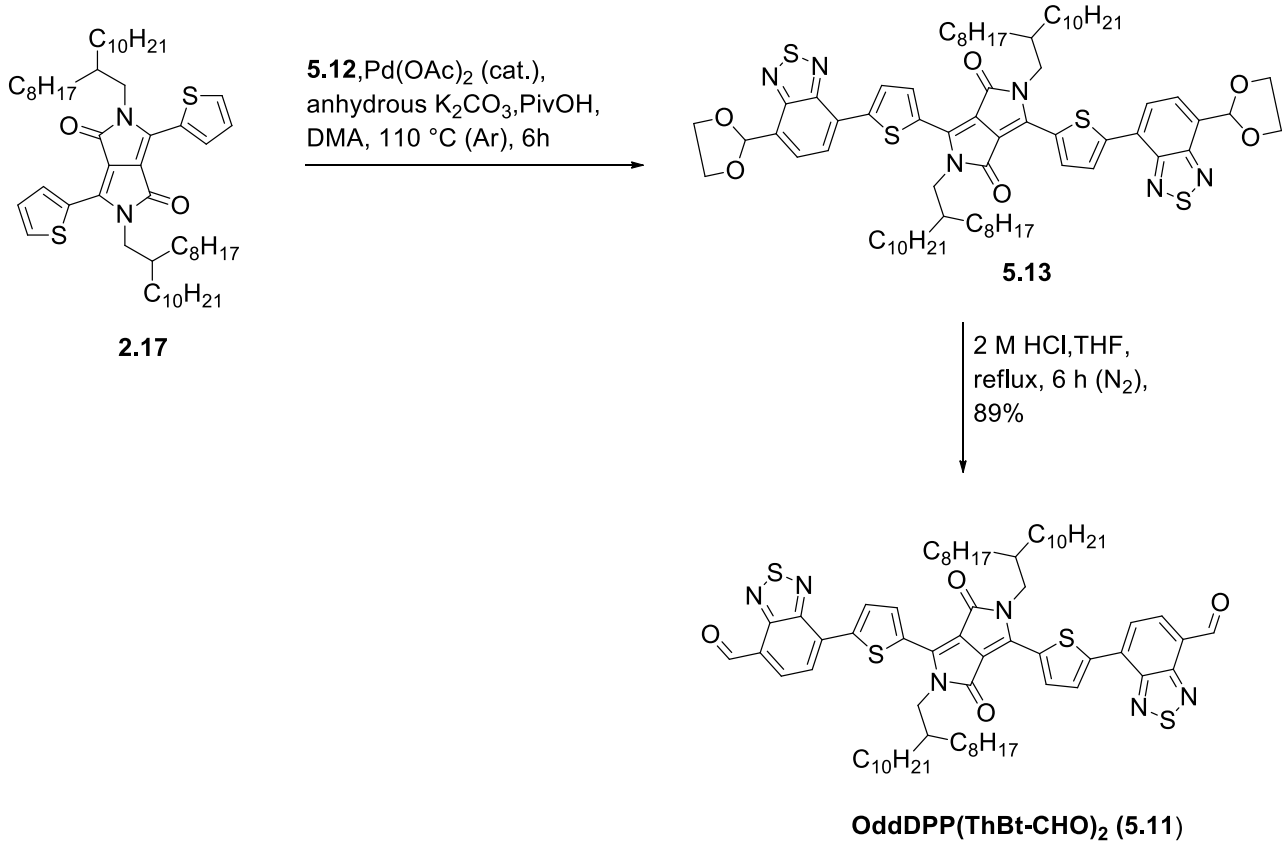


**Scheme 5.6.** Second route to **OddDPP(ThBt-CHO)$_2$** (**5.11**).

## 5.3 Synthesis of targets OddDPP(ThBt-DCV)$_2$, OddDPP(ThBt-B2A)$_2$, and OddDPP(ThBt-1,3-ind)$_2$

With sufficient **OddDPP(ThBt-CHO)$_2$** in hand, the next step was the synthesis of target molecules using condensation reaction conditions. The first target, **OddDPP(ThBt-DCV)$_2$** was synthesized by reacting **OddDPP(ThBt-CHO)$_2$** with excess malononitrile using pyridine as base in refluxing toluene heated at reflux. Purification of the product was first investigated using column chromatography over silica. During purification, the product was collected in a 10 cm$^3$ and the $^1$H NMR of each fraction was carried out. It was found that only in the first fraction was the product was pure (6%) with the other fractions, the $^1$H NMR indicating that that some of the dicyanovinylene groups have hydrolysed back to the aldehyde (see Figure 5.4, δ 10.7 ppm). Since, on silica some of the dicyanovinylene groups were found to have hydrolysed, further purification was carried out by recrystallisation. The recrystallisation was carried out first using ethanol/dichloromethane mixture and then with a toluene/ethanol mixture. However, in both experiments the product could not be isolated pure with a small aldehyde proton always observed in the $^1$H NMR spectrum.

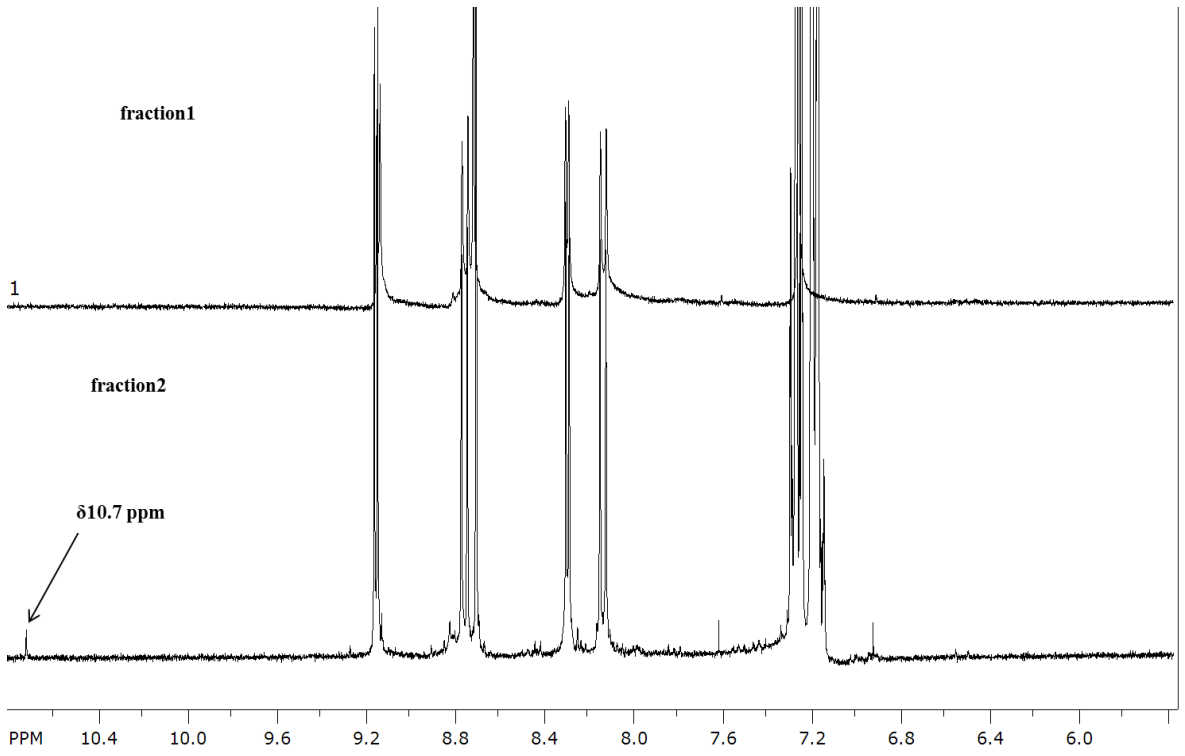


**Figure 5.4.** $^1$H NMR spectrum of fraction 1 and fraction 2 of **OddDPP(ThBt-DCV)$_2$**.

Fortunately, it was found that by re-subjecting the impure product under Knoevenagel reaction conditions the dicyanovinylene groups can be regained. Hence, the impure product was reacted with malononitrile and pyridine in toluene heated at reflux. After completion of the reaction the solvent, base and excess malononitrile were removed by short path distillation at 110 °C under vacuum (~0.2 mbar). Under these conditions $^1$H NMR spectrum showed that the product was pure and was obtained in a 59% yield (Scheme 5.7).

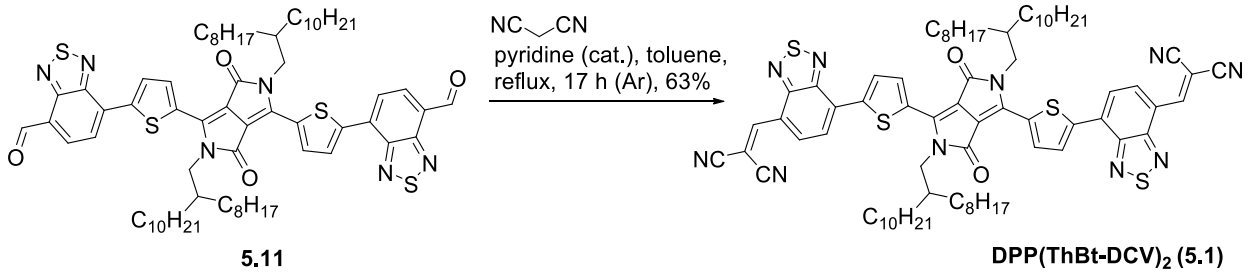


**Scheme 5.7.** Synthesis scheme to **OddDPP(ThBt-DCV)$_2$** (**5.1**).

The second target, **OddDPP(ThBt-B2A)$_2$**, also was synthesized using knoevenagel like conditions. **OddDPP(ThBt-CHO)$_2$** was reacted with *n*-butyl-2-cyanoacetate using piperidine as the base in toluene heated at 80 ºC (Scheme 5.8). Purification over silica was first attempted but, to avoid hydrolysis of the *n*-butyl-2-cyanoacetate groups on the silica, the column was neutralized by flushing with 5% triethyl amine in petroleum spirit three times before the column was finally flushed with neat petroleum spirit. Purification was then was achieved using a 3:2 ratio of chloroform/light petroleum spirit mixture as eluent, and the product was obtained in a 31% yield.

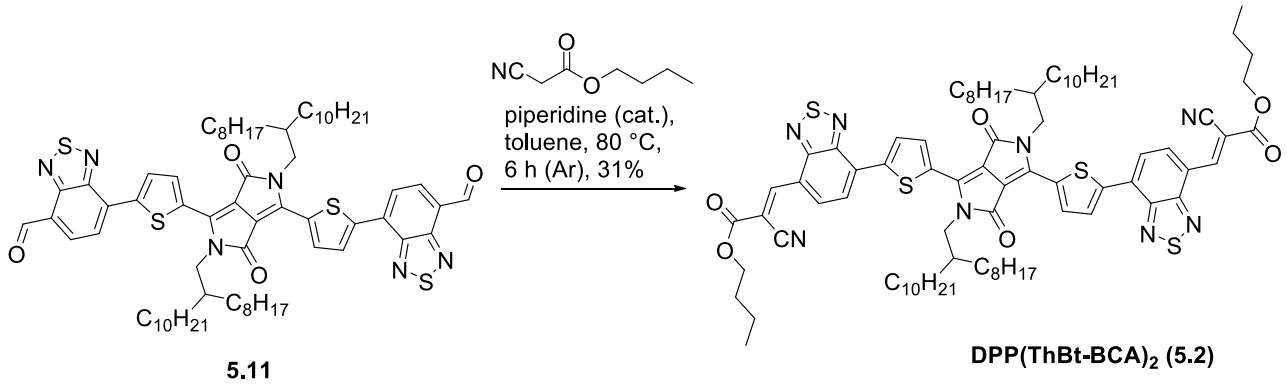


**Scheme 5.8.** Synthesis scheme to **OddDPP(ThBt-B2A)$_2$** (**5.2**).

The final target was proposed to have 1,3-indandione units attached to the **OddDPP(ThBt)$_2$**. With first two targets products successfully synthesized using pyridine or piperidine as the base in a toluene similar approach was taken for the preparation of **5.3**. **OddDPP(ThBt-CHO)$_2$** was reacted with 2.1 equivalents commercially available 1,3-indandione using pyridine as the base in toluene heated at 80 ºC for 22 h (Scheme 5.9). Purification of the crude product was investigated by column over silica. However, no product was obtained and during purification, it was observed that the purple coloured products could not be isolated, as it was highly polar and could not be eluted. Since, the first two targets **5.1** and **5.2** were green in colour, it was expected that when 1,3-indandione was incorporated into **OddDPP(ThBt-CHO)$_2$**, the product would also be green in colour.

A review of literature revealed that 1,3-indandiones are generally reacted with aldehydes either using piperidine as base in *tert*-butyl alcohol[93] or using neat acetic anhydride at 90 °C[160]. However, it was found that **5.11** were not soluble in either in *tert*-butyl alcohol or acetic anhydride, even at elevated temperature. To improve the solubility in acetic anhydride a mixed solvent system with toluene was used. **OddDPP(ThBt-CHO)$_2$** was completely soluble in the toluene/acetic anhydride mixture but, again, no product was found and the starting material was recovered in a 30% yield.

A deeper search into the reactivity of 1,3-indandione under these conditions revealed that, they can undergo self-condensation when reacted with pyridine or acetic anhydride to give primarily 1-(indan-1,3-dione-2-ylidene)indan-3-one (bindone), and or tribenzo[*a*,*f*,*k*]trindenone (truxenequinone)[161] (see Figure 5.5). Under the reaction conditions that were investigated, 1,3-indandione would have undergone self-condensation more readily than it would react with **OddDPP(ThBt-CHO)$_2$** because the ketone would be more electrophilic than the aldehyde.

As the reaction with pyridine or acetic anhydride failed to give desired product, finally, a reaction was carried out without using either of these reagents (see Table 5.1). Based on a literature procedure were dicyanovinylene groups were added to the DPP(Th)$_2$ using aluminum oxide in dichloromethane it was decided to use similar reaction condition for the current substrate **5.11**. Chloroform was used as solvent due to the good solubility of **OddDPP(ThBt-CHO)$_2$**. **OddDPP(ThBt-CHO)$_2$** was reacted with 1,3-indandione and aluminum oxide in chloroform at room temperature. The reaction did not proceed at room temperature and hence the reaction mixture was heated at reflux. However, the reaction still did not proceed and only the starting materials were recovered.

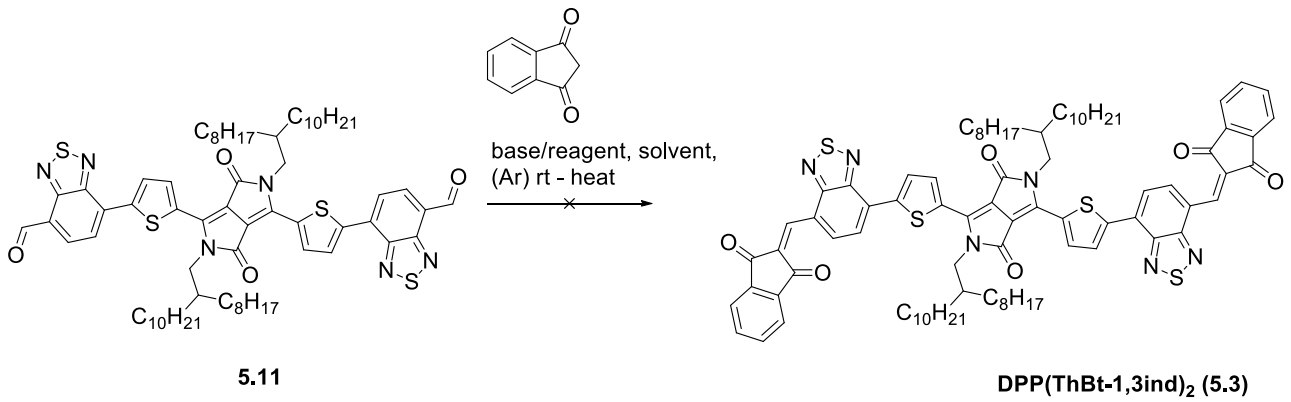


**Scheme 5.9.** Synthesis scheme to **OddDPP(ThBt-1,3ind)$_2$** (**5.3**).

| Reactions | Base/Reagent | solvent | Results |
|---|---|---|---|
| **1** | piperidine | toluene | No |
| **2** | acetic anhydride | toluene | No product was obtained and starting material was recovered in 30%. |
| **3** | $Al_2O_3$ | chloroform | Starting material were recovered in 90% yield |

**Table 5.1.** Summary of different reaction conditions investigated for synthesis of **5.3**.

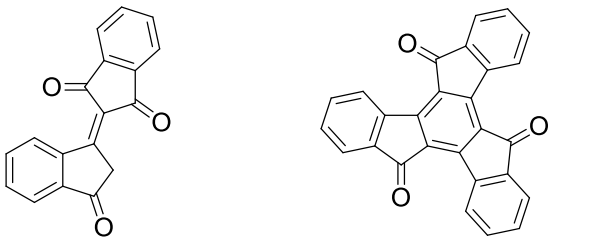


**Figure 5.5.** Chemical structure of bindone and truxenequinone.

Given the lack of reactivity of 5.11 with the indone this part of the project was stopped and characterisation of the two new materials was undertaken.

# 5.4 Physical properties

## 5.4.1 Thermal properties

The first measurements that were carried out on **OddDPP(ThBt-DCV)$_2$** and **OddDPP(ThBt-B2A)$_2$** were to determine the $T_d$ and whether they underwent any thermal phase transitions. **OddDPP(ThBt-DCV)$_2$** and **OddDPP(ThBt-B2A)$_2$** exhibited good thermal stability with 5% weight loss at 386 ºC and 343 ºC, respectively, under nitrogen. Comparison of $T_d$ of **OddDPP(ThBt)$_2$** and its derivatives (see Figure 5.6) shows that incorporation of the dicyanovinylene or *n*-butyl-2-cyanoacetate groups have lowered the thermal stability of the material. In particular, the $T_d$ was lowered by nearly 50 ºC with the incorporation of *n*-butyl-2-cyanoacetate groups. That been said the $T_d$s measured for are sufficiently high for them to be used in devices.

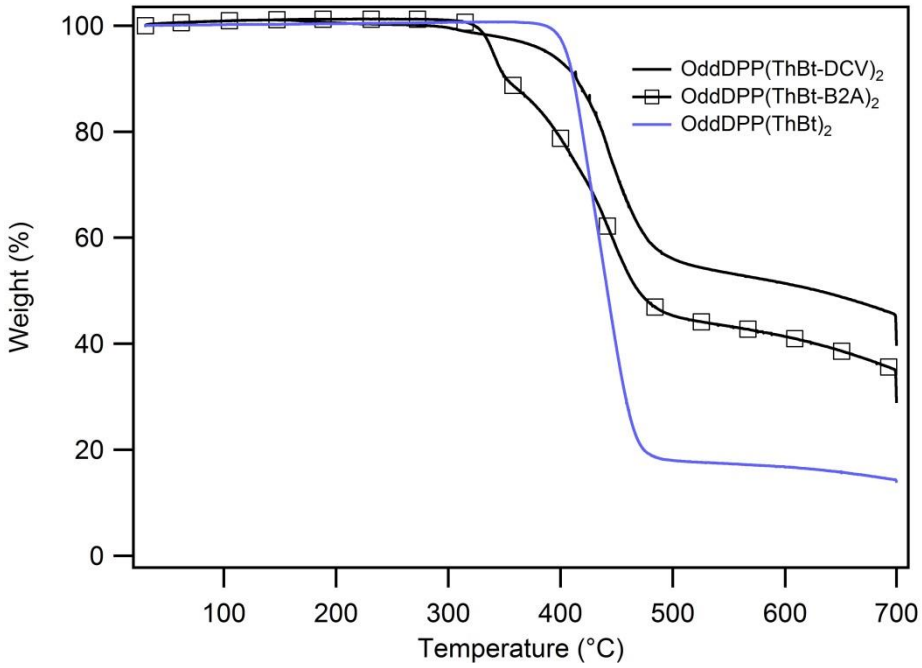


**Figure 5.6.** TGA traces for **OddDPP(ThBt-DCV)$_2$**, **OddDPP(ThBt-B2A)$_2$**, and **OddDPP(ThBt)$_2$** at 10 $^{o}$C min$^{-1}$ under $N_2$.

For **OddDPP(ThBt-DCV)$_2$** on the first heating scan a $T_g$ was observed at 192 ºC, followed by an endothermic transition corresponding to the melt at 258 ºC, at a scan rate of 100 ºC min$^{-1}$. On, cooling at the same scan rate crystallisation was observed to occur at 194 ºC (see Figure 5.7a). However, during the second heating and cooling scans no $T_g$ was observed and both the melt and $T_c$

was observed at slightly lower temperatures than the first scan (see Figure 5.7b). These results suggest that once the material is heated above the melting point then on colling it becomes a crystalline material. In comparison with the **OddDPP(ThBt)$_2$**, **OddDPP(ThBt-DCV)$_2$** exhibited similar phase transitions but, at higher temperatures. However, the difference in the scan rate for both experiments needs to be considered as well, as cooling rate can influence the phase tranisitons especially crystallisation process. The thermal properties of the **OddDPP(ThBt)$_2$** were measured at 10 ºC min$^{-1}$ while those of **OddDPP(ThBt-DCV)$_2$** were undertaken with a scan rate of 100 ºC min$^{-1}$.

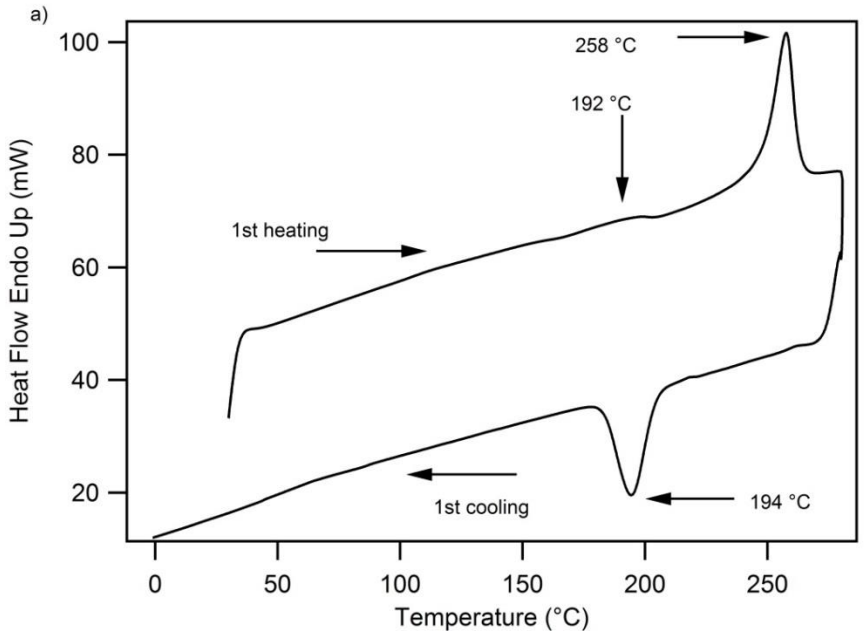


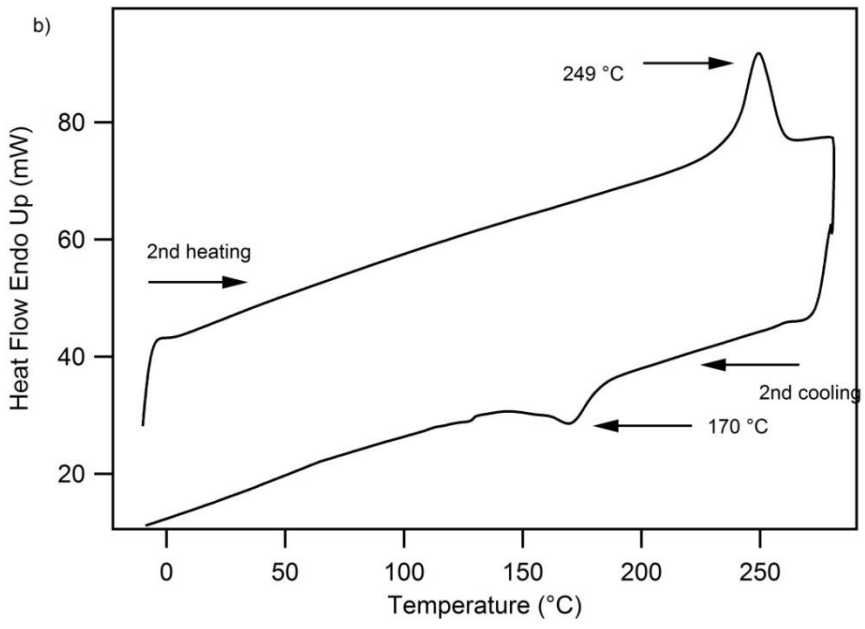

**Figure 5.7.** DSC traces for **OddDPP(ThBt-DCV)$_2$** a) 1st heating and cooling, and b) 2nd heating and cooling, at 100 $^{o}$C min$^{-1}$.

For the material having *n*-butyl-2-cyanoacetate groups **OddDPP(ThBt-B2A)$_2$** at the ends, different phase transition behaviour was observed by DSC scans. During the first heating scan at 100 ºC min$^{-1}$ an exothermic transition (crystallisation) at 186 ºC was observed, followed by an endothermic transition at 199 ºC, corresponding to a melt. On cooling only one $T_c$ was observed at 158 ºC (see Figure 5.8a). To investigate further regarding the different phase transitions that were observed during heating, the sample was heated and cooled at a different scan rates. The same sample when heated at a slow scan rate of 10 $^{o}$C min$^{-1}$, it exhibited similar crystallisation at 179 ºC followed by two endothermic transitions at 195 ºC and 197 ºC (see Figure 5.8b). However, at fast scan rate of 200 $^{o}$C min$^{-1}$, two endothermic transitions corresponding to the melt (179 ºC and 179 ºC) were observed (see Figure 5.8c), and no exothermic transitions were observed on heating. In contrast, during cooling under different scan rates only one $T_c$ was observed around ~158 ºC. These suggest that, the some of the material is not crystalline and it eventually crystallise when heated at slower scan rate (100 ºC and 10 ºC), but at a faster scan rate (200 ºC), it only shows melt. During the second and third heating and cooling scans at 100 ºC or 10 $^{o}$C min$^{-1}$, material exhibited identical phase transitions as the first.

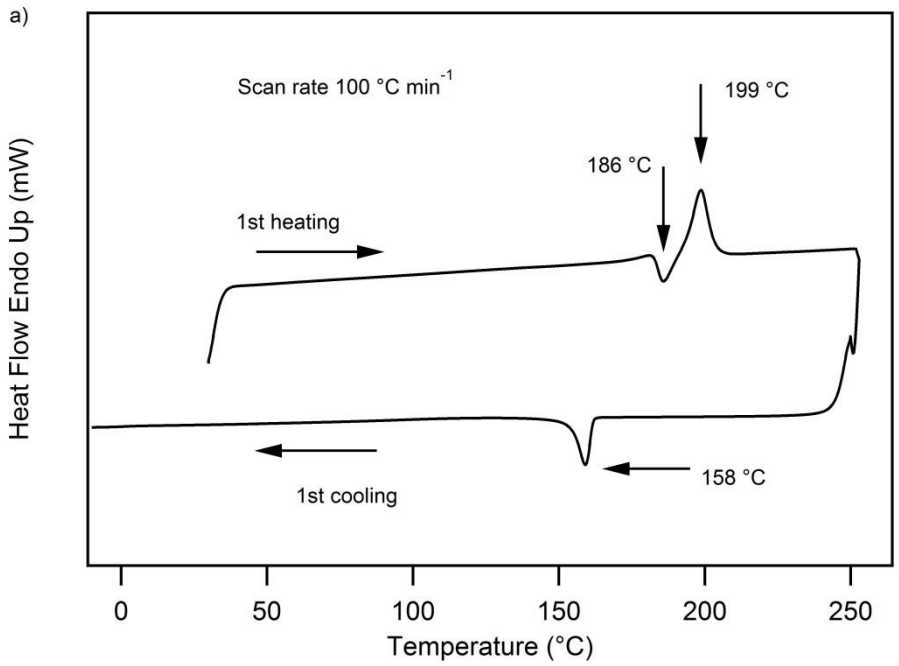

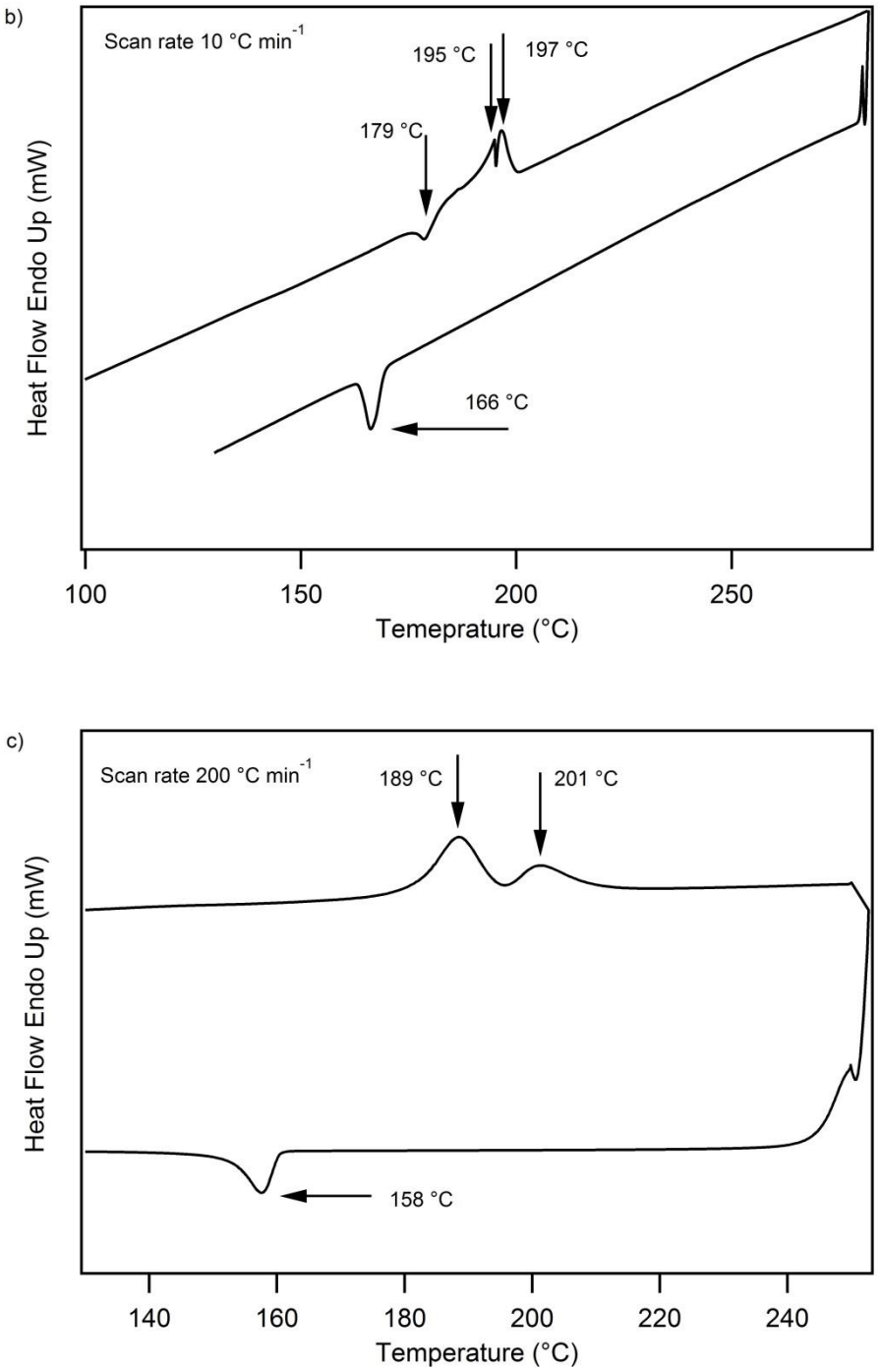


**Figure 5.8.** DSC traces for **OddDPP(ThBt-B2A)$_2$** at a) 100 $^{o}$C min$^{-1}$, b) 10 $^{o}$C min$^{-1}$, and c) 200 $^{o}$C min$^{-1}$.

| **Material** | $T_d$ **(°C)** | $T_g$ **(°C)** | $T_m$ **(°C)** | $T_c$ **(°C)** |
|---|---|---|---|---|
| **OddDPP(ThBt-DCV)$_2$** | 386 | 192 | 258 (1$^{st}$ heating), | 194(1$^{st}$ cooling), |

| | | | | |
|---|---|---|---|---|
| | | | 249 ($2^{nd}$ heating) | 170 ($2^{nd}$ cooling) |
| **OddDPP(ThBt-B2A)$_2$** | 343 | - | 199 | 186, 158 |

**Table 5.2**. Summary of TGA, DSC mesurments of **OddDPP(ThBt-DCV)$_2$** and **OddDPP(ThBt-B2A)$_2$**.

### 5.4.2 Optical properties

The UV-Vis-NIR absorption spectra of the DPP derivatives in chloroform and in thin films are shown in Figure 5.9. **OddDPP(ThBt-DCV)$_2$** and **OddDPP(ThBt-B2A)$_2$** exhibited absorption maxima at 703 nm and 680 nm in chloroform solution with molar absorption coefficient of 44 000 $M^{-1}$ $cm^{-1}$ and 53 000 $M^{-1}$ $cm^{-1}$, respectively. Incorporation of the dicyanovinylene groups lowered the molar absorption coefficient of **OddDPP(ThBt-DCV)$_2$** compared to **OddDPP(ThBt)$_2$** (48 000 $M^{-1}$ $cm^{-1}$ in dichloromethane). However, as the measurements were carried out in different solvents; the difference should not be over interpreted, especially if there is any charge transfer character. Incorporation of *n*-butyl-2-cyanoacetate groups onto **OddDPP(ThBt)$_2$** increased the molar absorption coefficient increased by 5 000 $M^{-1}$ $cm^{-1}$.

In solid state, **OddDPP(ThBt-DCV)$_2$** exhibited a significant shift to longer wavelength, around 150 nm, on both the onset and pear maximum of the absorption as well as the absorption being broadened. The strong shift in absorption maxima to longer wavelengths could come from planarisation or intermolecular interactions of the molecule in solid states, caused by incorporation of the dicyanovinylene groups. In comparison the maximum shifted by 119 nm in solid state absorption from the **OddDPP(ThBt)$_2$**. In contrast, incorporation of *n*-butyl-2-cyanoacetate groups, the maximum shifted to shorter wavelength by about 18 nm. This suggests less planarisation of the molecule, which might have arisen from by disordered caused by the *n*-butyl solubilising groups of the esters.

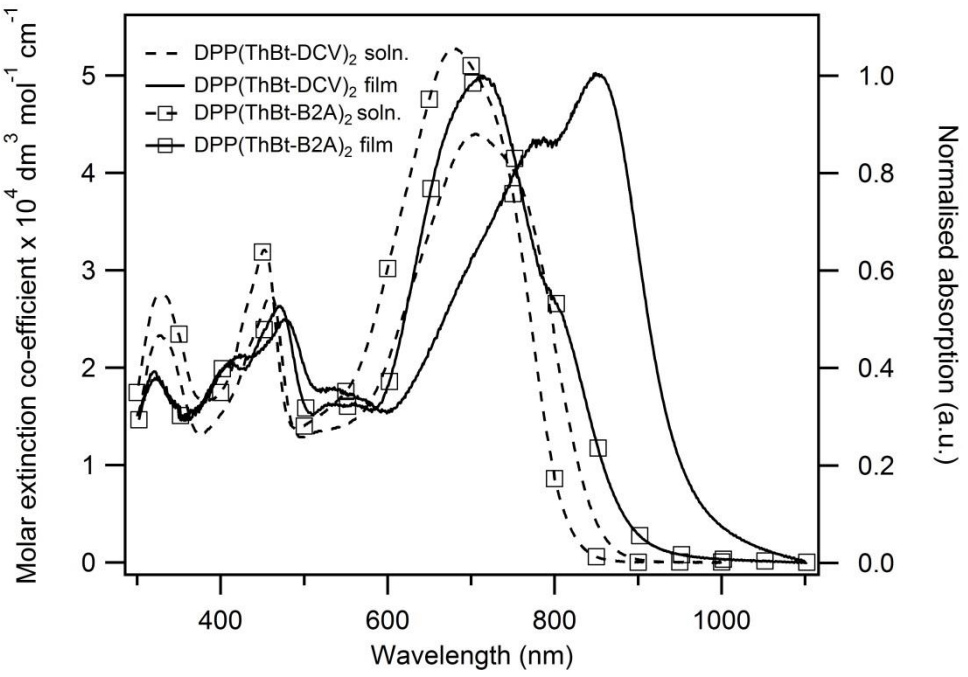


**Figure 5.9.** UV-Vis-NIR absorption spectra of **OddDPP(ThBt-DCV)$_2$** and **OddDPP(ThBt-B2A)$_2$** in solution and neat film.

| **Material** | **$\lambda_{max}$ (nm) solution** | **$\lambda_{max}$ (nm) film** |
|---|---|---|
| **OddDPP(ThBt-DCV)$_2$** | 765, 460, 329 | 853, 786, 478, 423, 324 |
| **OddDPP(ThBt-B2A)$_2$** | 680, 454, 330 | 799, 712, 469, 412, 319 |

**Table 5.3**. Summary of absorption measuments from solution (chloroform) and film of **OddDPP(ThBt-DCV)$_2$** and **OddDPP(ThBt-B2A)$_2$**.

A comparison of the normalized absorption spectrum of the **OddDPP(ThBt-B2A)$_2$** and P3HT (see Figure 5.10), suggest that above 700 nm, charge generation could only occur *via* the Channel II mechanism (i.e., hole transfer from the **OddDPP(ThBt-B2A)$_2$** to the P3HT). However, at wavelengths where both **OddDPP(ThBt-B2A)$_2$** and P3HT have absorption (700-400 nm) both Channels could play, depending on the relative IP and EA of the materials.

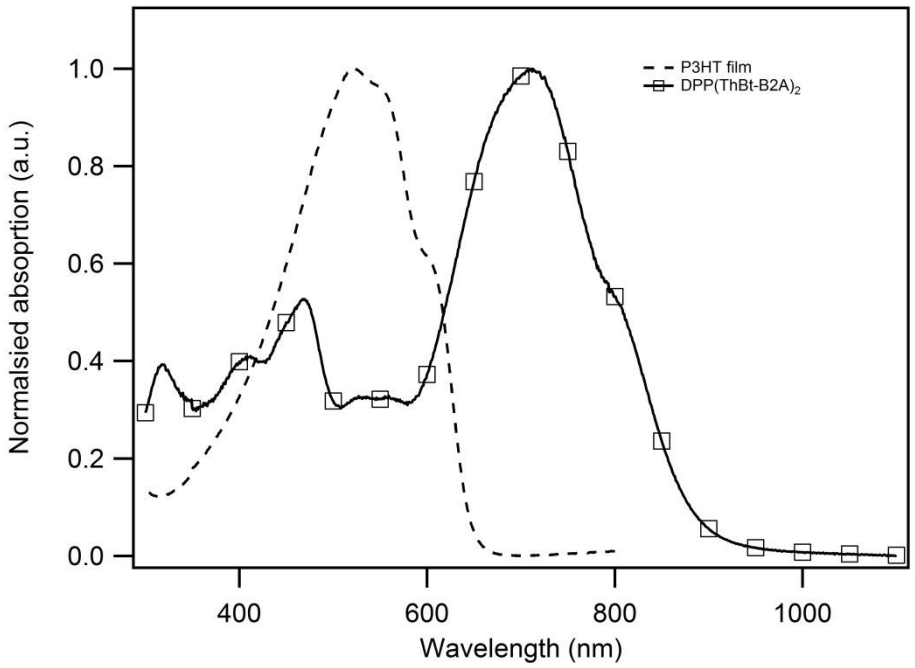


**Figure 5.10.** Thin film absorption spectrum of P3HT and **OddDPP(ThBt-B2A)$_2$** to compare the ranges of photon absorption.

### 5.4.3 Electrochemical studies

In order for a material to perform has an acceptor it requires the appropriate EA for charge generation, when blended with the donor material. Hence, the redox properties of the DPP derivatives had to be investigated. However, the **OddDPP(ThBt-DCV)$_2$** was not sufficiently soluble in dichloromethane or tetrahydrofuran to perform cyclic voltammetry (CV) measurements. **OddDPP(ThBt-B2A)$_2$**, was sufficiently soluble in dichloromethane and its redox properties studied using CV at a scan rate of 100 mV $s^{-1}$.

As a reminder **DPP(ThBt)$_2$** exhibited only two chemically reversible oxidation and reduction potentials at $E_{1/2}$ = 0.4 V and 0.7 V and -1.5 V and -1.8 V, respectively (see Chapter 3, section 3.2.3), and the HOMO (IP) and LUMO (EA) was estimated to -5.2 eV and -3.3 eV. However, **OddDPP(ThBt-B2A)$_2$** which has the electron withdrawing *n*-butyl-2-cyanoacetate groups, exhibited two chemically reversible oxidation and three chemically reversible reductions (see Figure 5.11) at $E_{1/2}$ = 0.5 V and 0.8 V and -1.0 V, -1.4 V and -1.7 V, respectively. The IP and EA were calculated from the $E_{1/2}$ of the first oxidation and reduction values and are reported against the ferrocence/ferrocenium couple (see Table 5.2). Thus **OddDPP(ThBt-B2A)$_2$** has a significantly higher EA than **OddDPP(ThBt)$_2$** but they have similar IPs.

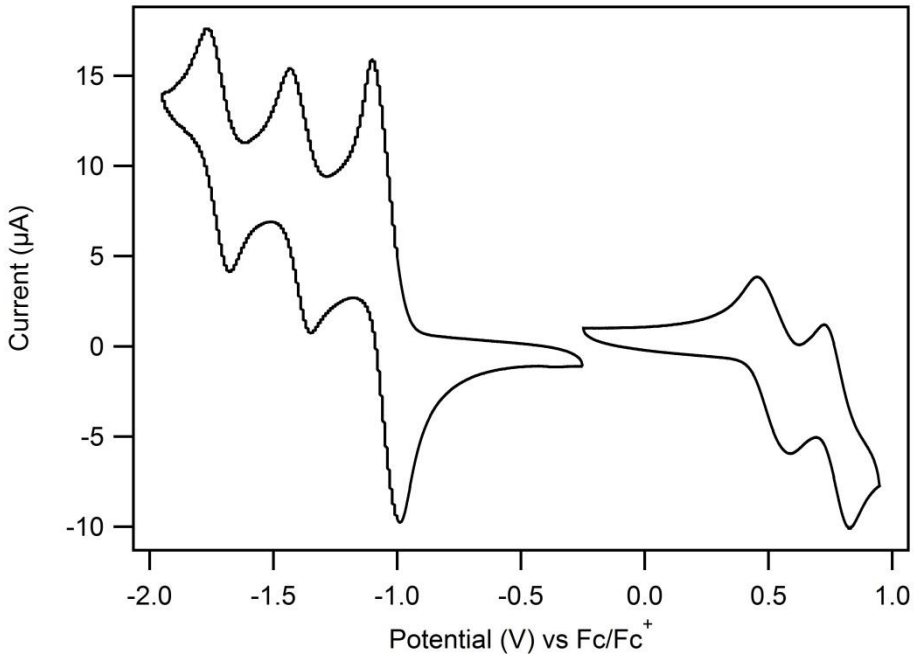


**Figure 5.11.** Cyclic voltammograms for **OddDPP(ThBt-B2A)$_2$** measured in dichloromethane under an argon atmosphere at a scan rate of 100 mV $s^{-1}$ with platinum as the working electrode.

A thin film of **OddDPP(ThBt-B2A)$_2$** as fabricated by spin-coating from chloroform onto a glass substrate. The IP of the material was then measured using Photoelectron Spectroscopy in air (PESA), from their thin films. The measurement was undertaken by Dr. Dani Stoltzfus. The measurement gave an IP values of -5.7 eV for **OddDPP(ThBt-B2A)$_2$**. Again it is important to note the difference between the IP determined by the two methods.

| **Materials** | **CV** | | **PESA** |
|---|---|---|---|
| | **HOMO (eV)[a]** | **LUMO (eV)[b]** | **IP (eV)[c]** |
| **OddDPP(ThBt-B2A)$_2$** | -5.3 | -3.8 | –5.7 |

[a] determined from the $E_{1/2}$ of the first oxidation; [b] determined from the $E_{1/2}$ of the first reduction; [c] determined from PESA.

**Table 5.4.** Summaries the results from CV measurements and PESA.

Given the poor solubility of **OddDPP(ThBt-DCV)$_2$** in organic solvents it was expected that, when solution processed the quality of the films formed would be poor for OPV devices. However, the **OddDPP(ThBt-B2A)$_2$** showed sufficient solubility in organic solvents and hence could be solution processed with P3HT. The EA of the material was similar to the EA of one of the best performing fullerene acceptor PC60BM (-3.6 eV) and one of the recently reported non-fullerene

acceptors FBR (-3.6 eV)[96]. This suggests that the **OddDPP(ThBt-B2A)$_2$** as sufficient energy offset (0.8 eV) to facilitate charge generation, when blended with P3HT (see Figure 5.12). However, the material has a slightly deeper EA (0.2 eV) compared to PC60BM, which is anticipated to give a lower Voc (~0.4 eV) in blend. The Voc is largely dependent in the offset on energy of the EA of the acceptor and the IP of the donor[40].

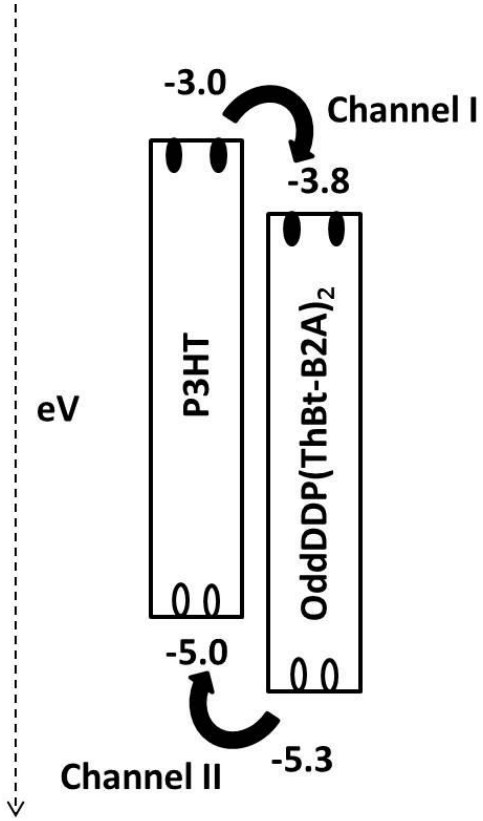


**Figure 5.12.** Diagrams showing the routes for charge generation between P3HT and **OddDPP(ThBt-B2A)$_2$**, and solid circles represent the movement of free electrons and free holes represented by hollow circles.

## 5.5 Bulk heterojunction devices

It was shown in previous sections that, **OddDPP(ThBt-B2A)$_2$**, has sufficient EA and have absorption longer than 700 nm to be investigated as Channel II material. However, before fabricating devices photoluminescence (PL) quenching experiment was carried out to determine whether the acceptor material is capable to separate charges when blended with P3HT.

### 5.5.1 Quenching results

In order to investigate the electron accepting ability of **OddDPP(ThBt-B2A)$_2$**, PL quenching experiments were carried out with different blend ratios of P3HT:**OddDPP(ThBt-B2A)$_2$**. Figure 5.13, shows that the, photoluminescence of the P3HT is quenched even at a low concentration of the acceptor. The quenching of the PL indicates that the radiative decay of the excited donor is inhibited meaning that the **OddDPP(ThBt-B2A)$_2$** should be capable of oxidising the excited state to form charge transfer states and then lead to charge generation. These measurements were carried out by Dr. Mike Hambsch.

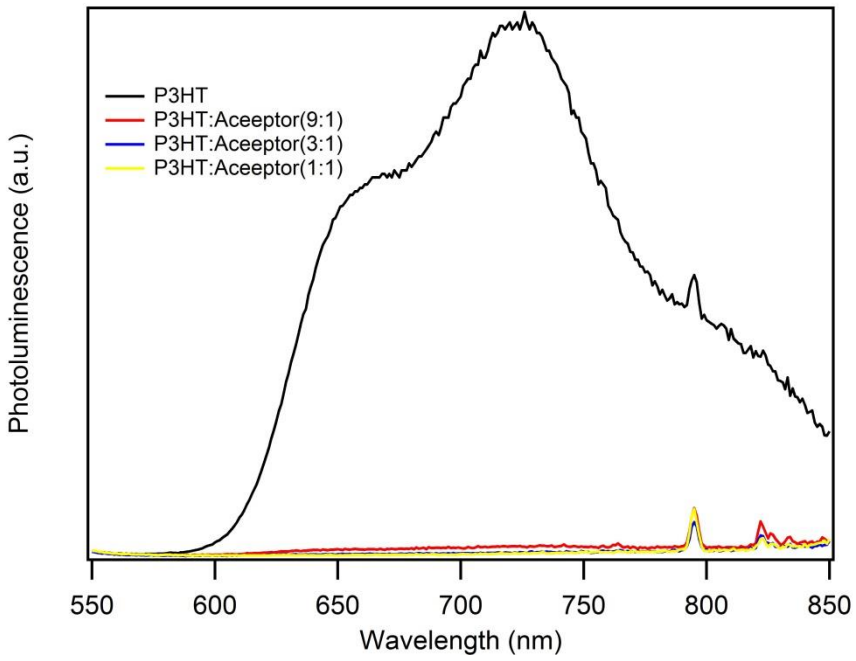


**Figure 5.13.** Thin film photoluminescence quenching results of the acceptor, **OddDPP(ThBt-B2A)$_2$**, with P3HT.

### 5.5.2 Device manufacture and transporting properties

The final stage of the study was the preparation of BHJ OPV devices. The devices had the following structure ITO (100 nm)/PEDOT:PSS (≈25 nm)/P3HT:**OddDPP(ThBt-B2A)$_2$**/Ca (15 nm)/Al (100 nm). The devices were fabricated from solutions of chloroform with 0.5% DIO and neat DCB, with different ratios of P3HT:**OddDPP(ThBt-B2A)$_2$** (1:1, 1:2 and 1:3) and the film thickness were 80-120 nm. However, the devices all performed poorly and the best device exhibited a maximum PCE = 0.1%, with $J_{sc}$ = 0. 40 ± 0.01 mA cm$^{-2}$, $V_{OC}$ = 0.47 ± 0.01 V and FF = 0.28 ±

0.01. As expected the device exhibited low Voc which is attributed to the low lying EA of the acceptor.

Figure 5.14 shows EQE spectrum of different ratios of P3HT:**OddDPP(ThBt-B2A)$_2$**. A device with ratio of 1:2 (P3HT:**OddDPP(ThBt-B2A)$_2$**) exhibited charge generation with an EQE of 1.4% at 682 nm. From the absorption spectra (see Figure 5.10) it would appear that at this wavelength the charge generation is purely through the Channel II mechanism (i.e, hole transfer from **OddDPP(ThBt-B2A)$_2$** to P3HT) as P3HT does not absorb at this wavelength. Between 600-300 nm both the donor and the acceptor absorb and hence, both Channel I and Channel II mechanisms could occur. A film fabricated with 1:3 ratio of P3HT:**OddDPP(ThBt-B2A)$_2$** exhibited similar EQE spectrum, but, with a maximum EQE of only 0.6%. Interestingly, it can also been seen that the device with 1:1 ratio of donor and acceptor exhibited no charge generation above 560 nm, and hence the device exhibited negligible PCE (0.002%).

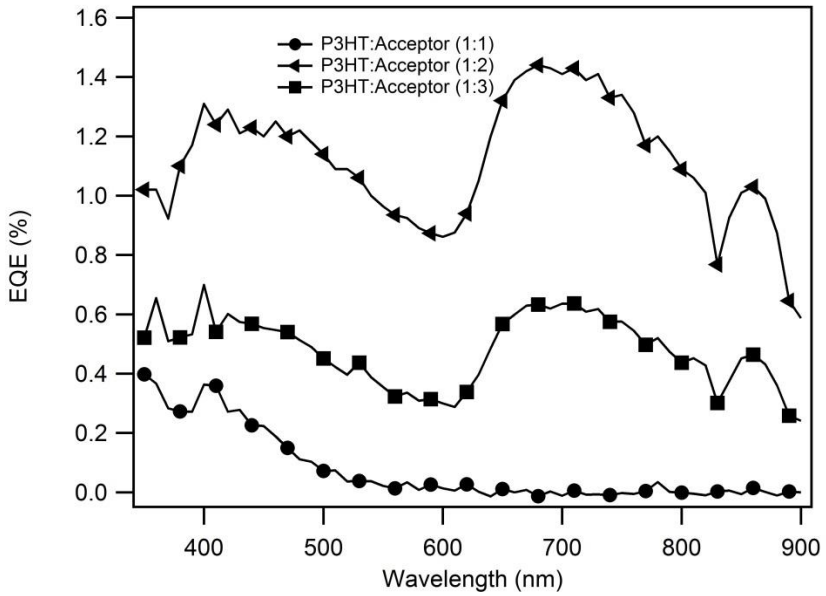


**Figure 5.14.** Display of EQE against wavelength for the different ratio of **P3HT:OddDPP(ThBt-B2A)$_2$** devices, fabricated from chloroform with 0.5% DIO.

Given that the photoluminescence quenching experiments indicated that, the P3HT:**OddDPP(ThBt-B2A)$_2$** blend film should be capable of photo excitation. The quite low efficiency may come from poor exciton dissociation as well as charge transport. To investigate whether the low photocurrent exhibited was due to poor charge carrier mobility in the blend films the transporting properties of the pristine and blend films were investigated using MIS-CELIV[78].

Both films were spin-coated from chloroform. The mobility measurements of the **OddDPP(ThBt-B2A)$_2$** pristine film showed that the material is bipolar with electron mobility higher by one order of magnitude than the hole mobility (see Table 5.5). However, the electron mobility in the blend with P3HT is two orders lower, which most likely is due to an unfavourable film structure for charge transport.

| **Materials** | **Ratio** | **Solvent** | $\mu_h$ **cm$^2$ V$^{-1}$ s$^{-1}$** | $\mu_e$ **cm$^2$ V$^{-1}$ s$^{-1}$** |
|---|---|---|---|---|
| **OddDPP(ThBt-B2A)$_2$** | - | Chloroform | $3 \times 10^{-4}$ | $1 \times 10^{-3}$ |
| **P3HT:OddDPP(ThBt-B2A)$_2$** | 1:2 | Chloroform | $1 \times 10^{-4}$ | $2 \times 10^{-5}$ |

**Table 5.5.** Summary of charge carrier mobilities of pristine and blend films.

# 5.6 Conclusion

**OddDPP(ThBt-DCV)$_2$** and **OddDPP(ThBt-B2A)$_2$** were successfully synthesized under condensation reaction conditions and fully characterized. The thin film absorption studies shows the **OddDPP(ThBt-DCV)$_2$**, has a strong red shift in its absorption did not have sufficient solubility to fabricate OPV devices by solution processing. The **OddDPP(ThBt-B2A)$_2$** showed better solubility and the EA measurement from CV showed that, charge generation should occur when blended with P3HT. The EQE spectrum showed Channel II charge generation at wavelength greater than 750 nm. However, the OPV devices performed poorly and the maximum PCE exhibited by the best device was only 0.1%. Mobility measurements of blend films showed electron mobilities two orders of magnitude less than the pristine film of the acceptor, suggesting unfavorable film structure leading to poor charge generation and charge extraction in blend films was the cause of the non-efficient performance.

# Chapter 6 – Synthesis, properties and BHJ devices of non-polymeric bisthienyl-DPP based materials with 9,9'-bifluorenylidene and its derivatives as end groups

# 6.1 Introduction

In previous Chapters it was shown that incorporating different groups onto the **OddDPP(Th)$_2$** unit influenced the properties and solubilities of the compounds, which in turn affected the device fabrication and performance. For example, when fluorenone or benzothiadiazole were incorporated, materials with different thermal and optical properties were obtained, which required different additives during device fabrication to achieve the best PCE. This chapter shows what happens to the physical properties and BHJ device performance when the basic structure of the end unit is kept same, and where the difference is simply the addition of electron donating or electron withdrawing groups onto the end unit. 9,9'-Bifluorenylidene (BF) (see Figure 6.1) was chosen as the basic end unit which was attached to the **OddDPP(Th)$_2$**, to give **OddDPP(ThBF)$_2$**. Additionally, electron donating methoxy (OMe) groups or electron withdrawing fluorine (F) atoms are incorporated to the 3' and 6' positions of the bifluorenylidene units of the **OddDPP(ThBF)$_2$**.

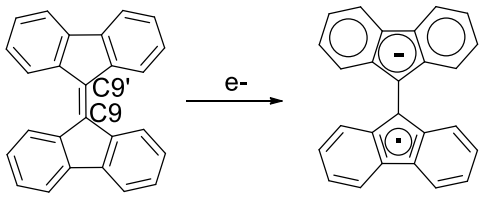


**Figure 6.1.** Chemical structure of 9,9'-bifluorenylidene (BF).

The reason why the BF unit was chosen was because it has been reported to have a high optical density (around 375-525 nm) and has a high electron affinity[86]. In addition, the BF unit has never been incorporated into a **OddDPP(Th)$_2$** like unit. In fact, there has only been one report of a BF unit conjugated with fluorene units to form a larger chromophore (TFBF). The material was reported as an electron acceptor (see Figure 6.2) and when used with P3HT as electron donor gave an OPV device with a PCE of 0.26%[162].

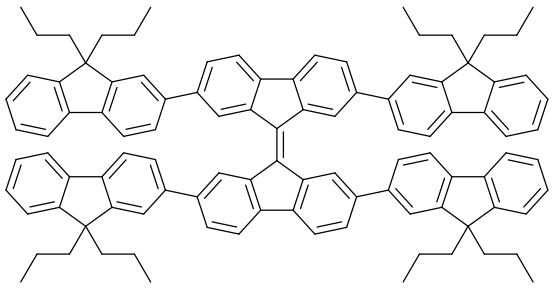

**Figure 6.2**. Chemical structure of tetrafluorene-9,9-bifluorenylidene (TFBF).

The first target compound consisted of the parent BF attached to the **DPP(Th)$_2$** unit, shown in Figure 6.3 [**OddDPP(ThBF)$_2$ (6.1)**]. In the second and third targets, the hydrogens at the 3'and 6' position of **DPP(ThBF)$_2$** are replaced with an electron-donating methoxy group [**OddDPP(ThBF(OMe)$_2$)$_2$ (6.2)**] or an electron withdrawing fluorine [**OddDPP(ThBF(F)$_2$)$_2$ (6.3)**], respectively, as shown in Figure 6.3.

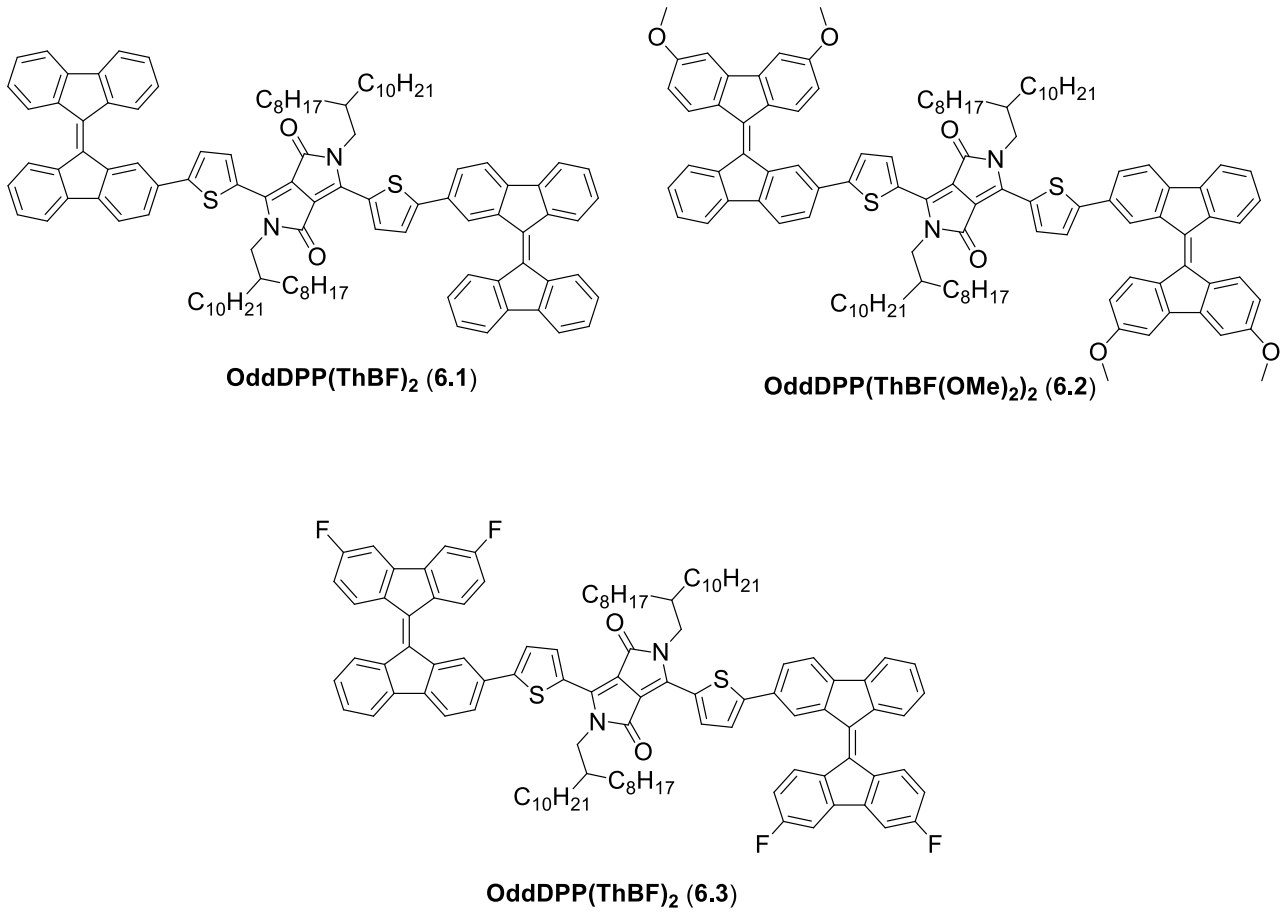


**Figure 6.3.** Chemical structures of **OddDPP(ThBF)$_2$** (**6.1**), **OddDPP(ThBF(OMe)$_2$)$_2$** (**6.2**), and **OddDPP(ThBF(F)$_2$)$_2$** (**6.3**).

## 6.2 Synthesis of the BF precursors

In order to attach the BF (and the subsequent derivatives) to the **OddDPP(Th)$_2$**, the brominated derivatives of the BFs (see Figure 6.4) needed to be first synthesized. The basic strategy to prepare the brominated derivatives of BFs **6.8**, **6.12**, and **6.16** was to couple synthesized 2-bromo-9-diazo-9*H*-fluorene (**6.5**) with the respective thiones **6.7**, **6.11**, and **6.16** (Scheme 6.2, 6.3 and 6.4), under Barton's two-fold extrusion diazo–thione coupling reaction conditions.

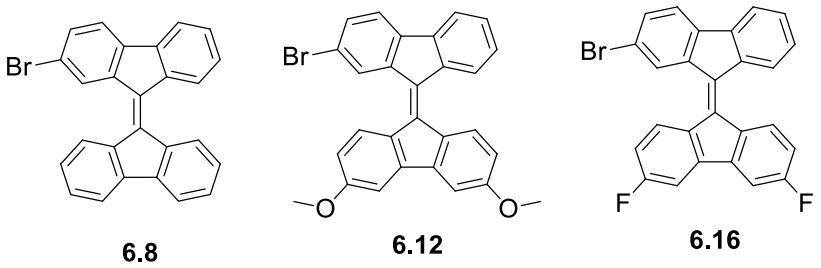


**6.8** **6.12** **6.16**

**Figure 6.4.** Chemical structure of **6.8**, **6.12**, and **6.16**.

In order to prepare 2-bromo-9,9'-bifluorenylidene (**6.8**), 2-bromofluorenone (**2.13**) was condensed with 4-methylbenzenesulfonohydrazide in refluxing acetonitrile (Scheme 6.1). Following completion of the reaction, the mixture was cooled down and filtered. The filtrate was then washed with cold acetonitrile to give **6.4** as yellow color solid. The solid was taken through to the next step without further purification. The next step involved the elimination of the tosyl group under basic conditions to synthesis the diazo-fluorene derivative (**6.5**) and this process was investigated using different solvents. Initially the hydrazide derivative was treated with 50% aqueous sodium hydroxide in 1,4-dioxane at 60 ºC to give **6.5** in a 21% yield, for the two steps (Scheme 6.1). However, difficulties arose with removal of the 1,4-dioxane (b.pt = 101 °C) following the reaction using Buchi Vacuum. 1,4-Dioxane was replaced with tetrahydrofuran (b.pt = 66 °C) and the reaction was carried out under similar reaction conditions as above to give **6.5** in a 22% yield, for the two steps (Scheme 6.1).

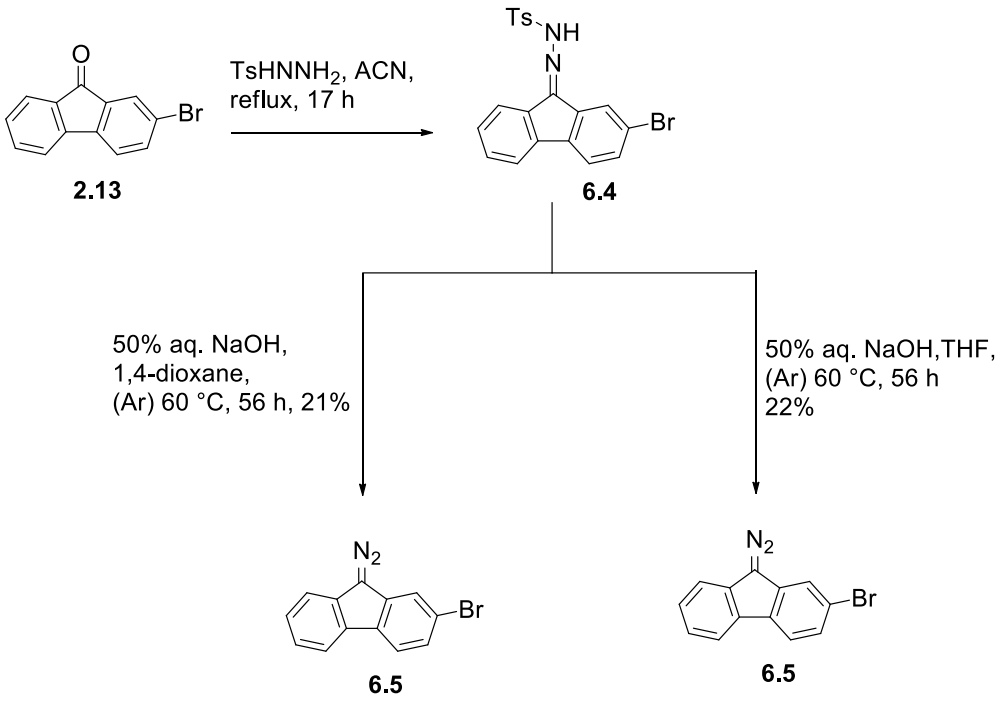


**2.13** **6.4** **6.5** **6.5**

**Scheme 6.1.** Synthetic scheme to **6.5**.

Following the preparation of sufficient **6.5**, the next step was to synthesize the thione derivatives. It has previously been reported that 9*H*-fluorene-9-thione undergoes self-condensation in toluene, when heated at reflux for longer periods[86, 162]. Hence the reaction was closely monitored by TLC in an effort to obtain the maximum quantity of thione. Taking this into consideration, a test reaction to synthesize 9*H*-Fluorene-9-thione (**6.7**) by treating commercially available fluorenone (**6.6**) with 0.5 equivalents of Lawesson's reagent in refluxing toluene under argon for 30 minutes (Scheme 6.2) was carried out. At the end of this time, the temperature of the reaction mixture was reduced to room temperature and the solvent completely removed in *vacuo*. Since **6.7** was anticipated to be unstable stable on silica, purification was carried out using rapid flash chromatography, with a dichloromethane/light petroleum spirit mixture (1:4) as eluent. An orange solid was obtained, which started turning into a yellow colour liquid upon exposure to air. **6.7** needed to be kept under an inert atmosphere (argon) after preparation and isolation and immediately reacted with **6.5** under Barton's two-fold extrusion diazo–thione coupling reaction conditions (Scheme 6.2). The reaction procedure involved a solution of **6.7** in tetrahydrofuran being added dropwise to a solution of **6.5** in tetrahydrofuran over 15 min before being stirred for 56 h at room temperature. Under these conditions **6.8** was formed in a 67% yield (Scheme 6.2).

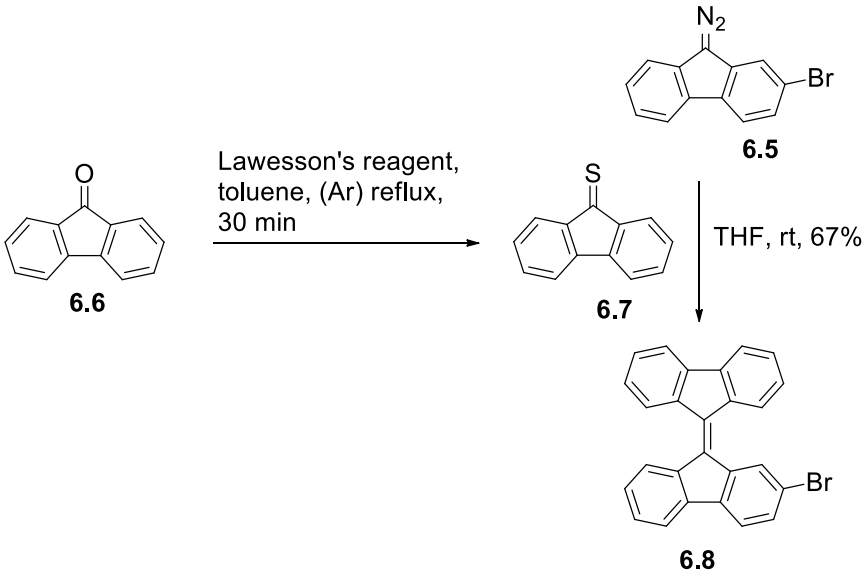


**Scheme 6.2.** Synthetic scheme to **6.7** and **6.8**.

To prepare the next precursor (**6.12**) it was proposed that, the same synthetic method would be followed. However, 3,6-dimethoxy-9*H*-fluoren-9-one (**6.10)** was not commercially available and had to be synthesized. A review of the literature revealed that benzophenone derivatives, which are commercially available, can be converted to the corresponding fluorenone by palladium catalyzed

intramolecular C-C bond formation through an oxidative C-H coupling[163, 164]. A typical reaction involving conversion of benzophenone and its derivatives to the corresponding fluorenone utilises an oxidant (e.g., silver(I) oxide or silver trifluoroacetate) with or without a base (potassium carbonate) in solvents such as trifluoroacetic acid, pivalic acid or acetic acid. High yields 74% and 73% have been reported for the conversion of benzophenone to the corresponding fluorenone when silver (I) oxide is used as an oxidant in trifluoroacetic acid, with or without base. Hence, the formation of the desired fluorenones was investigated under both these conditions. The first reaction was thus carried out with commercially available bis(4-methoxyphenyl)methanone (**6.9**), silver (I) oxide, and palladium (II) acetate catalyst in trifluoroacetic acid at reflux and this gave **6.10** in a 32% yield (Scheme 6.3). However, when potassium carbonate was added under similar reaction conditions used similar yield was obtained (Scheme 6.3). It has to be noted that trifluroacteic acid was added dropwise to the reaction mixture at room temperature. **6.10** was then converted to the BF derivative (**6.12**) first by converting **6.10** to **6.11** using Lawesson's reagent, followed by addition of freshly prepared **6.11** in tetrahydrofuran to a solution of **6.5**, to give **6.12** in a 71% yield (Scheme 6.4).

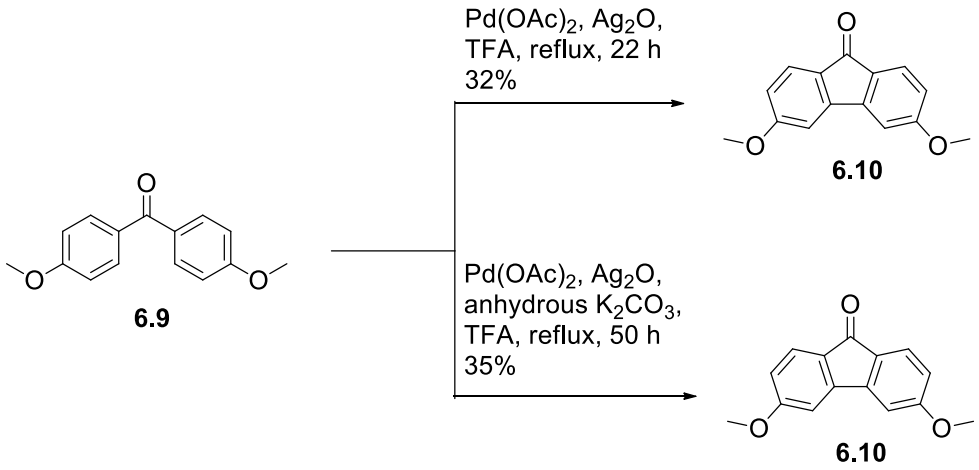


**Scheme 6.3.** Synthetic scheme to **6.10**.

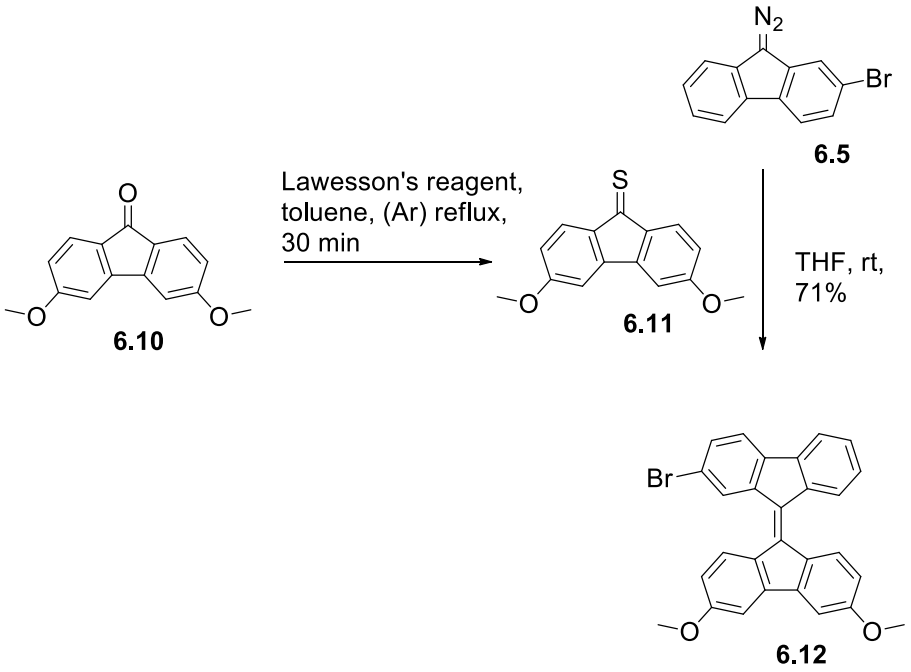


**Scheme 6.4.** Synthetic scheme to **6.11** and **6.12**.

Next, was the synthesis of final precursor **6.16**. Since the reaction with and without base gave similar yields in case of **6.10**. It was first decided to synthesize 3,6-difluoro-9*H*-fluoren-9-one from commercially available bis(4-fluorophenyl)methanone **6.13** without the use of base (Scheme 6.5). **6.13** were reacted with silver (I) oxide and palladium acetate in trifluoroacetic acid heated at reflux. Initially, the reaction was monitored by TLC and it was observed that the starting material and the product had very similar $R_f$ values despite trying different ratios of light petroleum spirit and dichloromethane as elunet. The reaction therefore needed to be monitored by $^1$H NMR. It was found that the reaction progressed slowly and even after 62 h the reaction did not go to completion. Nevertheless after this time, the reaction mixture was cooled down to room temperature and after purification by recrystallisation from ethanol **6.14** was isolated in a 19% yield with the starting material recovered in a 43% yield. Since, the reaction was found to progress slowly a second reaction under similar conditions but with the addition of potassium carbonate as base was undertaken. The reaction was carried out for 70 h and the reaction gave the same yield of **6.14** (19%) and, starting material was also recovered (34%). Finally, the reaction was carried out using base but heating also at reflux for 95 h and this gave **6.14** in a 64% yield with no starting material recovered. It was noted that, using fresh trifluoroacetic acid increased the reaction rate and made all the difference in the yield. It has been previously reported that, in general, benzophenones bearing electron donating substituents reacted more quickly than those bearing electron withdrawing substituents[163]. This to an extent explains the lower reactivity of **6.13**.

**6.11** as then converted to its respective thione **6.15** (Scheme 6.6), followed by dropwise addition of **6.15** (in tetrahydrofuran) to a solution of **6.5** in tetrahydrofuran. The reaction was stirred for 56 h at room temperature and purified using column chromatography. However, because a poor yield (< 1%) was obtained (Scheme 6.6), it was decided that the effect of temperature on the reaction needed to be investigated. In the next experiment, a solution of **6.15** in tetrahydrofuran was added to a solution of **6.5** in tetrahydrofuran and reacted for 5 min at room temperature before being heated at reflux for 17 h to give **6.16** in a 57% yield (Scheme 6.6). It has been reported in literature from X-ray diffraction studies of 12-(3,6-dimethoxy-9*H*-fluoren-9-ylidene)-12*H*-dibenzo[b,h]fluorene, which has the electron donating group (methoxy) at 3 and 6 positions, that there is an increase in length of the double bond between C9 and C9' for the compounds compared to 9,9'-bifluorenylidene[86]. It can therefore be postulated that when the methoxy groups are replaced by electron withdrawing groups like fluorine, the bond length would be shorter. Hence, in case of **6.16**, which has fluorine attached at the 3 and 6 positions, the steric hindrance between C9 and C9' hydrogens would be higher sterically hindering the coupling reaction from happening. This goes some way in explaining the low yield at room temperature and the sluggish nature of the reaction.

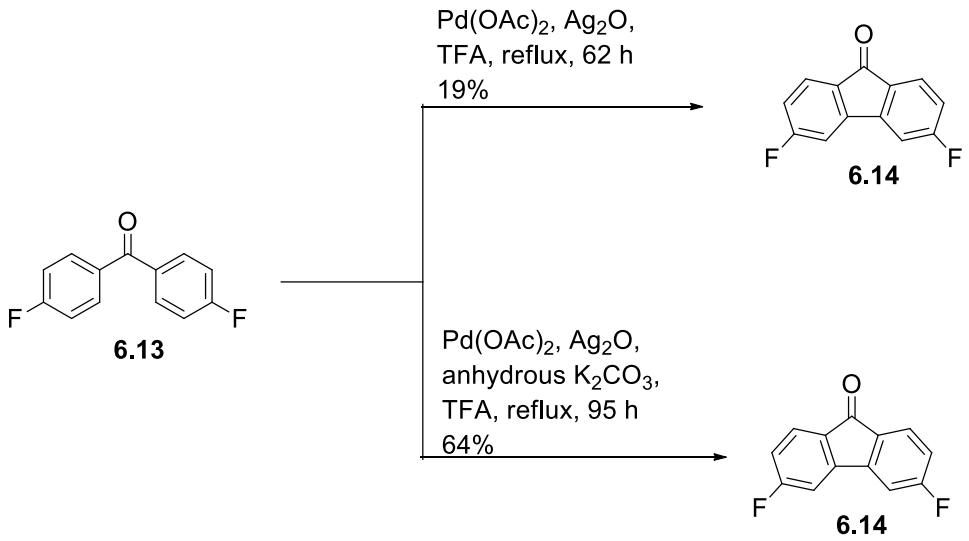


**Scheme 6.5.** Synthetic scheme to **6.14**.

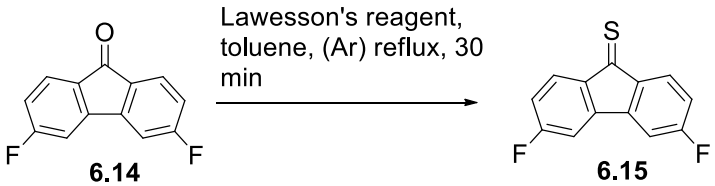

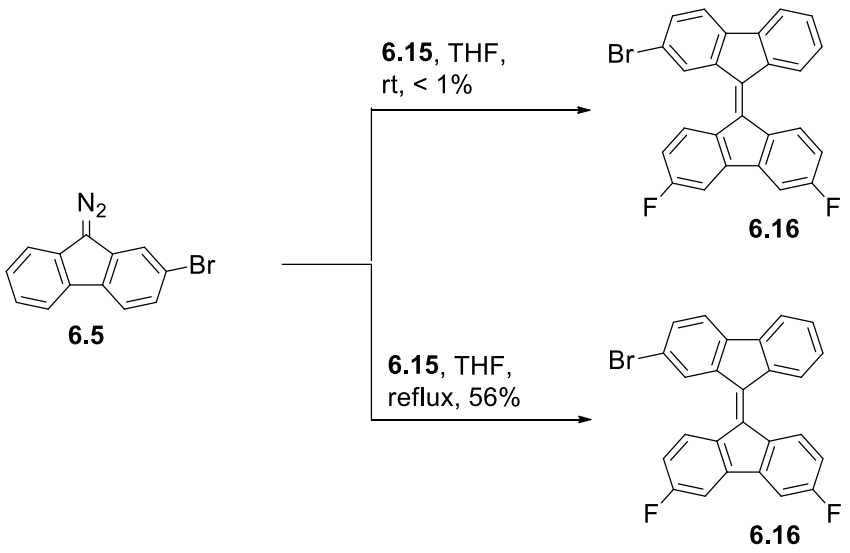


**Scheme 6.6.** Synthetic scheme to **6.15** and **6.16**.

## 6.3 Synthesis of targets OddDPP(ThBF)$_2$, OddDPP(ThBF(OMe)$_2$)$_2$, and OddDPP(ThBF(F)$_2$)$_2$

The final step in the synthesis involves the addition of precursor **6.6**, **6.12**, and **6.16** to the **OddDPP(Th)$_2$** unit. In the previous chapter, it was shown that direct arylation via C-H activation was a convenient way to synthesis DPP(ThAr)$_2$. Hence, the possibility of synthesizing the first target was investigated using direct arylation reaction conditions. Thus, a test reaction with **OddDPP(Th)$_2$** and **6.8** was carried out under direct arylation reaction conditions (Scheme 6.7). The reaction was monitored by TLC and despite consumption of the **OddDPP(Th)$_2$**, some **6.8** was still present after 6 h, so the reaction mixture was stirred for another 11 h before being cooled to room temperature and purified using column chromatography. The yield of the desired 6.1 was unfortunately low at 6%.

The low yield prompted further investigation into the synthesis of **OddDPP(ThBF)$_2$** under Suzuki-Miyuara cross coupling conditions. With a sufficient quantity of **OddDPP(Th-Br)$_2$** in hand, the bromo derivative of **6.8** was first converted to the boronic ester derivative under standard Miyaura borylation reaction conditions using [1,1'-bis-(diphenylphosphino)ferrocene]dichloropalladium(II) $PdCl_2$(dppf) as the catalyst and bis(pinacolato)diboron in 1,4-dioxane to give **6.17** in a 80% yield (Scheme 6.8). A test reaction was then carried out with **6.17** and **OddDPP(Th-Br)$_2$** using tetrakis(triphenylphosphino)palladium(0)

catalyst, and 2M aqueous potassium carbonate, in toluene and ethanol. Ethanol was used as the phase transfer solvent. The reaction went to completion in 6 h and **OddDPP(ThBF)$_2$** was obtained in an 86% yield (Scheme 6.8).

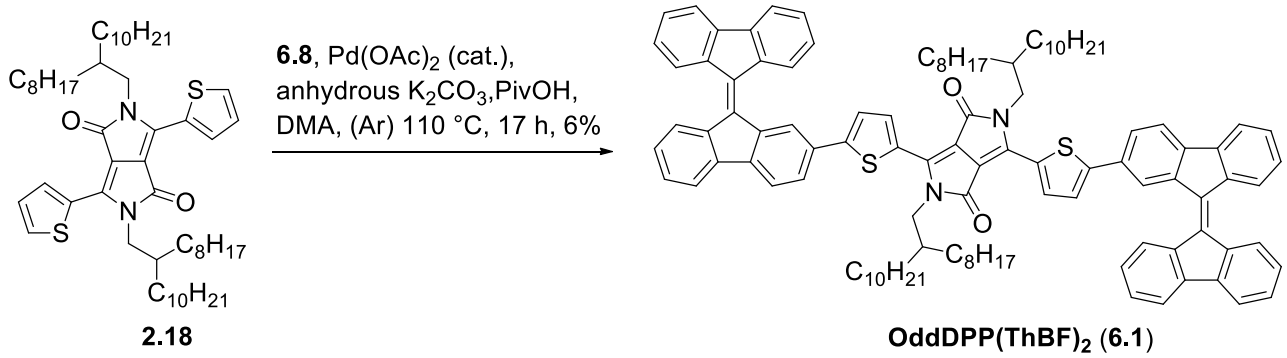


**Scheme 6.7.** First, synthetic scheme to **OddDPP(ThBF)$_2$ (6.1)**.

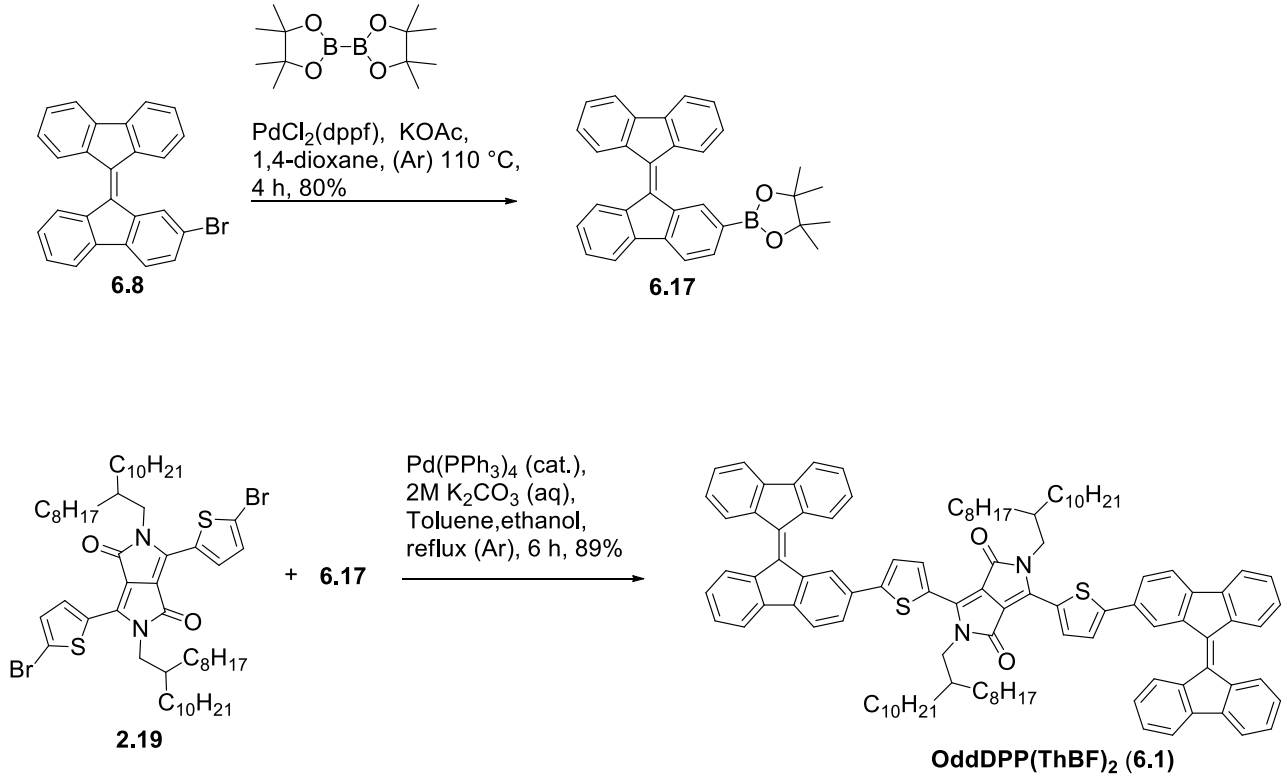


**Scheme 6.8.** Second, synthetic route to synthesize **OddDPP(ThBF)$_2$ (6.1)**.

With the synthesis of the first target of this series producing a good yield under Suzuki-Miyuara cross coupling conditions, it was decided to synthesize the second target under similar conditions. The **6.12** was converted to the boronic ester under standard Miyaura borylation reaction conditions

to give **6.18** in an 86% yield, which was then reacted with **OddDPP(Th-Br)$_2$** under Suzuki conditions to give **OddDPP(ThBF(OMe)$_2$)$_2$** in a 36% yield (Scheme 6.9).

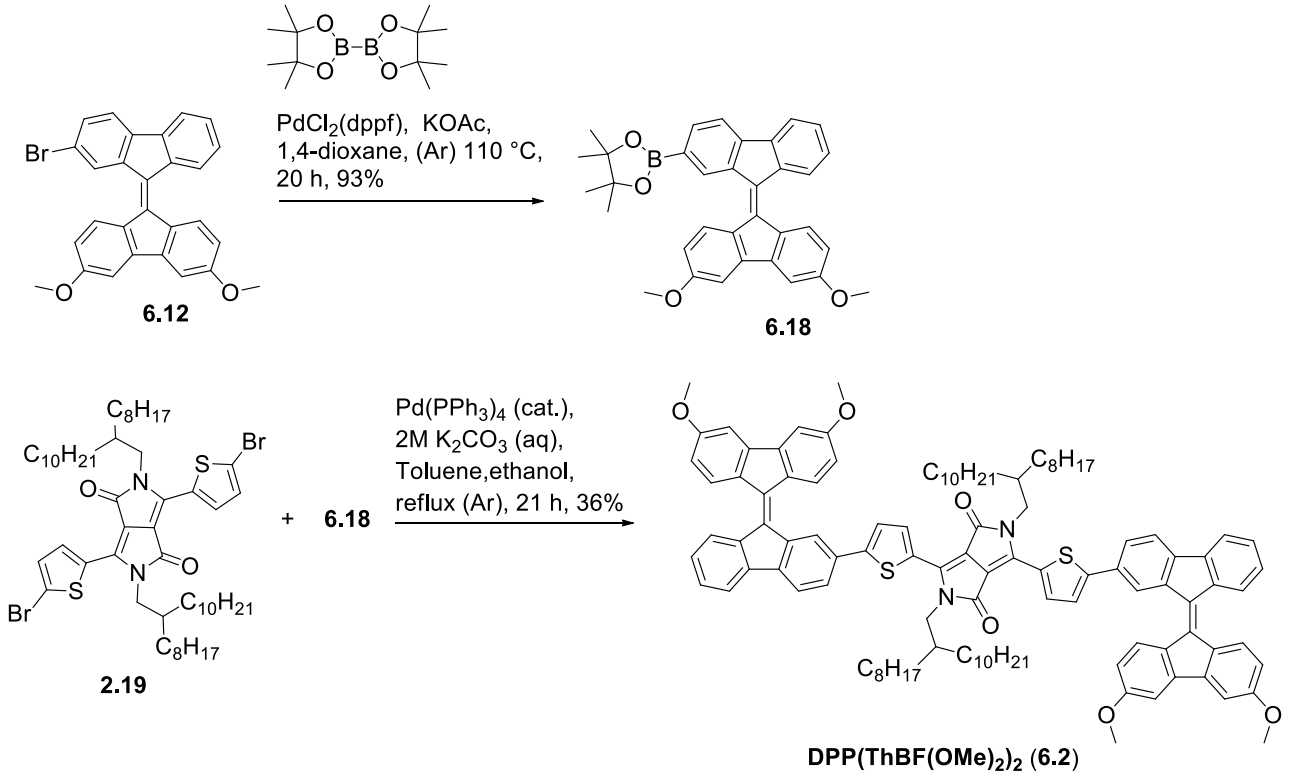


**Scheme 6.9.** Synthetic scheme to **OddDPP(ThBF(OMe)$_2$)$_2$** (**6.2**).

To obtain the final target of the series **OddDPP(ThBF(F)$_2$)$_2$** (**6.3**), **6.16** was reacted with [1,1'-bis-(diphenylphosphino)ferrocene]dichloropalladium(II) $PdCl_2$(dppf) as the catalyst and bis(pinacolato)diboron, potassium acetate as base in 1,4-dioxane at 110 ºC. The reaction was monitored by TLC but unfortunately the reaction did not go to completion even after 21 h. The starting material and product (**6.19**) were separated using column chromatography to give **6.19** in a 29% yield (scheme 6.10).

A test reaction was carried out with **6.19** and **OddDPP(Th-Br)$_2$ (2.19)**, under Suzuki-Miyuara cross coupling conditions. The reaction did not go to completion and most of the starting materials were recovered (see Scheme 6.11). The reaction was repeated with freshly distilled solvents under similar conditions, but again ~80% of the starting materials were recovered. It was decided to investigate the synthesis of **OddDPP(ThBF(F)$_2$)$_2$** under direct arylation reaction conditions. A test reaction was carried out with **6.16** and **OddDPP(Th)$_2$** using palladium acetate as catalyst and pivalic acid as co-catalyst, and potassium carbonate as base in *N*, *N*-dimethylacetamide

(DMA) at 110 °C (oil bath temperature) (scheme 6.11). The reaction went to completion in 6 h (monitored by TLC). Purification of the crude was first attempted using column chromatography over silica using chloroform/light petroleum spirit as the eluent. However, this was unsuccessful, but when the eluent as changed to a light petroleum spirit/toluene (4:1) mixture as eluent, some impurities was removed but the desired product was still was not pure. Recrystallization from ethanol/dichloromethane also failed to purify the product (see Figure 6.5, arrow showing impurities). Due to time constraints, further investigation on purification of **OddDPP(ThBF(F)$_2$)$_2$** was not carried out.

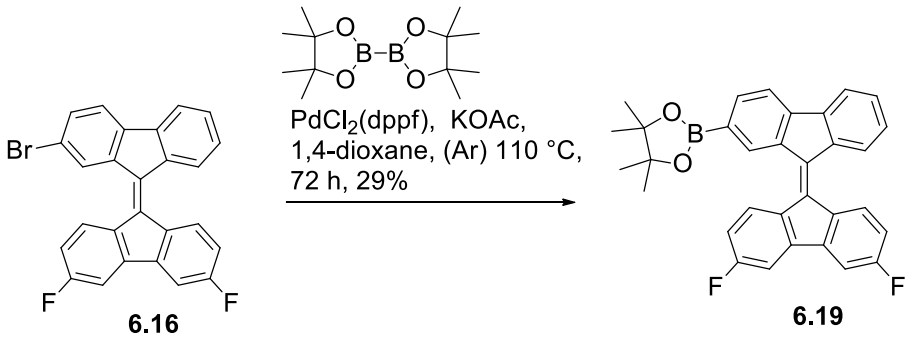


**Scheme 6.10.** Synthetic scheme to **6.19**.

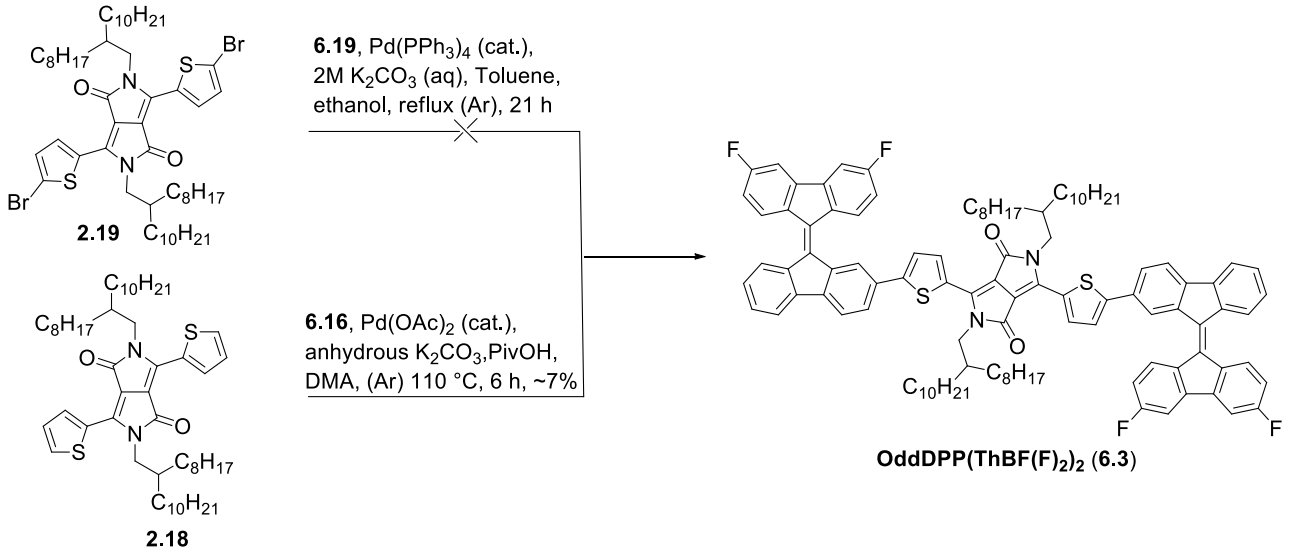


**Scheme 6.11.** Synthetic scheme to **OddDPP(ThBF(F)$_2$)$_2$ (6.3)**.

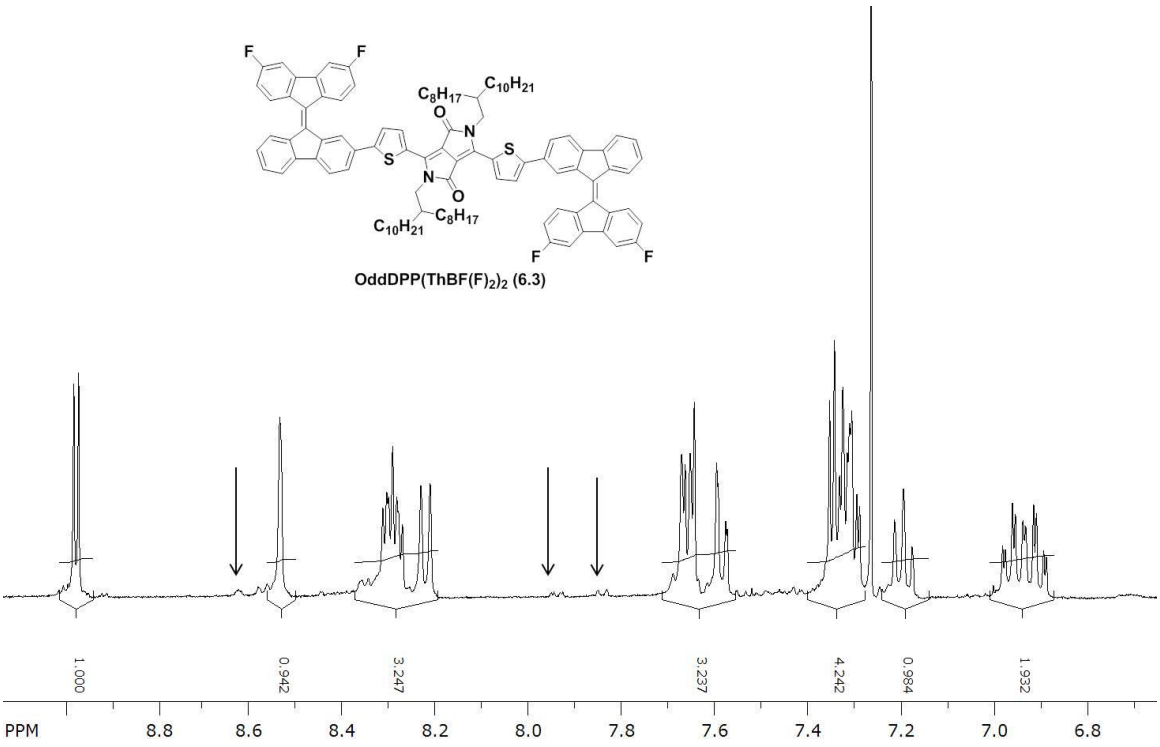


**Figure 6.5.** $^{1}$H NMR of the residue from ethanol/dichloromethane recrystallization of **DPP(ThBF(F)$_2$)$_2$**.

As **OddDPP(ThBF(F)$_2$)$_2$** could not be purified and hence only **OddDPP(ThBF)$_2$** and **OddDPP(ThBF(OMe)$_2$)$_2$** were further characterised and used in BHJ devices.

# 6.4 Physical properties

### 6.4.1 Thermal properties

The thermal properties were investigated using TGA and DSC. **OddDPP(ThBF)$_2$** and **OddDPP(ThBF(OMe)$_2$)$_2$** exhibited a 5% weight loss at 374 $^{o}$C and 379 $^{o}$C, respectively, at a scan rate of 10 $^{o}$C min$^{-1}$ under nitrogen (see Figure 6.6). The similar decomposition temperatures show that the methoxy groups did not have an effect on the thermal stability of the material.

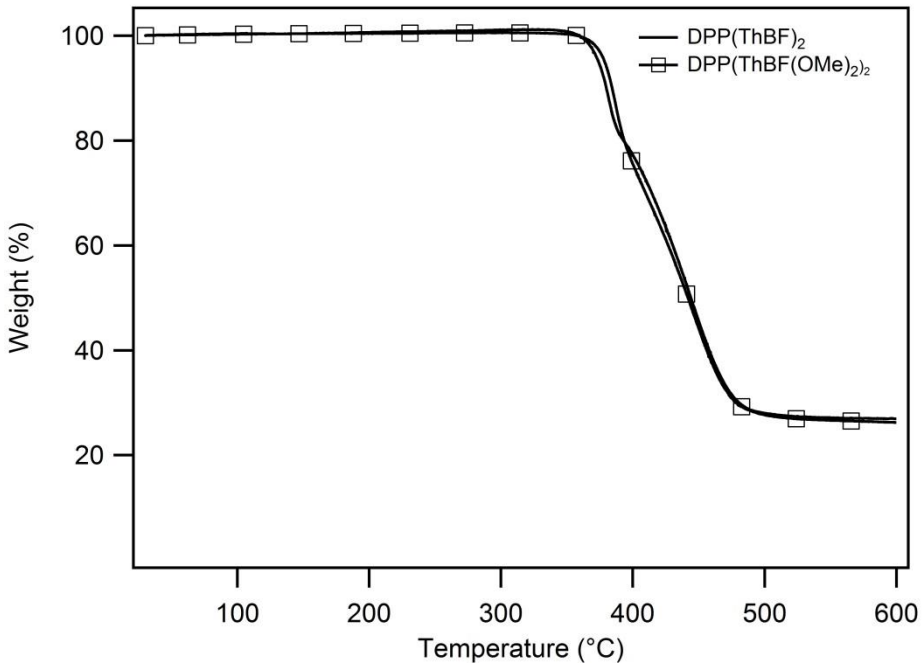


**Figure 6.6.** TGA traces for **OddDPP(ThBF)$_2$**, and **OddDPP(ThBF(OMe)$_2$)$_2$** at 10 $^{o}$C min$^{-1}$ under $N_2$.

The presence of thermal phase transitions was then studied using DSC. During the first heating scan, **OddDPP(ThBF)$_2$** exhibited a two endothermic transitions corresponding to melting points at 129 $^{o}$C and 153 $^{o}$C, at a scan rate of 100 $^{o}$C min$^{-1}$ (see Figure 6.7a). However, on cooling no thermal transition corresponding to crystallisation was found. On the second heating scan, the material exhibited a $T_g$ at 81 °C (see Figure 6.7b) but no crystallisation or melting transitions. The second cooling scan was identical to the first. Thus at this scan rate after melting the rapid cooling leads to amorphous **OddDPP(ThBF)$_2$** film and the inability to reorganise is expected to give poor transport properties.

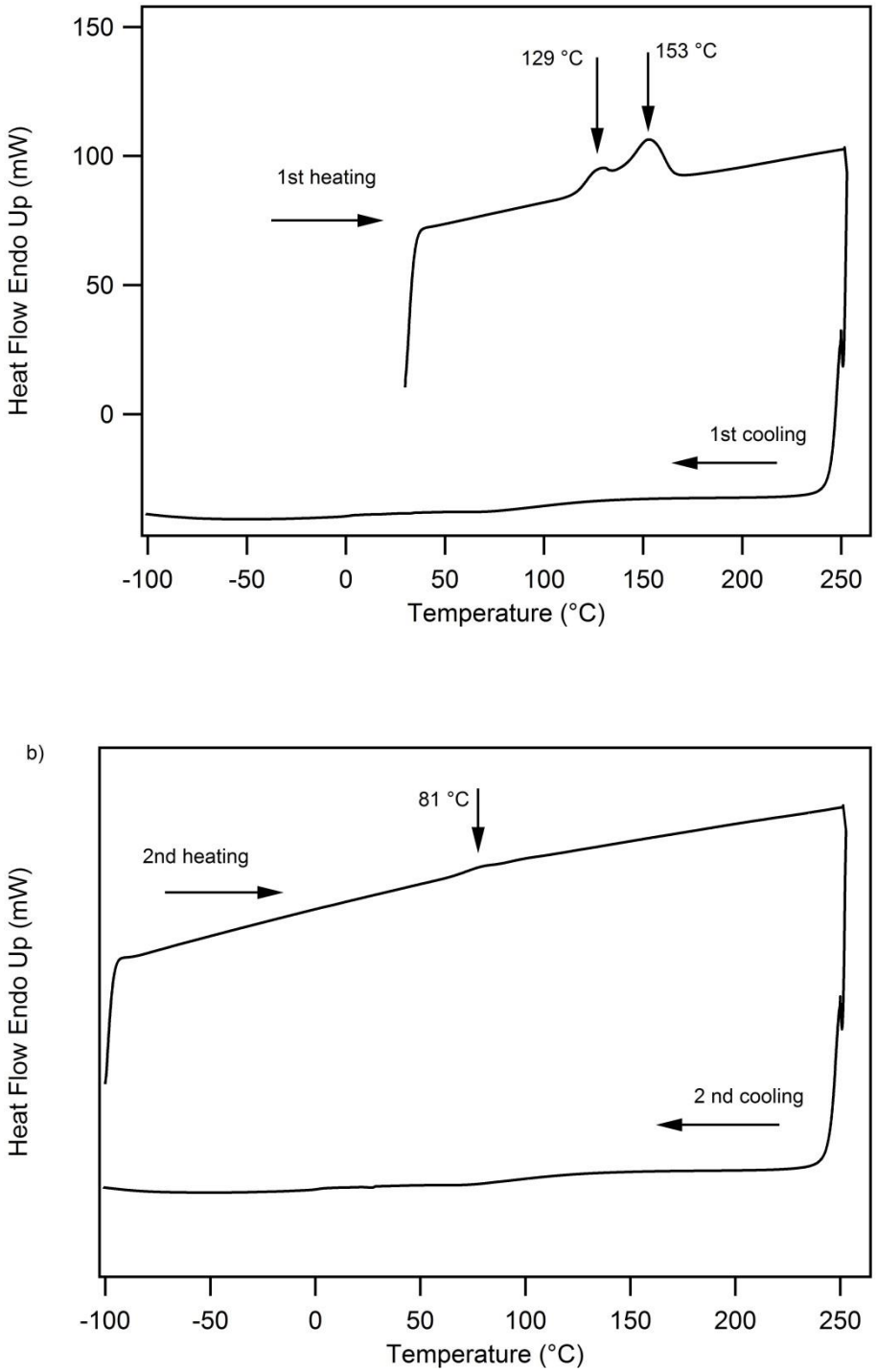


**Figure 6.7.** DSC traces for **OddDPP(ThBF)$_2$** a) 1st heating and cooling, and b) 2nd heating and cooling at scan rate of 100 $^{o}$C min$^{-1}$.

**OddDPP(ThBF(OMe)$_2$)$_2$** exhibited a $T_c$ at 148 °C and melted at 228 °C during the first heating scan (see Figure 6.8). Upon cooling, no thermal transitions were observed. During the second heating scan, in contrast, the material showed a $T_g$ at 96 °C and a subsequent crystallisation process at 173 °C before re-melting at 228 °C. Hence after cooling at this rate, **OddDPP(ThBF(OMe)$_2$)$_2$**

forms an amorphous material. Given the rapid nature of film formation during spin-coating or evaporation it would be expected that **OddDPP(ThBF(OMe)$_2$)$_2$** would form an amorphous film. However, heating the processed film above $T_g$ and new $T_c$ would be expected to give a more ordered film with better transport properties.

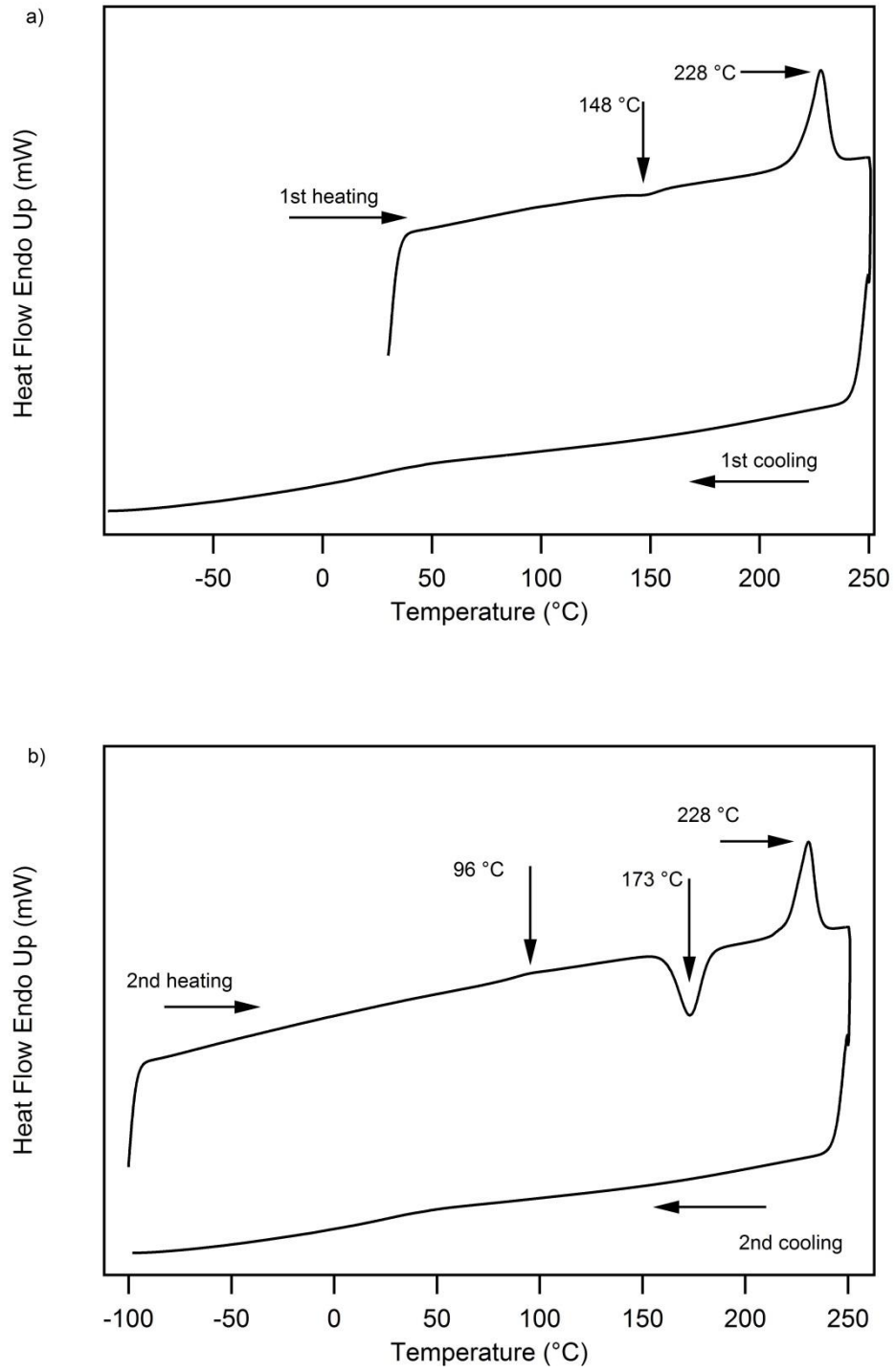


**Figure 6.8.** DSC traces for **OddDPP(ThBF(OMe)$_2$)$_2$** a) 1st heating and cooling, and b) 2nd heating and cooling at scan rate of 100 $^{o}$C min$^{-1}$.

| Material | $T_d$ (°C) | $T_g$ (°C) | $T_m$ (°C) | $T_c$ (°C) |
|---|---|---|---|---|
| **OddDPP(ThBF)$_2$** | 374 | 81 | 129, 153 | |
| **OddDPP(ThBF(OMe)$_2$)$_2$** | 379 | 96 | 228(1$^{st}$ heating), 148(2$^{nd}$ heating) | 148 (1$^{st}$ cooling), 173(2$^{nd}$ cooling) |

**Table 6.1**. Summary of TGA, DSC mesurments of **OddDPP(ThBF)$_2$** and **OddDPP(ThBF(OMe)$_2$)$_2$**.

### 6.4.2 Optical properties

Next, the optical properties of **OddDPP(ThBF)$_2$** and **OddDPP(ThBF(OMe)$_2$)$_2$** material were compared in solution and thin film using UV-Vis absorption spectroscopy (see Figure 6.9). **OddDPP(ThBF)$_2$** exhibited absorption maxima at 594 and 625 nm with molar exctinction coefficients of 51 000 $M^{-1}$ $cm^{-1}$ and 50 000 $M^{-1}$ $cm^{-1}$, respectively. **OddDPP(ThBF(OMe)$_2$)$_2$** exhibited absorption maxima at 488 nm and 631 nm with molar exctinction coefficients of 59 000 $M^{-1}$ $cm^{-1}$ and 57 000 $M^{-1}$ $cm^{-1}$, respectively. The absorption band from 370 to 550 nm is due to the π-π* transitions of the BF units whilst the absorption at longer wavelength is attributed to the **OddDPP(Th)$_2$** unit. With the incorporation of the methoxy group, the molar absorptivity of band corresponding to the BF unit increases by 13 000 $M^{-1}$ $cm^{-1}$. Interestingly, in thin films both the materials exhibited a red shift with the absorption maxima at 611 nm 663 nm, they had similar absorption profiles. The peak at 500 nm corresponding to BF for **OddDPP(ThBF(OMe)$_2$)$_2$** exhibited a red shift of about 30 nm compared to **OddDPP(ThBF)$_2$**.

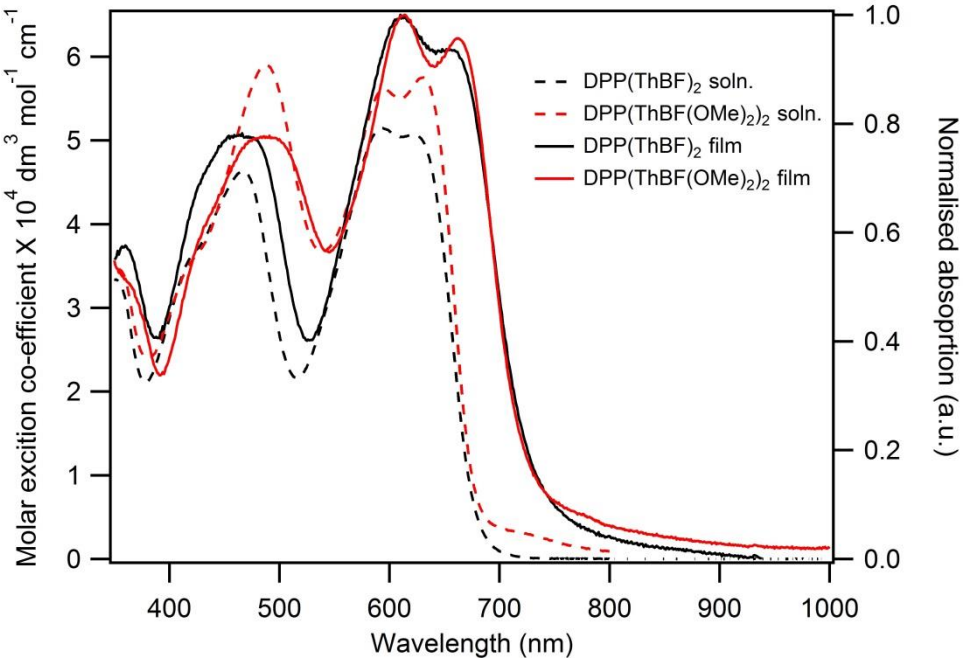


**Figure 6.9.** UV-Vis absorption spectra of **OddDPP(ThBF)$_2$** and **OddDPP(ThBF(OMe)$_2$)$_2$** in solution and neat film.

| **Material** | **$\lambda_{max}$ (nm) solution** | **$\lambda_{max}$ (nm) film** |
|---|---|---|
| **OddDPP(ThBF)$_2$** | 625, 594, 467, 421 | 657, 611, 464 |
| **OddDPP(ThBF(OMe)$_2$)$_2$** | 631, 595, 488, 420 | 662, 613, 488 |

**Table 6.2**. Summary of absorption measuments from solution (chloroform) and film of **OddDPP(ThBF)$_2$** and **OddDPP(ThBF(OMe)$_2$)$_2$**.

### 6.4.3 Electrochemical studies

In order to investigate the IP and EA of the materials, CV measurements were carried out using freshly dried and doubly distilled dichloromethane for both the oxidation and reduction measurements. The measurements used 0.1 M tetra-*n*-butylammonium perchlorate electrolyte (TBAP) solution and were carried out at a scan rate of 100 mV s$^{-1}$. The **OddDPP(ThBF)$_2$** exhibited three chemically reversible oxidations at $E_{1/2}$ = 0.3 V, 0.4 V, and 0.7 V, and, three chemically reversible reductions at $E_{1/2}$ = -1.4 V, -1.7 V, and -2.0 V (see Figure 6.10a). The IP and EA were

then estimated from the $E_{1/2}$ of the first oxidation and reduction relative to the ferrocene/ferrocenium couple. This gave a IP and EA of -5.2 eV and -3.3 eV, respectively, for **OddDPP(ThBF)$_2$**. **OddDPP(ThBF(OMe)$_2$)$_2$** in dichloromethane at the same scan rate of 100 mV s$^{-1}$, exhibited three chemically reversible oxidations at same potential ($E_{1/2}$ = 0.3 V, 0.4 V and 0.7 V) as for **OddDPP(ThBF)$_2$**. However, exhibited only two reversible reduction potential at $E_{1/2}$ = -1.6 V and -1.7 V (see Figure 6.10b). The subsequent scans were identical. A possible reason for unusual cyclic voltammagram reduction is the low solubility of **OddDPP(ThBF(OMe)$_2$)$_2$** in the electrolytic solution, which might have resulted in material depositing onto the electrode. Nevertheless, the $E_{1/2}$ of the first oxidation and reduction potential is sufficient for estimating the IP and EA, being -5.2 eV and -3.2 eV, respectively. The IP and EA are similar to the energy levels found for DPP derivatives shown in previous Chapter 3, which were used as donor materials. Hence, it was expected that the **OddDPP(ThBF)$_2$** and **OddDPP(ThBF(OMe)$_2$)$_2$** would be best used as donor material with PC70BM in BHJ devices.

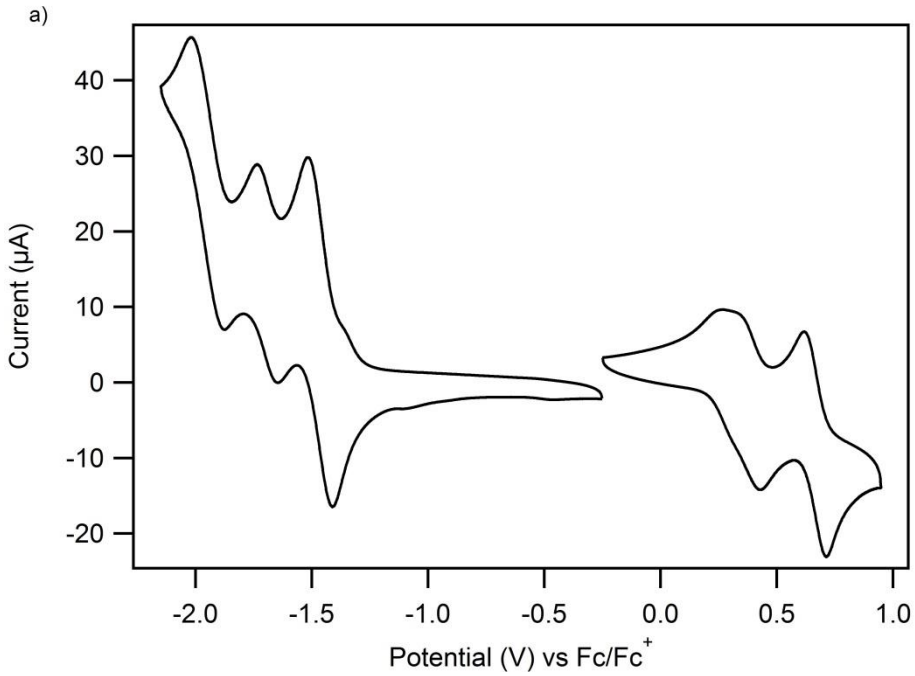

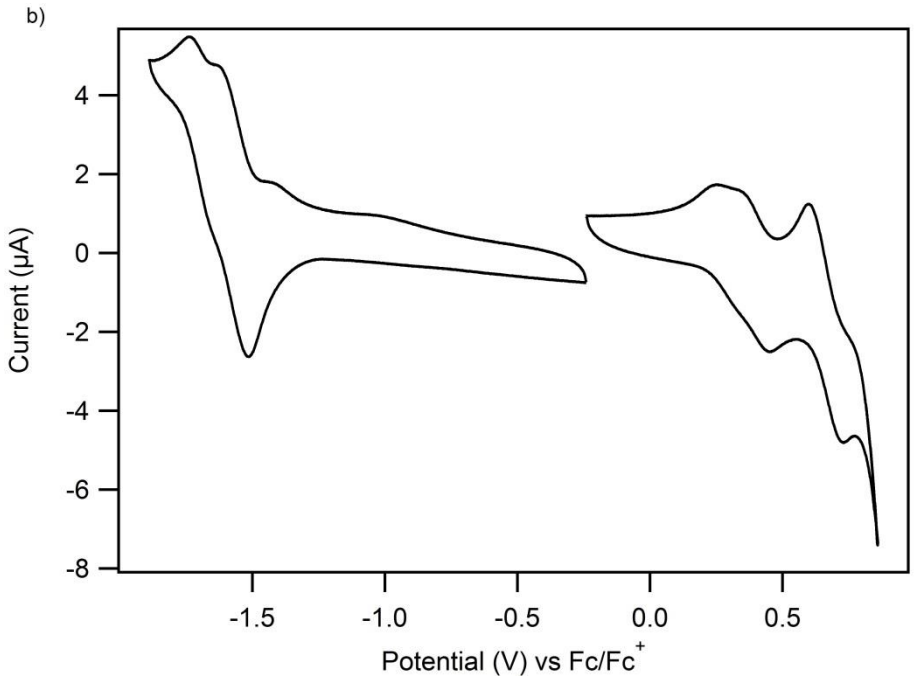


**Figure 6.10.** Cyclic voltammograms for a) **OddDPP(ThBF)$_2$** and b) **OddDPP(ThBF(OMe)$_2$)$_2$** measured in dichloromethane under an argon atmosphere at a scan rate of 100 mV $s^{-1}$ with platinum as the working electrode.

## 6.5 Bulk Heterojunction devices

Bulk heterojunction OPV devices were fabricated with the **OddDPP(ThBF)$_2$** or **OddDPP(ThBF(OMe)$_2$)$_2$** blended with PCBM to investigate the influence that chemical structural variations had on the processing conditions and device performance. Films were fabricated from neat chloroform, chloroform with 0.5% DIO, and chloroform with 10% DCB with different ratios of the donor and acceptor and the active layer thickness were 80 nm. The devices had the following structure ITO/MoOx (10 nm)/BHJ (80 nm)/Sm (1 nm)/Al (100 nm). The device fabrication and measurements were carried out by Dr. Hui Jin.

The first set of devices were fabricated with **OddDPP(ThBF)$_2$**:PC70BM with the blend ratios of donor:acceptor varying as follows: 4:1, 3:2, 1:1, 2:3,1:4, 1:19. Table 6.3 shows results only from the best devices. The devices with high donor content (donor:acceptor 4:1, 3:2) exhibited high Vocs (0.96 ± 0.01 eV) but with poor current densities ($J_{sc}$) and fill factors (FFs). However, the device performance showed the reverse when the acceptor (PCB70M) content in the blend was increased to 1:4 (donor:acceptor). The current density increased by almost thirty five fold, whilst the FF increased only marginally. However, Voc decreased to 0.84 ± 0.01 eV, which resulted in

PCEs of 0.9% for the devices. The film with the highest acceptor content 1:19 (donor:acceptor) exhibited a slightly lower Jsc, resulting in poorer device performance. A similar trend was also observed for blends films fabricated from chloroform with 10% DCB (see Table 6.4).

Another interestingly result found was the blend films of the **OddDPP(ThBF(OMe)$_2$)$_2$** and PC70BM, fabricated under similar conditions from chloroform and chloroform with 10% DCB exhibited the same trend (see Table 6.4).

| **Ratio (Donor:Acceptor) By weight** | **Voc (eV) ±0.01** | **$J_{sc}$ (mA cm$^{-2}$) ±0.1** | **FF ±0.01** | **PCE (%)** |
|---|---|---|---|---|
| **OddDPP(ThBF)$_2$**:PC70BM | | | | |
| 4:1 | 0.96 | 0.1 | 0.22 | 0.02 |
| 1:1 | 0.93 | 1.9 | 0.25 | 0.4 |
| 1:4 | 0.84 | 3.6 | 0.29 | 0.9 |
| 1:19 | 0.84 | 1.6 | 0.30 | 0.4 |
| **OddDPP(ThBF(OMe)$_2$)$_2$**:PC70BM | | | | |
| 4:1 | 0.92 | 0.1 | 0.22 | 0.02 |
| 1:1 | 0.88 | 1.9 | 0.25 | 0.4 |
| 1:4 | 0.81 | 3.5 | 0.30 | 0.9 |
| 1:19 | 0.82 | 1.4 | 0.32 | 0.4 |

**Table 6.3.** BHJ solar cell parameters of the best devices of **OddDPP(ThBF)$_2$** and **OddDPP(ThBF(OMe)$_2$)$_2$** blended with PC70BM processed from neat chloroform solvents.

| Ratio (Donor:Acceptor) By weight | Voc (eV) ±0.01 | $J_{sc}$ (mA $cm^{-2}$) ±0.1 | FF ±0.01 | PCE (%) |
|---|---|---|---|---|
| **OddDPP(ThBF)$_2$**:PC70BM | | | | |
| 4:1 | 0.94 | 0.06 | 0.21 | 0.01 |
| 1:1 | 0.94 | 1.6 | 0.25 | 0.4 |
| 1:4 | 0.84 | 3.6 | 0.30 | 0.9 |
| 1:19 | 0.84 | 1.3 | 0.31 | 0.3 |
| **OddDPP(ThBF(OMe)$_2$)$_2$**:PC70BM | | | | |
| 4:1 | 0.92 | 0.1 | 0.22 | 0.02 |
| 1:1 | 0.88 | 1.9 | 0.25 | 0.4 |
| 1:4 | 0.81 | 3.5 | 0.30 | 0.9 |
| 1:19 | 0.82 | 1.4 | 0.32 | 0.4 |

**Table 6.4.** BHJ solar cell parameters of the best devices of **OddDPP(ThBF)$_2$** and **OddDPP(ThBF(OMe)$_2$)$_2$** blended with PC70BM processed from different chloroform solvents with 10% DCB.

A comparison of donor:acceptor ratio of 1:1 and 1:4 for **OddDPP(ThBF)$_2$**:PC70BM and, **OddDPP(ThBF(OMe)$_2$)$_2$**:PC70BM fabricated from chloroform clearly suggest that when the acceptor (PC70BM ) content was increased the charge generation improved resulting in better $J_{sc}$. An EQE of ~32% and ~28% at 400 and 534 nm seen for the 1:4 blend film suggests charge generation occurs through both Channels, as both the donor and acceptor absorbs at these wavelengths (see Figure 6.11). The improvement in device performance with greater fullerene content in the film is consistent with the results for many narrow optical gap polymers.

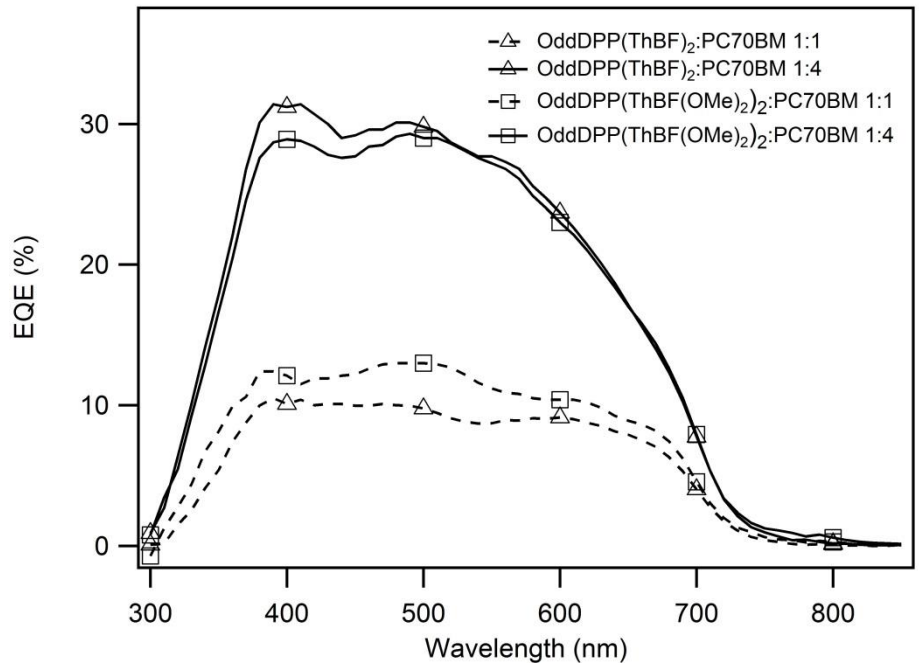


**Figure 6.11.** EQE against wavelength for the different ratios of **OddDPP(ThBF)$_2$**:PC70BM and **OddDPP(ThBF(OMe)$_2$)$_2$**:PC70BM of devices whereby the active films were formed by spin-coating from chloroform.

When the films were fabricated with different ratios of **OddDPP(ThBF)$_2$**:PC70BM from chloroform with 0.5% DIO, the devices exhibited a different trend. The films fabricated with higher content of either donor or acceptor performed poorly (see Table 6.3). Blends with 1:1, 3:2 and 2:3 ratios of donor to acceptor exhibited better device efficiencies, again mainly due to increase in the $J_{sc}$ and the FF. In contrast the devices fabricated from the **OddDPP(ThBF(OMe)$_2$)$_2$**:PC70BM, under similar conditions generally showed huge resistance and hence, the device performance could not be measured (see Table 6.5).

| **Ratio (Donor:Acceptor) By weight** | **Voc (eV) ±0.01** | **$J_{sc}$ (mA cm$^{-2}$) ±0.1** | **FF ±0.01** | **PCE%** |
|---|---|---|---|---|
| **OddDPP(ThBF)$_2$**:PC70BM | | | | |
| 4:1 | 0.66 | 1.1 | 0.26 | 0.2 |
| 3:2 | 0.70 | 6.6 | 0.48 | 2.2 |
| 1:1 | 0.69 | 6.8 | 0.56 | 2.6 |

| | | | | |
|---|---|---|---|---|
| 2:3 | 0.68 | 5.4 | 0.51 | 1.9 |
| 1:4 | 0.82 | 2.1 | 0.28 | 0.5 |
| 1:19 | 0.82 | 0.5 | 0.28 | 0.1 |
| **OddDPP(ThBF(OMe)$_2$)$_2$**:PC70BM | | | | |
| 4:1 | 0.58 | 0.2 | 0.21 | 0.02 |
| 1:19 | 0.78 | 0.8 | 0.32 | 0.2 |

**Table 6.5.** BHJ solar cell parameters of the best devices of **OddDPP(ThBF)$_2$** and **OddDPP(ThBF(OMe)$_2$)$_2$** blended with PC70BM processed from chloroform solvents with 0.5% DIO.

An EQE of 38% at 400 nm (see Figure 6.12) for 1:1 ratio of **OddDPP(ThBF)$_2$**:PC70BM device fabricated from chloroform with 0.5% DIO suggests, that the film structure favoured better charge generation, which led to a device with maximum PCE of 2.6% with $J_{sc}$ = 6.8 ± 0.1 mA cm$^{-2}$, Voc = 0.69 ± 0.01 eV, and FF = 0.56 ± 0.01. However, for the **OddDPP(ThBF(OMe)$_2$)$_2$**:PC70BM film fabricated under similar conditions with same blend ratio exhibited no charge generation (see Figure 6.12). The films fabricated with a higher acceptor content, a ratio of **OddDPP(ThBF)$_2$**:PC70BM 1:4, exhibited an increase in Voc to 0.82 ± 0.01 eV, but the $J_{sc}$ and FF reduced to 2.1 ± 0.1 mA cm$^{-2}$ and FF = 0.28 ± 0.01, respectively. This suggests a less favourable film structure for charge generation and extraction. Again, the films for **OddDPP(ThBF(OMe)$_2$)$_2$**:PC70BM, exhibited no charge generation at all (see Figure 6.12).

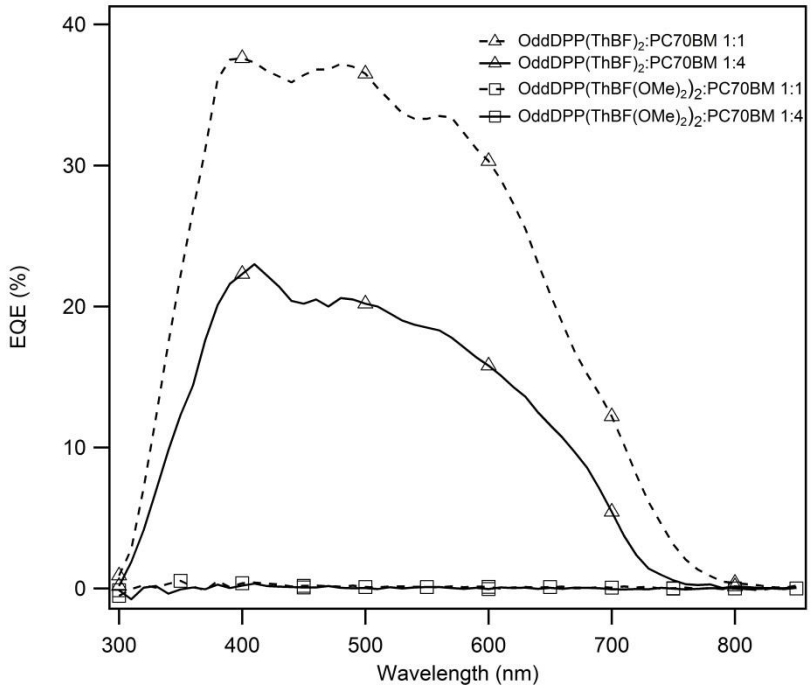


**Figure 6.12.** EQE against wavelength for the different ratios of **OddDPP(ThBF)$_2$**:PC70BM and, **OddDPP(ThBF(OMe)$_2$)$_2$**:PC70BM devices fabricated by spin coating the active films from chloroform and 0.5% DIO.

In order to further understand more about the influence of processing conditions on the films and their device performance it would be helpful to investigate their morphology, e.g., using Grazing Incidence Wide-angle X-ray scattering (GIWAX) technique. However, due to time constraints this is planned as a future study.

## 6.5 Conclusion

The final two targets **OddDPP(ThBF)$_2$** and **OddDPP(ThBF(OMe)$_2$)$_2$** were successfully synthesized and purified. However, the third target **OddDPP(ThBF(F)$_2$)$_2$** could not be purified in a timely manner for investigation into its properties. The DSC measurements showed that **OddDPP(ThBF)$_2$** and **OddDPP(ThBF(OMe)$_2$)$_2$** had different thermal phase transition behaviour at similar scan rates. However, the thin film absorption of the materials exhibited similar absorption profiles and their IPs and EAs were similar. In devices, the films fabricated from neat chloroform and chloroform with 10% DCB, with high acceptor content (1:4, donor:acceptor) exhibited maximum charge generation efficiency and better PCE. However, the films fabricated from chloroform with 0.5% DIO, exhibited better charge generation and device efficiency for a 1:1 ratio

of the **OddDPP(ThBF)$_2$**:PC70BM combination, the **OddDPP(ThBF(OMe)$_2$)$_2$**:PC70BM films showed no charge generation.

# Chapter 7- Conclusions, summary and furture directions

## 7.1 Conclusions and summary

Chapter 1 provided an introduction on the different types of photovoltaics cells and explained why there has been tremendous effort to develop organic photovoltaics cells (OPVs). Different types of OPV device architecture and the important parameters that determine the power conversion were introduced. The two main charge generation mechanisms were also described. A summary of the types of organic semiconductors that has been previously reported for use as either donor or acceptor materials was also reported. Polymer materials are widely studied as the electron donor in OPVs, but issues like regioregularity and batch-to-batch variations means that non-polymeric materials have now gained attention. In that context, diketopyrrolopyrrole based non-polymeric materials were introduced and reasons given as to why they have gained attention over the last 10 years. It was also shown how different research groups have fine-tuned the properties of the DPP derivatives to suit most commonly used polymer donor or fullerene based acceptor materials for charge generation and extraction in OPV devices.

In chapter 2, it was shown how the yield of the **DPP(Th)$_2$** unit can be improved by increasing the equivalents of sodium used and using catalytic amount of iron(II) chloride for sodium dissolution. The yield for the *N*-alkylation of the **DPP(Th)$_2$** unit with 2-octyldocdecyl solubilising groups was improved by using 18-crown-6 as a phase transfer catalyst. It was also shown that DPP(ThAr)$_2$ can be prepared either using standard Suzuki-Miyuara cross coupling conditions or by using direct arylation reaction conditions. The direct arylation reactions were found to be a faster and more convenient way to prepare DPP(ThAr)$_2$ than the standard Suzuki-Miyuara cross coupling conditions, as it does not require preparation of organometallic intermediates, which can be toxic and are labour intensive. The solubility was poor when the 2-ethylhexyl moiety was used as the solubilising group for **DPP(ThFl)$_2$** but is was found that the 2-octyldodecyl solubilising groups gave better solubility in chlorinated solvents, and enabled device fabrication.

In Chapter 3 it was seen that by having different end groups, fluorenone or benzothiadiazole units, on the **DPP(Th)$_2$** moiety the thermal phase transition behaviour of the materials were different. However, the materials exhibited a broad absorption across the UV-Visible spectrum with $\lambda_{max}$ above 600 nm. The redox properties of the DPP derivatives showed that they could be used with PC70BM as an acceptor. In an OFET configuration the materials showed hole mobilities in the range of $10^{-2}$-$10^{-3}$ cm$^2$ V$^{-1}$ s$^{-1}$. The mobility measurements from the MIS-CELIV technique showed that the two solution processable materials had sufficient mobility to be used as a hole transport

material in OPV devices. In OPV devices the role of solvent additives/solvent mixtures was found to be important in optimizing the ideal film structure to bring about maximum excition dissociation and efficient charge extraction. The EQE spectrum of devices comprised of **OddDPP(ThFl)$_2$** and **OddDPP(ThBt)$_2$** suggested that charge generation through the Channel I mechanism occurred at wavelengths longer than 700 nm. At shorter wavelengths charge generation via both Channel I and II was found to occur. However, **OddDPP(ThFl)$_2$** performed better as an electron donor in BHJ device and achieved maximum PCE of 4.1%.

In order to vary the charge transporting properties of **OddDPP(ThFl)$_2$** a series of sulphur containing derivatives was designed. However, only a dithiane derivative could be successfully synthesised and characterised. The thermal and optical properties of the dithiane derivative exhibited weak intermolecular interaction in films, which had direct impact on the OPV device performance. The best devices exhibited a poor PCE, with the highest being 0.4%.

In Chapter 5, a series of **OddDPP(ThBt)$_2$** derivatives were designed, synthesised, and characterised. It was shown that by incorporating different electron withdrawing groups the EA of DPP derivatives could be increased. The thin film absorption studies showed the **OddDPP(ThBt-DCV)$_2$**, had a much stronger red shift in absorption, compared to **OddDPP(ThBt-B2A)$_2$**. However, the **OddDPP(ThBt-DCV)$_2$** did not have sufficient solubility to fabricate OPV devices by solution processing, while **OddDPP(ThBt-B2A)$_2$** showed better solubility. The photoluminescence quenching experiments showed that by blending **OddDPP(ThBt-B2A)$_2$** with P3HT enabled charge generation, but the devices performed poorly. The EQE absorption spectrum of the device suggested that at wavelengths longer than 750 nm charge generation was purely through the Channel II pathway and at shorter wavelengths both Channel I and II, occurred. Mobility measurements of the blend films exhibited electron mobilities two orders of magnitude lower compared to the pristine film of the acceptor, suggesting an unfavourable film structure in blend for charge extraction, resulting in poor device performance.

In Chapter 6 the final two targets, **OddDPP(ThBF)$_2$** and **OddDPP(ThBF(OMe)$_2$)$_2$**, were successfully synthesized and purified. However, the third target **OddDPP(ThBF(F)$_2$)$_2$** could not be purified in time for investigation into its properties. Thermal analysis showed that the materials had different thermal phase transition behaviour. However, the thin film absorption of the materials exhibited similar absorption profile. In devices, the films fabricated from neat chloroform and chloroform with 10% DCB, with high acceptor content (1:4, donor:acceptor), for both the materials, were found to have the best PCE. However, the films fabricated from chloroform with 0.5% DIO,

exhibited an even better device efficiency but in this latter case for a 1:1 ratio of donor:acceptor (**OddDPP(ThBF)$_2$**:PC70BM). In contrast, OPV devices containing **OddDPP(ThBF(OMe)$_2$)$_2$**:PC70BM blends simply did not work.

In summary, it was shown that the DPP derivatives can be prepared under standard Suzuki-Miyuara cross coupling conditions or direct arylation conditions. The direct arylation reactions are more convenient ways to prepare these derivatives. 2-Octyldodecyl solubilising groups are the minimum required to enable these DPP derivatives to be solution processed. It was also shown that the incorporation of different end units onto DPP(Th)$_2$ moiety had direct impact on the physical properties and BHJ device performance.

### 7.2 Future directions

It is shown that DPP derivatives can function as both hole and electron charge transporting material in OPV devices. Hence, to utilise these adventegous properites of the DPP derivatives an intresting approach would be to fabricate a blend film with DPP derivatives. For example, OddDPP(ThBt)$_2$ was shown to have good hole mobility and its derivative OddDPP(ThBt-B2A)$_2$ with decent electron mobility similar with suffienct energy offset for charge generation. As the basic unit of the DPP derivatives are similar, it is anticpated to give films with better π–π stacking, which can lead to better charge transporting properties and eventually efficeint OPV devices.

In general, it might be better to have aromatic end groups on to the DPP(Th)$_2$ unit as it was shown in this work and in literature that, it can lead to better end-to-end interaction with adjacent molecules in films and is anticipated to increase the FF. This design statergy can be employed for engineering both donor and acceptor material to enhance its charge transporting proeprties.

# Chapter 8 - Experimental

## 8.1 General experimental

All commercial reagents were used as received unless otherwise noted. Solvents were distilled before use. Tetrahydrofuran was distilled from sodium and benzophenone under a nitrogen atmosphere before use. Light petroleum refers to the fraction with boiling point of 40–60 °C. $^{1}H$ and $^{13}C$ NMR spectra were recorded using a 400, or 500 MHz Bruker spectrometer in deuterated chloroform solution and chemical shifts (δ) were referenced to 7.26 ppm and 77.0 ppm for the proton and carbon spectra, respectively. Multiplicities are reported as singlet (s), doublet (d), triplet (t), and multiplet (m) and coupling constants (*J*) are in Hertz and quoted to the nearest 0.5 Hz. Assignments of proton peaks are as followings: Th H = thiophenyl H, Fl H = fluorenonyl H, and Bt H = benzothiadiazolyl H, BF H = 9,9'-bifluorenylidene. UV-vis absorption spectra were recorded on a Cary 5000 UV-Vis spectrophotometer in distilled (from $CaH_2$) dichloromethane using 10 × 10 mm quartz cuvettes and $\lambda_{max}$ values were quoted in nm and shoulders denoted as "sh". Fluorescence spectra were measured using a Jobin-Yvon Horiba Fluorolog in steady-state mode using a xenon lamp as the excitation source. Infrared spectra were recorded on a Perkin-Elmer Spectrum 100 FT-IR spectrometer with ATR attachment. Mass spectra were recorded on an Applied Biosystems Voyager-DE STR matrix-assisted laser-desorption ionisation-time of flight (MALDI-TOF) using 2,5-dihydroxybenzoic acid (DHB) as the matrix in positive reflectron mode. Cyclic voltammetry (CV) was performed in a standard three-electrode system at room temperature using a solution comprising 1 mM **2** and 0.1 M tetra-*n*-butylammonium hexafluorophosphate (TBAH, Alfa Aesar, electrochemical grade) as electrolyte in distilled (from $CaH_2$) dichloromethane, a glassy carbon, a Pt wire counter electrode and a $Ag/AgNO_3$ solution as the reference electrode at scan rate of 100 mV/s. The solutions were purged with argon and measured under an argon atmosphere. Thermal gravimetric analysis (TGA) was carried out on a Perkin-Elmer STA 6000 and differential scanning calorimetry (DSC) was performed by using PerkinElmer Diamond DSC. Melting points were measured on a BÜCHI Melting Point B-545. Elemental analyses were carried in School of Chemistry and Molecular Biosciences, the University of Queensland. Photoelectron spectroscopy in air (PESA) was performed by Dr. Dani Stoltzfus on ≈60 nm thick films on glass using a Riken Kekei AC-2 spectrometer.

### 8.1.2 OPV device Fabrication and measurement

Devices were prepared on pre-patterned indium-doped tin oxide (Kintec) substrates. The substrates were first cleaned in a warm detergent (Alconox), followed by ultra-sonication sequentially in an

Alconox solution, deionized water, acetone, and finally 2-propanol for approximately 6 min in each solution. The substrates were dried by blown with nitrogen. A thin (≈25 nm) layer of poly(ethylenedioxythiophene):poly(styrenesulfonic acid) (PEDOT:PSS, Baytron P VP Al 4083) was deposited by spin coating at 5000 rpm for 120 s. Substrates were then baked on a hot plate for 20 min at 170 $^{o}$C in air. For bulk heterojunction devices, stock solutions of DPP derivatives and PC70BM at varied concentrations in chloroform were prepared and mixed by blending DPP derivative:PC70BM in various ratios, and similarly when DPP derivative was used as acceptor, stock solutions of DPP derivatives and P3HT at varied concentrations in chloroform were prepared and mixed by blending DPP derivative:P3HT in various ratios. To that solution, 1,8-diiodooctane of different volumes or 10% 1,2-dichlorbenzne was added, unless otherwise stated. The remaining fabrication of bulk heterojunction devices was carried out inside a nitrogen filled glove box. Active layers were fabricated by spin coating the blend solution at 1300 rpm for 30 s onto the PEDOT:PSS layer and immediately covering with a petridish (9 cm diameter) until dry (≈5 min). The dry substrates were then baked at 60 $^{o}$C for 20 min before metallization. The devices made with PC70BM/P3HT were prepared in the same manner. Top aluminium electrodes (80 nm) were deposited by thermal evaporation. Aluminum was initially deposited at a rate of 0.4 Å/s, which was then increased to 1.5 Å/s under a vacuum of $1 \times 10^{-6}$ mbar. The electrode area was defined by a shadow mask with an active area of 0.2 cm$^2$. Each substrate contained 6 devices with at least one substrate fabricated for each blend ratio. Devices were tested unencapsulated in a nitrogen filled glove box using a spectrally corrected AM1.5G Abet Solar Simulator (white light J–V) and PV Measurements Inc EQE system in the small perturbation, chopped probe regime. On an average 4-6 devices were tested and the date presented is an average value.Solar Simulator spectral mismatch and absolute intensity was determined using an NREL calibrated photodiode. On average, the difference between the white light short circuit current and integrated EQE current was <10%.

### 8.1.3 OFET device fabrication and measurement

The top-contact bottom-gate OFET were comprised of 500 nm thick $SiO_2$ dielectric that was thermally grown on top of a heavily n-doped silicon wafer purchased from Silicon Quest, International, Inc. The $SiO_2$ substrates were cleaned in a Class 1000 clean room by ultra-sonication in acetone for 20 min followed by ultra-sonication in 2-propanol for 20 min. Substrates were then dried in nitrogen. All remaining fabrication and testing was performed inside a nitrogen filled MBraun glove box ($O_2$ and $H_2O$ levels < 0.1 ppm). The insulator surface was treated with octyltrichlorosilane (OTS), divinyltetramethyldisiloxane-bis(benzocyclobutane) (BCB), or poly(methyl methacrylate) (PMMA). Substrates treated with OTS were soaked for 24 h in a 3 mM

solution of OTS in toluene before removal and rinsing with toluene then annealed at 70 °C for 10 min. Solution of BCB (in mesitylene) was purchased from Dow Chemicals. BCB was spin-casted onto substrates at 2500 rpm for 30 s and then the films were annealed at 250 °C for 1 hour for crosslinking. PMMA (120,000 g/mol) solution of concentration 35 mg/cm$^3$ in *n*-propylacetate (P99.5%) was spin-cast onto the substrates at 2500 rpm for 30 s. The substrates were then backed on a hot plate at 150 °C for 30 min. The BCB and PMMA film thicknesses were measured to be about 260 nm and140 nm, respectively, using a Dektak 150 profilometer.

## 8.2 Chemical Synthesis

This section includes the experimental details comprising the preparation of novel compounds, as well as previously synthesized materials where a modification has been made to the earlier synthetic or purification procedure.

**Thiophene-2-carbonitrile** (**2.6**)

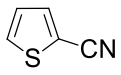


Triethylamine (21.0 g, 207 mmol) and **2.5** (22.0 g, 196 mmol) were added to a stirred solution of hydroxylamine hydrochloride (14.3 g, 207 mmol) in acetonitrile (800 cm$^3$), and the mixture was then heated at reflux for 2 h. Oxalyl chloride (24.9 g, 196 mmol) was then added dropwise to the refluxing mixture and after addition the reaction mixture was heated at reflux with stirring for 40 min before being allowed to cool down to room temperature. The acetonitrile was removed and chloroform (400 cm$^3$) and water (200 cm$^3$) were added, and after shaking the layers were separated. The organic layer was extracted with brine (100 cm$^3$), dried over anhydrous magnesium sulphate, and filtered. The solvent was completely removed to leave a yellow oily residue. The residue was purified in two stages; first, column chromatography over silica using light petroleum spirit/dichloromethane (7:3) as eluent, and second distillation under reduced pressure (130 °C, 21 mbar) to give **2.6** as a colorless oil (14.1 g, 66%). $^1$H NMR (500 MHz, $CDCl_3$) δ: 7.1 (dd, *J* = 4.0 & 5.0, 1 H, Th H), 7.59–7.57 (m, 2 H, Th H); $^{13}$C (125 MHz, $CDCl_3$) δ: 109.5, 114.1, 127.5, 132.5, 137.3; $\upsilon_{max}$/cm$^{-1}$ 2220 cm$^{-1}$ (CN). **2.6** had identical $^1$H and $^{13}$C NMR spectra as an authentic sample.[165]

**Di-*iso*-propylsuccinate** (**2.8**)

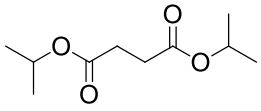

*Iso*-Propanol (750 $cm^3$) and **2.7** (20.0 g, 169 mmol) were added to the solid resulting from stirring sodium carbonate (39.5 g, 372 mmol) and thionyl chloride (42.0 g, 353 mmol) for 5 min. The mixture was stirred for 5 min before being heated at reflux for 3 h. After cooling to room temperature the pH was adjusted to 9 using aqueous sodium bicarbonate (10%, 150 $cm^3$). Dichloromethane (500 $cm^3$) and water (600 $cm^3$) were added and the mixture shaken. The layers were then separated and the organic layer was extracted with brine (100 $cm^3$) before being dried over anhydrous magnesium sulphate, and filtered. The solvent was removed to give colourless oil. The residue was purified by distillation under reduced pressure (95 °C, 0.85 mbar) to give **2.8** as a colorless oil (31.8 g, 93%). $^1$H NMR (300 MHz, $CDCl_3$) δ: 1.20 (d, *J* = 6.5, 12 H, $CH_3$), 2.55 (s, 4 H, $CH_2$), 4.94–5.06 (m, 2 H, O-CH), $^{13}$C (100 MHz, $CDCl_3$) δ: 21.8, 29.6, 68.0, 171.8; $\upsilon_{max}$/$cm^{-1}$ 1728 $cm^{-1}$ (C=O). **2.8** had identical $^1$H and $^{13}$C NMR spectra as an authentic sample.[166]

**3,6-Di(thiophen-2-yl)pyrrolo[3,4-c]pyrrole-1,4(2*H*,5*H*)-dione** (**2.9**)

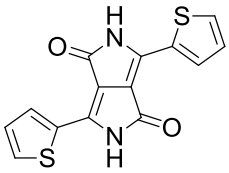

A mixture of sodium metal (3.50 g, 152 mmol) and a catalytic amount of ferric chloride (~2 mg, ~0.012) was carefully dissolved in 2-methyl-2-butanol (120 $cm^3$, 109 mmol). The mixture was then heated at reflux for 3 h, before being cool down to 50 °C (oil bath temperature). **2.6** (7.0 g, 64.1 mmol) was added and the mixture was heated at reflux for 5 min. A solution of **2.8** (6.20 g, 30.6 mmol) in 2-methyl-2-butanol (36 $cm^3$) was added drop wise for 5 h at the refluxing mixture and after addition the reaction mixture was heated at reflux with stirring for 36 h before being allowed to cool down to room temperature. The reaction mixture was quenched with water (90 $cm^3$) and acetic acid (8.5 $cm^3$), and then filtered. The residue was washed with water (500 $cm^3$) and methanol (250 $cm^3$) to give **2.9** as a dark purple solid (7.5 g, 81%). $^1$H NMR (300 MHz, $CDCl_3$) δ: 7.26 (t, *J* = 9.0, 2 H, Th H), 7.90 (d, *J* = 5.0, 2 H, Th H), 8.16 (d, *J* = 4.0, 2 H, Th H), 11.2 (s, 2 H, NH H);

$^{13}$C (100 MHz, $CDCl_3$) δ: 108.9, 129.2, 131.1, 131.8, 133.2, 136.7, 162.2. **2.9** had identical $^{1}$H and $^{13}$C NMR spectra as an authentic sample[167].

**2,5-Bis(2-ethylhexyl)-3,6-di(thiophen-2-yl)pyrrolo[3,4-c]pyrrole-1,4(2*H*,5*H*)-dione** (**2.10**)

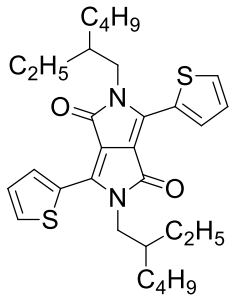


A mixture of **2.9** (7.00 g, 23.3 mmol), potassium carbonate (12.8 g, 92.6 mmol), and *N*,*N*-dimethylformamide (140 $cm^3$) was stirred at 80 °C (oil bath temperature) for an hour before being cooled down to room temperature. 2-Ethylhexylbromide (10.1 g, 104 mmol) was then added slowly (over 1 h). The mixture was then stirred at 80 °C (oil bath temperature) for 13 h, before being allowed to cool down to room temperature. Chloroform (500 $cm^3$) and water (1300 $cm^3$) were added and after shaking the layers were separated. The organic layer was extracted with brine (500 $cm^3$), dried over anhydrous magnesium sulphate, and filtered. The solvent was completely removed to leave a dark purple solid residue. The residue was purified using column chromatography over silica with light petroleum spirit/diethyl ether mixture (4:1) as eluent to give **2.10** as dark purple solid (5.4 g, 44%). $^{1}$H NMR (400 MHz, $CDCl_3$) δ: 0.80–0.87 (m, 12 H, $CH_3$), 1.17–1.42 (m, 16 H, $CH_2$), 1.77–1.90 (m, 2 H, CH), 3.94–4.06 (m, 4 H, $NCH_2$), 7.23–7.26 (m, 2 H, Th H), 7.60 (dd, *J* = 1.0 & 5.0, 2 H, Th H), 8.86 (dd, *J* = 1.0 & 4.0, 2 H, Th H); $^{13}$C (100 MHz, $CDCl_3$) δ: 10.5, 14.0, 23.0, 23.5, 28.3, 30.2, 39.1, 45.8, 107.9, 128.4, 129.8, 130.5, 135.3, 140.4, 161.7. **2.10** had identical $^{1}$H and $^{13}$C NMR spectra as an authentic sample.[111]

**3,6-Bis(5-bromothiophen-2-yl)-2,5-bis(2-ethylhexyl)pyrrolo[3,4-c]pyrrole-1,4(2*H*,5*H*)-dione** (**2.11**)

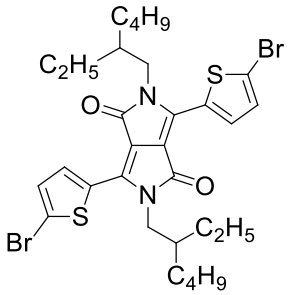

*N*-Bromosuccinimide (1.80 g, 10.3 mmol) was added to a solution of **2.10** (2.46 g, 4.68 mmol) in chloroform (137 $cm^3$) in the dark. After stirring at room temperature for 15 h, water (420 $cm^3$) was added, and after shaking, the layers were separated. The organic layer was extracted with brine (140 $cm^3$), dried over anhydrous magnesium sulphate, and filtered. The solvent was completely removed to leave a dark purple solid residue. The residue was purified using column chromatography over silica with light petroleum spirit/dichloromethane mixtures (1:3 to 1:4) as eluent to give **2.11** as dark purple solid (2.53 g, 79%). $^1$H NMR (400 MHz, $CDCl_3$) δ: 0.82–0.88 (m, 12 H, $CH_3$), 1.15–1.40 (m, 16 H, $CH_2$), 1.75–1.85 (m, 2 H, CH), 3.84–3.97 (m, 4 H, $NCH_2$), 7.20 (d, *J* = 4.0, 2 H, Th H), 8.61 (d, *J* = 4.5, 2 H, Th H); $^{13}$C (100 MHz, $CDCl_3$) δ: 10.4, 14.0, 23.0, 23.5, 28.3, 30.1, 39.1, 46.0, 108.0, 119.0, 131.1, 131.4, 135.4, 139.4, 161.4. **2.11** had identical $^1$H and $^{13}$C NMR spectra as an authentic sample.[168]

**2-Bromo-9*H*-fluoren-9-one** (**2.13**)

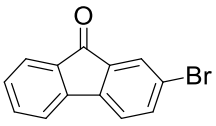

Aqueous sodium hydroxide (10 M, 335 $cm^3$) was added to a stirred mixture of **2.12** (20.0 g, 81.5 mmol) and catalytic tetra-*n*-butylammonium bromide (100 mg, 0.30 mmol) in toluene (500 $cm^3$). The mixture was stirred for 3 h at room temperature. The organic layer was separated and the aqueous layer was extracted with toluene (84 $cm^3$). The organic layers were combined and then washed with aqueous sodium bicarbonate solution (10 M, 150 $cm^3$), brine (50 $cm^3$), and then dried over anhydrous magnesium sulphate, and filtered. The solvent was completely removed to give a yellow residue. The residue was purified using column chromatography over silica using light

petroleum spirit/dichloromethane (7:3) as eluent to give **2.13** as a yellow solid (19.6 g, 93%). $^{1}$H NMR (400 MHz, $CDCl_3$) δ: 7.26–7. 30 (m, 1 H, Fl H), 7.34 (d, *J* = 5.65, 1 H, Fl H), 7.45–7.47 (m, 2 H, Fl H), 7.55 (d, *J* = 4.5, 1 H, Fl H), 7.61 (d, *J* = 5.5, 1 H, Fl H), 7.70 (s, 1 H, Fl H); $^{13}$C (100 MHz, $CDCl_3$) δ: 120.4, 121.7, 122.9, 124.6, 127.5, 129.4, 133.7, 135.0, 135.7, 137.1, 143.0, 143.6, 192.4; $\upsilon_{max}$/cm $^{-1}$ 1717 cm$^{-1}$ (C=O). **2.13** had identical $^{1}$H and $^{13}$C NMR spectra as an authentic sample.[169]

**2-(4,4,5,5-Tetramethyl-1,3,2-dioxaborolan-2-yl)-9*H*-fluoren-9-one** (**2.14**)

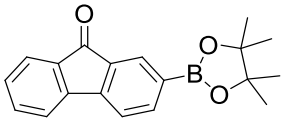


Method A

Bis(pinacolato)diboron (3.86 g, 15.2 mmol), potassium acetate (2.61 g, 26.6 mmol), [1,1'-bis-(diphenylphosphino)ferrocene]dichloropalladium(II) (162 mg, 0.22 mmol), **2.13** (2.30 g, 8.87 mmol) and *N*,*N*-dimethylformamide (67 cm$^3$) was sparged with argon for 15 min, and then heated at reflux for 27 h. After cooling to room temperature, chloroform (180 cm$^3$) and water (700 cm$^3$) were added. The mixture was shaken and the layers separated. The organic layer was washed with brine (150 cm$^3$), dried over anhydrous magnesium sulphate, and filtered. The solvent was completely removed to give a yellow residue. The residue was purified using column chromatography over silica using light petroleum spirit/dichloromethane (1:1) as eluent **2.14** as dark yellow needles (1.00 g, 45%). $^{1}$H NMR (400 MHz, $CDCl_3$) δ: 8.10 (s, 1 H, Fl H), 7.92 (d, *J* = 7.5, 1 H, Fl H), 7.64 (d, *J* = 7.5, 1 H, Fl H), 7.54–7.44 (m, 3 H, Fl H), 7.31–7.30 (m, 1 H, Fl H), 1.3 (s, 12 H, $CH_3$); $^{13}$C (100 MHz, $CDCl_3$) δ: 24.8, 84.1, 119.6, 120.7, 124.2, 129.5, 130.5, 133.3, 134.4, 141.4, 144.2, 146.9, 193.8. **2.14** had identical $^{1}$H and $^{13}$C NMR spectra as an authentic sample.[170]

Method B

Bis(pinacolato)diboron (2.35 g, 9.25 mmol), potassium acetate (2.2 g, 22.4 mmol), [1,1'-bis-(diphenylphosphino)ferrocene]dichloropalladium(II) (280 mg, 0.38 mmol), **2.13** (2.00 g, 7.71 mmol) and 1,4 –dioxane (30 cm$^3$) was sparged with argon for 10 min, and then heated at reflux for 3.5 h. After cooling to room temperature, diethyl ether (120 cm$^3$) and water (90 cm$^3$) were added.

The mixture was shaken and the layers separated. The organic layer was washed with brine (120 $cm^3$), dried over anhydrous magnesium sulphate, and filtered. The solvent was completely removed to give a yellow residue. The residue was purified by recrystallization from ethanol to give as dark yellow needles (1.4 g, 60%) and had identical $^1$H NMR and $^{13}$C NMR as obtained *via* method A.

**2,5-Bis(2-ethylhexyl)-3,6-bis(5-(9-oxo-9*H*-fluoren-2-yl)thiophen-2-yl)pyrrolo[3,4-c]pyrrole-1,4(2*H*,5*H*)-dione** (**2.1**)

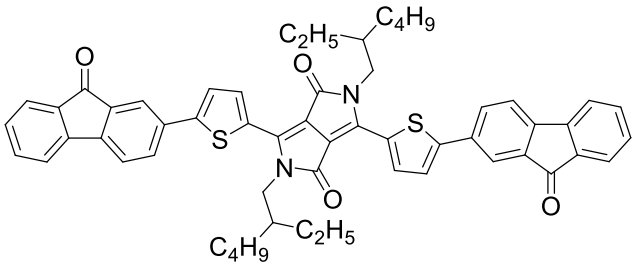


Tetrakis(triphenylphosphino)palladium(0) (85.0 mg, 0.073 mmol) was added to a deoxygenated mixture of **2.11** (1.00 g, 1.46 mmol), **2.14** (1.25 g, 4.09 mmol), tetrahydrofuran (30 $cm^3$) and aqueous potassium carbonate (2 M, 7.5 $cm^3$). The mixture was further deoxygenated by placement under vacuum and back filling with argon four times before being heated at reflux under argon for 20 h. The reaction was cooled to room temperature and the organic layer was separated. Aqueous layer was extracted with chloroform (3 x 250 $cm^3$). The organic layer and chloroform extracts were combined, washed with brine (330 $cm^3$), dried over anhydrous magnesium sulphate, and filtered. The filtrate was collected and the solvent was completely removed to give a dark blue residue. The residue was purified by column chromatography over silica using chloroform/light petroleum (4:1) as eluent. The isolated product was further purified by soxhlet extraction with toluene to give **2.1** as a dark blue solid (491 mg, 37%), mp 282–284 °C; $TGA_{(5\%)}$ 405 °C. Anal. Calcd $C_{56}H_{52}N_2O_4S_2$: C, 76.3; H, 6.0; N, 3.2; S, 7.3. Found: C, 76.2; H, 6.1; N, 3.3; S, 7.1%. $\upsilon_{max}$(solid)/$cm^{-1}$ 1717 (C=O), 1646 (C=O). $\lambda_{max}(CH_2Cl_2)$/nm 323 (log $\varepsilon/dm^3\ mol^{-1}\ cm^{-1}$ 4.40), 354 (4.51), 420 sh (4.21), 581 (4.72), 617 (4.72). $^1$H NMR (500 MHz, $CDCl_3$): δ 0.88–0.98 (m, 12 H, $CH_3$), 1.23–1.48 (m, 16 H, $CH_2$), 1.86–1.98 (m, 2 H, CH), 4.00–4.10 (m, 4 H, $NCH_2$), 7.27 (dt, *J* = 1 & 7, 2 H, Fl H), 7.45–7.52 (m, 8 H, Fl H, Th H), 7.63 (d, *J* = 7.5, 2 H, Fl H), 7.73 (dd, *J* = 2 & 8, 2 H, Fl H), 7.86 (d, *J* = 2, 2 H, Fl H), 8.94 (d, *J* = 4, 2 H, TH H). $^{13}$C NMR (125 MHz, $CDCl_3$): δ 10.7, 14.2, 23.2, 23.8, 28.7, 30.5, 39.4, 46.2, 108.7, 120.7, 121.1, 121.7, 124.7, 125.1, 129.4, 129.5, 132.0, 134.2, 134.5, 135.1, 135.2, 136.9, 139.8, 144.1, 144.3, 148.3, 161.8, 193.3. *m/z* [MALDI: DHB]: Anal. Calcd for

$C_{56}H_{52}N_2O_4S_2$: 880.3 (100%), 881.3 (65%), 882.3 (31%), 883.3 (11%), 884.3 (3%). Found: 880.3 (48%), 881.3 (100%), 882.3 (41%), 883.3 (18%), 884.2 (7%).

**9-(Bromomethyl)nonadecane** (**2.16**)

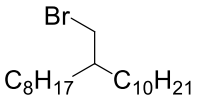


**2.15** (25.0 g, 83.7 mmol) and triphenylphosphine (44.0 g, 167 mmol) were dissolved in dichloromethane (75 $cm^3$) and cooled to 0 °C, before *N*-bromosuccinimide (22.4g, 125 mmol) was added. After stirring the reaction for 24 h at room temperature, the solvent was completely removed to give a colourless oily residue. The residue was purified using column chromatography over silica using light petroleum spirit as eluent to give **2.16** as colourless oil (25.4 g, 84%). **2.16** had identical $^1H$ and $^{13}C$ NMR spectra as an authentic sample[171].

**2,5-Bis(2-octyldodecyl)-3,6-di(thiophen-2-yl)pyrrolo[3,4-c]pyrrole-1,4(2H,5H)-dione** (**2.17**)

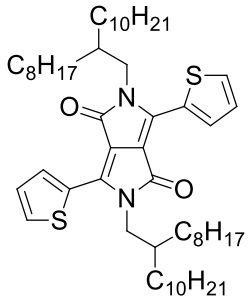


A mixture of **2.9** (4.50 g, 14.9 mmol), potassium carbonate (8.30 g, 60.0 mmol), 18-Crown-6 (1.60 g, 6.05 mmol) and *N*,*N*-dimethylformamide (45 $cm^3$) was stirred at 80 °C (oil bath temperature) for an hour before being cooled down to room temperature. 2-Octyldodecylbromide (19.0 g, 52.5 mmol) was then added slowly (over 1 h). The mixture was then stirred at 80 °C (oil bath temperature) for 16 h, before being allowed to cool down to room temperature and carefully poured into a mixture of ice and water (≈ 500 $cm^3$). The mixture was extracted with chloroform (3 X 100 $cm^3$). The Chloroform extracts were combined washed with brine (150 $cm^3$), dried over anhydrous magnesium sulphate, and filtered. The solvent was completely removed to leave a dark purple solid residue. The residue was purified using column chromatography over silica with diethyl ether/light petroleum spirit mixture (1:9 to 1:1) as eluent to give **2.17** as dark purple solid (3.86 g, 30%). $^1H$

NMR (300 MHz, $CDCl_3$) δ: 0.84 – 0.90 (m, 12 H, $CH_3$), 1.17–1.34 (m, 16 H, $CH_2$), 1.86–1.98 (m, 2 H, CH), 4.01–4.08 (m, 4 H, $NCH_2$), 7.25–7.28 (m, 2 H, Th H), 7.61 (dd, *J* = 1.0 & 5.0, 2 H, Th H), 8.86 (dd, *J* = 1.0 & 4.0, 2 H, Th H); $^{13}C$ (125 MHz, $CDCl_3$) δ: 14.1, 22.64, 22.67, 26.2, 29.27, 29.33, 29.48, 29.54, 29.6, 29.99, 31.2, 31.86, 31.90, 37.7, 46.2, 107.9, 128.4, 129.8, 130.4, 135.2, 140.4, 161.7. **2.17** had identical $^1H$ and $^{13}C$ NMR spectra as an authentic sample.[58]

**3,6-Bis(5-bromothiophen-2-yl)-2,5-bis(2-octyldodecyl)pyrrolo[3,4-c]pyrrole-1,4(2H,5H)-dione** (**2.18**)

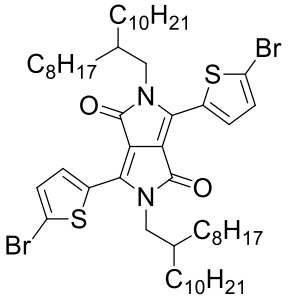


*N*-Bromosuccinimide (714.5 mg, 4.01 mmol) was added to a solution of **2.17** (2.22 g, 2.57 mmol) in chloroform (75 $cm^3$) in the dark. After stirring at room temperature for 22 h, before the solvent was completely removed to leave a dark purple solid residue. The residue was purified using column chromatography over silica with dichloromethane/light petroleum spirit mixtures (1:1) as eluent to give **2.18** as dark purple solid (1.93 g, 74%). $^1H$ NMR (300 MHz, $CDCl_3$) δ: 0.83–0.90 (m, 12 H, $CH_3$), 1.19–1.30 (m, 16 H, $CH_2$), 1.77–1.93 (m, 2 H, CH), 4.01–4.08 (m, 4 H, $NCH_2$), 7.18 (d, *J* = 4.0, 2 H, Th H), 8.60 (d, *J* = 4.0, 2 H, Th H); $^{13}C$ (125 MHz, $CDCl_3$) δ: 14.1, 22.64, 22.67, 26.2, 29.27, 29.34, 29.47, 29.53, 29.6, 29.95, 31.2, 31.85, 31.9, 37.7, 46.3, 107.9, 118.9, 131.1, 131.4,135.3, 139.3, 161.3. **2.18** had identical $^1H$ and $^{13}C$ NMR spectra as an authentic sample.[58]

**2,5-Bis(2-octyldodecyl)-3,6-bis(5-(9-oxo-9*H*-fluoren-2-yl)thiophen-2-yl)pyrrolo[3,4-c]pyrrole-1,4(2*H*,5*H*)-dione** (**2.2**)

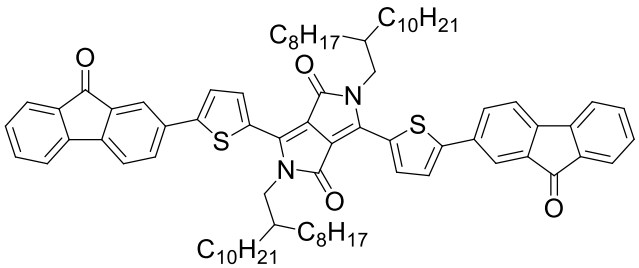

Method A

Tetrakis(triphenylphosphino)palladium(0) (104 mg, 0.090 mmol) was added to a deoxygenated mixture of **2.18** (1.83 g, 1.79 mmol), **2.14** (1.53 g, 5.01 mmol), tetrahydrofuran (55 $cm^3$) and aqueous potassium carbonate (2 M, 14.5 $cm^3$). The mixture was further deoxygenated by placement under vacuum and back filling with argon four times before being heated at reflux under argon for 22 h. The reaction was cooled and the two layers were separated. The aqueous layer was extracted with chloroform (2 x 200 $cm^3$). The organic layer and chloroform extracts were combined, washed with brine (100 $cm^3$), dried over anhydrous magnesium sulphate, and filtered. The filtrate was collected and the solvent was completely removed to give a dark blue residue. The residue was purified by column chromatography over silica using dichloromethane/light petroleum (4:1) as eluent. The isolated product was further purified by recrystallization from toluene to give **2.2** as a dark blue solid (1.18 g, 54%), mp 238–240 °C; $TGA_{(5\%)}$ 399 °C. Anal. Calcd for $C_{80}H_{100}N_2O_4S_2$: C, 78.9; H, 8.3; N, 2.3; S, 5.3. Found: C, 78.65; H, 8.35; N, 2.2; S, 5.0%. $\upsilon_{max}$(solid)/$cm^{-1}$ 1717 (C=O), 1646 (C=O). $\lambda_{max}$($CH_2Cl_2$)/nm 323 (log ε/$dm^3$ $mol^{-1}$ $cm^{-1}$ 4.35), 354 (4.47), 420 sh (4.17), 581(4.68), 617 (4.68). $^1$H NMR (500 MHz, $CDCl_3$) δ 0.80–0.85 (m, 12 H, $CH_3$), 1.15–1.40 (m, 64 H, $CH_2$), 1.93–2.01 (m, 2 H, CH), 4.03-4.08 (m, 4 H, $NCH_2$), 7.28 (dt, *J* = 1.5 & 7, 2 H, Fl H), 7.45–7.52 (m, 8 H, Fl H, Th H), 7.64 (d, *J* = 7, 2 H, Fl H), 7.73 (dd, *J* = 2 & 8, 2 H, Fl H), 7.87 (d, *J* = 1.5, 2 H, Fl H), 8.92 (d, *J* = 4, 2 H, Th H). $^{13}$C NMR (125 MHz, $CDCl_3$): δ 14.1, 22.7, 26.4, 29.3, 29.4, 29.57, 29.65, 29.66, 29.7, 30.1, 31.3, 31.89, 31.92, 37.9, 46.4, 108.5, 120.5, 120.9, 121.4, 124.5, 124.9, 129.30, 129.33, 131.7, 134.1, 134.3, 134.9, 135.0, 136.7, 139.6, 143.9, 144.0, 148.0, 161.5, 193.0. *m/z* [MALDI: DHB]: Anal. Calcd for $C_{80}H_{100}N_2O_4S_2$: 1216.7 (100%), 1217.7 (92%), 1218.7 (52%), 1219.7 (22%), 1220.7 (7%), 1221.7 (2%). Found: 1216.3 (44%), 1217.3 (100%), 1218.3 (91%), 1219.3 (49%), 1220.2 (22%), 1221.2 (4%).

Method B

Palladium acetate(II) (1.60 mg, 0.007 mmol) was added to a deoxygenated mixture of **2.17** (87.0 mg, 0.101 mmol), **2.13** (66.0 mg, 0.255 mmol), anhydrous potassium carbonate (35.0 mg, 0.253 mmol), pivallic acid (3.2 mg, 0.031 mmol) and *N*,*N*-dimethylacetamide (0.5 $cm^3$). The mixture was further deoxygenated under vacuum and back filling with argon four times before being heated in an oil bath held at 110 °C under argon for 4 h. The mixture was allowed to cool to room temperature and poured into a mixture of ice and water mixture (≈20 $cm^3$). The mixture was extracted with chloroform (3 x 20 $cm^3$). The chloroform extracts were combined, washed with brine

(20 $cm^3$), dried over anhydrous magnesium sulphate, and filtered. The filtrate was collected and the solvent was completely removed to give a dark blue residue. The residue was purified by column chromatography over silica using dichloromethane/light petroleum (4:1) and then chloroform/light petroleum (2:3) as eluent to give **2.2** as a dark blue solid (60.3 mg, 49%) and had identical $^1$H NMR and $^{13}$C NMR as obtained *via* method A.

**4-Bromobenzo[c][1,2,5]thiadiazole** (**2.20**)

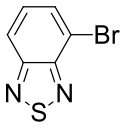


To a solution of **2.19** (10.0 g, 73.4 mmol) and hydrobromic acid 37% (50 $cm^3$, 2.22 mmol) heated at 120 °C, bromine (11.7 g, 73.2 mmol) in hydrobromic acid 37% (10 $cm^3$) was added dropwise for 5 h, before cool down to room temperature. The reaction mixture was then quenched with 50% aqueous sodium thiosulphate pentahydrate (50 $cm^3$). Dichloromethane (200 $cm^3$) was added shaken and layer separated. The aqueous phase was then extracted with dichloromethane (2 x 50 $cm^3$) and separated. The combined organics was then washed with 50% aqueous sodium bicarbonate solution (2 x 50 $cm^3$), dried over anhydrous magnesium sulphate, filtered and solvent completely removed to get yellow residue. The residue was purified by recrystallization from methanol to give **2.20** as white solid (9.94 g, 62%). $^1$H NMR (300 MHz, $CDCl_3$) δ: 7.34–7.39 (m, 1 H, Bt H), 7.72 (dd, *J* = 1 &7, 1 H, Bt H), 7.85 (dd, *J* =1 & 9, 1 H, Bt H); $^{13}$C (125 MHz, $CDCl_3$) δ: 114.2, 120.7, 129.7, 131.8, 153.1, 154.4. **2.20** had identical $^1$H and $^{13}$C NMR spectra as an authentic sample[158].

**3,6-Bis(5-(benzo[c][1,2,5]thiadiazol-4-yl)thiophen-2-yl)-2,5-bis(2-octyldodecyl)pyrrolo[3,4-c]pyrrole-1,4(2*H*,5*H*)-dione** (**2.3**)

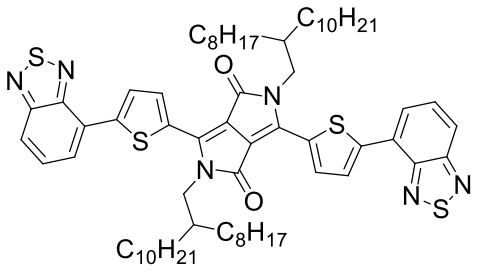

Palladium acetate(II) (21.0 mg, 0.093 mmol) was added to a deoxygenated mixture of **2.17** (1.10 g, 1.28 mmol), **2.20** (687 mg, 3.19 mmol), anhydrous potassium carbonate (442 mg, 3.20 mmol), pivallic acid (40.0 mg, 0.392 mmol) and *N*,*N* -dimethylacetamide (3.5 $cm^3$). The mixture was further deoxygenated by placement under vacuum and back filling with argon four times before being heated in an oil bath held at 110 °C under argon for 6 h. The mixture was allowed to cool to room temperature and poured into a mixture of ice and water mixture (≈50 $cm^3$). The mixture was extracted with chloroform (2 x 200 $cm^3$). The chloroform extracts were combined, washed with brine (200 $cm^3$), dried over anhydrous magnesium sulphate, and filtered. The filtrate was collected and the solvent was completely removed to give a dark blue residue. The residue was purified by column chromatography over silica using dichloromethane/light petroleum (1:4 to 3:2) as eluent to give **2.3** as a dark blue solid (702 mg, 49%), mp 137–139 °C; $TGA_{(5\%)}$ 404 °C. Anal. Calcd for $C_{66}H_{92}N_6O_2S_4$: C, 70.2; H, 8.3; N, 7.4; S, 11.4. Found: C, 70.1; H, 8.25; N, 7.4; S, 10.9%. $\upsilon_{max}$(solid)/$cm^{-1}$ 1659 (C=O), 1545 (C=N). $\lambda_{max}(CH_2Cl_2)$/nm 314 (log ε/$dm^3$ $mol^{-1}$ $cm^{-1}$ 4.58), 415 (4.37), (4.69), 636 sh (4.64). $^1$H NMR (400 MHz, $CDCl_3$): δ 0.77–0.84 (m, 12 H, $CH_3$), 1.11–1.43 (m, 64 H, $CH_2$), 1.98–2.08 (m, 2 H, CH), 4.12–4.6 (m, 4 H, $NCH_2$), 7.64 (dd, *J* = 8 & 8, 2 H, Bt H), 7.96 (d, *J* = 8, 4 H, Bt H), 8.16 (d, *J* = 4, 2 H, Th H), 9.07 (d, *J* = 4, 2 H, Th H). $^{13}$C NMR (125 MHz, $CDCl_3$): δ 14.1, 22.6, 22.7, 26.4, 29.32, 29.34, 29.59, 29.63, 29.64, 29.68, 30.1, 31.3, 31.86, 31.89, 38.1, 46.5, 108.8, 121.2, 125.8, 126.5, 128.2, 129.5, 131.2, 136.2, 140.0, 144.2, 151.9, 155.4, 161.7. *m/z* [MALDI: DHB]: Anal. Calcd for $C_{66}H_{92}N_6O_2S_4$: 1128.6 (100%), 1129.6 (80%), 1130.6 (50%), 1131.6 (22%), 1132.6 (8%), 1133.6 (3%). Found: 1228.3 (42%), 1129.3 (100%), 1130.3 (61%), 1131.3 (31%), 1132.3 (15%), 1133.3 (10%).

**2,5-Bis(2-octyldodecyl)-3,6-bis(5-(spiro[[1,3]dithiane-2,9'-fluoren]-2'-yl)thiophen-2-yl)pyrrolo[3,4-c]pyrrole-1,4(2H,5H)-dione** (**4.3**)

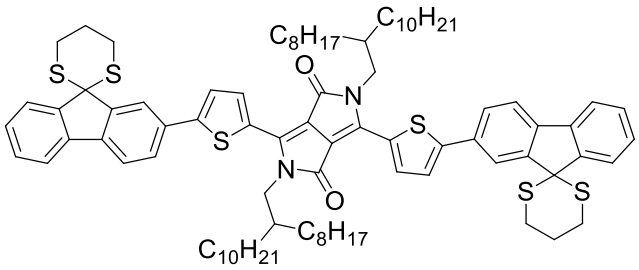


1,3-Propanedithiol (80.4 mg, 0.742 mmol) was added to a deoxygenated mixture of **2.2** (348.1 mg, 0.285 mmol), aluminum chloride (88.0 mg, 0.659 mmol), and 1,2-Dichloroethane (8 $cm^3$). The mixture was further deoxygenated by placement under vacuum and back filling with argon four times before being heated at reflux under argon for 22 h. The reaction was cooled to room

temperature and quenched with water (100 $cm^3$). Aqueous layer was extracted with chloroform (2 × 75 $cm^3$). The organic layer and chloroform extracts were combined, washed with brine (50 $cm^3$), dried over anhydrous magnesium sulphate, and filtered. The filtrate was collected and the solvent was completely removed to give a dark blue residue. The residue was purified by column chromatography over silica using chloroform/light petroleum (1:1 to 3:2) as eluent to give **4.3** as a dark blue solid (315.5 mg, 79%), mp 144–146 °C; $TGA_{(5\%)}$ 303 °C. Anal. Calcd $C_{86}H_{112}N_2O_2S_6$: C, 73.9; H, 8.1; N, 2.0; S, 13.7. Found: C, 73.8; H, 8.2; N, 1.9; S, 13.8%. $\upsilon_{max}$(solid)/$cm^{-1}$ 1654 (C=O). $\lambda_{max}(CH_2Cl_2)$/nm 360 (log ε/$dm^3$ $mol^{-1}$ $cm^{-1}$ 4.56), 401 sh (4.32), 578 (4.76), 615 (4.77). $^1$H NMR (500 MHz, $CDCl_3$): δ 0.82–0.87 (m, 12 H, $CH_3$), 1.18–1.39 (m, 64 H, $CH_2$), 1.98–2.06 (m, 2 H, CH), 2.40-2.46 (m, 4H, $CH_2$), 3.26-3.44 (m, 8 H, S $CH_2$) 4.08-4.17 (m, 4 H, $NCH_2$), 7.36–7.44 (m, 4 H, Fl H, Th H), 7.53 (d, *J* = 4, 2 H, Fl H), 7.68-7.73 (m, 6 H, Fl H), 7.94 (d, *J* = 7 Hz, 2 H, Fl H), 8.17 (s, 2 H, Fl H) 9.00 (d, *J* = 4, 2 H, TH H). $^{13}$C NMR (125 MHz, $CDCl_3$): δ 14.1, 22.7, 24.27, 26.32, 26.33, 27.8, 29.3, 29.4, 29.6, 29.62, 29.66, 29.79, 30.11, 30.12, 31.3, 31.89, 31.92, 37.98, 46.4, 52.5, 108.4, 120.6, 120.9, 121.9, 123.97, 124.7, 127.0, 128.4, 128.95, 132.95, 136.9, 137.1, 138.8, 139.8, 149.5, 150.2, 150.6, 161.7. *m/z* [MALDI: DHB]: Anal. Calcd for $C_{86}H_{112}N_2O_2S_6$: m/z: 1396.7 (98%), 1397.7 (100%), 1398.7 (77%), 1399.7 (44%), 1400.7 (21%), 1401.7 (8%), 1402.7 (3%). Found: 1396.5 (100%), 1397.5 (78%), 1398.5 (44%), 1399.5 (36%), 1400.6 (18%), 1401.7 (6%), 1401.95 (5%).

**3-Methylbenzene-1,2-diamine** (**5.5**)

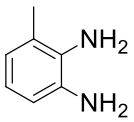


A suspension of **5.4** (25.0 g, 164.3 mmol), aluminum foil (15.8 g, 421.3 mmol) and ammonium chloride (30.0 g, 681.1 mmol) in methanol (500 $cm^3$) was heated at reflux for 20 h before cool down to room temperature. The reaction mixture was then diluted with dichloromethane (500 $cm^3$) and filtered. The residue is washed with dichloromethane (500 $cm^3$). The filtrate is then taken and reduced under vacuum and then passed through a pad of celite and washed with dichloromethane (500 $cm^3$). The solvent is completely removed to get brown oil, which was dried under high vacuum at room temperature to give **5.5** as a dark brown solid (18.1 g). **5.5** was taken to next step without further purification.

**4-Methylbenzo[c][1,2,5]thiadiazole** (**5.6**)

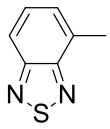

A solution of **5.5** (18.1 g, 148.1 mmol), triethylamine (59.9 g, 529.9 mmol) and dichloromethane (350 $cm^3$) was cooled in an ice bath, to which thionyl chloride (35.2 g, 295.7 mmol) was slowly added dropwise and upon addition the solution was heated at reflux for 3 h, before cool down to room temperature. The solvents were then removed *via* distillation and to the residue water (150 $cm^3$) was added and pH was adjusted to 1 with concentrated hydrochloric acid 37%. The mixture is then purified by steam distillation to give **5.6** as an yellow oil (11.4 g, 46%). $^1$H NMR (300 MHz, $CDCl_3$) δ 2.11 (s, 3 H, $CH_3$), 7.13-7.22 (m, 1 H, Bt H), 7.28-7.38 (m, 1 H, Bt H), 7.67 (d, $J$ = 8, 1 H, Bt H). $^{13}$C NMR (125 MHz, $CDCl_3$): δ 17.6, 118.6, 127.6, 129.2, 131.3, 154.6, 155.1. **5.6** had identical $^1$H and $^{13}$C NMR spectra as an authentic sample[96, 172].

**4-Bromo-7-methylbenzo[c][1,2,5]thiadiazole** (**5.7**)

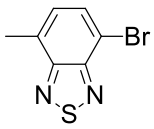

**5.6** (11.3 g, 75.3 mmol) in hydrobromic acid 37% (50 $cm^3$) was heated at reflux and to that bromine (18.0 g, 112.9 mmol) in hydrobromic acid 37% (9 $cm^3$) was added dropwise and upon completion of the addition the solution was heated at reflux for 20 h, before cool down to room temperature. The solution was poured into the mixture of ice and water (~ 100 $cm^3$). The suspension was extracted with dichloromethane (2 × 300 $cm^3$). And the combined extracts were washed with sodium bisulphite ~10% solution W/V (200 $cm^3$), saturated sodium bicarbonate (200 $cm^3$), and water (200 $cm^3$), and then dried over sodium sulphate and the solvents removed to get ~19 g of dark brown solid. **5.7** were taken to next step without further purification.

**4-Bromo-7-(dibromomethyl)benzo[c][1,2,5]thiadiazole** (**5.9**)

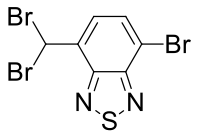


A solution of **5.7** (~19.0 g), *N*-bromosuccinimide (29.7 g, 166.8 mmol) and 1,1'-Azobis(cyclohexanecarbonitrile) (1.26 g, 5.16 mmol) in chlorobenzene was heated at 110 for 48 h. The solution was cooled to room temperature and filtered. The residue was washed with dichloromethane. The filtrate was then washed with water (2 × 100 $cm^3$) and dried over anhydrous sodium sulphate and the solvents completely removed to give yellow residue. The residue was purified by column chromatography over silica using dichloromethane/light petroleum (3:2) as eluent to give **5.9** as a yellow solid (15.0 g, 52%). $^1$H NMR (300 MHz, $CDCl_3$) δ 7.39 (s, 1 H, CH), 7.83-8.02 (m, 2 H, Bt H). $^{13}$C NMR (125 MHz, $CDCl_3$): δ 33.8, 115.9, 129.5, 131.9, 133.4, 149.7, 152.9. **5.9** had identical $^1$H and $^{13}$C NMR spectra as an authentic sample[96, 173].

**7-Bromobenzo[c][1,2,5]thiadiazole-4-carbaldehyde** (**5.10**)

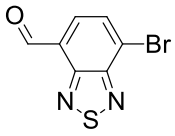


A solution of **5.9** (9.8 g, 25.38 mmol), sodium acetate (20. 5 g, 250.8 mmol) in acetic acid (200 $cm^3$) was heated at reflux for 17 h, before cool down to room temperature. The reaction mixture was further cooled in an ice bath and water (100 $cm^3$) was added. The precipitate obtained was filtered and washed with water (100 $cm^3$) and ethanol (150 $cm^3$). The residue obtained was dried under vacuum to give off-white solid. The solid was dissolved in dichloromethane (100 $cm^3$) and extracted with saturated sodium bicarbonate solution (2 x 100 $cm^3$) and water (100 $cm^3$). The organic phase was then dried over sodium sulphate and solvents completely removed to give **5.10** as a pale yellow solid (3.9 g, 64%). $^1$H NMR (300 MHz, $CDCl_3$) δ 8.02 (m, 2 H, Bt H), 10.7 (s, 1 H, CHO H). $^{13}$C NMR (125 MHz, $CDCl_3$): δ 121.9, 126.8, 131.7, 132.1, 152.3, 154.0, 188.3 **5.10** had identical $^1$H and $^{13}$C NMR spectra as an authentic sample[173].

**7,7'-(5,5'-(2,5-Bis(2-octyldodecyl)-3,6-dioxo-2,3,5,6-tetrahydropyrrolo[3,4-c]pyrrole-1,4-diyl)bis(thiophene-5,2-diyl))bis(benzo[c][1,2,5]thiadiazole-4-carbaldehyde)** (**5.11**)

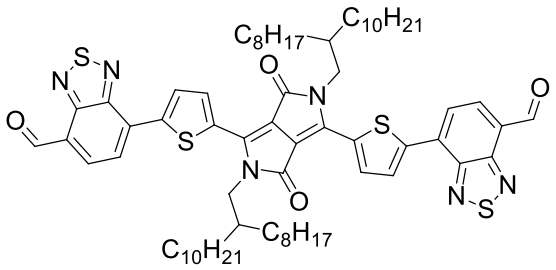

Palladium acetate(II) (6.00 mg, 0.026 mmol) was added to a deoxygenated mixture of **2.17** (86.3 mg, 0.100mmol), **5.10** (62.7 mg, 0.257 mmol), anhydrous potassium carbonate (40.6 mg, 0.293 mmol), pivallic acid (3.20 mg, 0.031 mmol) and *N*,*N* -dimethylacetamide (0.5 $cm^3$). The mixture was further deoxygenated by placement under vacuum and back filling with argon four times before being heated in an oil bath held at 110 °C under argon for 6 h. The mixture was allowed to cool to room temperature. Water (20 $cm^3$) and chloroform (20 $cm^3$) were added shaken and layer separated. The organics were combined, washed with brine (10 $cm^3$), dried over anhydrous sodium sulphate, and filtered. The filtrate was collected and the solvent was completely removed to give a dark green residue. The residue was purified by column chromatography over silica using chlorofrom/light petroleum spirit (4:1) as eluent to give **5.11** as a dark green solid (35.5 mg, 30%), mp 204–206 °C; $TGA_{(5\%)}$ 386 °C. Anal. Calcd for $C_{68}H_{92}N_6O_4S4$: C, 68.9; H, 7.8; N, 7.1; S, 10.8. Found: C, 68.9; H, 8.1; N, 6.8; S, 10.7%. $\upsilon_{max}$(solid)/$cm^{-1}$ 1687 (C=O), 1670 (C=O). $\lambda_{max}$($CH_2Cl_2$)/nm 328 (log ε/$dm^3$ $mol^{-1}$ $cm^{-1}$ 4.68), 432 (4.56), 643 (4.79). $^1$H NMR (300 MHz, $CDCl_3$) δ 0.78–0.85 (m, 12 H, $CH_3$), 1.13–1.43 (m, 64 H, $CH_2$), 1.92–2.10 (m, 2 H, CH), 4.11–4.14 (m, 4 H, $NCH_2$), 8.09 (d, *J* = 8, 2 H, Bt H), 8.23 (d, *J* = 8, 2 H, Bt H), 8.27 (d, *J* = 5, 2 H, Th H), 9.12 (d, *J* = 4, 2 H, Th H), 10.7 (s, 2 H, CHO H). $^{13}$C NMR (100 MHz, $CDCl_3$): δ 14.1, 22.6, 26.3, 29.3, 2959, 29.62, 29.65, 30.1, 31.3, 31.85, 31.87, 38.2, 46.6, 109.6, 124.6, 126.2, 129.95, 131.5, 131.9, 133.5, 136.5, 139.9, 143.0, 152.2, 153.6, 161.5, 188.1. *m/z* [MALDI: DHB]: Anal. Calcd for $C_{68}H_{92}N_6O_4S_4$: 1184.6 (100%), 1185.6 (82%), 1186.6 (52%), 1187.6 (24%), 1188.6 (9%), 1189.6 (3%). Found: 1184.4 (59%), 1185.5 (100%), 1186.5 (87%), 1187.5 (44%), 1188.4 (29%), 1189.5 (12%), 1190.5 (3%).

**4-Bromo-7-(1,3-dioxolan-2-yl)benzo[c][1,2,5]thiadiazole** (**5.12**)

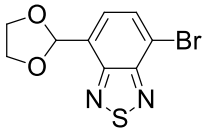

A solution of **5.10** (1.09 g, 4.48 mmol), ethylene glycol (6.67 g, 107 mmol) and *p*-toluenesulphonic acid (91.3 mg, 0.480 mmol) in toluene ( 100 $cm^3$) were taken in a round bottom flask fitted with Dean and Stark apparatus and was heated at reflux for 26 h before being cool down to room temperature. Water (150 $cm^3$) was added and after shaking the layers were separated. The aqueous layer was extracted with diethyl ether (2 X 50 $cm^3$). The toluene layer and diethyl ether extracts were combined dried over anhydrous sodium sulphate, and filtered. The filtrate was collected and the solvent was completely removed to give a yellow residue. The residue was purified by recrystallization from methanol to give **5.12** as off white solid (1.10 g, 86%), mp 97–99 °C; $TGA_{(5\%)}$ 187 °C. Anal. Calcd for $C_9H_7BrN_2O_2S$: C, 37.7; H, 2.5; N, 9.8; S, 11.2. Found: C, 37.9; H, 2.4; N, 9.5; S, 11.5%. $\lambda_{max}(CH_2Cl_2)$/nm 301 (log ε/$dm^3\,mol^{-1}\,cm^{-1}$ 4.53), 306 (4.58), 313 (4.64), 337 (4.18). $^1$H NMR (300 MHz, $CDCl_3$) δ 4.11–4.24 (m, 4 H, $CH_2$), 6.46 (s, 1 H, CH), 7.64 (dd, *J* = 0.6 & 0.6, 1 H, Bt H), 7.84 (d, *J* = 8, 1 H, Bt H). $^{13}$C NMR (125 MHz, $CDCl_3$): δ 65.7, 100.4, 115.1, 126.8, 130.2, 136.6, 152.6, 153.6. *m/z* (ESI) 310.9 ($M+Na^+$).

**3,6-Bis(5-(7-(1,3-dioxolan-2-yl)benzo[c][1,2,5]thiadiazol-4-yl)thiophen-2-yl)-2,5-bis(2-octyldodecyl)pyrrolo[3,4-c]pyrrole-1,4(2H,5H)-dione** (**5.13**)

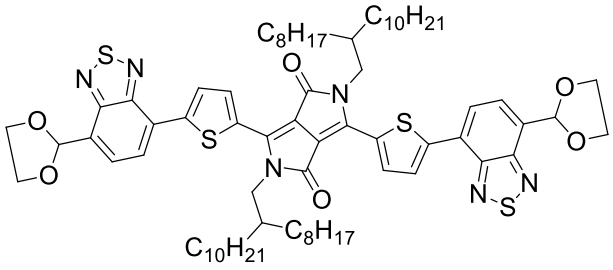


Palladium acetate(II) (36.4 mg, 0.162 mmol) was added to a deoxygenated mixture of **2.17** (835.5 mg, 0.969 mmol), **5.12** (699.1 g, 2.43 mmol), anhydrous potassium carbonate (339.5 mg, 2.45 mmol), pivallic acid (36.1 mg, 0.353 mmol) and *N*,*N*-dimethylacetamide (3.0 $cm^3$). The mixture was further deoxygenated under vacuum and back filling with argon four times before being heated in an oil bath held at 110 °C under argon for 6 h. The mixture was allowed to cool to room temperature and poured into a mixture of ice and water (≈ 100 $cm^3$) and stirred for 1 h at room temperature, filtered and washed with water (100 $cm^3$) and methanol (150 $cm^3$). The residue obtained was dried under vacuum for 20 h at 50 °C to give **5.13** as dark blue solid (~ 1.13g). The residue was taken to next step without further purification. *m/z* [MALDI: DHB]: Anal. Calcd for $C_{72}H_{100}N_6O_6S_4$: 1272.7 (100%), 1273.7 (87%), 1274.7 (56%), 1275.7 (26%), 1276.7 (11%), 1277.7 (4%), 1278.7 (1.0%). Found: 1272.4 (66%), 1273.4 (100%), 1274.4 (84%), 1275.4 (54%), 1276.4 (25%), 1277.4 (11%), 1278.4 (4%).

**7,7'-(5,5'-(2,5-Bis(2-octyldodecyl)-3,6-dioxo-2,3,5,6-tetrahydropyrrolo[3,4-c]pyrrole-1,4-diyl)bis(thiophene-5,2-diyl))bis(benzo[c][1,2,5]thiadiazole-4-carbaldehyde)** (**5.11**)

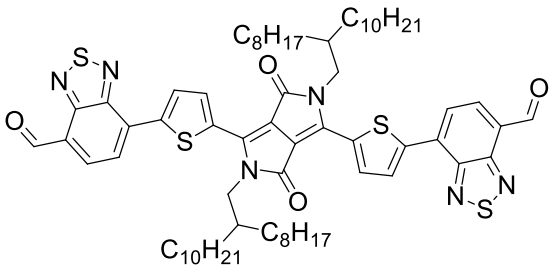

Method B

Hydrochloric acid (3 M, 10 $cm^3$) were added to a stirred solution of **5.13** (~ 1.13 g, ~ 0.887 mmol) in tetrahydrofuran (75 $cm^3$) and the mixture was then heated at reflux for 6 h before being cool down to room temperature. Water (100 $cm^3$) and chloroform (150 $cm^3$) were added and after shaking the layers were separated. The aqueous layer was extracted with chloroform (2 X 150 $cm^3$). The chloroform extracts were combined, washed with brine (100 $cm^3$), dried over anhydrous sodium sulphate, and filtered. The filtrate was collected and the solvent was completely removed to give a dark green residue. The residue was purified by column chromatography over silica using dichloromethane/light petroleum spirit (4:1) as eluent to give **5.11** as a dark green solid (904.7 mg, 73%), and had identical $^1H$ and $^{13}C$ NMR as obtained from Method A.

**2,2'-((7,7'-(5,5'-(2,5-Bis(2-octyldodecyl)-3,6-dioxo-2,3,5,6-tetrahydropyrrolo[3,4-c]pyrrole-1,4-diyl)bis(thiophene-5,2-diyl))bis(benzo[c][1,2,5]thiadiazole-7,4-diyl))bis(methanylylidene))dimalononitrile** (**5.1**)

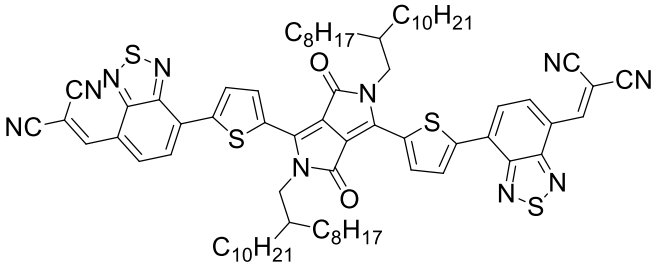

**5.11** (355.2 mg, 0.299 mmol), malononitrile (118.4 mg, 1.79 mmol), and pyridine (4.90 mg, 0.061 mmol) in toluene (15 $cm^3$) were heated at reflux under argon for 17 h. The mixture was allowed to

cool to room temperature. Water (50 $cm^3$) was added and extracted with chloroform (2 × 25 $cm^3$). The chloroform extracts were combined, washed with brine (25 $cm^3$), dried over anhydrous sodium sulphate, and filtered. The chloroform extracts were combined, washed with brine (25 $cm^3$), dried over anhydrous magnesium sulphate, and filtered. The filtrate was collected and the solvent was completely removed to give a dark green residue. The residue was purified by column chromatography over silica using chloroform/light petroleum (4:1) as eluent to give **5.1** as a dark green solid (233.9 mg, 63%), mp 252–254 °C; $TGA_{(5\%)}$ 386 °C. Anal. Calcd for $C_{74}H_{92}N_{10}O_2S_4$: C, 69.3; H, 7.2; N, 10.9; S, 10.0. Found: C, 69.2; H, 7.3; N, 10.7; S, 9.8%. $\upsilon_{max}$(solid)/$cm^{-1}$ 1665 (C=O), 2226 (C≡N). $\lambda_{max}(CH_2Cl_2)$/nm 328 (log ε/$dm^3$ $mol^{-1}$ $cm^{-1}$ 4.37), 460 (4.44), 704 (4.64). $^1$H NMR (300 MHz, $CDCl_3$): δ 0.77–0.85 (m, 12 H, $CH_3$), 1.13–1.43 (m, 64 H, $CH_2$), 1.92–2.11 (m, 2 H, CH), 4.11-4.13 (m, 4 H, $NCH_2$), 8.14 (d, *J* = 8, 2 H, Bt H), 8.30 (d, *J* = 5, 2 H, Th H), 8.72(s, 2 H, vinyl H), 8.76 (d, *J* = 8, 2 H, Bt H) 9.15 (d, *J* = 4, 2 H, Th H). $^{13}$C NMR (125 MHz, $CDCl_3$): δ 14.1, 22.6, 22.7, 26.3, 29.3, 29.34, 29.59, 29.63, 29.65, 29.7, 30.15, 31.2, 31.85, 31.9, 38.3, 46.6, 83.2, 109.9, 112.9, 113.6, 122.8, 124.9, 130.2, 130.4, 131.4,134.2, 136.9, 139.7, 142.98, 151.1, 151.6, 154.1, 161.2. *m/z* [MALDI: DHB]: Anal. Calcd for $C_{74}H_{92}N_{10}O_2S_4$: 1280.6 (100%), 1281.6 (90%), 1282.6 (58%), 1283.6 (28%), 1284.6 (11%), 1285.6 (4.0%), 1286.6 (1%). Found: 1280.5 (25%), 1281.5 (64%), 1282.5 (48%), 1283.5 (43%), 1284.5 (24%), 1285.5 (13.0%), 1286.63 (4%).

**(2E,2'E)-Dibutyl3,3'-(7,7'-(5,5'-(2,5-bis(2-octyldodecyl)-3,6-dioxo-2,3,5,6-tetrahydropyrrolo[3,4-c]pyrrole-1,4-diyl)bis(thiophene-5,2-diyl))bis(benzo[c][1,2,5]thiadiazole-7,4-diyl))bis(2-cyanoacrylate))** (**5.2**)

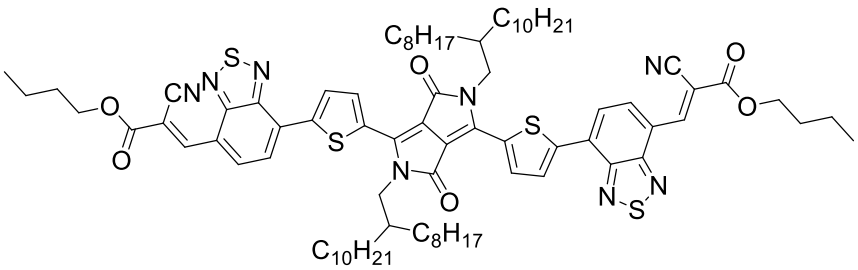


**5.11** (363.6 mg, 0.306 mmol), butyl 2-cyanoacetate (347.5 mg, 2.45 mmol), and pyridine (5.22 mg, 0.061 mmol) in toluene (10 $cm^3$) were heated at 80 °C under argon for 6 h. The mixture was allowed to cool to room temperature. Water (50 $cm^3$) was added and extracted with chloroform (2 × 25 $cm^3$). The chloroform extracts were combined, washed with brine (25 $cm^3$), dried over anhydrous sodium sulphate, and filtered. The filtrate was collected and the solvent was completely removed to give a dark green residue. The residue was purified by column chromatography over

silica using chloroform/light petroleum (3:2) as eluent to give **5.2** as a dark green solid (136.9 mg, 31%), mp 198–200°C; $TGA_{(5\%)}$ 343 °C. Anal. Calcd for $C_{82}H_{110}N_8O_6S_4$: C, 68.8; H, 7.7; N, 7.8; S, 9.0. Found: C, 68.6; H, 7.8; N, 7.9; S, 8.6%. $\upsilon_{max}$(solid)/$cm^{-1}$ 1720 (C=O), 1664 (C=O), 2222 (C≡N). $\lambda_{max}$($CHCl_3$)/nm 328 (log ε/$dm^3$ $mol^{-1}$ $cm^{-1}$ 4.44), 452 (3.50), 636 (4.72). $^1$H NMR (300 MHz, $CDCl_3$): δ 0.79–0.85 (m, 12 H, octyldodecyl $CH_3$), 1.00 (t, *J* = 15, 6 H, butyl $CH_3$), 1.14–1.63 (m, 66 H, octyldodecyl $CH_2$, butyl $CH_2$), 1.70–1.81 (m, 4H, butyl $CH_2$) 1.98–2.08 (m, 2 H, CH), 4.09–4.12 (m, 4 H, $NCH_2$), 4.29 (t, *J* = 13, 4 H, $OCH_2$), 8.05 (d, *J* = 8, 2 H, Bt H), 8.20 (d, *J* = 4, 2 H, Th H), 8.78 (d, *J* = 8, 2 H, Bt H), 9.06 (s, 2 H, vinyl H), 9.16 (d, *J* = 4, 2 H, Th H). $^{13}$C NMR (125 MHz, $CDCl_3$): δ 13.69, 14.1, 19.1, 22.6, 26.29, 29.35, 29.6, 29.66, 29.71, 30.2, 30.5, 31.2, 31.85, 31.88, 38.3, 46.6, 66.7, 103.8, 109.5, 115.6, 123.4, 124.9, 129.6, 129.9, 133.5, 136.85, 139.5, 143.0, 146.5, 151.0, 154.6, 161.1, 161.9. *m/z* [MALDI: DHB]: Anal. Calcd for $C_{82}H_{110}N_8O_6S_4$: 1430.7 (100%), 1431.7 (99%), 1432.7 (67%), 1433.7 (34%), 1434.7 (14%), 1435.7 (5%), 1436.7 (2%). Found: 1430.5 (49%), 1431.5 (100%), 1432.5 (90%), 1433.5 (71%), 1434.5 (27%), 1435.5 (5%), 1436.7 (8%).

**_N_'-(2-bromo-9_H_-fluoren-9-ylidene)-4-methylbenzenesulfonohydrazide** (**6.4**)

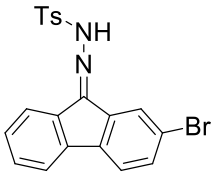


**2.13** (10.3 g, 39.9 mmol), 4-Methylbenzenesulfonhydrazide (9.32 g, 50.0 mmol) in acetonitrile (160 $cm^3$) were heated at reflux under nitrogen for 17 h, before being cool down to room temperature, filtered and washed with cold acetonitrile (100 $cm^3$). The residue obtained was dried under vacuum (~0.2 mbar) for 19 h to give **6.4** as yellow solid (~ 6.24 g). **6.4** were taken to next step without further purification.

**2-Bromo-9-diazo-9_H_-fluorene** (**6.5**)

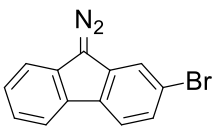


Method A

50% sodium hydroxide (aqueous) (30 $cm^3$) were added to a stirred solution of **6.4** (~ 4.48 g, ~ 10.50 mmol) in 1,4-dioxane (60 $cm^3$) and the mixture was then heated at reflux for 15 h before being cool down to room temperature. The aqueous and organic layers were separated. The aqueous layer was extracted with ethyl acetate (2 x 50 $cm^3$). The ethyl acetate extracts and organic layer were combined, washed with brine (100 $cm^3$), dried over anhydrous sodium sulphate, and filtered. The filtrate was collected and the solvent was completely removed to give a pink residue. The residue was purified by column chromatography over silica using light petroleum spirit /dichloromethane (3:2) as eluent to give **6.5** as a pink solid (597.7 mg, 21%). **6.5** had identical $^1H$ and $^{13}C$ NMR spectra as an authentic sample[174].

Method B

50% sodium hydroxide (aqueous) (50 $cm^3$) were added to a stirred solution of **6.4** (~ 6.24 g, ~ 14.6 mmol) in tetrahydrofuran (150 $cm^3$) and the mixture was then heated at reflux for 56 h before being cool down to room temperature. The aqueous and organic layers were separated. The aqueous layer was extracted with ethyl acetate (2 x 50 $cm^3$). The ethyl acetate extracts and organic layer were combined, washed with brine (100 $cm^3$), dried over anhydrous sodium sulphate, and filtered. The filtrate was collected and the solvent was completely removed to give a pink residue. The residue was purified by column chromatography over silica using light petroleum spirit /dichloromethane (3:2) as eluent to give **6.5** as a pink solid (2.34 g, 22%). **6.5** had identical $^1H$ and $^{13}C$ NMR spectra as an authentic sample[174].

**3,6-Dimethoxy-9*H*-fluoren-9-one** (**6.10**)

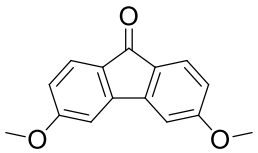


Method A

Palladium acetate(II) (102 mg, 0.454 mmol) was added to a deoxygenated mixture of **6.9** (1.06 g, 4.37 mmol), silver(I) oxide (2.02 g, 8.71 mmol). The mixture was further deoxygenated under vacuum and back filling with argon four times before trifluoroacetic acid (3 $cm^3$) was added and heated in an oil bath held at reflux under argon for 22 h. The mixture was allowed to cool to room

temperature and passed through celite plug and washed with dichloromethane (100 $cm^3$). Water (50 $cm^3$) was added shaken and layer separated. The organic layers were then washed with brine (50 $cm^3$) dried over anhydrous sodium sulphate and filtered. The filtrate was collected and the solvent was completely removed to give a yellow residue. The residue was purified by column chromatography over silica using light petroleum spirit/diethyl ether (3:2) as eluent to give **6.10** as a yellow solid (336.5 mg, 32%)**.** $^1$H NMR (300 MHz, $CDCl_3$): δ 3.84 (s, 6 H, $OCH_3$), 6.67 (dd, *J* = 2 & 8, 1 H), 6.89 (d, *J* = 2, 1 H), 7.50 (d, *J* = 8, 1 H). $^{13}$C NMR (125 MHz, $CDCl_3$): δ 55.6, 106.9, 112.9, 125.5, 128.1, 145.7, 164.9, 191.2. **6.10** had identical $^1$H and $^{13}$C NMR spectra as an authentic sample[163].

Method B

Palladium acetate(II) (445 mg, 1.98 mmol) was added to a deoxygenated mixture of **6.9** (2.41 g, 9.92 mmol), silver(I) oxide (6.88 g, 29.6 mmol), and anhydrous potassium carbonate (4.78 g, 34.5 mmol). The mixture was further deoxygenated under vacuum and back filling with argon four times before trifluoroacetic acid (18 $cm^3$) was added and heated in an oil bath held at reflux under argon for 50 h. The mixture was allowed to cool to room temperature and passed through celite plug and washed with dichloromethane (200 $cm^3$). The water (100 $cm^3$) was added shaken and layer separated. The organic layers were combined washed with brine (200 $cm^3$) dried over anhydrous sodium sulphate and filtered. The filtrate was collected and the solvent was completely removed to give a yellowish brown residue. The residue was purified by column chromatography over silica using light petroleum/diethylether (3:2) as eluent to give **6.10** as a yellow solid (833 mg, 35%) and had identical $^1$H and $^{13}$C NMR spectra as obtained *via* Method A.

**3,6-Difluoro-9*H*-fluoren-9-one** (**6.14**)

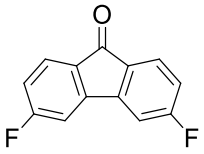


Method A

Palladium acetate(II) (121 mg, 0.538 mmol) was added to a deoxygenated mixture of **6.13** (1.09 g, 5.00 mmol), silver(I) oxide (2.31 g, 10.0 mmol). The mixture was further deoxygenated under

vacuum and back filling with argon four times before trifluoroacetic acid (3 $cm^3$) was added and heated in an oil bath held at reflux under argon for 62 h. The mixture was allowed to cool to room temperature and passed through celite plug and washed with dichloromethane (100 $cm^3$). Water (50 $cm^3$) was added shaken and layer separated. The organic layers were then washed with brine (50 $cm^3$) dried over anhydrous sodium sulphate and filtered. The filtrate was collected and the solvent was completely removed to give a yellow residue. The residue was purified by recrystallisation from ethanol to give **6.14** as a yellow solid (210.3 mg, 19%), $^1$H NMR (300 MHz, $CDCl_3$): 6.96-7.04 (m, 2 H), 7.18 (d, *J* = 2 & 8, 2 H), 7.67 (d, *J* = 5, & 8, 2 H). $^{13}$C NMR (125 MHz, $CDCl_3$): δ 106.6, 108.9, 116.1, 116.4, 126.4, 126.5, 130.7, 145.69, 145.7, 145.8, 165.5, 168.9, 190.3. **6.14** had identical $^1$H and $^{13}$C NMR spectra as an authentic sample[163].

Method B

Palladium acetate(II) (291 mg, 1.29 mmol) was added to a deoxygenated mixture of **6.13** (1.41 g, 5.22 mmol), silver(I) oxide (4.43 g, 19.1 mmol) and anhydrous potassium carbonate (3.12 g, 22.5 mmol). The mixture was further deoxygenated under vacuum and back filling with argon four times before trifluoroacetic acid (10 $cm^3$) was added and heated in an oil bath held at reflux under argon for 95 h. The mixture was allowed to cool to room temperature and passed through celite plug and washed with dichloromethane (100 $cm^3$). Water (150 $cm^3$) was added shaken and layer separated. The organic layers were then washed with brine (100 $cm^3$) dried over anhydrous sodium sulphate and filtered. The filtrate was collected and the solvent was completely removed to give a brown residue. The residue was purified in two stages, first using column chromatography over silica using light petroleum/dichloromethane (1:4) as eluent, second recrystallisation from ethanol to give **6.14** as a yellow solid (722.2 mg, 64%) and had similar $^1$H NMR and $^{13}$C NMR as obtained from method A.

**9*H*-fluorene-9-thione** (**6.7**)

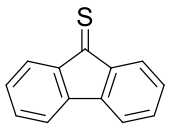


Lawesson's reagent (6.04 g, 14.9 mmol) was added to a deoxygenated mixture of **6.6** (5.40 g, 30.0 mmol) and toluene (90 $cm^3$). The mixture was further deoxygenated under vacuum and back filling

with argon four times before heated at reflux for 30 min. The reaction mixture was then allowed to cool to room temperature and the solvent was completely removed to give a dark green residue. The residue was purified by column chromatography over silica using light petroleum/dichloromethane (4:1) as eluent to give **6.7** as a green solid (1.68 g) and was used immediately.

**3,6-Dimethoxy-9*H*-fluorene-9-thione** (**6.11**)

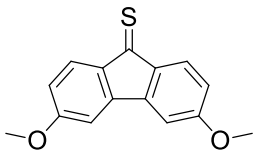


Lawesson's reagent (1.30 g, 3.21 mmol) was added to a deoxygenated mixture of **6.10** (1.55 g, 6.45 mmol) and toluene (13 $cm^3$). The mixture was further deoxygenated under vacuum and back filling with argon four times before heated at reflux for 20 min. The reaction mixture was then allowed to cool to room temperature and the solvent was completely removed to give a dark red residue. The residue was purified by column chromatography over silica using light petroleum/dichloromethane (3:2 to 2:3) as eluent to give **6.11** as a red solid (1.34 g) and was used immediately.

**3,6-Difluoro-9*H*-fluorene-9-thione** (**6.15**)

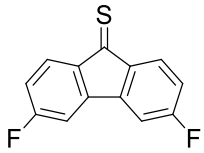


Lawesson's reagent (623.9 mg, 1.54 mmol) was added to a deoxygenated mixture of **6.14** (659.6 mg, 3.04 mmol) and toluene (10 $cm^3$). The mixture was further deoxygenated under vacuum and back filling with argon four times before heated at reflux for 30 min. The reaction mixture was then allowed to cool to room temperature and the solvent was completely removed to give a green residue. The residue was purified by column chromatography over silica using light petroleum/dichloromethane (2:3) as eluent to give **6.15** as a green solid (388.7 mg) and was used immediately.

**2-Bromo-9,9'-bifluorenylidene** (**6.8**)

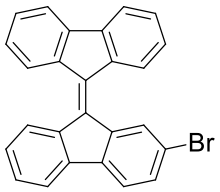


To a solution of **6.5** (2.34 g, 8.63 mmol) in 150 $cm^3$ of anhydrous tetrahydrofuran was added **6.7** (1.68 g, 8.55 mmol) dissolved in anhydrous tetrahydrofuran (250 $cm^3$), dropwise. The reaction mixture was then stirred for 63 h at room temperature before the solvents was completely removed to give an orange residue. The residue was purified by column chromatography over silica using light petroleum/dichloromethane mixture (4:1) as eluent to give **6.8** as an orange solid (2.35 g, 67%), mp 148–150 °C; $TGA_{(5\%)}$ 323 °C. Anal. Calcd $C_{26}H_{15}Br$: C, 76.7; H, 3.7. Found: C, 76.6; H, 3.7%. $\lambda_{max}(CH_2Cl_2)$/nm 458 (log $\varepsilon/dm^3\ mol^{-1}\ cm^{-1}$ 4.43). $^1H$ NMR (400 MHz, $CDCl_3$): δ 7.17–7.27 (m, 3 H), 7.31–7.37 (m, 3 H), 7.44 (dd, *J* = 2 & 8, 1 H), 7.56 (d, *J* = 8, 1 H), 7.66 – 7.71 (m, 3 H), 8.30 (d, *J* = 8, 1 H), 8.36 (dd, *J* = 5 & 8, 2 H), 8.50 (d, *J* = 2, 1 H). $^{13}C$ NMR (100 MHz, $CDCl_3$): δ 119.9, 119.98, 120.1, 120.5, 121.0, 126.6, 126.7, 126.8, 127.0, 127.2, 129.1, 129.3, 129.6, 129.7, 131.6, 137.9, 137.97, 138.0, 139.5, 139.8, 139.9, 140.3, 141.5, 141.6, 142.3. *m/z* [MALDI: DHB]: Anal. Calcd for $C_{26}H_{15}Br$: 406.0 (99%), 407.0 (29%), 408.0 (100%), 409.0 (28%), 410.0 (4%). Found: 405.9 (100%), 406.9 (44%), 407.9 (97%), 408.9 (39%), 409.9 (6%).

**2-Bromo-3',6'-dimethoxy-9,9'-bifluorenylidene** (**6.12**)

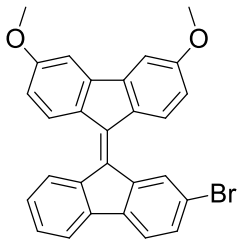


To a solution of **6.5** (1.50 g, 5.53 mmol) in 100 $cm^3$ of anhydrous tetrahydrofuran was added **6.11** (1.34 g, 5.22 mmol) dissolved in tetrahydrofuran (200 $cm^3$), dropwise. The mixture was then stirred for 67 h at room temperature before the solvents was completely removed to give a red residue. The residue was purified by column chromatography over silica using light petroleum/dichloromethane mixture (3:2) as eluent to give **6.12** as a red solid (1.84 g, 71%), mp 183–185 °C; $TGA_{(5\%)}$ 317 °C. Anal. Calcd $C_{28}H_{19}O_2Br$: C, 71.96; H, 4.1. Found: C, 71.6; H, 4.1%. $\lambda_{max}(CH_2Cl_2)$/nm 475 (log

ε/$dm^3$ $mol^{-1}$ $cm^{-1}$ 4.49). $^1$H NMR (400 MHz, $CDCl_3$): δ 3.93 (d, *J* = 4, 6 H, $OCH_3$), 6.72–6.80 (m, 2 H), 7.14 (t, *J* = 3, 2 H), 7.19–7.26 (m, 2 H), 7.30 (dt, *J* = 1 & 7, 1 H), 7.41 (dd, *J* = 2 & 8 , 1 H), 7.57 (d, *J* = 8, 1 H), 7.69 (d, *J* = 7, 1 H), 8.17 (d, *J* = 9, 1 H), 8.22 (d, *J* = 9, 1 H), 8.29 (d, *J* = 8, 1 H), 8.43 (d, *J* = 2, 1 H). $^{13}$C NMR (100 MHz, $CDCl_3$): δ 55.61, 55.63, 105.2, 105.4, 113.0, 119.8, 120.2, 120.9, 126.0, 126.8, 128.10, 128.14, 128.2, 128.6, 130.5, 131.7, 131.8, 134.8, 138.2, 139.1, 139.5, 140.1, 141.95, 143.15, 143.2, 161.30, 161.35. *m/z* [MALDI: DHB]: Anal. Calcd for $C_{28}H_{19}O_2Br$: 466.1 (97%), 467.1 (31%), 468.1 (100%), 469.1 (31%), 470.1 (5%). Found: 465.9 (99%), 466.9 (66%), 467.9 (100%), 468.9 (65%), 469.9 (21%).

**2-Bromo-3',6'-difluoro-9,9'-bifluorenylidene** (**6.16**)

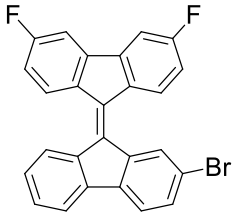


Method A

To a solution of **6.5** (345.1 mg, 1.27 mmol) in 15 $cm^3$ of anhydrous tetrahydrofuran was added **6.15** (312.4 g, 1.34 mmol) dissolved in tetrahydrofuran (30 $cm^3$), dropwise. The mixture was then stirred for 56 h at room temperature before the solvents was completely removed to give a red residue. The residue was purified by column chromatography over silica using light petroleum/dichloromethane mixture (4:1) as eluent to give **6.16** as a red solid (25.3 mg, 0.43%) and had identical $^1$H and $^{13}$C NMR as obtained from Method B.

Method B

To a solution of **6.5** (480.2 mg, 1.75 mmol) in 100 $cm^3$ of anhydrous tetrahydrofuran was added dropwise **6.15** (388.7 mg, 1.67 mmol) dissolved in tetrahydrofuran (100 $cm^3$) at room temperature. The reaction was then heated at reflux for 22 h, before cool down to room temperature and solvent completely removed to give a red residue. The residue was purified by column chromatography over silica using light petroleum as eluent to give **6.16** as a red solid (434.3 mg, 56%), mp 223–225 °C; $TGA_{(5\%)}$ 214 °C. Anal. Calcd $C_{26}H_{13}F_2Br$: C, 70.5; H, 2.96; Found: C, 70.7; H, 3.0%. $\lambda_{max}(CH_2Cl_2)$/nm 457 (log ε/$dm^3$ $mol^{-1}$ $cm^{-1}$ 4.28). $^1$H NMR (400 MHz, $CDCl_3$): δ 6.86–7.06 (m, 2

H) 7.18–7.39 (m, 4 H), 7.44 (d, *J* = 8, 1 H), 7.55(d, *J* = 8, 1 H), 7.67 (d, *J* = 7.5, 1 H), 8.18–8.27 (m, 2 H), 8.27–8.33 (m, 1 H), 8.37 (s, 1 H). *m/z* [MALDI: DHB]: Anal. Calcd for $C_{26}H_{13}F_2Br$: 442.0 (99%), 443.0 (29%), 444.0 (100%), 445.0 (28%), 446.0 (4%). Found: 441.9 (100%), 442.9 (41%), 443.9 (100%), 444.9 (39%), 445.9 (5%).

**2-([9,9'-Bifluorenylidene]-2-yl)-4,4,5,5-tetramethyl-1,3,2-dioxaborolane** (**6.17**)

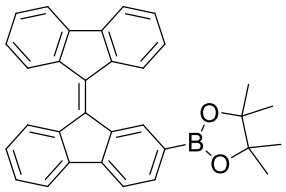


Bis(pinacolato)diboron (2.03 g, 7.99 mmol), potassium acetate (1.71 g, 17.4 mmol), [1,1'-bis-(diphenylphosphino)ferrocene]dichloropalladium(II) (80.0 mg, 0.109 mmol), **6.8** (1.01 g, 2.47 mmol) and 1,4-dioxane (12 $cm^3$) was sparged with argon for 10 min, and then heated at 110 °C for 22 h. After cooling to room temperature, the reaction mixture was passed through celite plug, washed with diethyl ether (150 $cm^3$). Water (400 $cm^3$) was added, shaken and the layers separated. The organic layer was washed with brine (100 $cm^3$), dried over anhydrous sodium sulphate, and filtered. The solvent was completely removed to give a red oily residue. The residue was purified by recrystallisation from ethanol/dichloromethane mixture to give **6.17** as red solid (891 mg, 80%), mp 225–227 °C; $TGA_{(5\%)}$ 329 °C. $\lambda_{max}(CH_2Cl_2)$/nm 460 (log ε/$dm^3$ $mol^{-1}$ $cm^{-1}$ 4.45). $^1$H NMR (300 MHz, $CDCl_3$): δ 1.32 (s, 12 H), 7.17–7.26 (m, 3 H), 7.30–7.37 (m, 3 H), 7.69–7.80 (m, 5 H) 8.32-8.43 (m, 3 H), 8.84 (s, 1 H). $^{13}$C NMR (100 MHz, CDCl3): δ 24.8, 83.7, 119.2, 119.7, 119.8, 120.3, 126.6, 126.7, 126.79, 126.84, 126.95, 127.3, 129.0, 129.09, 129.12, 133.4, 135.6, 137.6, 138.2, 138.5, 138.8, 140.7, 141.0, 141.17, 141.24, 141.4, 143.7. m/z [MALDI: DHB]: Anal. Calcd for $C_{32}H_{27}BO_2$: 453.2 (23%), 454.2 (100%), 455.2 (35%), 456.2 (6%). Found: 453.1 (25%), 454.1 (100%), 455.1 (41%), 456.1 (6%).

**2-(3',6'-Dimethoxy-[9,9'-bifluorenylidene]-2-yl)-4,4,5,5-tetramethyl-1,3,2-dioxaborolane** (**6.18**)

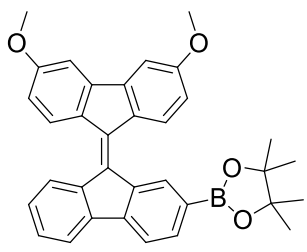

Bis(pinacolato)diboron (2.31 g, 9.09 mmol), potassium acetate (2.10 g, 21.3 mmol), [1,1′-Bis(diphenylphosphino)ferrocene]dichloropalladium(II), complex with dichloromethane (341.9 mg, 0.418 mmol), **6.12** (1.40 g, 2.99 mmol) and 1,4 –dioxane (11 $cm^3$) was sparged with argon for 10 min, and then heated at reflux for 20 h. After cooling to room temperature, the reaction mixture was passed through celite plug, washed with diethyl ether (100 $cm^3$). Water (100 $cm^3$) was added, shaken and the layers separated. The organic layer was washed with brine (50 $cm^3$), dried over anhydrous sodium sulphate, and filtered. The solvent was completely removed to give a red oily residue. The residue was purified by column chromatography over silica using light petroleum/dichloromethane (3:2) as eluent. The isolated product was further purified by removing unreacted Bis(pinacolato)diboron using sublimation technique under vacuum (0.02 m bar) at 110 °C to give **6.18** as a dark red solid (1.42 g, 93%), mp 136–138 °C; $TGA_{(5\%)}$ 344 °C. Anal. Calcd $C_{34}H_{31}O_4B$: C, 79.4; H, 6.1. Found: C, 79.1; H, 6.4%. $\lambda_{max}(CH_2Cl_2)$/nm 476 (log ε/$dm^3$ $mol^{-1}$ $cm^{-1}$ 4.48). $^1$H NMR (300 MHz, $CDCl_3$): δ 1.32 (s,12 H), 3.94 (d, *J* = 4, 6 H, $OCH_3$), 6.73–6.78 (m, 2 H), 7.16–7.17 (m, 2 H), 7.19–7.26 (m, 2 H), 7.29–7.34 (m, 1 H), 7.72–7.78 (m, 3 H), 8.26 (dd, *J* = 9 & 10, 2 H), 8.34 (d, *J* = 8, 1 H), 8.77 (s, 1 H).$^{13}$C NMR (100 MHz, CDCl3): δ 24.8, 24.9, 55.5, 55.6, 83.4, 83.7, 104.6, 104.96, 112.8, 113.3, 119.1, 120.2, 126.1, 126.97, 128.0, 128.2, 128.3, 132.1, 132.4, 132.8, 134.5, 136.2, 137.69, 138.9, 140.3, 140.7, 142.8, 143.1, 160.95. m/z [MALDI: DHB]: Anal. Calcd for $C_{34}H_{31}BO_4$: 513.2 (23%), 514.2 (100%), 515.2 (37%), 516.2 (8%), 517.2 (1%). Found: 513.1 (36%), 514.1 (100%), 515.1 (52%), 516.1 (18%), 517.1 (4%).

**2-(3',6'-Difluoro-[9,9'-bifluorenylidene]-2-yl)-4,4,5,5-tetramethyl-1,3,2-dioxaborolane** (**6.19**)

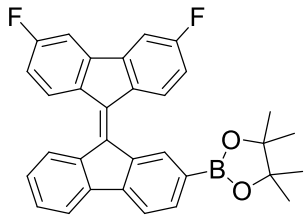


Bis(pinacolato)diboron (799 mg, 3.14 mmol), potassium acetate (722 mg, 7.35 mmol), [1,1'-bis-(diphenylphosphino)ferrocene]dichloropalladium(II) (123.3 mg, 0.150 mmol), **6.16** (461.7 mg, 1.04 mmol) and 1,4 –dioxane (7 cm3) was sparged with argon for 10 min, and then heated at reflux for 72 h. After cooling to room temperature, the reaction mixture was passed through celite plug, washed with diethyl ether (100 $cm^3$). Water (100 $cm^3$) was added, shaken and the layers separated. The organic layer was washed with brine (50 $cm^3$), dried over anhydrous sodium sulphate, and

filtered. The solvent was completely removed to give a red solid residue. The residue was purified by column chromatography over silica using light petroleum /dichloromethane (4:1) as eluent to give **6.19** as a dark red solid (149.1 mg, 29%), mp 245–247 °C. $\lambda_{max}(CH_2Cl_2)$/nm 455 (log ε/dm$^3$ mol$^{-1}$ cm$^{-1}$ 4.45). m/z [MALDI: DHB]: Anal. Calcd for $C_{32}H_{25}O_2F_2B$: 489.2 (23%), 490.2 (100%), 491.2 (34%), 492.2 (6%). Found: 489.2 (7%), 490.2 (27%), 491.2 (11%), 492.2 (2%).

**3,6-bis(5-([9,9'-bifluorenylidene]-2-yl)thiophen-2-yl)-2,5-bis(2-octyldodecyl)pyrrolo[3,4-c]pyrrole-1,4(2H,5H)-dione** (**6.1**)

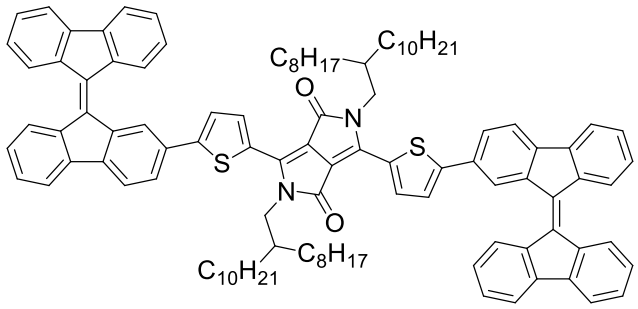


Tetrakis(triphenylphosphino)palladium(0) (29.3 mg, 0.025 mmol) was added to a deoxygenated mixture of **2.19** (255.9 mg, 0.251 mmol), **6.17** (455.3 mg, 1.00 mmol), 4:1 toluene/ethanol mixture (5 cm$^3$) and aqueous potassium carbonate (2 M, 2 cm$^3$). The mixture was further deoxygenated by placement under vacuum and back filling with argon four times before being heated at 100 °C under argon for 6 h. The reaction was cooled down to room temperature. Water (25 cm$^3$) and dichloromethane (100 cm$^3$) were added, shaken and layer separated. The aqueous layer was further extracted with dichloromethane (3 x 50 cm$^3$). The organics were combined, washed with brine (50 cm$^3$), dried over anhydrous sodium sulphate, and filtered. The filtrate was collected and the solvent was completely removed to give a dark green residue. The residue was purified by column chromatography over silica using light petroleum /dichloromethane (3:2 to 2:3) as eluent to give **6.1** as a dark green solid (337.8 mg, 89%), mp 148–150 °C; $TGA_{(5\%)}$ 374 °C. Anal. Calcd for $C_{106}H_{116}N_2O_2S_2$: C, 84.1; H, 7.7; N, 1.85; S, 4.2. Found: C, 83.7; H, 7.8; N, 1.7; S, 4.1%. $\upsilon_{max}$(solid)/cm$^{-1}$ 1660 (C=O), 1548 (C=C). $\lambda_{max}(CH_2Cl_2)$/nm 467 (log ε/dm$^3$ mol$^{-1}$ cm$^{-1}$ 4.66), 417 sh (4.56), 593 (4.70), 622 (4.70). $^1$H NMR (500 MHz, $CDCl_3$) δ 0.78–0.83 (m, 12 H, $CH_3$), 1.12–1.27 (m, 64 H, $CH_2$), 1.85–2.00 (m, 2 H, CH), 3.97-4.00 (m, 4 H, $NCH_2$), 7.18 -7.26 (m, 6 H, 6 BF H), 7.30 -7.37 (m, 8 H, 2 Th H, 6 BF H), 7.59 (dd, *J* = 1 & 8, 2 H, BF H), 7.66 – 7.71 (m, 8 H, BF H), 8.37 (dd, *J* = 3 & 8, 6 H, BF H), 8.70 (s, 2 H, BF H), 9.00 (d, *J* = 4, 2 H, Th H). $^{13}$C NMR (125 MHz, $CDCl_3$): δ 14.1, 22.7, 26.3, 29.32, 29.36, 29.59, 29.63, 29.67, 30.1, 31.2, 31.86, 31.90, 37.8, 46.4, 108.1, 119.95, 120.1, 120.3, 124.1, 124.2, 126.5, 126.7, 126.8, 126.9, 126.98, 127.2, 128.5,

129.3, 129.5, 129.7, 131.1, 137.99, 138.9, 139.98, 140.6, 141.3, 141.4, 141.6, 141.97, 149.8, 161.6. *m/z* [MALDI: DHB]: Anal. Calcd for $C_{106}H_{116}N_2O_2S_2$: 1512.8 (82%), 1513.9 (100%), 1514.9 (68%), 1515.9 (33%), 1516.9 (13%), 1517.9 (4%), 1518.9 (1%). Found: 1512.7 (44%), 1513.7 (100%), 1514.1 (94%), 1515.7 (66%), 1516.7 (42%), 1517.7 (22%), 1518.7 (7%).

**3,6-bis(5-(3',6'-dimethoxy-[9,9'-bifluorenylidene]-2-yl)thiophen-2-yl)-2,5-bis(2-octyldodecyl)pyrrolo[3,4-c]pyrrole-1,4(2H,5H)-dione** (**6.2**)

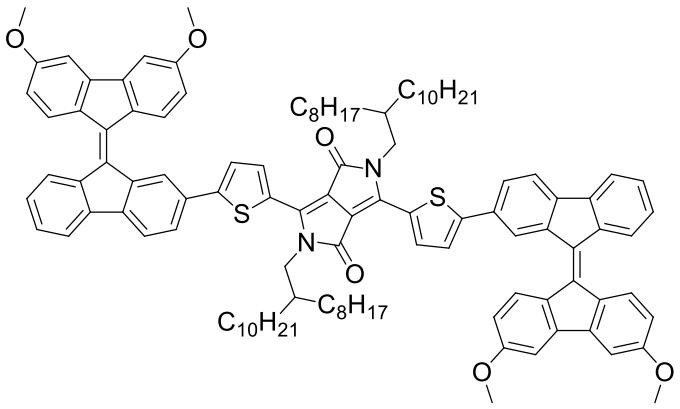


Tetrakis(triphenylphosphino)palladium(0) (88.5 mg, 0.076 mmol) was added to a deoxygenated mixture of **2.19** (514.3 mg, 0.504 mmol), **6.18** (1.03 g, 2.00 mmol), 4:1 toluene/ethanol mixture (6 $cm^3$) and aqueous potassium carbonate (2 M, 2 $cm^3$). The mixture was further deoxygenated by placement under vacuum and back filling with argon four times before being heated at 100 °C under argon for 21 h. The reaction was cooled down to room temperature. Water (25 $cm^3$) and dichloromethane (150 $cm^3$) were added, shaken and layer separated. The aqueous layer was extracted with dichloromethane (3 x 25 $cm^3$). The combined organics were washed with brine (50 $cm^3$), dried over anhydrous sodium sulphate, and filtered. The filtrate was collected and the solvent was completely removed to give a dark green residue. The residue was purified by column chromatography over silica using light petroleum /dichloromethane (1:4) as eluent to give **6.2** as a dark green solid (252.8 mg, 31%), mp 224–226 °C; $TGA_{(5\%)}$ 379 °C. Anal. Calcd for $C_{110}H_{124}N_2O_6S_2$: C, 80.8; H, 7.65; N, 1.7; S, 3.9. Found: C, 80.5; H, 7.7; N, 1.7; S, 3.5%. $\upsilon_{max}$(solid)/$cm^{-1}$ 1653 (C=O), 1548 (C=C). $\lambda_{max}(CH_2Cl_2)$/nm 488 (log ε/$dm^3$ $mol^{-1}$ $cm^{-1}$ 4.77), 470 sh (4.56), 595 (4.75), 631 (4.76). $^1$H NMR (400 MHz, $CDCl_3$) δ 0.77–0.82 (m, 12 H, $CH_3$), 1.13–1.29 (m, 64 H, $CH_2$), 1.87–2.25 (m, 2 H, CH), 3.94 (d, *J* = 9, 6 H, $OCH_3$), 3.98-4.06 (m, 4 H, $NCH_2$), 6.72–6.79 (m, 4 H, BF H), 7.14–7.32 (m, 8 H, BF H, Th H), 7.38 (d, *J* = 4, 2 H, BF H), 7.57 (d, *J* = 8, 2 H, BF H), 7.70 (d, *J* = 8, 4 H, BF H), 8.24 (d, *J* = 9, 4 H, BF H), 8.31 (d, *J* = 8, 2 H, BF H), 8.65 (s, 2 H, BF H), 9.00 (d, *J* = 4, 2 H, Th H). $^{13}$C NMR (100 MHz, $CDCl_3$): δ 14.1, 22.65, 22.7,

26.3, 29.3, 29.4, 29.6, 29.65, 29.67, 29.69, 30.1, 31.2, 31.88, 31.91, 37.8, 46.3, 55.6, 55.62, 105.2, 105.5, 108.1, 112.75, 12.97, 120.0, 120.2, 123.5, 124.1,125.55, 126.1, 126.9, 128.1, 128.2, 128.39, 131.2, 131.8, 131.85, 135.3, 137.1, 138.7, 139.0, 139.6, 139.9, 140.7, 141.6, 143.1, 143.28, 150.2, 161.3, 161.4, 161.6. *m/z* [MALDI: DHB]: Anal. Calcd for $C_{110}H_{124}N_2O_6S_2$: 1632.9 (79%), 1633.9 (100%), 1634.9 (71%), 1635.9 (36%), 1636.9 (14%), 1637.9 (5%), 1638.9 (1%). Found: 1632.6 (51%), 1633.6 (94%), 1634.6 (79%), 1635.6 (49%), 1636.6 (22%), 1637.6 (8%), 1638.6 (4%).

**3,6-bis(5-(3',6'-difluoro-[9,9'-bifluorenylidene]-2-yl)thiophen-2-yl)-2,5-bis(2-octyldodecyl)pyrrolo[3,4-c]pyrrole-1,4(2H,5H)-dione** (**6.3**)

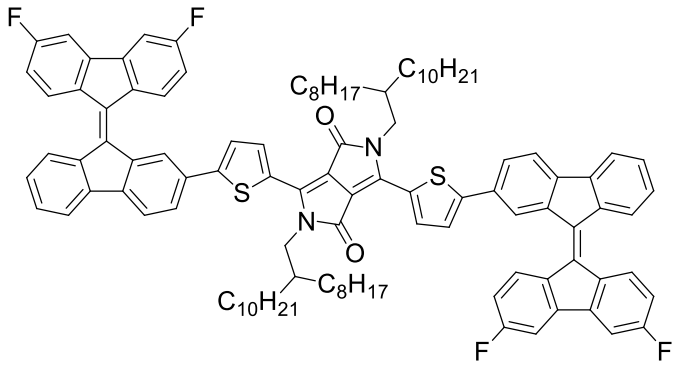


Palladium acetate(II) (11.9 mg, 0.053 mmol) was added to a deoxygenated mixture of **2.18** (217.2 mg, 0.252 mmol), **6.16** (390.7 mg, 0.881 mmol), anhydrous potassium carbonate (89.8 mg, 0.649 mmol), pivallic acid (11.3 mg, 0.110 mmol) and *N*,*N* -dimethylacetamide (2.5 $cm^3$). The mixture was further deoxygenated by placement under vacuum and back filling with argon four times before being heated in an oil bath held at 110 °C under argon for 7 h. Water (100 $cm^3$) and dichloromethane (150 $cm^3$) was added, shaken and layer separated. The aqueous layer was then extracted with dichloromethane (2 x 100 $cm^3$). The organic layer and dichloromethane extracts were combined washed with brine (50 $cm^3$), dried over sodium sulphate, and filtered. The filtrate was collected and solvent completely removed to get dark green residue. The residue was purified by column chromatography over silica using dichloromethane/light petroleum (3:2) as eluent to give **6.3** as a dark green solid (~41.3 mg, ~7%), Anal. Calcd for $C_{106}H_{112}F_4N_2O_2S_2$: 1584.8 (82.4%), 1585.8 (100.0%), 1586.8 (67.8%), 1587.8 (33.1%), 1588.8 (12.8%), 1589.8 (4.1%), 1590.8 (1.1%). Found: 1584.6 (69.2%), 1585.6 (100.0%), 1586.6 (96.5%), 1587.6 (54.6%), 1588.6 (22.8%), 1589.6 (8.5%), 1590.6 (2.9%).

# Chapter 9- Bibilogrpahy

1. R. Maceiras, M. Rodrí guez, A. Cancela, S. Urréjola and A. Sánchez, *Applied Energy*, 2011, **88**, 3318-3323.
2. http://cleantechnica.com/2015/02/18/bp-energy-outlook-proclaims-possible-25-carbon-emissions-increase-2035/, February 18th, 2015.
3. https://www.worldenergy.org/wp-content/uploads/2013/10/WER_2013_8_Solar_revised.pdf, 2013.
4. G. K. Singh, *Energy*, 2013, **53**, 1-13.
5. D. M. Chapin, C. S. Fuller and G. L. Pearson, *J. Appl. Phys.*, 1954, **25**, 676-677.
6. T. Saga, *NPG Asia Mater*, 2010, **2**, 96-102.
7. M. A. Green, K. Emery, Y. Hishikawa, W. Warta and E. D. Dunlop, *Progress in Photovoltaics: Research and Applications*, 2011, **19**, 565-572.
8. N. Espinosa, M. Hosel, D. Angmo and F. C. Krebs, *Energy & Environmental Science*, 2012, **5**, 5117-5132.
9. C. J. Brabec, *Sol. Energy Mater. Sol. Cells*, 2004, **83**, 273-292.
10. R. Søndergaard, M. Hösel, D. Angmo, T. T. Larsen-Olsen and F. C. Krebs, *Mater. Today*, 2012, **15**, 36-49.
11. R. F. Service, *Science*, 2014, **344**, 458.
12. S. E. Habas, H. A. S. Platt, M. F. A. M. van Hest and D. S. Ginley, *Chem. Rev.*, 2010, **110**, 6571-6594.
13. N. J. Jeon, H. G. Lee, Y. C. Kim, J. Seo, J. H. Noh, J. Lee and S. I. Seok, *J. Am. Chem. Soc.*, 2014, **136**, 7837-7840.
14. H. Zhou, Q. Chen, G. Li, S. Luo, T.-b. Song, H.-S. Duan, Z. Hong, J. You, Y. Liu and Y. Yang, *Science*, 2014, **345**, 542-546.
15. S. Luo and W. A. Daoud, *Journal of Materials Chemistry A*, 2015, **3**, 8992-9010.
16. N. K. Noel, S. D. Stranks, A. Abate, C. Wehrenfennig, S. Guarnera, A.-A. Haghighirad, A. Sadhanala, G. E. Eperon, S. K. Pathak, M. B. Johnston, A. Petrozza, L. M. Herz and H. J. Snaith, *Energy & Environmental Science*, 2014, **7**, 3061-3068.
17. F. Hao, C. C. Stoumpos, D. H. Cao, R. P. H. Chang and M. G. Kanatzidis, *Nat Photon*, 2014, **8**, 489-494.
18. D. Natali and M. Caironi, *Adv. Mater.*, 2012, **24**, 1357-1387.
19. C. Tang, X.-D. Liu, F. Liu, X.-L. Wang, H. Xu and W. Huang, *Macromol. Chem. Phys.*, 2013, **214**, 314-342.
20. R. Gaudiana, *The Journal of Physical Chemistry Letters*, 2010, **1**, 1288-1289.
21. http://www.heliatek.com/newscenter/latest_news/neuer-weltrekord-fur-organische-solarzellen-heliatek-behauptet-sich-mit-12-zelleffizienz-als-technologiefuhrer/?lang=en#, January 16, 2013.
22. D. L. Morel, A. K. Ghosh, T. Feng, E. L. Stogryn, P. E. Purwin, R. F. Shaw and C. Fishman, *Appl. Phys. Lett.*, 1978, **32**, 495-497.

23. A. K. Ghosh and T. Feng, *J. Appl. Phys.*, 1978, **49**, 5982-5989.
24. C. W. Tang, *Appl. Phys. Lett.*, 1986, **48**, 183-185.
25. M. Hiramoto, H. Fujiwara and M. Yokoyama, *J. Appl. Phys.*, 1992, **72**, 3781-3787.
26. N. S. Sariciftci, L. Smilowitz, A. J. Heeger and F. Wudl, *Science*, 1992, **258**, 1474-1476.
27. S. Morita, A. A. Zakhidov and K. Yoshino, *Solid State Commun.*, 1992, **82**, 249-252.
28. P. E. Shaw, A. Ruseckas and I. D. W. Samuel, *Adv. Mater.*, 2008, **20**, 3516-3520.
29. H. Hoppe, T. Glatzel, M. Niggemann, W. Schwinger, F. Schaeffler, A. Hinsch, M. C. Lux-Steiner and N. S. Sariciftci, *Thin Solid Films*, 2006, **511–512**, 587-592.
30. M. Knupfer, *Appl. Phys. A*, 2003, **77**, 623-626.
31. D. Credgington, F. C. Jamieson, B. Walker, T.-Q. Nguyen and J. R. Durrant, *Advanced Materials*, 2012, **24**, 2135-2141.
32. B. Walker, A. B. Tamayo, X.-D. Dang, P. Zalar, J. H. Seo, A. Garcia, M. Tantiwiwat and T.-Q. Nguyen, *Adv. Funct. Mater.*, 2009, **19**, 3063-3069.
33. F. Padinger, R. S. Rittberger and N. S. Sariciftci, *Adv. Funct. Mater.*, 2003, **13**, 85-88.
34. S. Huttner, M. Sommer, A. Chiche, G. Krausch, U. Steiner and M. Thelakkat, *Soft Matter*, 2009, **5**, 4206-4211.
35. P. Sonar, E. L. Williams, S. P. Singh, S. Manzhos and A. Dodabalapur, *PCCP*, 2013, **15**, 17064-17069.
36. J. K. Park, C. Kim, B. Walker, T.-Q. Nguyen and J. H. Seo, *RSC Advances*, 2012, **2**, 2232-2234.
37. Y. Yao, J. Hou, Z. Xu, G. Li and Y. Yang, *Adv. Funct. Mater.*, 2008, **18**, 1783-1789.
38. G. Li, V. Shrotriya, J. Huang, Y. Yao, T. Moriarty, K. Emery and Y. Yang, *Nat Mater*, 2005, **4**, 864-868.
39. F. Zhang, K. G. Jespersen, C. Björström, M. Svensson, M. R. Andersson, V. Sundström, K. Magnusson, E. Moons, A. Yartsev and O. Inganäs, *Adv. Funct. Mater.*, 2006, **16**, 667-674.
40. C. J. Brabec, A. Cravino, D. Meissner, N. S. Sariciftci, T. Fromherz, M. T. Rispens, L. Sanchez and J. C. Hummelen, *Adv. Funct. Mater.*, 2001, **11**, 374-380.
41. G. Yu, J. Gao, J. C. Hummelen, F. Wudl and A. J. Heeger, *Science*, 1995, **270**, 1789-1791.
42. Q. Zhou, Q. Hou, L. Zheng, X. Deng, G. Yu and Y. Cao, *Appl. Phys. Lett.*, 2004, **84**, 1653-1655.
43. N. Blouin, A. Michaud and M. Leclerc, *Adv. Mater.*, 2007, **19**, 2295-2300.
44. J. Peet, J. Y. Kim, N. E. Coates, W. L. Ma, D. Moses, A. J. Heeger and G. C. Bazan, *Nat Mater*, 2007, **6**, 497-500.
45. S. C. Price, A. C. Stuart, L. Yang, H. Zhou and W. You, *J. Am. Chem. Soc.*, 2011, **133**, 4625-4631.
46. H. Zhou, L. Yang, A. C. Stuart, S. C. Price, S. Liu and W. You, *Angew. Chem. Int. Ed.*, 2011, **50**, 2995-2998.
47. M. T. Lloyd, J. E. Anthony and G. G. Malliaras, *Mater. Today*, 2007, **10**, 34-41.

48. J. Roncali, P. Leriche and A. Cravino, *Adv. Mater.*, 2007, **19**, 2045-2060.
49. X. Sun, Y. Zhou, W. Wu, Y. Liu, W. Tian, G. Yu, W. Qiu, S. Chen and D. Zhu, *The Journal of Physical Chemistry B*, 2006, **110**, 7702-7707.
50. M. T. Lloyd, A. C. Mayer, A. S. Tayi, A. M. Bowen, T. G. Kasen, D. J. Herman, D. A. Mourey, J. E. Anthony and G. G. Malliaras, *Org. Electron.*, 2006, **7**, 243-248.
51. N. Kopidakis, W. J. Mitchell, J. van de Lagemaat, D. S. Ginley, G. Rumbles, S. E. Shaheen and W. L. Rance, *Appl. Phys. Lett.*, 2006, **89**, 103524.
52. K. N. Winzenberg, P. Kemppinen, G. Fanchini, M. Bown, G. E. Collis, C. M. Forsyth, K. Hegedus, T. B. Singh and S. E. Watkins, *Chem. Mater.*, 2009, **21**, 5701-5703.
53. A. B. Tamayo, B. Walker and T.-Q. Nguyen*, *The Journal of Physical Chemistry C*, 2008, **112**, 11545-11551.
54. A. B. Tamayo, X.-D. Dang, B. Walker, J. Seo, T. Kent and T.-Q. Nguyen, *Appl. Phys. Lett.*, 2009, **94**, 103301.
55. http://www.heliatek.com/wp-content/uploads/2013/01/130116_PR_Heliatek_achieves_record_cell_effiency_for_OPV.pdf, Heliatek.
56. Yanming Sun, Gregory C. Welch, Wei Lin Leong, Christopher J. Takacs, G. C. Bazan and A. J. Heeger, *Nature Materials ,* , 2012, **11**, 44–48.
57. J. Zhou, X. Wan, Y. Liu, Y. Zuo, Z. Li, G. He, G. Long, W. Ni, C. Li, X. Su and Y. Chen, *J. Am. Chem. Soc.*, 2012, **134**, 16345-16351.
58. O. P. Lee, A. T. Yiu, P. M. Beaujuge, C. H. Woo, T. W. Holcombe, J. E. Millstone, J. D. Douglas, M. S. Chen and J. M. J. Fréchet, *Adv. Mater.*, 2011, **23**, 5359-5363.
59. Y. Li, P. Sonar, L. Murphy and W. Hong, *Energy & Environmental Science*, 2013, **6**, 1684-1710.
60. H. Bürckstümmer, A. Weissenstein, D. Bialas and F. Würthner, *The Journal of Organic Chemistry*, 2011, **76**, 2426-2432.
61. Y. Qu, J. Hua and H. Tian, *Org. Lett.*, 2010, **12**, 3320-3323.
62. Y. Jiang, Y. Wang, J. Hua, S. Qu, S. Qian and H. Tian, *J. Polym. Sci., Part A: Polym. Chem.*, 2009, **47**, 4400-4408.
63. Z. Qiao, Y. Xu, S. Lin, J. Peng and D. Cao, *Synth. Met.*, 2010, **160**, 1544-1550.
64. M. Tantiwiwat, A. Tamayo, N. Luu, X.-D. Dang and T.-Q. Nguyen, *The Journal of Physical Chemistry C*, 2008, **112**, 17402-17407.
65. S. Qu and H. Tian, *Chem. Commun.*, 2012, **48**, 3039-3051.
66. D. G. Farnum, G. Mehta, G. G. I. Moore and F. P. Siegal, *Tetrahedron Lett.*, 1974, **15**, 2549-2552.
67. B. Alain C. Rochat, B. Luigi Cassar and E. Abul Iqbal, US 4415685 (Nov, 1983) Iqbal et al., US, 1986.
68. O. Wallquist and R. Lenz, *Macromolecular Symposia*, 2002, **187**, 617-630.

69. Z. Hao and A. Iqbal, *Chem. Soc. Rev.*, 1997, **26**, 203-213.
70. B. Walker, C. Kim and T.-Q. Nguyen, *Chem. Mater.*, 2010, **23**, 470-482.
71. L. Huo, J. Hou, H.-Y. Chen, S. Zhang, Y. Jiang, T. L. Chen and Y. Yang, *Macromolecules*, 2009, **42**, 6564-6571.
72. J. Y. Letian Dou, Jun Yang, Chun-Chao Chen, Youjun He, Seiichiro Murase, Tom Moriarty, Keith Emery, Gang Li & Yang Yang, *Nature Photonics* 2012, **6**, 180–185.
73. P. P. Khlyabich, B. Burkhart, C. F. Ng and B. C. Thompson, *Macromolecules*, 2011, **44**, 5079-5084.
74. M. A. Naik and S. Patil, *J. Polym. Sci., Part A: Polym. Chem.*, 2013, **51**, 4241-4260.
75. L. Jun, Z. Yan, T. Huei Shuan, G. Yunlong, D. Chong-An, Y. Gui, L. Yunqi, L. Ming, L. Suo Hon, Z. Yuhua, S. Haibin and S. O. Beng, *Scientific Reports*, 2012, **2**.
76. M. Chandrasekharam, M. A. Reddy, K. Ganesh, G. D. Sharma, S. P. Singh and J. L. Rao, *Org. Electron.*, 2014, **15**, 2116-2125.
77. Y. Lin, L. Ma, Y. Li, Y. Liu, D. Zhu and X. Zhan, *Advanced Energy Materials*, 2013, **3**, 1166-1170.
78. A. Armin, G. Juska, M. Ullah, M. Velusamy, P. L. Burn, P. Meredith and A. Pivrikas, *Advanced Energy Materials*, 2014, **4**, n/a-n/a.
79. V. D. Mihailetchi, J. K. J. van Duren, P. W. M. Blom, J. C. Hummelen, R. A. J. Janssen, J. M. Kroon, M. T. Rispens, W. J. H. Verhees and M. M. Wienk, *Adv. Funct. Mater.*, 2003, **13**, 43-46.
80. Y. Fang, A. K. Pandey, A. M. Nardes, N. Kopidakis, P. L. Burn and P. Meredith, *Advanced Energy Materials*, 2013, **3**, 54-59.
81. A. a. F. Eftaiha, J.-P. Sun, I. G. Hill and G. C. Welch, *Journal of Materials Chemistry A*, 2014, **2**, 1201-1213.
82. T. Ye, R. Singh, H.-J. Butt, G. Floudas and P. E. Keivanidis, *ACS Applied Materials & Interfaces*, 2013, **5**, 11844-11857.
83. R. Singh, E. Aluicio-Sarduy, Z. Kan, T. Ye, R. C. I. MacKenzie and P. E. Keivanidis, *Journal of Materials Chemistry A*, 2014, **2**, 14348-14353.
84. J. Zhao, Y. Li, H. Lin, Y. Liu, K. Jiang, C. Mu, T. Ma, J. Y. Lin Lai, H. Hu, D. Yu and H. Yan, *Energy & Environmental Science*, 2015, **8**, 520-525.
85. S. Tatemichi, M. Ichikawa, T. Koyama and Y. Taniguchi, *Appl. Phys. Lett.*, 2006, **89**, 112108.
86. F. G. Brunetti, X. Gong, M. Tong, A. J. Heeger and F. Wudl, *Angew. Chem. Int. Ed.*, 2010, **49**, 532-536.
87. M. Rabinovitz, I. Agranat and A. Weitzen-Dagan, *Tetrahedron Lett.*, 1974, **15**, 1241-1244.
88. Y. Cohen, J. Klein and M. Rabinovitz, *J. Chem. Soc., Chem. Commun.*, 1986, 1071-1073.
89. X. Gong, M. Tong, F. G. Brunetti, J. Seo, Y. Sun, D. Moses, F. Wudl and A. J. Heeger, *Adv. Mater.*, 2011, **23**, 2272-2277.

90. J. T. Bloking, X. Han, A. T. Higgs, J. P. Kastrop, L. Pandey, J. E. Norton, C. Risko, C. E. Chen, J.-L. Brédas, M. D. McGehee and A. Sellinger, *Chem. Mater.*, 2011, **23**, 5484-5490.
91. C. H. Woo, T. W. Holcombe, D. A. Unruh, A. Sellinger and J. M. J. Fréchet, *Chem. Mater.*, 2010, **22**, 1673-1679.
92. P. Sonar, G.-M. Ng, T. T. Lin, A. Dodabalapur and Z.-K. Chen, *J. Mater. Chem.*, 2010, **20**, 3626-3636.
93. K. N. Winzenberg, P. Kemppinen, F. H. Scholes, G. E. Collis, Y. Shu, T. Birendra Singh, A. Bilic, C. M. Forsyth and S. E. Watkins, *Chem. Commun.*, 2013, **49**, 6307-6309.
94. Y. Kim, C. E. Song, S.-J. Moon and E. Lim, *Chem. Commun.*, 2014, **50**, 8235-8238.
95. L. Chen, L. Huang, D. Yang, S. Ma, X. Zhou, J. Zhang, G. Tu and C. Li, *Journal of Materials Chemistry A*, 2014, **2**, 2657-2662.
96. S. Holliday, R. S. Ashraf, C. B. Nielsen, M. Kirkus, J. A. Röhr, C.-H. Tan, E. Collado-Fregoso, A.-C. Knall, J. R. Durrant, J. Nelson and I. McCulloch, *J. Am. Chem. Soc.*, 2015, **137**, 898-904.
97. B. P. Karsten, J. C. Bijleveld and R. A. J. Janssen, *Macromol. Rapid Commun.*, 2010, **31**, 1554-1559.
98. A. M. Raynor, A. Gupta, H. Patil, A. Bilic and S. V. Bhosale, *RSC Advances*, 2014, **4**, 57635-57638.
99. H. Patil, W. X. Zu, A. Gupta, V. Chellappan, A. Bilic, P. Sonar, A. Rananaware, S. V. Bhosale and S. V. Bhosale, *PCCP*, 2014, **16**, 23837-23842.
100. Y. Kim, C. E. Song, E. J. Ko, D. Kim, S. J. Moon and E. Lim, *RSC Advances*, 2015, **5**, 4811-4821.
101. W. Porzio, S. Destri, M. Pasini, U. Giovanella, T. Motta, M. D. Iosip, D. Natali, M. Sampietro, L. Franco and M. Campione, *Synth. Met.*, 2004, **146**, 259-263.
102. F. Lincker, N. Delbosc, S. Bailly, R. De Bettignies, M. Billon, A. Pron and R. Demadrille, *Adv. Funct. Mater.*, 2008, **18**, 3444-3453.
103. Z. Xinran, B. Hugo, J. K. Auke, S. Jeremy, K. Youngju, R. J. Kline, J. R. Lee, D. A. Thomas, S. Henning, S. Kigook, H. Martin, Z. Weimin, M. Iain and M. D. Dean, *Nature Communications*, 2013, **4**.
104. Y.-J. Cheng, S.-H. Yang and C.-S. Hsu, *Chem. Rev.*, 2009, **109**, 5868-5923.
105. M. Grzybowski and D. T. Gryko, *Advanced Optical Materials*, 2015, **3**, 280-320.
106. C. J. H. Morton, R. Gilmour, D. M. Smith, P. Lightfoot, A. M. Z. Slawin and E. J. MacLean, *Tetrahedron*, 2002, **58**, 5547-5565.
107. C. J. H. Morton, R. L. Riggs, D. M. Smith, N. J. Westwood, P. Lightfoot and A. M. Z. Slawin, *Tetrahedron*, 2005, **61**, 727-738.
108. R. L. Riggs, C. J. H. Morton, A. M. Z. Slawin, D. M. Smith, N. J. Westwood, W. S. D. Austen and K. E. Stuart, *Tetrahedron*, 2005, **61**, 11230-11243.
109. P.-L. T. Boudreault, A. Najari and M. Leclerc, *Chem. Mater.*, 2010, **23**, 456-469.

110. F. Kazemi, A. R. Kiasat and B. Mombaini, *Phosphorus, Sulfur, and Silicon and the Related Elements*, 2004, **179**, 1187-1191.
111. G.-Y. Chen, C.-M. Chiang, D. Kekuda, S.-C. Lan, C.-W. Chu and K.-H. Wei, *J. Polym. Sci., Part A: Polym. Chem.*, 2010, **48**, 1669-1675.
112. B. Zhao, K. Sun, F. Xue and J. Ouyang, *Org. Electron.*, 2012, **13**, 2516-2524.
113. H.-C. Chang, T. Shiozaki, A. Kamata, K. Kishida, T. Ohmori, D. Kiriya, T. Yamauchi, H. Furukawa and S. Kitagawa, *J. Mater. Chem.*, 2007, **17**, 4136-4138.
114. Y. Li, S. P. Singh and P. Sonar, *Adv. Mater.*, 2010, **22**, 4862-4866.
115. W. C. Guida and D. J. Mathre, *The Journal of Organic Chemistry*, 1980, **45**, 3172-3176.
116. H. Bai, P. Cheng, Y. Wang, L. Ma, Y. Li, D. Zhu and X. Zhan, *Journal of Materials Chemistry A*, 2014, **2**, 778-784.
117. K. Okamoto, J. Zhang, J. B. Housekeeper, S. R. Marder and C. K. Luscombe, *Macromolecules*, 2013, **46**, 8059-8078.
118. S.-Y. Liu, M.-M. Shi, J.-C. Huang, Z.-N. Jin, X.-L. Hu, J.-Y. Pan, H.-Y. Li, A. K. Y. Jen and H.-Z. Chen, *Journal of Materials Chemistry A*, 2013, **1**, 2795-2805.
119. J. Dhar, N. Venkatramaiah, A. A and S. Patil, *Journal of Materials Chemistry C*, 2014, **2**, 3457-3466.
120. L. A. Estrada, J. E. Yarnell and D. C. Neckers, *The Journal of Physical Chemistry A*, 2011, **115**, 6366-6375.
121. B. W. D'Andrade, S. Datta, S. R. Forrest, P. Djurovich, E. Polikarpov and M. E. Thompson, *Org. Electron.*, 2005, **6**, 11-20.
122. J. Yu, K. H. Lee, Y. Zhang, M. F. G. Klein, A. Colsmann, U. Lemmer, P. L. Burn, S.-C. Lo and P. Meredith, *Polymer Chemistry*, 2011, **2**, 2668-2673.
123. J. R. Lakowicz, *Principles of Fluorescence Spectroscopy*, Springer,
New York, 2006.
124. B. Ebenhoch, S. A. J. Thomson, K. Genevičius, G. Juška and I. D. W. Samuel, *Org. Electron.*, 2015, **22**, 62-68.
125. A. Wan, J. Hwang, F. Amy and A. Kahn, *Org. Electron.*, 2005, **6**, 47-54.
126. A. Kumatani, Y. Li, P. Darmawan, T. Minari and K. Tsukagoshi, *Sci. Rep.*, 2013, **3**.
127. G. Generali, F. Dinelli, R. Capelli, S. Toffanin, F. di Maria, M. Gazzano, G. Barbarella and M. Muccini, *The Journal of Physical Chemistry C*, 2011, **115**, 23164-23169.
128. C. Yu, Z. Liu, Y. Yang, J. Yao, Z. Cai, H. Luo, G. Zhang and D. Zhang, *Journal of Materials Chemistry C*, 2014.
129. W. Kang, M. Jung, W. Cha, S. Jang, Y. Yoon, H. Kim, H. J. Son, D.-K. Lee, B. Kim and J. H. Cho, *ACS Applied Materials & Interfaces*, 2014, **6**, 6589-6597.
130. A. Ko Ko Kyaw, D. Hwan Wang, H.-R. Tseng, J. Zhang, G. C. Bazan and A. J. Heeger, *Appl. Phys. Lett.*, 2013, **102**, 163308.
131. C. Jouanin, J. P. Albert and C. Gout, *J. Phys. France*, 1976, **37**, 595-602.

132. J. Liu, Y. Sun, P. Moonsin, M. Kuik, C. M. Proctor, J. Lin, B. B. Hsu, V. Promarak, A. J. Heeger and T.-Q. Nguyen, *Adv. Mater.*, 2013, **25**, 5898-5903.
133. G. Wei, R. R. Lunt, K. Sun, S. Wang, M. E. Thompson and S. R. Forrest, *Nano Lett.*, 2010, **10**, 3555-3559.
134. H. Fan, H. Shang, Y. Li and X. Zhan, *Appl. Phys. Lett.*, 2010, **97**, 133302.
135. V. Gupta, A. K. K. Kyaw, D. H. Wang, S. Chand, G. C. Bazan and A. J. Heeger, *Sci. Rep.*, 2013, **3**.
136. W. Li, K. H. Hendriks, W. S. C. Roelofs, Y. Kim, M. M. Wienk and R. A. J. Janssen, *Adv. Mater.*, 2013, **25**, 3182-3186.
137. A. L. Briseno, Q. Miao, M.-M. Ling, C. Reese, H. Meng, Z. Bao and F. Wudl, *J. Am. Chem. Soc.*, 2006, **128**, 15576-15577.
138. Y. Sun, L. Tan, S. Jiang, H. Qian, Z. Wang, D. Yan, C. Di, Y. Wang, W. Wu, G. Yu, S. Yan, C. Wang, W. Hu, Y. Liu and D. Zhu, *J. Am. Chem. Soc.*, 2007, **129**, 1882-1883.
139. W. Jiang, Y. Zhou, H. Geng, S. Jiang, S. Yan, W. Hu, Z. Wang, Z. Shuai and J. Pei, *J. Am. Chem. Soc.*, 2011, **133**, 1-3.
140. Y. Y. Mohamad SB, Melø TB, Jávorfi T, Partali V, Sliwka HR, Razi Naqvi K, *Journal of Photochemistry and Photobiology. B, Biology*, **84**, 135-140.
141. W. S. Yoon, S. K. Park, I. Cho, J.-A. Oh, J. H. Kim and S. Y. Park, *Adv. Funct. Mater.*, 2013, **23**, 3519-3524.
142. C. D. Wessendorf, G. L. Schulz, A. Mishra, P. Kar, I. Ata, M. Weidelener, M. Urdanpilleta, J. Hanisch, E. Mena-Osteritz, M. Lindén, E. Ahlswede and P. Bäuerle, *Advanced Energy Materials*, 2014, **4**, n/a-n/a.
143. V. Sachweh and H. Langhals, *Chem. Ber.*, 1990, **123**, 1981-1987.
144. T. C. Pijper, D. Pijper, M. M. Pollard, F. Dumur, S. G. Davey, A. Meetsma and B. L. Feringa, *The Journal of Organic Chemistry*, 2010, **75**, 825-838.
145. E. Spinner, *The Journal of Organic Chemistry*, 1958, **23**, 2037-2038.
146. D. M. Wiles, B. A. Gingras and T. Suprunchuk, *Can. J. Chem.*, 1967, **45**, 469-473.
147. M. Jesberger, T. P. Davis and L. Barner, *Synthesis*, 2003, **2003**, 1929-1958.
148. M. Ghandi, S. J. Tabatabaei Rezaei, A. Yari and A. Taheri, *Tetrahedron Lett.*, 2008, **49**, 5899-5901.
149. W.-Y. Wong, G.-L. Lu, K.-H. Choi and Z. Lin, *Eur. J. Org. Chem.*, 2003, **2003**, 365-373.
150. B. S. Ong, *Tetrahedron Lett.*, 1980, **21**, 4225-4228.
151. G. Ren, E. Ahmed and S. A. Jenekhe, *Advanced Energy Materials*, 2011, **1**, 946-953.
152. T. Zhou, T. Jia, B. Kang, F. Li, M. Fahlman and Y. Wang, *Advanced Energy Materials*, 2011, **1**, 431-439.
153. L. Wang, P. Li, Z. Wu, J. Yan, M. Wang and Y. Ding, *Synthesis*, 2003, **2003**, 2001-2004.
154. G. A. Heropoulos, S. Georgakopoulos and B. R. Steele, *Tetrahedron Lett.*, 2005, **46**, 2469-2473.

155. C. Boix and M. Poliakoff, *J. Chem. Soc., Perkin Trans. 1*, 1999, 1487-1490.
156. D. Nagaraja and M. A. Pasha, *Tetrahedron Lett.*, 1999, **40**, 7855-7856.
157. A. J. Nunn and J. T. Ralph, *Journal of the Chemical Society (Resumed)*, 1965, 6769-6777.
158. K. Pilgram, M. Zupan and R. Skiles, *J. Heterocycl. Chem.*, 1970, **7**, 629-633.
159. P. L. Vanelle, C.T.; Meuche, J.; Maldonado, J.; Crozet, M.P., *Hetrocycles* 1997, **45**, 955-962.
160. M. Hirade, T. Yasuda and C. Adachi, *The Journal of Physical Chemistry C*, 2013, **117**, 4986-4991.
161. K. Jacob, M. Sigalov, James Y. Becker, A. Ellern and V. Khodorkovsky, *Eur. J. Org. Chem.*, 2000, **2000**, 2047-2055.
162. O. Y. Park, H. U. Kim, J.-H. Kim, J. B. Park, J. Kwak, W. S. Shin, S. C. Yoon and D.-H. Hwang, *Sol. Energy Mater. Sol. Cells*, 2013, **116**, 275-282.
163. H. Li, R.-Y. Zhu, W.-J. Shi, K.-H. He and Z.-J. Shi, *Org. Lett.*, 2012, **14**, 4850-4853.
164. P. Gandeepan, C.-H. Hung and C.-H. Cheng, *Chem. Commun.*, 2012, **48**, 9379-9381.
165. P. Anbarasan, H. Neumann and M. Beller, *Chemistry – A European Journal*, 2011, **17**, 4217-4222.
166. R. O. Kan, *J. Am. Chem. Soc.*, 1964, **86**, 5180-5183.
167. S. Stas, S. Sergeyev and Y. Geerts, *Tetrahedron*, 2010, **66**, 1837-1845.
168. C. H. Woo, P. M. Beaujuge, T. W. Holcombe, O. P. Lee and J. M. J. Fréchet, *J. Am. Chem. Soc.*, 2010, **132**, 15547-15549.
169. C.-S. Li, Y.-H. Tsai, W.-C. Lee and W.-J. Kuo, *The Journal of Organic Chemistry*, 2010, **75**, 4004-4013.
170. R. Grisorio, P. Mastrorilli, G. Ciccarella, G. P. Suranna and C. F. Nobile, *Tetrahedron Lett.*, 2008, **49**, 2078-2082.
171. T. Nakanishi, Y. Shirai and L. Han, *Journal of Materials Chemistry A*, 2015, **3**, 4229-4238.
172. T. Miyazaki, M. Shibahara, J.-i. Fujishige, M. Watanabe, K. Goto and T. Shinmyozu, *The Journal of Organic Chemistry*, 2014, **79**, 11440-11453.
173. L.-Y. Lin, Y.-H. Chen, Z.-Y. Huang, H.-W. Lin, S.-H. Chou, F. Lin, C.-W. Chen, Y.-H. Liu and K.-T. Wong, *J. Am. Chem. Soc.*, 2011, **133**, 15822-15825.
174. D. Pijper and B. L. Feringa, *Angew. Chem. Int. Ed.*, 2007, **46**, 3693-3696.